Single-molecule Dynamics and Localization of mRNAs, ribosomal Protein L1 and the membrane remodeling protein DynA in *Bacillus subtilis*

Dissertation

zur Erlangung des Grades eines

Doktor der Naturwissenschaften

(Dr. rer. nat.)

im Fachbereichs Chemie der Philipps-Universität Marburg

Vorgelegt von

Laura Sattler, M.Sc.

geboren in Wetzlar

Marburg, Dezember 2021

Die Untersuchungen zur vorliegenden Dissertation wurden in der Zeit von April 2017 bis April 2021 unter Leitung von Herrn Prof. Dr. Peter L. Graumann an der Philipps-Universität Marburg, unter Finanzierung des DFG geförderten „Transregional Collaborative Research Centers“ TRR174, durchgeführt.

Vom Fachbereich Chemie der Philipps-Universität Marburg
(Hochschulkennziffer 1180) als Dissertation angenommen am 10.02.2022

Erstgutachter: Prof. Dr. Peter L. Graumann
Fachbereich Chemie, Philipps-Universität Marburg

Zweitgutachter: Prof. Dr. Gert Bange
Fachbereich Chemie, Philipps-Universität Marburg

Tag der Disputation: 02.03.2022

Eidesstattliche Erklärung

Ich erkläre, dass eine Promotion noch an keiner anderen Hochschule als der Philipps-Universität Marburg, Fachbereich Chemie, versucht wurde.

Hiermit versichere ich, dass die vorliegende Dissertation:

"Single-molecule Dynamics and Localization of mRNAs, ribosomal Protein L1 and the membrane remodeling protein DynA in *Bacillus subtilis*"

selbstständig, ohne unerlaubte Hilfe Dritter angefertigt und andere als die in der Dissertation angegebenen Hilfsmittel nicht benutzt habe. Alle Stellen, die wörtlich oder sinngemäß aus veröffentlichten oder unveröffentlichten Schriften entnommen sind, habe ich als solche kenntlich gemacht. Dritte waren an der inhaltlich-materiellen Erstellung der Dissertation nicht beteiligt; insbesondere habe ich hierfür nicht die Hilfe eines Promotionsberaters in Anspruch genommen. Kein Teil dieser Arbeit ist in einem anderen Promotions- oder Habilitationsverfahren verwendet worden. Mit dem Einsatz von Software zur Erkennung von Plagiaten bin ich einverstanden.

Marburg, 7.12.2021

Ort/Datum

(Laura Sattler)

Unterschrift (Vor- und Nachname)

Summary

In this work, single-molecule tracking, in combination with SMTracker software, is the main microscopy method to generate and analyze data. This allows various processes to be studied in a millisecond time range with a high optical resolution in living cells/bacteria. Due to new findings, including improved methods, a number of theories that were previously considered established have to be reconsidered. This also applies to protein biosynthesis in bacteria. A temporal and spatial separation of transcription and translation of these two processes is becoming increasingly likely at least in some bacteria. However, the extent to which this occurs is still unclear. Two general models exist for this, which attempt to explain where mRNA translation takes place and whether this is a process separate from transcription or coupled to it: 1.) The mRNA remains close to its transcription site, with the bacterial chromosome acting as a template - where both, coupling of transcription and translation and separation, are possible - or 2.) mRNAs localize where the protein to be encoded is later required. Transcription and translation are thus rather spatially and temporally separated from each other. Importantly, these models may apply differently to different bacterial species.

This work focuses mainly on the question of where translation of different mRNAs takes place in the Gram-positive bacterium *Bacillus subtilis* and what dynamics they exhibit. For this work, the already often used RNA labelling method, the MS2-system, was used, which had to be modified a little in advance in order to achieve optimal results. The results show that already one and two repeats of the MS2-binding sequence are sufficient to detect mRNAs with the MS2-system. In this context, it could be shown that unspecific binding of the MS2-binding protein occurs and affects the growth of cells expressing it, regardless of the co-expression of the associated binding site. Nevertheless, detection of mRNAs is still possible.

To address the question of where translation occurs in *B. subtilis*, mRNAs encoding soluble, membrane and extracellular proteins were used. The localization of these mRNAs provides insight into where translation might take place. The results of this work do not fit exclusively to either model 1) or model 2), but have features of both models. All tested mRNAs show a localization at the poles and the surrounding of the nucleoid, whereas mRNAs encoding membrane proteins show a tendency towards the membrane. The co-expression and co-localization of a mRNA, *ypbR-ypzF*, and one of the proteins encoded from it, DynA,

supports the assumption that a mRNA and its protein product could colocalize.

This investigation further includes the dynamics of mRNAs, which previous studies have mainly determined in an indirect or theoretical way. The understanding of how mRNAs move in the cell is best explained by assuming at least two, possibly three populations, with a static population likely representing the translation of mRNA, a possible transition complex with the ribosomal subunits, as well as a freely diffusing population existing if three populations are assumed. The square displacement analysis also shows that the diffusion constants and thus the speed of the mRNAs appear to be size-independent and that mRNAs can move anywhere in the cell within a few seconds, although they are noticeably slower than cytosolic proteins.

The assembly of the ribosome also plays an important role here and is probably already indirectly reflected by the mRNA study. The data generated of the ribosomal protein of the 50S subunit, by using single-molecule tracking further supports this. In addition to its localization, for the first time in a Gram-positive bacterium, its dynamics were investigated. Here, more than three populations can be assumed, whereby the static population, which represents a possible translation, corresponds to the static population of the investigated mRNAs. In addition, a fast, freely diffuse population can be observed, as well as the formation of a transition complex with several intermediates, which argues for the dynamic, complex structure of the ribosome and agrees with the mRNA data. Furthermore, the localization data match and support the results obtained from the mRNAs.

The bacterial dynamin-like protein, DynA from *B. subtilis*, was not only used for co-localization analyses with its mRNA transcript, but was also further characterized. This protein is involved in cell division, where it plays an important role in membrane fusion of the newly divided cells. In addition, cells lacking DynA are less resistant to phage attack and membrane stress induced by chemical reagents. However, the type of membrane stress responsible for DynA recruitment is not fully understood. Using epifluorescence microscopy and single-molecule tracking, I was able to show that DynA only responds to specific stresses, probably induced pores in the membrane caused by attacking components of lipid II. Furthermore, by studying the dynamics of DynA, three different populations of mobility could be found. A static population that is involved in membrane fusion, including during cell division and repair of membrane damage - a process that occurs relatively quickly -, a slow mobile population that searches for possible membrane damage, and a population for probably freely diffusing DynA

molecules that has a cytoplasmic localization not known so far. Importantly, even a slight change in the number of DynA molecules is enough to repair the damage caused by the antibiotics.

Zusammenfassung

In dieser Arbeit ist das Verfahren der Einzelmolekül-Verfolgung, in Kombination mit der SMTracker Software, die wichtigste Mikroskopiemethode, um Daten zu generieren und zu analysieren. Damit können verschiedenen Prozesse im Millisekundenbereich mit einer hohen optischen Auflösung in lebenden Zellen/Bakterien untersucht werden.

Durch neue Erkenntnisse, u.a. durch verbesserte Methoden, müssen verschiedene, bis dahin als etabliert betrachtete Theorien, überdacht werden. So auch die Proteinbiosynthese in Bakterien. Eine zeitliche und räumliche Trennung von Transkription und Translation dieser beiden Prozesse in verschiedenen Bakterienspezies wird immer wahrscheinlicher. In welchem Ausmaß dies geschieht, ist jedoch noch unklar. Dafür existieren zwei generelle Modelle, die zu erklären versuchen, wo die mRNA-Translation stattfindet und ob dies ein von der Transkription getrennter oder damit gekoppelter Vorgang ist: 1.) Die mRNA verbleibt in der Nähe ihres Transkriptionsortes, wobei das bakterielle Chromosom als Vorlage fungiert – bei dem sowohl eine Kopplung von Transkription und Translation als auch eine Trennung möglich ist -, oder 2.) mRNAs lokalisieren sich dort, wo das zu kodierende Protein später benötigt wird. Transkription und Translation sind damit eher räumlich und zeitlich voneinander getrennt. Wichtig ist, diese Modelle können für verschiedene Bakterienspezies unterschiedlich zutreffend sein.

Diese Arbeit beschäftigt sich im Wesentlichen mit der Frage, wo die Translation verschiedener mRNAs in dem Gram-positiven Bakterium *Bacillus subtilis* stattfindet und welche Dynamiken sie aufweisen. Für diese Arbeit wurde die bereits vielfacht genutzte RNA-Markierungsmethode, das MS2-System, verwendet, das vorab ein wenig abgeändert werden musste, um optimale Ergebnisse zu erzielen. Die Ergebnisse zeigen, dass bereits ein und zwei Wiederholungen der MS2-Bindesequenz ausreichend sind, um mRNAs mit dem MS2-System zu detektieren. In diesem Zusammenhang konnte aufgezeigt werden, dass eine unspezifische Bindung des MS2-Bindeproteins auftritt und das Wachstum von Zellen, die dies exprimieren, unabhängig von der Koexpression der dazugehörigen Bindestelle, beeinflusst. Trotzdem ist der Nachweis von mRNAs damit möglich.

Um der Frage nachzugehen, wo die Translation in *B. subtilis* stattfindet, wurden mRNAs, die für lösliche, membranständige und extrazelluläre Proteine kodieren, verwendet. Die Lokalisierung dieser mRNAs gibt einen Einblick, wo die Translation stattfinden könnte. Die Ergebnisse dieser Arbeit passen dabei weder ausschließlich zu Modell 1) noch zu Modell 2),

besitzen jedoch Merkmale beider Modelle. Sämtliche getesteten mRNAs weisen eine Lokalisation an den Polen und der Umgebung des Nukleoids auf, wobei mRNAs, die für Membranproteine kodieren, eine Tendenz zur Membran aufzeigen. Die Koexpression und Kolokalisation einer mRNA, *ypbR-ypzF*, und eines der daraus kodierten Proteine, DynA, unterstützt die Annahme, dass eine mRNA und ihr Proteinprodukt kolokalisieren könnten.

Diese Untersuchung umfasst ferner die Dynamiken von mRNAs, die in bisherigen Studien hauptsächlich auf indirekte oder theoretische Weise ermittelt wurde. Die Erkenntnis, wie sich mRNAs in der Zelle bewegen, lässt sich am besten durch die Annahme von mindestens zwei, möglicherweise drei Populationen erklären, wobei eine statische Population wahrscheinlich die Translation der mRNA abbildet, ein möglicher Übergangskomplex mit den ribosomalen Untereinheiten vorhanden ist, sowie eine frei diffuse Population existiert, wenn von drei Populationen ausgegangen wird. Die quadratische Verschiebungsanalyse (*square displacement analysis*) zeigt zudem, dass die Diffusionskonstanten und damit die Geschwindigkeit der mRNAs größenunabhängig zu seinen scheint und sich mRNAs innerhalb weniger Sekunden überall in der Zelle hinbewegen können, wobei sie deutlich langsamer sind als cytosolische Proteine.

Auch der Zusammenbau des Ribosoms spielt hierbei eine wichtige Rolle und wird wahrscheinlich bereits indirekt durch die mRNA Untersuchung wiedergegeben. Die generierten Daten des ribosomalen Proteins der 50S Untereinheit, L1, mittels Einzelmolekül-Verfolgung unterstützt dies zusätzlich. Neben dessen Lokalisation wurde erstmals in einem Gram positiven Bakterium, dessen Dynamik untersucht. Hier kann von mehr als drei Populationen ausgegangen werden, wobei die statische Population, die eine mögliche Translation darstellt, der statischen Population der untersuchten mRNAs entspricht. Daneben kann eine schnelle, frei diffuse Population beobachtet werden, sowie die Bildung eines Übergangskomplexes mit mehreren Zwischenprodukten, was für den dynamischen, komplexen Aufbau des Ribosoms spricht und mit den mRNA Daten übereinstimmt. Des Weiteren passen die Lokalisationsdaten zu den gewonnenen Ergebnissen der mRNAs und untermauert diese.

Das bakterielle Dynamin-ähnliche Protein, DynA von *B. subtilis*, wurde nicht nur für Kolokalisationsanalysen mit seinem mRNA-Transkript verwendet, sondern auch weitergehend charakterisiert. Dieses Protein ist an der Zellteilung beteiligt und spielt dort eine wichtige Rolle bei der Membranfusion der sich frisch geteilten Zelle. Darüber hinaus sind Zellen, denen DynA

fehlt, weniger resistent gegenüber Phagenbefall und Membranstress, der durch chemische Reagenzien induziert wird. Welche Art von Membranstress für die Rekrutierung von DynA verantwortlich ist, ist jedoch nicht vollständig geklärt. Mit Hilfe von Epifluoreszenzmikroskopie und Einzelmolekül-Verfolgung konnte ich zeigen, dass DynA nur auf spezielle Stressfaktoren reagiert, wahrscheinlich induzierte Poren in der Membran, die durch das Angreifen von Komponenten des Lipid II entstehen. Außerdem konnte bei der Untersuchung der Dynamik von DynA drei unterschiedliche Populationen der Mobilität gefunden werden. Eine statische Population, die an der Membranfusion beteiligt ist, u. a. während der Zellteilung und bei der Behebung von Membranschäden– ein Vorgang, der verhältnismäßig schnell vonstattengeht -, eine langsam mobile Population, die nach möglichen Membranschädigungen sucht, sowie eine Population für wahrscheinlich frei diffundierende DynA-Moleküle, die eine bisher nicht bekannte zytoplasmatische Lokalisation aufweist. Wichtig dabei ist, dass bereits eine geringfügige Änderung in der Anzahl der DynA-Moleküle ausreichend ist, um die durch die Antibiotika verursachten Schäden zu beheben.

Contents

Table of Figures

Introduction

Article I

Article II

Unpublished Results

Discussion

Material and Methods

1. INTRODUCTION

1.1 RNAs were essential for the origin of life

In the beginning, life on Earth was remarkably different from today. This is, of course, common knowledge. Still, the question how life began on Earth is not fully uncovered. Different theories exist. Besides religious believes, first, it was thought, life arises from dead material, also called abiogenesis, and was already theorized by the Greek philosopher Aristoteles (384–322 B.C.). In the 20th's century, new theories emerged. In the 1950th, Stanley Miller and Harold C. Urey performed experiments to demonstrate that by energizing inorganic compounds, organic material like amino acids, fatty acids and also later on lipids could be generated, by developing the theory and experimental set-ups of Aleksandr Oparin and J. B. S. Haldane further [1]. The theory of the primordial soup was born [2]. Based on this theory, the RNA-world theory was developed and first mentioned by Carl Woese [3] and was made famous by Walter Gilbert [4]. It states that ribonucleotide acids (RNA), were the initial factor of the beginning of life, through their ability to store genetic information and catalyze chemical reactions in primitive cells [3, 5]. Experiments in the 21st century showed that RNAs may have originated from the primordial soup [6]. The RNA world theory relies on the assumption that RNAs, among other things, have an autocatalytic activity and can perform self-replication, which both were found in *Escherichia coli* in the 1980ths [7]. Not to dive too deeply into this theory, also several problems occur. RNAs are too complex that they have developed out of nothing. Here, the pre-RNA world theory states that early simple RNA-like polymers evolved into the more complex RNA, whereas various models are used to explain this [8, 9]. In the 80th's critics came up, because the setting of the assumed prehistoric conditions for the primordial soup would not be correct, and the theory of the primordial-sandwich was announced by Günter Wächtershäuser. This theory suggests that life began with a chemo-autotrophic metabolism by reducing iron and sulfur with elemental hydrogen to produce different biomolecules, including complex ones [10, 11]. Of course, other theories also exist. A famous one is the panspermatism, where life came to Earth by meteorites, etc. [12]. To this day, no theory could prove its total accuracy and even more theories exist. It is not known, what was first, the simple metabolic activity, the RNA world, or the RNA-peptide coevolution theory, to name a few, or a combination of different theories. However, it is indisputable that ribonucleotide acids play an important role in modern life. Different processes in cells are only

possible, because of different kinds of RNAs. Ribosomal RNA (rRNA), transfer-RNAs (tRNA), messenger RNAs (mRNA) are the most well-known RNAs, but also processes like splicing in eukaryotes might have been originated from an early RNA-world [5]. Also, non-coding RNAs (ncRNAs) play an important role, as we start to realize, how many processes in cells are regulated by them [13-15], like the inactivation of chromosomes [16] and how important all different kinds of RNAs are, therefore.

1.2 Protein biosynthesis in general – Transcription in eukaryotes and prokaryotes

RNAs play an important role in a lot of different processes, especially in protein biosynthesis, where the activity of genes is regulated by riboswitches [17] or the regulation of alternative response mechanisms by non-coding RNAs [18]. Still, most famously is the role of RNAs while translation. Without Ribosomes, tRNAs and mRNAs, live in the complex way as we know it, would not be possible. However, the genetic information is stored in deoxyribonucleotide acid (DNA), because the deoxyribose and its phosphate-sugar backbone make the DNA chemically more stable. This, together with its double-helical structure, improves the stability and reparations can be performed easier and making it the more suitable solution for storing information [19]. A brief overview of protein biosynthesis and the differences between eukaryotes and prokaryotes will help to understand the aim of this work.

In general, protein biosynthesis is necessary to express new proteins in all cell types and is therefore necessary for the metabolism of cells, regardless of single-cell organisms such as bacteria and archaea (prokaryotes) or more complex organisms which are made up of more than one cell (eukaryotes) [20]. Transcription and translation happen at different places, depending on whether the cell is prokaryotic or eukaryotic. In eukaryotes, transcription occurs in the nucleus, the mature mRNA leaves the nucleus, and the mRNA is translated in the cytoplasm (**Fig. 1.1.A**) or in the rough endoplasmic reticulum (rough ER) of the nucleus if a nuclear localization sequence (NLS) for nucleus localized proteins is present [21] (**Fig. 1.3D**). In prokaryotes, where less compartmentalization is present, transcription occurs in the nucleoid [22], while translation also occurs there or also (**Fig. 1.1.B**) – as recent studies have shown - in the cytoplasm, the membrane and the poles [23]. This will be later on discussed further.

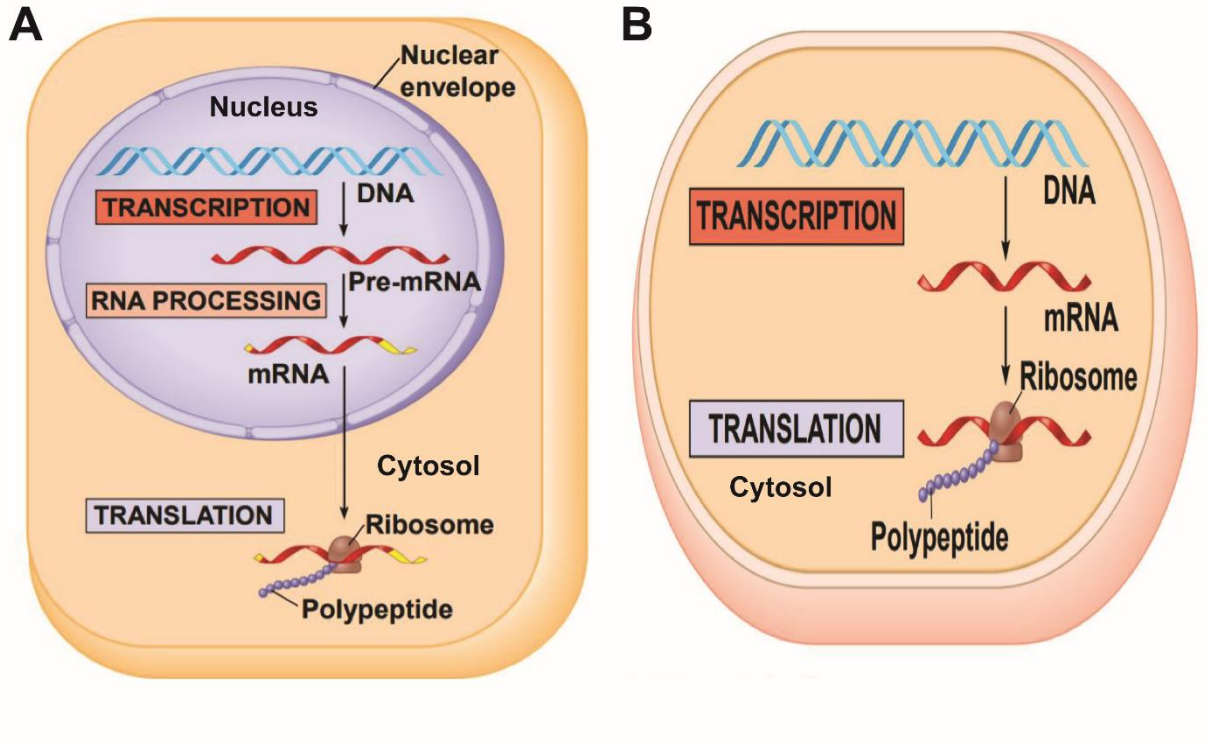

Fig. 1.1 Schematic overview of protein biosynthesis in eukaryotes and prokaryotes.

In eukaryotes (**A**) depicts the separated process of transcription of the DNA (blue) in the nucleus (violet area) and translation of the mRNA (red) into a protein/polypeptide in the cytosol (brown area). The intermediate step of RNA processing of the pre-mRNA (red) is depicted in the nucleus. The post-transcriptional modifications are shown in yellow. (**B**) depicts a spatial non-separated transcription and translation event in prokaryotes in the nucleoid. Figure adapted and modified after Campbell *et al.* [21].

In short, a gen needs to be transcribed from the DNA into what is called messenger RNA, which is then translated into the protein (**Fig. 1.2**). Transcription of other types of RNAs occurs in a similar manner, but they are not called mRNA [21]. During transcription, a RNA-polymerase (RNAP) reads the target DNA segment complementary from 5'-to 3' into the mRNA [24]. Transcription can be categorized into three different phases: Initiation, elongation and termination [24]. They differ between eukaryotes and prokaryotes [21]. Only brief examples are used to illustrate the main differences, because this is not the main topic of this work.

The initiation of transcription in procaryotes involves a so-called sigma factor (σ-factor), which is part of the RNA-polymerase and recognizes the promoter upstream of the target gene, detaches from the RNA-polymerase and allow transcription elongation to follow

[20]. In eukaryotes, on the other hand, different transcription factors are necessary for the binding of the RNA-polymerase to the DNA [25-27].

During elongation, the RNA-polymerase reads the DNA and transcribes it into a complementary strand from 5’ to 3’, exchanging thymidine for uracil while the other three bases (adenine, guanine, and cytosine) remain the same. Importantly, the mRNA is no longer a double-stranded molecule, as DNA is, but single-stranded. The RNA-polymerase contains a proofreading mechanism that operates differently from the DNA-polymerase during replication [28, 29]. In addition, in eukaryotes, several types of specific elongation factors are involved in this step [30].

Two mechanisms for termination in prokaryotes are known. In the Rho-dependent way, a termination protein, Rho, binds to a specific sequence on the mRNA, which then leads to the termination of transcription [31]. In Rho-independent termination, a hairpin is folded after the stop codon sequence and the RNA-polymerase dissociates from the DNA [32]. In eukaryotes, termination for rRNAs follows a similar pattern to the Rho-dependent way, although here other termination proteins are involved and lead to a disassembly of Pol I [33]. Pol II, the RNA-polymerase that transcribes for mRNAs, dissociates from DNA mainly by recognition of the so-called poly-A-tail, thereby stopping transcription. Again, different factors are involved here [34] and thus, both transcription termination ways are factor-dependent. Only for the transcription of non-coding RNAs is a factor-independent mechanism known [34].

After transcription, translation of the mRNA takes place. Before this is possible, several post-transcriptional modifications take place – mainly in eukaryotes but also to some extend in prokaryotes –, which may be responsible for the correct localization of mRNA [35].

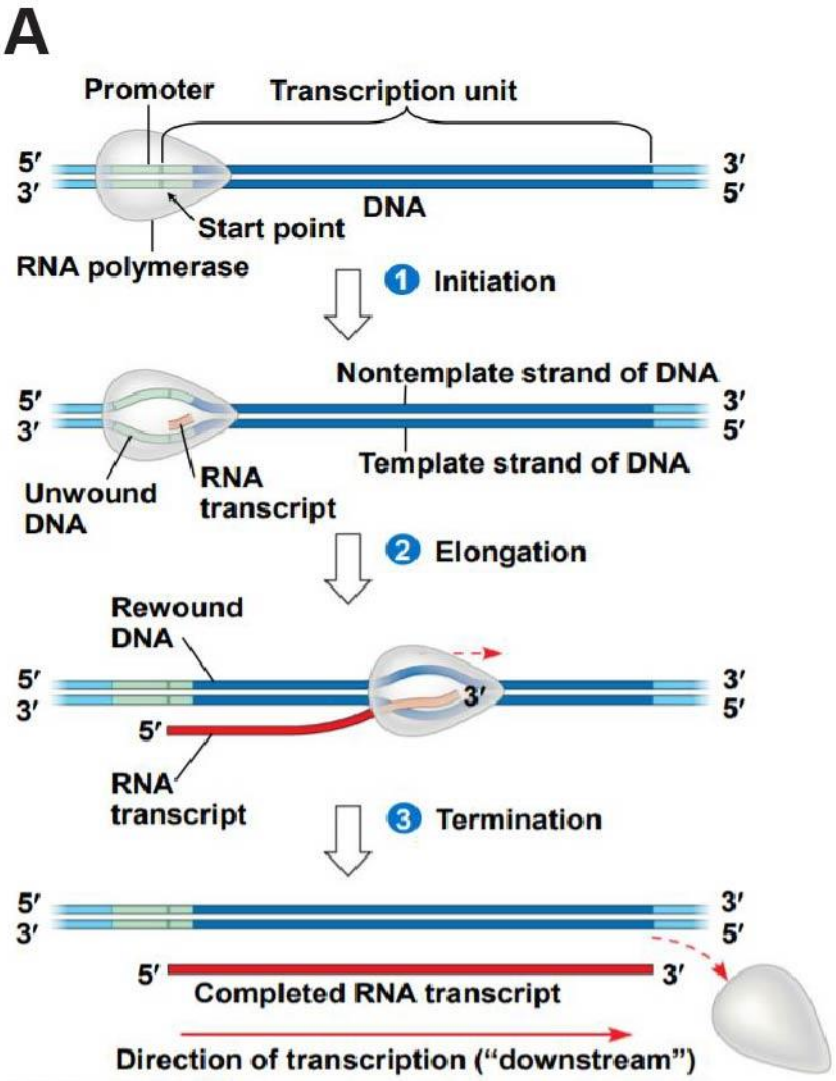

Fig. 1.2 Schematic overview of transcription in eukaryotes and prokaryotes.

The three steps of transcription, 1) initiation, 2) elongation and 3) termination are depicted in (**A**). The process of the binding of the RNA-polymerase (gray) to the DNA at the promotor region, as well as the elongation of the mRNA transcript from 5' to 3' end and the termination of the RNA-polymerase, are illustrated. The doubled-stranded DNA is shown in blue, while the single-stranded mRNA transcript is shown in red. The promotor is illustrated in green. The factors, which differ between eukaryotes and prokaryotes, are not shown. Figure adapted after Campbell *et al.* [21].

1.2.2 Post-transcriptional modifications in eukaryotes

Different mechanisms are known to regulate the mRNA even after the transcription, but also still during transcription. Both will be illustrated shortly here. Before the mRNA leaves the nucleoid in its mature form, it is known as the so-called precursor mRNA (pre-mRNA) [36] (**Fig.**

1.1A). One pre-mRNA consists of coding regions, called exons, and non-coding regions, called introns [37]. Several introns can be found in one pre-mRNA. By cutting them out – called splicing – the mRNA consists only of exons and can be translated into a protein. Along the way, exons can also be cut out, depending on the intron localization. This is also known as alternative-splicing. Thereby, more than one protein can be translated from one mRNA. Splicing is mainly mediated by the spliceosome, which consists of small nuclear ribonucleoproteins (snRNPs) [38], but the rare event of self-splicing by ribozymes is also known, which are introns capable of catalytic reactions and might be a hint to the RNA-world theory [39].

Another post-transcriptional modification is the 5'-capping (**Fig. 1.1.A**). Here, a methylated guanosine is connected to the mRNA at its 5'-end via a 5' to 5' triphosphate linkage [40]. Other ways of capping also exist, but this is the most widespread [41]. The capping has different functions. It regulates the nuclear export [42], promotes translation [43] and the intron excision [44], as well as it protects the mRNA from exonucleases [45].

The last well-known post-transcriptional modification of the pre-mRNA actually occurs already during transcription. The so-called poly-A-tail is a 3'-end modification (**Fig. 1.1.A**). In this process, several adenosine phosphates are localized behind each other [46]. This structure is necessary for the transcription termination and is found mainly in mRNAs [47] and rarely in ncRNAs [48], but also functions as a protector against degradation when the poly(A)-binding protein binds to it [49]. Besides this, it is also important for the transport of the mature mRNA from the nucleus to the cytoplasm [50]. Similar to alternative splicing, there is also alternative polyadenylation [51]. If the poly-A-tail at the 3'-end is shorter, the mRNA is more likely to be translated [52]. This mechanism can be used to react to extracellular stimuli [53].

1.2.3 Post-transcriptional modifications in prokaryotes

Even though post-transcriptional modifications also occur in prokaryotes, the main focus is on eukaryotes. They are often similar to the post-transcriptional modifications in eukaryotes, but are less complex and they do not occur for each mRNA transcript. An example of this would be the existence of introns in prokaryotes. It was thought that prokaryotes do not need them, because of the existence of operons, in which more than one gene is transcribed into the mRNA and therefore, more than one protein can be translated from this polycistronic mRNA and thus, providing more diversity [54]. Self-splicing introns of tRNAs were already known [55],

but not in mRNAs. Although the number is quite low, introns have been found in mRNAs, with their possible function to gain a bigger gene variety, but also to obtain new genes with new functions, which underlines the RNA-world theory further [56].

As in eukaryotes, the 5'-end can be protected from degradation, but with a triphosphorylated 5'-end, rather than a 5'-cap [57]. The folding of secondary structures at the 5'-end leads to a longer half-time and thus, a longer lifetime of mRNAs, too [58, 59], which can also be achieved by the Shine-Dalgarno sequence, also known as the ribosome binding site (RBS) in the 5'-UTR (untranslated regions), which is purine-rich [58, 59]. Even though this is not a real post-transcriptional modification, the RBS, as the name already suggests, plays an important role in ribosomes binding [60].

The final post-transcription modification , again as in eukaryotes, is the poly-A-tail, done by the polyadenylate polymerases [61]. In eukaryotes, it protects the mRNA from degradation, whereas in prokaryotes, the approximately 30 nucleotide (nt) long sequence [62] at the 3'-end leads to a faster degradation, because a special secondary structure cannot fold for protection and can even recruit the RNase [63]. A second type of adenylation exists, in which the polynucleotide phosphorylase extends the 3'-end mainly with adenosines, which also leads to a faster degradation [64]. This type can also be found in mitochondria [65] and plastids in eukaryotes [66].

Despite the existence of similar post-transcriptional modifications in eukaryotes and prokaryotes, they differ mainly in their composition and function. However, after transcription and post-transcriptional modifications, translation of the mRNAs occurs in eukaryotes and prokaryotes, to obtain proteins.

1.3 Translation in general

The following explanation of translation is mainly based on the processes in eukaryotes, even though the actual process of translation is similar between eukaryotes and prokaryotes. In short, here, the mRNA is translated into its corresponding protein. This completes protein biosynthesis. As with transcription, three main processes can be distinguished in translation: Initiation, elongation and termination (**Fig. 1.3**).

In the translation initiation, mRNA, transfer-RNA (tRNA), the small (40S in eukaryotes and 30S in prokaryotes) and large (60S in eukaryotes and 50S in prokaryotes) ribosomal subunits form the translation-initiation-complex [67, 68] (**Fig. 1.4A**). The whole composition of the translation-complex demonstrates the importance of RNAs in all life form. Furthermore,

the ribosome is a ribozyme, which means, it consists of rRNAs and proteins, whereas the main catalytic processes are performed by the ribosomal components. Translation would still be possible without the proteins of the ribozyme, but at a slower rate [20]. The tRNA is the carrier of the different amino acids, which are needed to make a protein. To ensure the correctness of the amino acids, transferred by the tRNA, the tRNA owns an anticodon region. One amino acid is made up of three base pairs of the mRNA, which are called a codon. Thus, the anticodon is complementary to the codon of the mRNA. The first codon always encodes for the amino acid methionine. This ensures the correct reading frame of the codons. The very process of attaching the correct amino acid to the tRNA requires energy, in this case ATP. The transfer of the amino acid in the translation complex again needs energy, this time GTP (**Fig. 1.4A**). In eukaryotes, several proteins are involved in the formation of the translation-initiation-complex. The initiation factors recognize the 5'-cap and the 5'-UTR and mediate the binding to the small ribosomal subunit. Different initiation factors also play a role in the proper ribosome assembly. Unlike in prokaryotes, the order of the binding of mRNA and tRNA is important. The small ribosomal subunit scans the mRNA until it reaches the start codon at the 3'-end. The tRNA is brought to the P-site (peptidyl-tRNA-binding site), the initiation factors dissolve, and the large ribosomal subunit can bind to it [20]. Only a few mRNAs can be translated without a 5'-cap, which occurs mainly under special stress conditions and apoptosis [69]. Minor differences from eukaryotes can be observed in the assembly of the translation-initiation-complex in prokaryotes. Here, the correct binding of the ribosome to the mRNA is mediated by the RBS at the 5'-UTR – which is recognized by the 16S rRNA, part of the 30S subunit - and the ribosome scans to the start codon at the 3'-end. In addition, the first tRNA carries a N-formyl-methionyl and various initiation factors are used [70].

During elongation, the polypeptide chain is stretched to form the finished protein. In the fully assembled ribosome, there are three different sites – all part of the small subunit. First, the $tRNA^{Met}$ binds to the P-site, even though this is the middle one. The next charged tRNA binds to the A-site (aminoacyl-tRNA-binding site), which is at 5'-end upstream of the P-site and via cleavage and catalyzed fusion, the amino acid of the tRNA at the P-site is transferred to the tRNA with the new amino acid. The no longer charged tRNA of the P-site moves to the E-site (exit site), leaving the ribosome and the tRNA with the extended polypeptide chain moves to the P-site, leaving the A-site free again (**Fig. 1.4B,C**). That the tRNAs can move between the three different sites is possible because the mRNA actually

moves on in the ribosome by one codon. Therefore, the translation occurs from 5'-to 3'. Those steps repeat until the stop codon is reached. One difference between eukaryotes and prokaryotes is mainly the use of different elongation proteins [21, 70].

The stop codon initiates the termination of translation. No amino acid exists for the three different triplets, the stop codon is built up. A release factor in eukaryotes binds to the available free A-site and catalyzes the hydrolyses of the peptide chain and the tRNA at the P-site. In prokaryotes, two different release factors exist, which is the main difference here compared to eukaryotes [71]. When the polypeptide chain leaves the ribosome, it is folded and modified into a functional protein [21]. Meanwhile, the ribosome disassembles. Again, several proteins are involved and GTP is again used as energy. The different parts of the disassembled ribosome are recycled and used for the next translation [70].

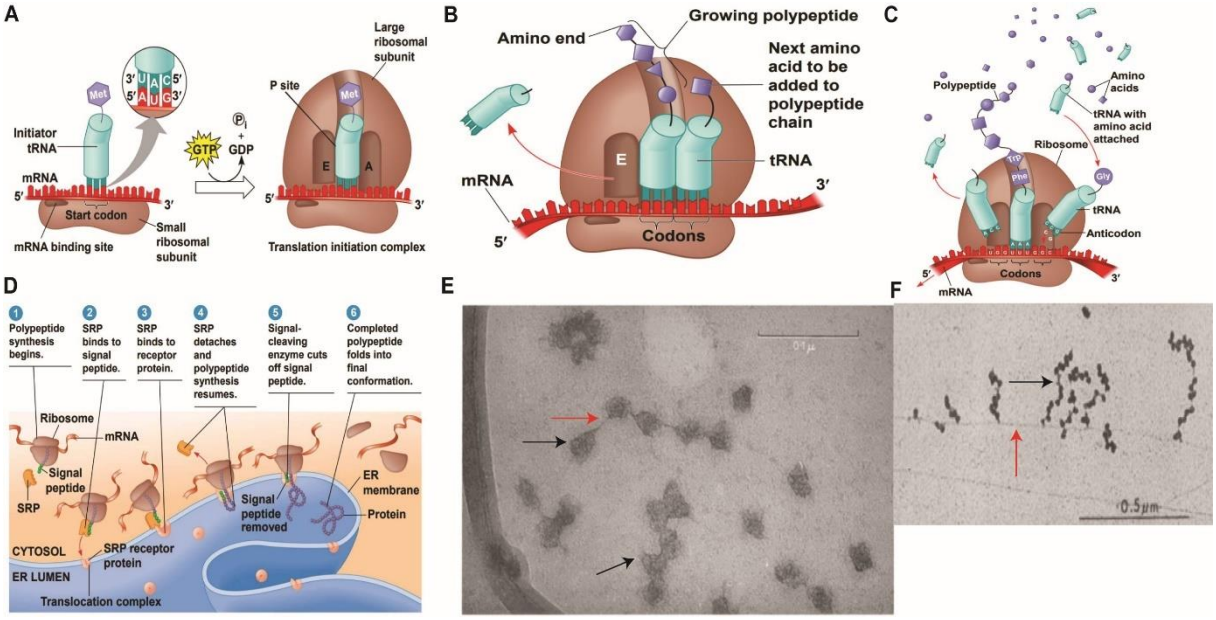

Fig. 1.3 Schematic overview of translation and electron microscopy of polyribosomes.

(**A**) illustrates the assembly of the ribosome out of the small and large ribosomal subunits (brown). The mRNA (red) is bound to the small ribosomal subunit. In green is the tRNA depicted, while the blue hexagons represent amino acids bound to the tRNA and/or the polypeptide chain and the needed energy in the form of GTP and GDP. (**B**) depicts the process of growth of the polypeptide chain, while (**C**) shows an overall overview of the translation event. "E" stays for exit site, "P" for peptidyl-tRNA-binding site and "A" for aminoacyl-tRNA-binding site. In (**D**) the translation of proteins from the nucleus is illustrated, whereas the mRNAs consist of a NLS. The nucleus with the rough ER is shown in blue, while the components

of the translation complex and the process itself are similar to (**A**)-(**C**). (**E**) shows an electron microscope picture of polyribosomes, indicated by a black arrow, which are separated and possibly bound to a strand of mRNA, indicated by a red arrow. The tested polyribosomes were gained from a mouse cell line of reticulocytes, stained by uracil acetate. The scalebar is 0.1 µm. (**F**) also shows an electron microscope picture of polyribosomes, indicated by a black arrow, which are bound to a strand of mRNA. DNA is also visible, indicated by a red arrow. The tested polyribosomes were gained from *E. coli* cells. Figure adapted and modified after Campbell *et al.* [21], Slayter *et al.* [72] and Miller *et al*. [73].

1.4 The "new way" of transcription and translation in bacteria

In eukaryotes, transcription and translation are spatially and temporally separated, due to the complex compartmentation. While transcription occurs in the nucleus, translation happens in the cytoplasm (ribosomes are not bound to a membrane) (**Fig. 1.1A**) or in the rough ER and the outer membrane of the nucleus, where ribosomes are bound to the membrane of the rough ER, if the proteins consist of a NLS [20, 35] (**Fig. 1.3D**). Prokaryotes, on the other hand, do not have this high compartmentation and therefore, it was assumed, there is no need to separate transcription and translation. In the early '60s, the finding of polyribosomes on mRNA while transcription of this mRNA was still occurring further strengthened this theory [73, 74] (**Fig. 1.3F**). The term "polyribosomes" describes a group of multiple ribosomes that are simultaneously bound to one mRNA. All of those ribosomes translate the mRNA at the same time, therefore saving time in protein production. This does not automatically mean that the mRNA to be translated is also transcribed at the same time. Later on, polyribosomes where also found in eukaryotic cells, such as in different cell lines of mice and rats [75, 76] and in sarcoma cells [77]. Due to the strict separation of transcription and translation in eukaryotes, polyribosomes are only found on mature mRNAs, where transcription is already complete (**Fig. 1.3.E**).

In regards of the development and advantage of different methods and microscopes, this old theory of a combined process of transcription and translation needs to be renewed. But why? Several groups have found some interesting information leading to the rethinking of this old theory. This include the new findings on the location of ribosomes [78, 79] and mRNAs localization [80, 81], as well as the realization that prokaryotes are also organized without being particularly compartmentalized [82] like eukaryotes. However, the following findings focus on bacteria and not archaea, where further studies are needed to be sure,

whether or not this is also the case for archaea or not. First, I will provide more information on the organization in prokaryotes and then continue with the new information on the ribosome and mRNA localization, as well as introduce new models for the transcription and translation in bacteria.

As mentioned earlier, although bacterial cells do not have a fixed structure for compartmentalization like eukaryotes, they are also highly organized in a more dynamic way. All different types of proteins show a subcellular localization in bacteria. Cytoskeletal elements such as the actin-like MreB [83, 84] and ParM [85] or the tubulin-like FtsZ [86], while not forming a structure as in eukaryotes, are essential for the organization of other proteins in the bacterial cell. Proteins of the divisome must localize to the correct area in the cell for a proper cell division, which in most bacteria the septal region [87], but can also be asymmetrical, as in *Bacillus subtilis* in sporulation [88, 89]. Here, for example, FtsZ, which forms the Z-ring during cell division, is essential. The chances are high that proteins diffusive through the cell, till they found a fitting interaction partner and therefore localize at the correct spot, still, this can be considered as a simple way of organization in bacterial cells. Also, the rod shape of different bacteria species leads to a localization of hydrophobic proteins at the membrane of the poles or in the cytoplasm, close to the poles [90, 91]. In rod-shaped bacteria, like *Escherichia coli*, chemotaxis components are localized at the poles [92], as well as various components of the degradosome [93], and the pole-to-pole oscillation of the Min-system, which is responsible for the correct localization of the formation of the Z-ring of the divisome [94]. Hereby, this demonstrates, how the localization of one protein affects the localization of other proteins and the functionality of different processes in a bacterial cell. The localization of the chromosome also plays an important role. For sporulation in *B. subtilis,* the localization of the origin of replication is crucial [95]. Something similar was observed for *Caulobacter crescentus* [96]. Furthermore, the nucleoid of bacteria also appears to be dynamic. In *C. crescentus* and *E. coli,* an ellipsoidal distribution has been shown [97], with the poles free of it [98] or with only specific chromosomal regions near the poles, as in *C. crescentus* [97]. Also, depending on whether the cells grow slowly or fast, the nucleoid is denser in slow-growing *E. coli* than in fast-growing ones [99]. All those examples demonstrate that bacterial cells have an organization and structure for the ongoing processes. Of course, this organization also applies to all proteins and RNAs involved in transcription and translation.

It is not of a big surprise that transcription occurs in the nucleoid. The RNA-

polymerases mainly overlap with the nucleoid [79]. This makes sense because the RNAP can only transcribe DNA into mRNA when it is bound to the chromosomal DNA. As already indicated by the presence of polyribosomes on mRNAs that have not yet been fully transcribed, translation appears to occur simultaneously while the mRNA is still being transcribed [22, 73]. Also, an interaction of the RNAP with ribosomal subunits, as well as with the ribosome, found in *E. coli*, underlines this further [100]. However, this does not appear to be true for all mRNAs in every bacterial species. Interestingly, in the same study where the group of J. C. Weisshaar observed an overlap of RNAPs with the nucleoid, they did not found many ribosomes in the nucleoid in *E. coli* [79]. Only 4% or less of the 70S ribosome overlapped with the RNAPs [101]. This seems to be contradicted to the findings of an interaction between RNAP and the ribosome. Still, another study performed in *E. coli,* showed that the nucleoid was mainly composed of the small 30S and large 50S subunits of the ribosome, whereas the slower 70S ribosome was mostly excluded and found in the cytoplasm around the nucleoid lobe [102]. This would still fit with the findings that the RNAP interacts with the ribosomal subunits [100]. The large number of monomeric subunits of the ribosome in the nucleoid would also explain the observed nucleoid expansion in the exponential growth phase [78]. Most of the work was performed in *E. coli*, but something similar was observed in *B. subtilis*, too [23]. Those findings led to a renewal of the old theory that transcription and translation occur at the same time and without any spatial separation in each bacterial species [22].

If transcription and translation appear to be separated in space and time, where does translation take place? One explanatory model, suggested by the Amster-Choder group, is that mRNAs are translated near their site, where the associated protein is later found (**Fig. 1.4B-D**). In *E.* coli, they found the mRNAs for cytoplasmatic proteins, *cat* and *lacI*, in the cytoplasm, whereas the mRNA for the membrane protein BglG was found at the membrane [81]. Other groups found similar localization behavior in different bacteria, like polar localization of *flaA* in *Campylobacter jejuni* [103] and *nifH* in *Klebsiella oxytoca* [104]. Again in *E. coli*, different mRNAs for soluble proteins or the extracellular were found in the cytoplasm and mRNAs for membrane proteins were found at the membrane [105]. Nevertheless, these findings should not be regarded as true to all bacteria, especially since some results underline the old model of a coupling of transcription and translation in bacteria. [73, 100]. Another model is still close to the old theory. The suggestion of Jacobs-Wagner's group is that the transcript stays near to its transcription site. The mRNA does not move far away from the nucleoid, so to speak,

because the chromosome serves as a template for the localization of the mRNA (**Fig. 1.4E**). Their findings in *C. crescentus* lead to this model [80]. In the same study, they also observed a co-localization of ribosomes with the nucleoid, which is different to the previously described findings in *B. subtilis* and partially in *E. coli*. However, in the work of the Jacobs-Wagner group, they also found the mRNA *lacZ* of *E. coli* close to its transcription site. This is contradicted by the finding of *lacZ* in the cytoplasm by another group, also performed in *E. coli* [106]. The differences here were the techniques to label the mRNAs.

It is obvious that both models lack conviction and may describe only a part of the truth. Polyribosomes can be found where DNA is still being transcribed and the resulting mRNA is simultaneously already being translated. In addition, as described earlier, RNAP and the ribosomes interact with each other to some degree. Therefore, in a few bacteria, transcription and translation are coupled to a certain degree [73, 100]. At the same time, however, there is evidence that a mRNA is translated by multiple ribosomes, i.e. a polyribosome, but this is not spatially and/or temporally linked to transcription, as shown by findings in *E. coli* and *B. subtilis*. Thus, a combination of the old and new models also seems to be possible and might be closer to the truth.

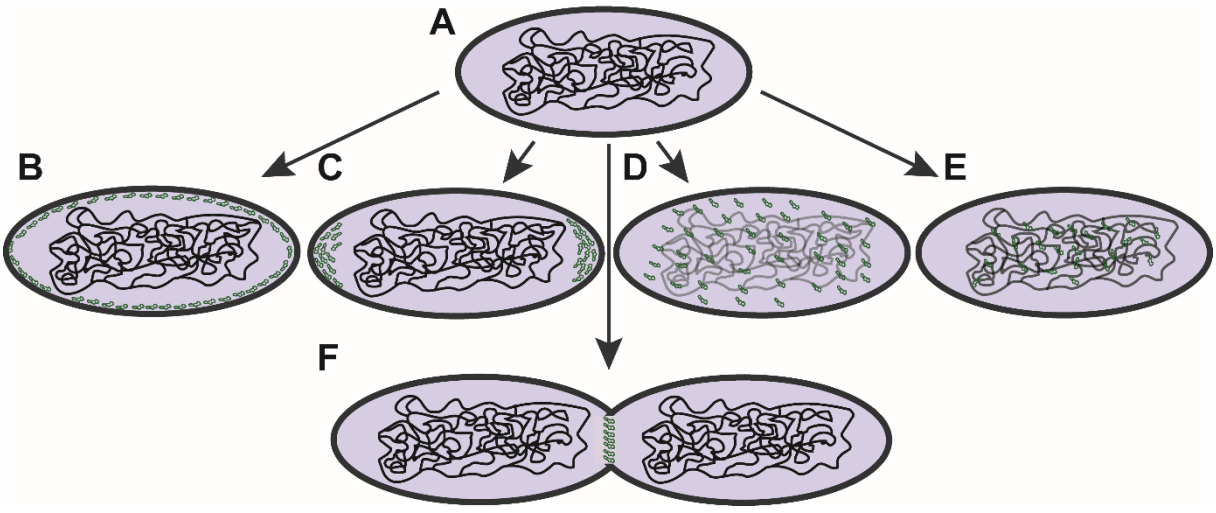

Fig. 1.4 Different schematic models for mRNA localization during translation in prokaryotes. (**A**) depicts a schematic bacterial cell with the bulk DNA in black, with higher density in the middle. Membrane localization of the mRNA (**B**). (**C**) shows polar localization. (**D**) illustrates a helical localization throughout the cytoplasm, while (**E**) shows mRNA localization near the transcription site in the DNA bulk. mRNA localization at the septal area while cell division (**F**).

The mRNA is depicted in green, DNA in black, cytosol in grey-blue and the cell membrane is depicted by a dark grey-blue.

1.4.1 The chosen mRNAs in *Bacillus subtilis*

To gain further insight into the behavior and localization of mRNAs, several mRNAs from *B. subtilis* were selected for this purpose. Single-molecule tracking (SMT) was used to analyse the localization of polycistronic and monocistronic mRNAs, as well as their dynamics. Most studies focused on only a few mRNAs, mainly encoding for membrane proteins [80, 81, 107], some of which were tested by various groups and led to different and contradicting results, as demonstrated by the above-mentioned example of *lacI* [80, 106]. In this work, I will analyse 9 different mRNAs, whereas two are monocistronic and the other seven being polycistronic mRNAs. Of those 9 mRNAs, one mRNA encodes an extracellular protein, three encode soluble proteins, two encode membrane proteins and three encode soluble and membrane proteins in one operon. Besides this, two different types of constructs were made. Four constructs have two MS2-binding sites (MS2BS) (**Fig. 1.5A+D**), while eight constructs have only one MS2-binding site (**Fig. 1.5B+E**). The MS2-binding site is presented in more detail in **1.5.1**. In addition, the four constructs with two MS2-binding sites have a translation terminator shortly behind them, while the other constructs have this after around 1700 bp and are therefore also referred to as artificial mRNAs.

From here on, the different mRNAs will be introduced. I will start with the mRNAs with two MS2BS, followed by the constructs with one MS2BS. Those mRNAs with two MS2-binding sites are four polycistronic mRNAs (*mreB-minD*, *spoIIIE-ymfC*, *ypbR-ypzF* and *rnc-ftsY*). With the exception of *ypbR-ypzF*, these mRNAs encode mainly for membrane proteins or proteins localized at the poles and the septum. FtsY is a signal-recognition particle (SRP) protein and is essential for the correct translation and insertion of membrane proteins and their integration into the membrane [108, 109]. It is mainly located at the membrane, as well as partially in the periphery [109] and the cytoplasm[108]. *rnc* encodes for the essential endoribonuclease RNase III [110] that is a substrate specific RNase IIIE, which is important for foreign toxin gene silencing and localizes in the cytoplasm [111, 112]. SMC, on the other hand, localizes partially at the poles and mainly in the nucleoid, where it plays an important role in chromosome condensation and segregation [113-115]. Here, it is part of the condensing complex and is necessary for origin segregation [116]. MreB, MreC and MreD are all cell shape-determining proteins and belong to the Rod complex. They are essential for the lateral cell wall synthesis

[117]. Therefore, their localization is at the membrane [118]. It has been reported that MreB can be also found in the cytoplasm, but only in stationary growth phase [119]. Since no cells of the stationary growth phase were used, this does not play any role. The other two proteins encoded by this operon are MinC and MinD and part of the Min-system [120]. They function as cell division inhibitors [121] and are localized at the poles and septum. The last operon, which encodes for membrane proteins, is *spoIIIE-ymfC*. YmfC is a transcription factor of the HutC subfamily and belongs to the GntR family [122] and therefore should be localized in the nucleoid and the cytoplasm. SpoIIIE on the other hand, the other protein encoded by this operon, is an ATP-dependent dsDNA translocase, which plays an important role in the transport of the forespore chromosome before sporulation occurs [123]. The last mRNA with two MS2-binding sites is the *ypbR-ypzF* operon. According to SubtiWiki, there is currently no information known about the encoding product of *ypbS* and *ypzF*, nor their functions. *ypbR* on the other side encodes for YpbR, mainly known as DynA. This protein from the bacterial dynamin-like family [124] is also tested and further analysed in this work. DynA aids in membrane fusion of the invaginating dividing septum [125] and is also involved in membrane fusion after lesion [124], but more about this in **1.7.2**. DynA is a membrane-associated protein which is also localized to the septum and diffuses freely in the cytoplasm.

The mRNAs with one MS2BS are artificial constructs because the late presence of the translation terminator (**Fig. 1.5B+E**). In addition to *rnc-ftsY*, *mreB-minD* and *ypbR-ypzF*, which are also constructed with one MS2-binding site, five more mRNA constructs were made. Those are *comN-secDF*, *rplJ-rplL*, *rplK-rplA* and *ylxM-rplS* for polycistronic mRNAs and *hag* for a monocistronic mRNA. The operons of *rplJ-rplL* and *rplK-rplA* encode only for ribosomal proteins of the different ribosomal subunits - where *rplA* encodes for L1 [126] -, localized mainly in the cytoplasm, around the nucleoid and the poles [127]. *comN-secDF* encodes for ComN, which mediates the post-transcriptional control of the *comE* operon and is mainly localized at the cell poles and the division site [128, 129]. SecDF, the other protein encoded this operon, is a pre-protein translocase subunit (ATPase) and is part of the Sec-pathway and thus localized at the membrane [130, 131]. This is followed by YlxM and Ffh, both proteins of the signal recognition particle and are encoded by the *ylxM-rplS* operon. Those two proteins are mainly localized to the membrane and the periphery, like FtsY [132-134]. RpsP [67] and RplS [126] are ribosomal proteins of the small and large subunit and thus localized at the poles, in the cytoplasm and around the nucleoid. The 16S rRNA processing RNase encoded from the

rimM mRNA of the *ylxM-rplS* operon plays a role in the maturation of the 16S rRNA and is found in the cytoplasm [135]. *trmD*, also a mRNA of the *ylxM-rplS* operon, encodes a tRNA methyltransferase that plays an essential role in translation and is located in the cytoplasm [136]. According to SubtiWiki, there is currently no information known about the encoded product of the other two mRNAs of the *ylxM-rplS* operon, *ylqC* and *ylqD* nor their functions. The last mRNA to be analysed was *hag*. This mRNA is an exception. So far, all mRNAs encode for membrane or soluble proteins in the cell, but *hag* translates for flagellin proteins, whose subunits build the flagellum of *B. subtilis*. The flagellin proteins, therefore, are located outside of the cell, in the extracellular [137].

The chosen mRNAs show a big diversity for the encoded proteins. Membrane proteins, soluble proteins and even an extracellular protein are encoded by the monocistronic mRNAs and the operons. Moreover, some of those proteins, encoded by the chosen mRNAs, are essential for *B. subtilis*, such as MreB and Ffh, whereas others are not. With this larger selection of mRNAs, a nice overview of the behavior and localization of different mRNAs can be provided.

1.5 Different methods for RNA labeling

To find out more about the behavior of the selected mRNAs, a suitable labeling method is necessary. As the contradicted results of *lacI* in *E. coli* demonstrate [80, 106], the labeling technique plays an important role and can potent also influence the behavior of the tested mRNA. A pool of different methods is available, some which have a good potential and need further development, while others are widely used to this day. An overview of different labeling techniques of mRNAs, in prokaryotes and eukaryotes, will be provided.

Some methods for RNA labeling are used in both, prokaryotes and eukaryotes, but one new RNA labeling method is only used in eukaryotes, the CRISPR/Cas9 system of *Streptococcus pyogenes*, which has been successfully used for genome engineering in eukaryotes [138]. Since CRISPR (clustered regularly-interspaced short palindromic repeats) belongs to the basic and adaptive immune systems of prokaryotes, this method cannot be used for them. Because the CRISPR/Cas9 system recognizes RNA and not DNA double-strands [139], a so-called protospacer adjacent motif (PAM) is required as part of the oligonucleotide [140] and hybridizes with the target RNA. The CRISPR-associated nuclease Cas9 [139] – fused together with a fluorophore - then recognizes this and the RNA is visualized. Even though the influence on the cells from the system itself is not strong and may be less than of other systems, this

labeling method cannot be used in prokaryotes and therefore, other methods are needed.

The following methods are used in eukaryotes and prokaryotes. In fixed cells, FiSH (fluorescence *in situ* hybridization) is a common tool for labeling RNAs and was an early on established method. Here, the sample is directly labeled with a fluorophore, but this method might have problems with the sensitivity and a possible autofluorescence of the sample and a dye is necessary, potentially leading to background noise [141]. A more advanced version of FiSH is smFiSH, in which a 20-50 base long fluorophore-labeled probe, complementary to the target RNA, binds to the RNA and therefore visualizes the RNA. The use of more of the 20 base long labels demonstrated a better signal-to-noise ratio, including the background of autofluorescence [142]. There are more FiSH-modified RNA labeling methods, but because they are all used in fixed cells, this cannot be used for the purpose of this work to analyse mRNAs in living cells. However, the use of RNA molecular beacons is in general interesting. Here, a beacon consists of a short loop-structure. The 5'-end is fused to a fluorophore, while the 3'-end is fused to a quencher that absorbs the emitted energy of the fluorophore, as long as they are in close proximity, which is the case when the beacon is in its loop state. By binding complementary to the target RNA, the loop structure is no longer existent and the emission from the fluorophore is no longer absorbed [143, 144]. Another approach would be fluorescent *in situ* RNA sequencing. Also in fixed cells, by using a reverse transcriptase, the RNA is converted into circular DNA (cDNA) and then crosslinked to a cDNA library, all performed *in situ*. After this, the cDNA can be sequenced using a complex way of SOLiD (solid-ligation) sequencing [145]. Using wide-field epifluorescence microscopy or a confocal, the result can be detected, hence, this can be very time-intensive. At the same time, different types of tissue, eukaryotic and prokaryotic cells can be analysed with this method [146]. Continuing with labeling systems for live cell imaging, a more recent method is the use of aptamers, which consists of a short RNA sequence [147]. With this, it binds to synthetic dyes that mimic various fluorophores. After binding, a conformation change occurs and the dye emits a fluorescent signal. In the beginning, the signal-to-noise ratio was not good enough [148] but has improved [149]. Also, some dyes are cytotoxic to cells, such as malachite [147]. In recent years, this method has been used more often, but it still needs some improvement. Aptamers can also be used in fixed cells.

Over the years, several components of phages - originated from bacteriophages - are mainly used to label RNAs in living cells. The use of a recognition or

binding sequence, attached to the target mRNA, is recognized by a special protein of the phage and binds to it. Because this protein is fused to a fluorophore, the fluorophore binds indirectly to the target mRNA, therefore making the mRNA visible. One of those systems is the Lambda N22 (λN22) system, which uses the N protein of the λ phage. This protein is 22 amino acids small and binds a short RNA structure, called boxB. The boxB itself is 15 nucleotides short and forms a loop-structure. 4-16 repeats of the boxB is a common number to tag the target RNA, while the N protein is fused to a fluorophore [150]. This system is mainly used in eukaryotes [151] especially in mammalians [150]. The other indirect labelling method using phage components, is the MS2-system and is discussed in more detail in **1.5.1**. In general, a disadvantage of those phage-based indirect labelling methods is the high number of repeats of the aptameric binding sites, as well as a possible unspecific binding of the RNA tag to a RNA-binding protein or instability while replication and transcription, due to too many repeats of the RNA tag.

1.5.1 The MS2-system

When considering the available methods for live-cell imaging, the use of the λN22 was dismissed early on, because its more or less exclusive use in eukaryotes does not provide sufficient evidence that this system is also suitable for bacterial cells. In contrast, the other phage-based indirect labelling system - the MS2-system -, has been used for many years and has been used successfully in both, eukaryotes and prokaryotes. Here, a 19 nt short binding sequence is tagged to the target mRNA. In most reports, 6-12 repeats of the MS2-binding site (MS2BS) are used [81, 107, 152], in the beginning as many as 96 repeats [153]. The dimeric coat protein of the bacteriophage MS2 – 13.7 kDa small - recognizes the RNA loop structure of the binding site and binds to it [154, 155] (**Fig. 1.5D+E**). A fluorophore, similar to the λN22-system, is fused to the coat protein. Although the MS2-system is a well-established RNA-labeling method, further improvement is needed. To ensure the correctness of replication and transcription, a fusion of the MS2BS to the 3'-end of the target mRNA is useful [81]. Due to the natural occurrence of the MS2 coat protein as a dimer, the use of at least six repeats of the MS2BS, twice the amount of the coat protein – which will be further on referred to as MS2 tag -, will bind to it. An influence of this massive complex on the mRNA cannot be excluded. Therefore, this number must be reduced, but signal still needs to be detectable. By using only one or two MS2-binding sites, the influence of the MS2-system itself should be drastically reduced (**Fig. 1.5**). Also, the likelihood of an unspecific binding to RNA-binding proteins is also

reduced. To ensure the detection of the signal, a good fluorophore, as well as a sensitive microscopy technique, like single-molecule tracking, are necessary. By cloning the MS2 tag behind a xylose promoter, its expression can be controlled. With this setup, detection of mRNAs in *B. subtilis* was possible.

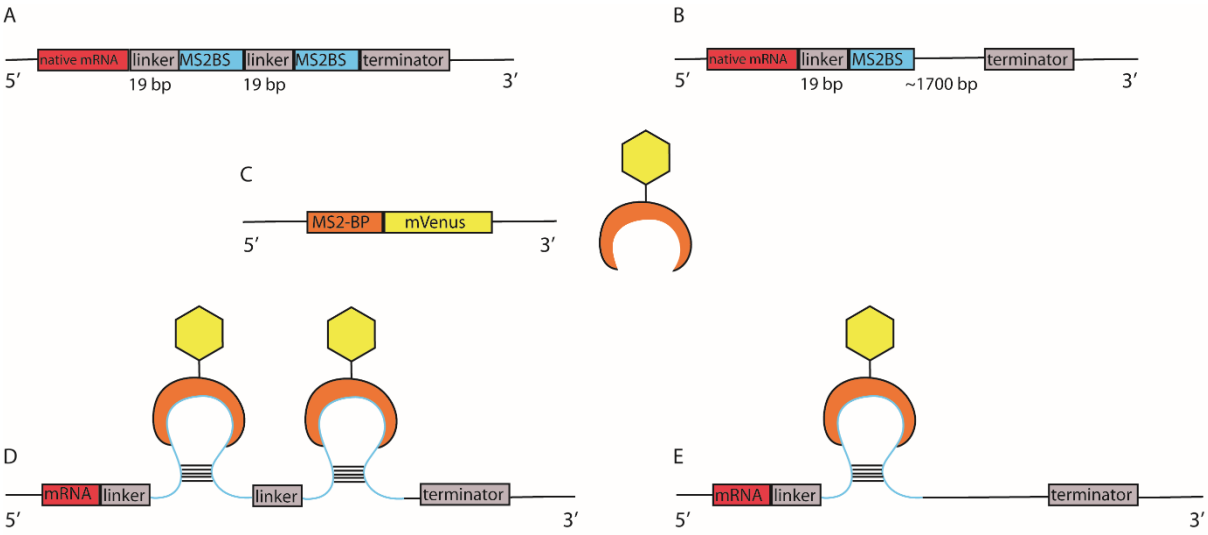

Fig. 1.5 Illustration of the labeling of the target mRNA with the MS2-system.

At the 3’ end of the target mRNA (red) one (**B**) or two (**A**) MS2-binding sequences (blue) are fused to it via a short linker region (gray). A transcription terminator (gray) follows directly after this (**A**) or roughly 1700 bp later (**B**). (**C**) depicts the dimeric MS2-binding protein (orange) fused to the fluorescence protein mVenus (yellow) at the 3’ end. (**D**) and (**E**) show how the MS2BP-mVenus construct binds to the stem loops of the MS2BS (blue), whereas (**D**) consists of two MS2BS, while (**E**) consists of one MS2BS.

1.6 Fluorescence microscopy – different methods for single-molecule tracking

The microscopy methods used in this work are based on wide-field fluorescence microscopy, similar to epifluorescence microscopy, where the sample is illuminated in a wide-field manner [156]. Besides the composition of a bright-field microscope, an additional illumination with UV-light is added, as well as specific excitation filters to ensure the use of the correct wavelength for excitation of the fluorophore, used in the sample. An additional filter, the beam splitter, is necessary. It leads the longer wavelength signal, emitted by the sample, to the ocular while blocking the excitation wavelength. A camera is often used in this way to detect and capture the signal and record it as an image or movie. For a more detailed description, see **5.5.1.1**.

Another method for microscopy, is single-molecule tracking (SMT) or single-particle tracking (SPT). Different SMT methods exist, but important for SMT, which is the basic principle behind it, is the observation of single molecules or particles in a medium. This is accomplished by taking a fast series of images – usually assembled as a video - and analysing the coordinates of the signal in two and/or three dimensions, which is called trajectories. Tracks – i.e., the signal of one molecule - are detected based on the coordinates of trajectories of two or more consecutive frames that are in the nearest position to each other [157, 158]. With this principle, the dynamic of molecules can be analysed, as well as the diffusion coefficients can be measured, using a suitable statistic tool, in this work, the software SMTracker version 1.5 and 2.0 [159, 160]. In general, the detection of a signal takes place by using the point spread function (PSF) and by fitting the gaussian function to the PSF, the center of the signal can be identified. How precise this is, depends on the number of fluorescent molecules, used to label the sample [161]. A good signal-to-noise ratio is also important for this. This can be achieved by using only a small detection volume of less than one femtoliter [162].

Different microscopes and setups are used. A distinction can be made between feedback SMT and non-feedback SMT. Feedback SMT means that the laser has to follow the diffusing molecules or the diffusive molecules have to be relocated to the center of the laser focus by moving the whole stage [163]. By using single-photon-counting detectors and time-correlated single-photon counting (TCSPC) – a fluorophore is excited and the deactivation probability of it is measured by assuming that the excitation is proportional to the fluorescence intensity when it got excited [164] -, SMT of diffusive molecules in three dimensions might be easier compared to non-feedback SMT.

For non-feedback SMT, early attempts were made by using total-internal-reflection microscopy (TIRM). Wide-field illumination is used, so that a larger area of the sample can be observed. Hence, the depth cannot be analysed and is therefore a good tool for *in vitro* experiments [165]. Another microscope of the non-feedback SMT is SPT photoactivated localization microscopy (PALM) [166, 167]. Here, photoactivatable fluorescent proteins (PA-FP) are fused to the target molecule. First, a short wavelength, often from the blue light spectrum, is used for a few frames to activate the PA-FP. A longer wavelength is used next, to excite the activated PA-FP, which then emits a fluorescent signal until it bleaches out. Once activated, a PA-FP cannot be reused. Those activation and exciting steps can be repeated to

gain more information in one cell [166]. The frequent use of blue light can be damaging to cells and lead to an arrest of growth or even death [168]. Therefore, another technique of SMT can or should be used as well.

In our group, we use an inverted microscope with a similar setup to the one of epifluorescence microscopy. Instead of using wide-field illumination, a slim laser is used for a strong excitation of the fluorophores, with the intensity of the excitation being a factor of around 100 higher than compared with epifluorescence [169]. To achieve this, the slim excitation laser is directed at a specific spot on the sample. It underfills the back aperture of the objective lens, which then leads to a concentrated, parallel illumination of the selected spot. Much faster bleaching on this particular area can be achieved with this and therefore the single-molecule level – where only a few molecules still show fluorescence - is reached within a few frames. Newly synthesized, functional fluorophores are also visible and can be used for SMT when the sample is excited again. Furthermore, the damage of the cells is minimized [123].

The approach of SMT leads to a better understanding of processes in living cells, like protein-folding [170], virus infections [171], gene regulation [172], translation [173] and of course the behavior of mRNA [75]. SMT is used here to enlarge the knowledge of mRNA, its localization behavior and dynamics, as well as those of the protein DynA.

1.7 The Dynamin superfamily

A great variety of proteins belong to the dynamin superfamily. The first real description of dynamin protein and its importance to organisms was found in mutants of *Drosophila melanogaster* [174]. Members of the dynamin superfamily are found in eukaryotes and prokaryotes [84, 175]. All members of this family are large GTPases. They are characterized by a large GTPase domain of around 300 amino acids, a low binding affinity to GTP, and their oligomerization-dependent GTPase (guanosine triphosphatase) activity, which differs from other GTPases [176] like Ras-like GTPases [177]. Besides this, they possess a middle domain and a GTPase effector domain (GED). Due to new findings of the structure, the nomenclature changed and they were renamed as G-domain, stalk, neck and lipid-binding domain [178]. Since older paper used the old nomenclature, it is also used here for better understanding. The GTPase domain further consists of a GTP-binding motif necessary for the guanine-nucleoid binding and hydrolysis [179]. An oligomerization to dimers or tetramers occurs through the interaction of the GTPase domain with the middle domain and GED, which can also interact

with itself [180, 181]. In eukaryotes, proline-rich domains (PRD), SRC-homology-3 domain and pleckstrin-homology (PH) domains often exist for specific targeting of organelles, such as mitochondria and chloroplasts [182, 183]. Also, most of the dynamins in this superfamily can interact with lipid membranes via the PH domain [184]. Dynamin proteins in eukaryotes are also often referred to as the "classical dynamins." They are involved, for example, in the scission of clathrin-coated vesicles from the parent membrane [183], in phagocytosis [185], cytokinesis [186], budding [179] and during the rearrangements of actin [182]. A variety of processes are regulated by dynamins, but all are somehow involved in membrane fission or fusion [187]. It is plausible to assume that hemifusion occurs as an intermediate state to ensure membrane integrity. This would also explain why different types of dynamins are able to do membrane fusion and fission [188, 189].

Besides the classical dynamins, dynamin-like proteins exist, too. Those proteins are similar to the classical dynamins, but lack the proline-rich domain and are involved in mitochondrial division [190]. Other members of the subfamily belong to the dynamin superfamily, like Mx-like proteins [191], mitofusin/Fzo1 proteins [192], and OPA1/Mgm1 proteins [193], to name a few. They lack domains such as the proline-rich domain or the pleckstrin-homology domain, but have additional domains, sequences or regions, like a transmembrane domain [194]. With those additional domains and sequences, binding to the membrane can still occur [193] They are found in numerous eukaryotes, like in plants, yeast, several mammalians, etc. [192, 195, 196]. It has not been shown for all of them, but at least a few proteins of the subfamily also oligomerizes [197].

1.7.1 Bacterial dynamin-like proteins

In addition to classical dynamins, dynamin-like proteins and all different kinds of proteins of the subfamily of the dynamin superfamily, all of which are found in eukaryotes, homologues in prokaryotes can be found, too. They are called bacterial dynamin-like proteins (BDLP) and were first reported in 2006 [198]. Five years later, it was reported that BDLPs also have the ability to catalyze membrane fusion [199]. BDLPs can be found in Gram-negative and positive bacteria, as well as in archaea, where they have been found in *Methanomicrobia* [178]. Often, two different BDLPs exist in bacteria and can be found in operons, too [199] (**Fig. 1.6A**). To belong to the dynamin superfamily, the bacterial dynamin-like proteins also need the special structure of the G-domain (old nomenclature: GTPase domain), the stalk domain (old nomenclature: middle domain and GED), the neck domain (old nomenclature: part of the

GTPase, middle domain and GED) and a lipid-binding domain. Still, differences among BDLPs - with the G-domain being highly conserved - as well as with eukaryotic members of the dynamin superfamily exist in many forms [198, 200-202]. The same counts for the way, how hydrolysis of GTP and dimerization occur [176, 198, 202, 203]. However, dimerization itself occurs mainly through the G-domain [62, 198, 202]. For lipid-binding, most BDLPs do this via the paddle, located at the top of the stalk domain [202]. Because BDLPs and the other eukaryotic members of the dynamin superfamily still share a lot in common, it is not too farfetched to assume that the BDLP evolved first in evolution and different changes led to the high variety of dynamin and dynamin-like proteins in eukaryotes that we know today.

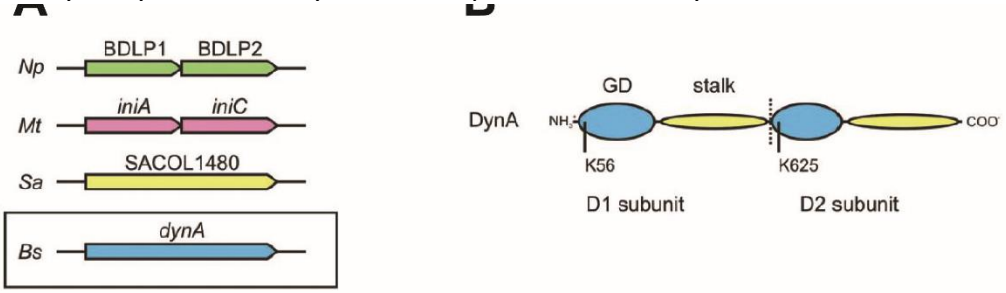

Fig. 1.6 Overview of the genetic organization of different bacterial dynamin-like proteins of different organisms.

(**A**) shows the composition of the BDLPs in *Nostoc punctiforme* (Np) and *Mycobacterium tuberculosis* (Mt) with two different genes encoding for it, while *Staphylococcus aureus* COL (Sa) and *Bacillus subtilis* (Bs) show only one longer gene, which encode for the BDLPs. A more detailed structure of the protein DynA with its two subunits is schematically depicted in (**B**), whereas the two GTPase domains are (GD) colored in blue. In yellow the helical regions, which probably consists of the stalk region with the trunk, neck and paddle domains, are depicted. The positions of the lysins K56 and K625 of the P-loop are also shown. Figure adapted and modified after Bramkamp *et al.* [199].

1.7.2 The bacterial dynamin-like protein DynA in *B. subtilis*

DynA is one of the best-studied bacterial dynamin-like proteins. It is a protein of *B. subtilis* and is expressed by the gene *ypbR.* A closer look at DynA reveals some special features, compared to the other BDLPs. First of all, DynA is the only protein in *B. subtilis* and is an intrinsic dimer, rather than two different proteins that function together like the other BDLPs [199, 204] (**Fig. 1.6B**). This could be due to a gene-fusion event in the past and is therefore a two-headed BDLP.

DynA consists of two subunits, D1 and D2, which form the intrinsic dimer and consist of the G-domain, stalk and loop (**Fig. 1.6B, Fig. 1.7**). DynA does not have a transmembrane domain like other BDLPs and D2 does not have a paddle region either. Therefore, D1 is essential for membrane-binding, which is also a surprise that only one subunit is enough for this (**Fig. 1.7B**). Also, D1 is mainly responsible for membrane fusion, whereas D2 plays a minor role in it, but is necessary for the stability of the whole complex [204]. DynA localizes at the membrane. A deletion of *dynA* in combination with *mreB* or *floT* leads to an exacerbation of the effects on cell shape and growth compared to an only deletion of *mreB* or *floT* [125, 205]. Furthermore, DynA localizes at the septal area during cell division and therefore, similar to dynamin in eukaryotes might play a role in cytokines. The fact that correct localization only occurs as long as MinJ is expressed further supports this assumption [199]. Further possible interaction partners, like YneK, RNaseY and YwqG, are also depend on MinJ expression [206]. YneK possibly binds to D1, YwqG to both subunits, whereas RNaseY requires the full-length protein for interaction [206] (**Fig. 1.7B**). Even though DynA can catalyze membrane fusion in *trans* alone in *in vitro, in vivo* this is not so effective. Therefore, those different interaction partners might be necessary [204]. Furthermore, DynA has been shown to do hemifusion as an intermediate state before membrane fusion finally occurs. Also, suggested for other members of the dynamin superfamily, the detachment of the membrane, and therefore the final step in membrane fusion, occurs due to the hydrolysis of GTP to GDP [199, 204]. Interestingly, unlike the other proteins of the dynamin superfamily, DynA does not require any nucleotide for hydrolysis, but Mg^{2+} [199].

Besides its function in cell division, DynA may also play a role in membrane integrity (**Fig. 1.7A**). Under membrane stress, *dynA* deletion leads to an increase in the sensitivity of cells toward membrane stress [125]. Furthermore, antibiotic stress-induced membrane stress as well as phage-induced membrane leakage leads to an increase of foci and a better resistance if DynA is expressed [124].

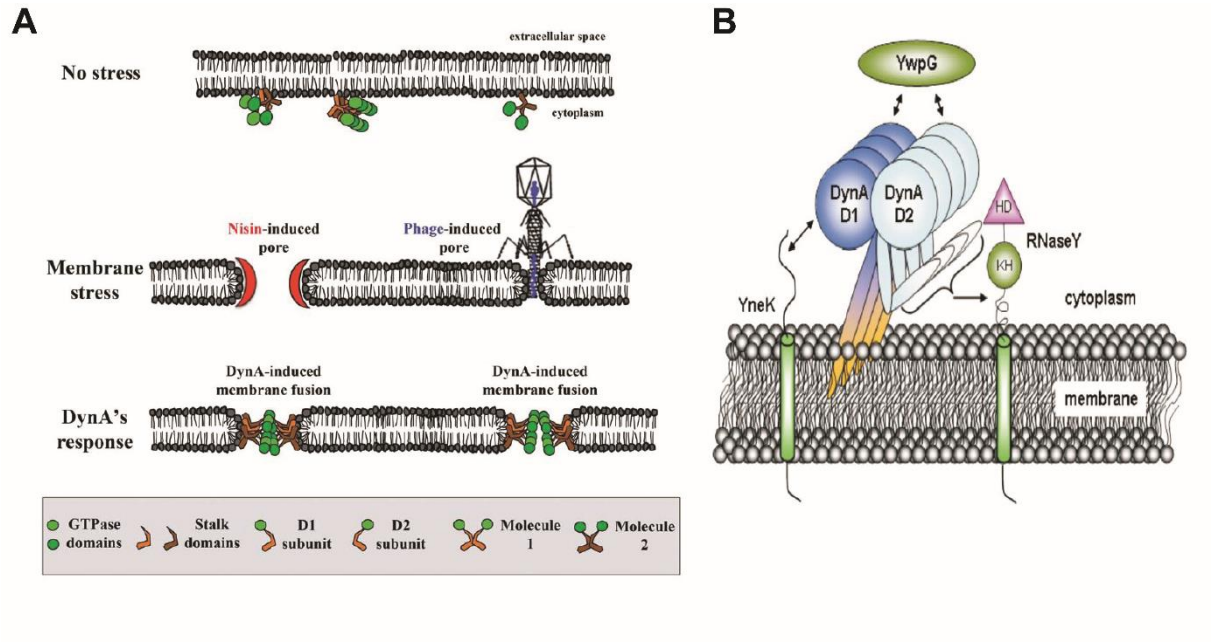

Fig. 1.7 Models of membrane fusion mediated by DynA.

(**A**) depicts the cell membrane without any membrane leakage in the top, where DynA proteins are already bound to it. Beneath this, membrane leakage through Nisin-treatment and phage infection is illustrated. At the bottom, DynA-induced membrane fusion is shown, whereas the binding to the membrane occurs with the stalk domains and the intrinsic dimer fusion via the GTPase domains of the two subunits D1 and D2. (**B**) represents a model, how DynA – bound to the membrane - interacts with three different proteins (YneK, YwpG and RNaseY) and which parts of DynA might be necessary for the interaction. YneK possibly interacts with the D1 subdomain, YwpG possibly interacts with both subdomains D1 and D2, while RNaseY possibly needs the full-length DynA protein for interaction. Figure adapted and modified after Bramkamp *et al.* [124, 206].

1.8 Aim of research

In recent years, the importance of RNAs in bacteria has been recognized and thus the focus has been on a variety of RNAs, their function and behavior. In this context, skepticism has arisen about well-accepted models and theories, especially about the way, transcription and translation occur in bacteria. Are they connected in a spatial and temporary manner, or are they separated in one way or another, as in eukaryotes? To gain more insight into it, this work focuses on one specific area of this topic: where does translation take place in bacteria? To address this question, various mRNAs from the Gram-positive bacteria *Bacillus subtilis* - a well-studied model organism -, are tested, to get a more detailed inside into the localization

behavior, as well as the dynamics of mRNAs.

In addition, one protein, DynA, which is the translated product of one of the mRNAs tested, was selected for further characterization. Members of the dynamin superfamily are highly necessary for eukaryotes and prokaryotes. Yet, much is not known about the representatives of the bacterial dynamin-like proteins. However, DynA of *B. subtilis* is a better-studied member of the bacterial dynamin-like proteins. In spite of everything, substantial questions remain to be not fully answered. Those are about its function, how it fuses membranes and whether it protects the cell from various stress factors and what are those? Therefore, as part of this work, different stress factors were used to analyse the response of DynA to them, as well as the general dynamics of DynA, and the dynamics of DynA under several stress conditions.

2 MANUSCRIPTS

Personal contribution to published work:

The majority of this work has been published (first article) or at least accepted in for publication (second article):

Article I

Laura Sattler and Peter L. Graumann, November 2021

Real time messenger RNA dynamics in *Bacillus subtilis.* Frontiers in Microbiology, 12:760857

Article II

Laura Sattler and Peter L. Graumann, 2021

Assembly of *Bacillus subtilis* dynamin into membrane-protective structures in response to environmental stress is mediated by moderate changes in dynamics at a single molecule level. Accepted in Microbial Physiology.

I designed and carried out all experiments and analysed the data. Furthermore, I wrote both manuscripts together with Prof. Dr. Peter L. Graumann, created all figures and tables and revised the manuscripts during the publishing process together with Prof. Dr. Peter L. Graumann. In addition, I greatly acknowledge the always helpful support from my supervisor Prof. Dr. Peter L. Graumann.

2.1 Article I

Real time messenger RNA dynamics in *Bacillus subtilis*

2.1.1 Abstract

Messenger RNA molecules have been localized to different positions in cells, and have been followed by time-lapse microscopy. We have used MS2-mVenus labeled mRNA and single-particle tracking to obtain information on the dynamics of single mRNA molecules in real time. Using single-molecule tracking (SMT), we show that several mRNA molecules visualized via two MS2-binding sites and MS2-mVenus expressed in *Bacillus subtilis* cells show free diffusion through the entire cell, and constrained motion predominantly close to the cell membrane, and at the polar regions of the cells. Because constrained motion of mRNAs likely reflects molecules complexed with ribosomes, our data support the idea that translation occurs at sites surrounding the nucleoids. Squared displacement analyses show the existence of at least two distinct populations of molecules with different diffusion constants, or possibly of three populations, e.g. freely mobile mRNAs, mRNAs in transition complexes, or in complex with polysomes. Diffusion constants between differently sized mRNAs did not differ dramatically, and were much lower than that of cytosolic proteins. These data agree with the large size of mRNA molecules and suggest that within the viscous cytoplasm, size variations do not translate into mobility differences. However, at observed diffusion constants, mRNA molecules would be able to reach all positions within cells in a frame of seconds. We did not observe strong differences in the location of confined motion for mRNAs encoding mostly soluble or membrane proteins, indicating that there is no strong bias for localization of membrane protein-encoding transcripts for the cell membrane.

Importance

In contrast to dynamics of proteins, little is known about real time motion of mRNA molecules in bacteria. We have added MS2-binding sites to several mRNAs in *Bacillus subtilis* cells, and followed motion of MS2-mVenus at a single molecule level. We find that mRNAs show dynamics similar to those of ribosomes, in spite of their polymeric nature, and similar to those found in eukaryotic cells. Our data suggest that while mRNAs are preferentially translated at

subpolar regions in cells, where also 70S ribosomes are accumulated, they can move through cells in a time frame of few seconds. Thus, in general, mRNAs appear to be mobile to reach any position in the cell in a short time frame, they are preferentially located at the cell poles and close to the cell membrane, facilitating rapid translation and insertion of membrane proteins.

2.1.2 Introduction

In the past, it has been a common model that transcription and translation occur at the same space and time in bacteria [1], because of the fact that, in general, bacteria are non-compartmentalized cells, unlike eukaryotes. Over the years, with the advance of powerful light microscopes and fluorescence labeling techniques, a new awareness of the organization and the inner structure of bacteria has arisen. Even though bacteria lack internal membrane systems similar to those found in eukaryotes, they possess a high degree of three-dimensional organization. Model bacteria such as *Escherichia coli* and *Bacillus subtilis* show a compacted structure called the nucleoid, containing the chromosome, which occupies the central space of the cell, but is absent at the cell poles or in the middle of large cells prior to cell division [2]. The cytoplasm is crowded with different enzymes diffusing through the cell [3], whereas the RNA degradation machinery of *E. coli* and *B. subtilis* can be mainly found at the cell membrane [4-6]. Transcription and translation occur spatially and temporarily coupled in *Caulobacter crescentus cells* [7], in which the chromosome fills the entire cell, whereas in *E. coli* and *B. subtilis*, both processes occur largely separated from each other [8], as transcription takes place mainly at the periphery of the nucleoid [9], and translation at the cell poles. Different studies showed that only a minority of ribosomes, approximately 20%, are localized within the nucleoid, while 80% are localized in the cytoplasm surrounding the nucleoid, the membrane and the poles [10, 11]. At the same time, only 4% of the RNA polymerase (RNAP) molecules and the ribosomes overlap in the nucleoid [12]. Thus, in different bacterial species, transcription and translation can take place in close spatial proximity; that is, genes and ribosomes can be found at the same place, or largely separated, when the chromosome is organized as a nucleoid. In the latter case, the question arises how RNA moves from its places of synthesis on the nucleoids to the cell poles, and further, if mRNA might be translated near sites where the encoded protein is used, for example, in case of cell division proteins, or membrane proteins that specifically localize to the cell poles. Different models for mRNA

localization have been discussed. For *C. crescentus*, the Jacobs-Wagner group has shown that mRNAs stay near their transcription sites, whose subcellular location in turn depends on its position of the chromosome, whose ordered arrangement serves as a spatial template [13]. Considering a bacterium having a nucleoid, a target gen locus would move out of the bulky nucleoid to the periphery, where RNAPs would transcribe the gene(s), and a coupling with translation (e.g. attenuation) would be possible [9]. A second principle model, suggested by the Amster-Choder group, is, that the mRNA is translated near the localization, where its encoded protein would later on localize. They could identify three different patterns for RNA localization, along the membrane, near the poles and a helical distribution in the cytoplasm, for different proteins. Note that not all of the tested mRNAs could be found at the same spot as their corresponding protein product [14]. Midcell localization was observed in another study, where an involvement of the signal-recognition pathway (SRP) for membrane proteins was assumed [15]. In addition, mRNA encoding for membrane proteins has been found to be more associated with cell membranes than mRNA for soluble proteins [16, 17]. Off note, different models could be possible in different bacteria species.

To address the question, where translation occurs in the Gram-positive bacterium *B. subtilis*, and to gain insight into the mode of diffusion of mRNAs, we decided to use the MS2-system of the bacteriophage [18, 19]. MS2 coat protein binds as a dimer to a 19 nt long RNA loop structure, such that MS2 fused to fluorophore would bind to and visualize mRNA in living cells. In order to overcome low signal intensity, a large number of repeats of the binding site have been used, fixed cells or other larger arrays such as λN22 in eukaryotes [20]. More recently, six repeats of the MS2-binding site have been commonly used [21], which still considerably enlarge the molecules, also keeping in mind the many MS2-GFP molecules binding to the array. Because of inhibition or delayed degradation of mRNA [22], different modifications were done over time by different groups [23]. Other labeling techniques can be used with possibly less influence, such as fluorescence *in situ* hybridization (FISH) in fixed cells [21], but do not allow to capture dynamics. In order to limit adverse effects, we decided to use only one or two MS2-binding sites fused to the 3'-end of the mRNA sequence. Our goal was to determine if motion of mRNA can be explained by assuming Brownian motion, using *B. subtilis* as a model bacterium, or if the polymers move largely by anomalous diffusion, or show no motion at all. We also set out to attempt determining diffusion constants, in order to find out if large mRNAs show markedly different dynamics than small molecules. We also wished

to address the question of mRNA operons encoding for membrane proteins membrane-proximal localization can be observed, as was described for some cases before, or if mRNAs can be mobile throughout the non-compartmentalized bacterial cells. Using single-molecule tracking (SMT), we found evidence for different populations having distinct average diffusion constants, indicating low mobility of mRNA bound to a ribosome during translation, and mobile populations, in which mRNA could be bound to a partially assembled ribosome or even freely diffusing molecules. Our data show that, for model mRNAs, diffusion can occur throughout the entire cells, whereas static motion occurs mostly at the periphery of the cell. Our data are in agreement with translation occurring at specific subcellular places, but show a high degree of mobility to reach these sites.

2.1.3 Results

2.1.3.1 Use of MS2-mVenus to Investigate mRNA diffusing at Single-Molecule Level in Live Cells

In contrast to other studies using the MS2-system for mRNA detection, in this work, we only use one and two MS2-binding sites instead of six or more [14, 24] and MS2 coat protein [18, 19] fused to the bright, monomeric GFP derivate mVenus [25]. Rather than using fixed cells [26] and bulky MS2-GFP tags or slow acquisition speeds (4 Hz) [27], we imaged using slim-field illumination and stream acquisition in the milliseconds range [28-30]. We reasoned that at an integration time of 75 ms, we would not track freely diffusing MS2-mVenus molecules, for which ≤ 20 ms would be required [5 ms are necessary to track free mVenus [31]], but predominantly track MS2 molecules bound to their target mRNA molecules. To test this assumption, we imaged MS2-mVenus via SMT with two different exposure times. We chose 8 ms to capture freely diffusive molecules, or 75 ms, where we would likely miss out freely diffusive molecules.

Jump distance (JD) analysis (**Fig. 1A,C,E**) is based on squared displacement analyses [32, 33], showing the probability of particles taking certain steps during a given time interval, assuming two-dimensional Brownian motion. We used several tests in order to evaluate if a single or more populations with an average diffusion constant can explain the observed JD distribution, using Rayleigh distributions. Probability-probability plots shown in **Fig. 1B,D,F** plot the deviation between modelled data (red dotted line) and observed data (blue solid line), and lack of deviation indicates a high quality for the goodness of the fit [32]. Based on tests

and the probability plots, MS2-mVenus tracked with 8 ms exposure time showed two populations, which best explain the data (**Fig. 1A,B**), having diffusion coefficients (DC) of D_2 with 0.55 $\mu m^2 s^{-1}$, likely freely diffusive MS2-mVenus, and D_1 of 0.11 $\mu m^2 s^{-1}$, that is, a slow-mobile population, likely consisting of MS2 bound to mRNA (**Fig. 1G,H**). A DC of 0.55 $\mu m^2 s^{-1}$ is surprisingly low for a small protein fused to mVenus, but at the acquisition speed used, we do not believe that our analyses is hampered by technical limitations. **Fig. S1** shows that assuming a third population does not increase the goodness of the fit (compare panel **B** and **D**) and was therefore discarded.

On the other hand, for MS2-mVenus tracked with an exposure time of 75 ms, three populations can explain the data better than assuming two populations (**Fig. S1E-H**). The most mobile population of MS2-mVenus at 75 ms had a diffusion constant of 0.094 $\mu m^2 s^{-1}$, very similar to that of the slower population tracked with 8 ms (**Fig. 1G**). The intermediate population D_2 had a DC of 0.012 $\mu m^2 s^{-1}$ and a size of 43.7%, similar to the fast-mobile population with 43.6%. D_1 with 0.003 $\mu m^2 s^{-1}$ weight only 12.7%. Most likely, the latter population represents MS2 bound to mRNA being translated by polysomes, the largest structure expected for mRNA to be present in. Very similar DCs were obtained for cells expressing *ypbR-ypzF* mRNA having two MS2-binding sites (**Fig. 1 E,F, 2E-H**). Here, the triple fit covered best the whole data set. These data suggest that MS2 protein binds to mRNA other than its target mRNA with considerable affinity. Although this caveat compromises specific claims, we found that the static fraction is much larger for cells carrying mRNA with MS2-binding sites, 25% of MS2-mVenus molecules showed static motion compared to 13% in cells lacking the MS2-binding site, and likewise, the intermediate mobile population was larger (49 versus 44%), whereas the high mobility fraction was smaller (26% versus 44% in cells lacking MS2-binding sites). These findings suggest that the high mobility fraction represents mostly MS2 bound to non-specifically recognized targets, whereas the other two fractions contain a large portion of MS2 bound to its specifically recognized mRNAs.

As a further argument for a considerable degree of specificity, we analysed the presence of MS2-mVenus molecules in an average size cell of 3 x 1 µm, into which all tracks obtained from hundreds of cells are projected. For example, a “heat map”, where white areas show a low probability of distribution and red to black a high concentration of molecules, shows that MS2-mVenus diffuses throughout the cell with no clear preference to a certain area (**Fig. 1I, J**), whereas the presence of the MS2-binding sites on *ybpR-ypzF* mRNA shows a

preferential localization towards the periphery of cells (**Fig. 1K**). Of note, expression of MS2-mVenus at low level does not strongly affect exponential growth, but cells reached a lower density than cells lacking the fusion protein (**Fig. S2**). We speculate that MS2 might bind to one ribosomal RNA, a highly abundant molecule that would strongly compete with few mRNAs carrying two MS2-binding sites. With this caveat in mind, we went on to analyse if differences might be observed for different mRNA molecules.

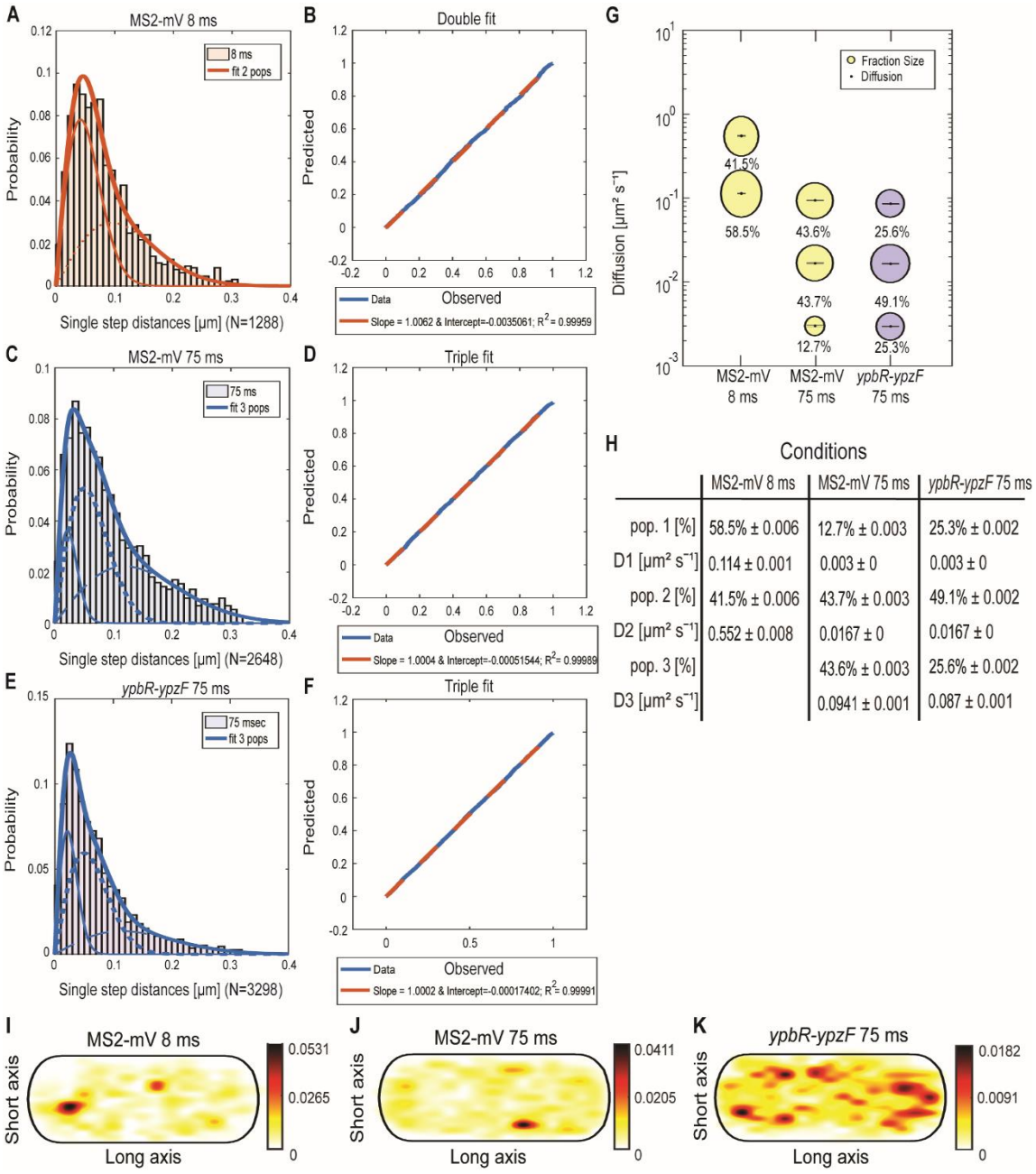

Fig. 1 Analyses of single molecule dynamics of MS2-mVenus expressed in *B. subtilis* cells during exponential growth.

(**A,C,E**) Jump distance analysis shows probability of displacements 8 ms acquisition (**A**) or 75 ms acquisition (**C,E**). (**B, D, F**) Probability-probability plot display the goodness of the fit of

predicted (red dotted lines) and determined data (blue solid lines). Triple Rayleigh fit models are shown in blue, double fits are depicted in red. Different dotted lines represent the subpopulations, solid lines represent the sum of the subpopulations. (**G**). Bubble plot shows the size of the fractions (proportional to the area) and corresponding diffusion coefficients. MS2-mVenus only is shown in yellow, in the presence of *ypbR-ypzF* carrying two binding sites in purple. (**I-K**) heat maps for MS2-mVenus tracked with 8 ms (**I**), 75 ms (**J**) - and in the presence of tagged *ypbR-ypzF* mRNA. White to red: low to the high probability of distribution of tracks.

Table 1 Genes Contained in mRNA Constructs and For What Proteins They Encode For

	Length	Genes	essential	encodes for
comN-secDF [1]	2950 bp	*comN, secDF*	no	membrane proteins
rnc-ftsY [1,2]	5301 bp	*rnc, smc, ftsY*	yes	soluble and membrane-associated proteins
hag [1]	915 bp	*hag*	no	extracellular protein
mreB-minD[1,2]	3894 bp	*mreB, mreC, mreD, minC, mind*	yes and no	soluble and membrane proteins
rplJ-rplL[1]	873 bp	*rplJ, rplL*	yes	soluble proteins
rplK-rplA[1]	1264 bp	*rplK, rplA*	no	soluble proteins
spoIIIE-ymfC[2]	3191 bp	*spoIIIE, ymfC*	no	soluble and membrane proteins
ylxM-rplS[1]	4395 bp	*ylxM, ffh, rpsP, ylqC, ylgD, rimM, trmD, rplS*	yes and no	soluble proteins
ypbR-ypzF[1,2]	4059	*ypbR, ypbS, ypzF*	no	soluble and membrane-associated proteins

[1] artificial mRNAs with one MS2BS and 1700 bp extra (not added in the table)
[2] mRNAs with two MS2BS

2.1.3.2 mRNA Moves as Three Distinctly Measurable Fractions of Mobility Within cells

We analysed four different polycistronic mRNAs. The *ypbR-ypzF* operon comprises open reading frames (ORFs) for soluble and membrane-associated proteins (**Table 1**). *ypbR* encodes for DynA, a soluble protein involved in membrane fusion after lesions [34] and appears to aid in membrane fusion of the invaginating division septum [35]. The products of *ypbS* and *ypzF* are of presently unknown function. The *rnc-ftsY* operon encodes three different proteins. FtsY is the membrane-associated receptor for the signal recognition particle [36] and localizes at the membrane, but also diffuses through the cell [37]. RNase Y is also membrane-associated [6], whereas SMC localizes to the nucleoids [31]. The *mreB-minD* operon comprises genes for cell shape-determining proteins MreB (soluble), MreC and MreD (membrane proteins), part

of the Rod complex for lateral cell wall synthesis [38, 39]. MreB forms filamentous structures underneath the cell membrane [40]. MinC and MinD, encoded at the 3' end of the operon, are part of the membrane-associated Min system [41] and function as cell division inhibitors [42], localizing at the septum and cell poles. The fourth mRNA, operon *spoIIIE-ymfC*, encodes for YmfC, a transcription factor of the GntR family [43] and membrane protein SpoIIIE, an ATP-dependent dsDNA translocase [44, 45]. MreB and MreC are essential proteins, and the deletion of FtsY leads to extremely slow growth of *B. subtilis*. Addition of two MS2-binding sites did not considerably slow down growth of cells compared with cells only expressing MS2-mVenus (**Fig. S2**), indicating that both mRNAs retain functionality. Although we cannot test for functionality of the other two tagged mRNAs during exponential growth (note that SpoIIIE is constitutively expressed, and plays an additional role during sporulation), we assume that the two binding sites do not cause a major defect in terms of mRNA dynamics.

Fig. 2A-G reinforces the idea that the distribution of *ypbR-ypzF* tracks is best explained assuming the presence of three populations. The same holds true for the other three tagged mRNAs, indicating that three distinct diffusion constants could be a general property for mRNA molecules (**Fig. 2I-J**).

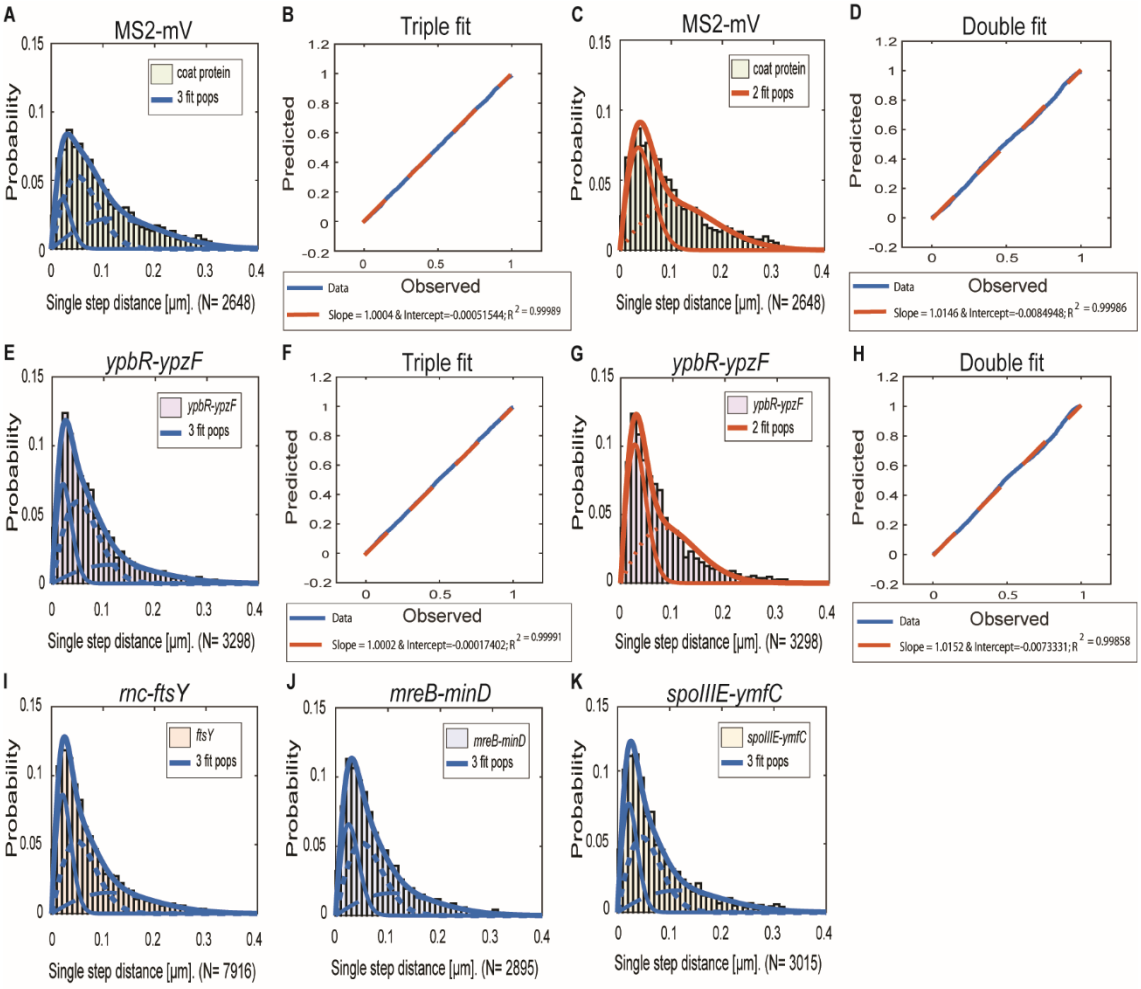

Fig. 2 Jump Distance Analyses of four MS2-tagged mRNAs.

Triple fits are shown in blue, double fits in red. (**A-D**) Cells expressing MS2-mVenus only, (**E-K**) cells additionally containing MS2-binding sites fused to mRNAs. (**E-H**) MS2-mVenus + *ypbR-ypzF*_MS2-binding site 2x, (**I**) MS2-mVenus + *rnc-ftsY*_MS2-binding site 2x, (**J**) MS2-mVenus + *mreB-minD*_MS2-binding site 2x and (**K**) MS2-mVenus + *spoIIIE-ymfC*_MS2-binding site 2x.

For all tagged mRNAs, the diffusion constants for the most mobile populations D_3 are similar between MS2-mVenus alone and bound to the mRNAs. In MS2-mVenus the mobile fraction has D = 0.094 ± 0.001 $\mu m^2 s^{-1}$, *ypbR-ypzF* 0.09 ± 0.001 $\mu m^2 s^{-1}$, *rnc-ftsY* 0.083 ± 0.001 $\mu m^2 s^{-1}$, *mreB-minD* 0.078 ± 0.001 $\mu m^2 s^{-1}$ and *spoIIIE-ymfC* 0.09 ± 0.001 $\mu m^2 s^{-1}$ (**Fig. 3**). Note that errors stated in **Fig. 3B** refer to fitting errors, whereas all data are combined from tracks of three independent biological replicates (for statistics, see **Table S1**). The intermediate mobile diffusion constant (D_2) is roughly one order of magnitude lower, with 0.019 ± 0 $\mu m^2 s^{-1}$ for MS2-mVenus and *ypbR-ypzF.* For *rnc-ftsY,* D is 0.016 ± 0 $\mu m^2 s^{-1}$, for *mreB-minD* 0.017 ± 0 $\mu m^2 s^{-1}$ and for *spoIIIE-ymfC* ,D = 0.015 ± 0 $\mu m^2 s^{-1}$ (**Fig. 3**). Those two populations diffuse faster

or slower compared to a study about mRNA diffusion, suggesting 0.05 ± 0 $\mu m^2 s^{-1}$ for mRNAs moving out of the nucleoid into the ribosome-rich area in *E. coli* [46]. Thus, for *ypbR-ypzF, rnc-ftsY, mreB-minD* and *spoIIIE-ymfC,* the high mobility population could represent free mRNA, and the intermediate-mobile population could consist of partially assembled ribosomes, where the mRNA is already bound to the smaller subunit S30, before the large subunit start to associate [47]. We will discuss SMT of the ribosomal protein L1 later on. The static population D_3 does not differ considerably between MS2-mVenus expressed alone or with mRNA containing binding sites (**Fig. 3**). The diffusive coefficient with 0.003 ± 0 $\mu m^2 s^{-1}$ for MS2-mVenus, *ypbR-ypzF, rnc-ftsY* and *spoIIIE-ymfC* and and/or with 0.0042 ± 0 $\mu m^2 s^{-1}$ for *mreB-minD* is extremely low, suggesting engagement of mRNA with polysomes. Of note, our measured diffusion constants are in good agreement with those found for eukaryotic cells [48, 49].

MS2-mVenus alone has a large high-mobility population of 43.6% and a large intermediate mobile fraction (43.7%), but a small static fraction (12.7%). For *ypbR-ypzF* compared with MS2-mVenus control, the highly mobile population decreases to 25.6% ± 0.002, whereas the static population increases to 25.3% ± 0.002. Also, the intermediate mobile population with 49.1% ± 0.002 is larger than that for "MS2-mVenus-only". Static populations on the other mRNAs were also more than twofold larger than that of MS2-mVenus alone (**Fig. 3**), suggesting that static fractions are dominated by MS2-mVenus specifically bound to its cognate mRNA. Based on this, we can assume that approximately one-third to half of our data in the strains expressing tagged mRNA are tracked MS2 coat protein bound to the binding site on the chosen mRNA, and leaving a large but not overwhelming degree of background noise of MS2 coat protein binding to unspecific targets, most likely RNA, in the cells.

Considering the size of mRNAs, the three big mRNAs, operons *ypbR-ypzF* with 4059 bp, *mreB-minD* with 3894 bp, and *rnc-ftsY* with 5477 bp (or 4627 bp when the *smc* promoter is used) and the smaller mRNA *spoIIIE-ymfC* with 873 bp (**Table 1**) show similar diffusion constants (**Fig. 3**). Thus, to a first approximation, the size of mRNA does not appear play a decisive role for mRNA diffusion, nor for the mobility of assembled polysomes.

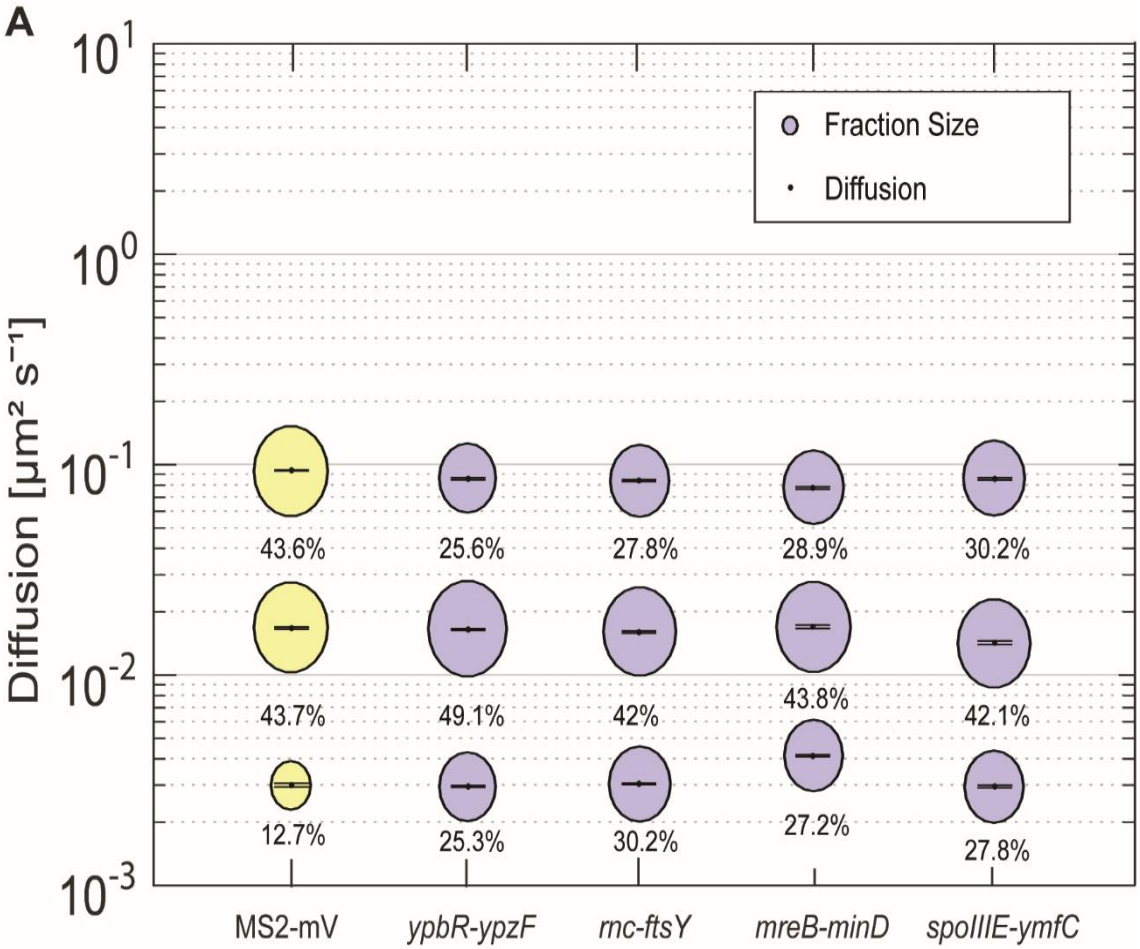

	MS2-mV	*ypbR-ypzF*	*rnc-ftsY*	*mreB-minD*	*spoIIIE-ymfC*
pop. 1 [%]	12.7% ± 0.003	25.3% ± 0.002	30.2% ± 0.003	27.2% ± 0.005	27.8% ± 0.005
D1 [µm² s⁻¹]	0.003 ± 0	0.003 ± 0	0.003 ± 0	0.00419 ± 0	0.003 ± 0
pop. 2 [%]	43.7% ± 0.003	49.1% ± 0.002	42% ± 0.002	43.8% ± 0.003	42.1% ± 0.004
D2 [µm² s⁻¹]	0.0167 ± 0	0.0167 ± 0	0.0158 ± 0	0.0172 ± 0	0.0145 ± 0
pop. 3 [%]	43.6% ± 0.003	25.6% ± 0.002	27.8% ± 0.002	28.9% ± 0.003	30.2% ± 0.004
D3 [µm² s⁻¹]	0.0941 ± 0.001	0.087 ± 0.001	0.0828 ± 0.001	0.0778 ± 0.001	0.0869 ± 0.001

Fig. 3 Dynamics of different mRNAs for soluble, membrane and membrane-associated proteins in comparison to MS2-mVenus.

For the determination of the diffusive coefficient and the fraction size, square displacement analysis (SQD) was used. (**A**) The bubble plot shows the size of the fraction where each bubble is proportional to the area of its corresponding diffusion coefficients. MS2-mVenus alone is shown in yellow whereas the different mRNAs are shown in purple. Table (**B**) states the SQD results.

2.1.3.3 Single-Molecule Tracking Reveals a Similar Behavior of Ribosomal Protein L1 Compared to mRNA

To address the nature of the different populations of MS2 tagged mRNA, we performed SMT of the ribosomal protein L1, which is part of the large subunit of the ribosome [50, 51]. L1-BFP has been shown to be fully functional and to localize mainly at the cell poles, and around the nucleoids using epifluorescence [11]. We performed SMT using 75 ms stream acquisition for comparison with the mRNA data, and 20 ms to be able to detect possibly freely diffusive L1. Highest density of L1-mVenus molecules was observed at the cell poles, septum area and at the membrane (**Fig. 4A,B**), in agreement with earlier epifluorescence experiments [11].

Jump distance (JD) analyses suggest that assuming two populations for L1-mVenus can explain the observed data well, but three populations increase the quality of the overall fit (**Fig. S3**). Square displacement analysis (SQD) shows that L1, tracked with 20 ms exposure time, has a high-mobile population of 40.2%, with D = 0.34 $\mu m^2 s^{-1}$, a slow mobile population of 48.7%, with D = 0.06 $\mu m^2 s^{-1}$, and a static population of only 11%, with D = 0.016 $\mu m^2 s^{-1}$ (**Fig. 4E,F**). We can assume that the high-mobile fraction consists of L1 within diffusing large subunit, as D_3 is similar to that determined by the Elf group for free subunits that diffuse through the entire cell [52]. The other two populations likely represent L1 bound to 70S subunits plus mRNA. In *E. coli* a DC of 0.04 $\mu m^2 s^{-1}$ was assumed for a translating ribosome [12]. Our investigation suggests that more than a single form of translating ribosomes exists or different forms of ribosome/mRNA complexes with distinct mobilities. In comparison, L1-mVenus tracked with longer integration time, DCs as all fractions decreased, likely because many fast diffusing L1 molecules (e.g., in the free large subunit) are not captured at a 75 ms integration time. Here, the fastest population moves with a diffusion coefficient of 0.1 ± 0 $\mu m^2 s^{-1}$, which lies in between the mobile and intermediate mobile fractions from the 20 ms condition. Likely, many fast diffusing L1 molecules (in the free large subunit) are not captured at 75 ms integration time. The static population has a lower DC at 75 ms compared to 25 ms, with D = 0.003 $\mu m^2 s^{-1}$, because it can be more accurately determined at slower stream acquisition.

Interestingly, at 75 ms integration time, the DC of the static population of L1 with 0.003 $\mu m^2 s^{-1}$ and of the mRNAs with 0.003 $\mu m^2 s^{-1}$ for *ypbR-ypzF, rnc-ftsY* and *spoIIIE-ymfC* and 0.004 $\mu m^2 s^{-1}$ for *mreB-minD* were very similar (**Fig. 4F**). Thus, we propose that this population might be polysomes in full swing, and/or mRNA for membrane proteins being translated at the SecYEG translocon after delivery through the SRP system.

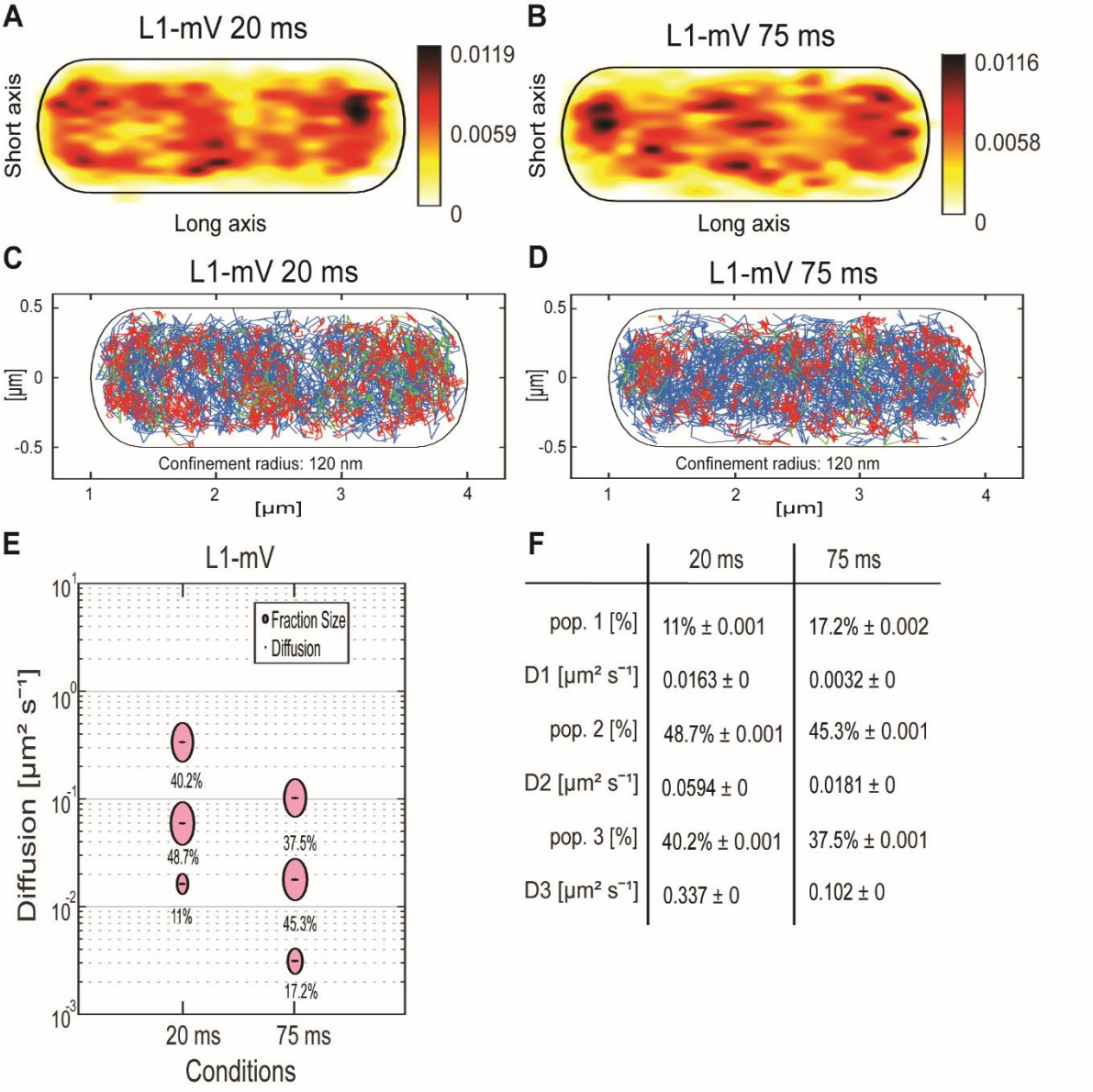

Fig. 4 Analyses of a ribosomal L1-mVenus protein fusion using SMT with 20 and 75 ms stream acquisition.

(**A+B**) all tracks of L1-mVenus are projected into a standardized cell of 1 x 3 µm. From white to red, low to the high probability of localization for tracking with an exposure time of 20 ms (**A**) and 75 ms (**B**). (**C+D**) Confinement maps. Blue represents freely diffusive tracks, red tracks showing confined motion within a 120 nm circle for a minimum of 8 steps, green tracks showing mixed behavior. (**E**) The bubble plot shows the size of the fractions, each bubble is proportional to the area of its corresponding diffusion coefficients. (**F**) Squared displacement analysis (SQD) was used for the determination of the diffusion constants and fraction sizes.

2.1.3.4 Analyses of Confined Motion Shows Preferential Low Mobility of mRNA at Sites Corresponding to Translating Ribosomes

Heat maps for all four analysed mRNAs showed a tendency for a preferential localization towards the cell periphery (**Fig. 5A-D**), different from the relatively even distribution of MS2-mVenus only (**Fig. 1J**), with the *ypbR-ypzF* transcript revealing the strongest accumulation at the cell poles (**Fig. 5A**). In order to gain spatial information of different dynamics within the cell, we set up confinement maps, which visualize low molecule mobility in cells. Confined motion was assumed for molecules that stay within in a circle of 120 nm (roughly three times the localization error in this study) for a minimum of 8 steps and longer. Such tracks represent molecules that stay associated with a defined subcellular position, likely bound to a large, static complex, and are represented by red tracks in **Fig. 5E-H**. Of note, these molecules will largely overlap with the population of molecules showing the slowest diffusion constant and thus to 50% and more represent MS2-mVenus bound to its specific mRNA molecules rather that non-specifically bound MS2-mVenus (see above). While freely diffusing molecules, indicated by blue tracks, are found throughout the cells, confined motion is enriched at the cell periphery, and is depleted from the central places of the cell (**Fig. 5E-H**). The exception is the cell middle, where in large cells (tracks of all sizes of cells are projected into the standardized cell), the segregated nucleoids make space for the invaginating septum, and where ribosomes are also accumulated. The trend for depletion at spaces of nucleoids is also seen for L1 protein representing the ribosomes (**Fig. 4D**), especially for the 75 ms acquisitions. In general, localization behavior of mRNAs is similar to that of L1 (**Fig. 4A-D**). As confined motion likely represents translating polysomes, that of labeled mRNAs likewise will account for transcripts being actively translated.

According to the model of the Amster-Choder group [14], mRNAs may be enriched near the area where its encoded protein will be active. For the four mRNA molecules, we found small but noticeable differences in the probability of confined motion, as apparent from the histograms of the short (*y*) cell axis or long (*x*) axis distributions (**Fig. 5I-L**). *ypbR-ypzF* mRNA showed a relatively even distribution with depletion of confined tracks from the cell center (**Fig. 5J**). For *rnc-ftsY,* enrichment at the septal area can be seen in the *x*-axis histogram (**Fig. 5I**), with a high probability of confined tracks near the cell membrane, as well as in the septal area (**Fig. 5F**). FtsY has been shown to diffuse through the entire cell in *Shewanella putrefaciens*, but to move in confined motion close to the cell membrane [37]. Thus, while

enrichment at the septal area might suggest preferred translation at this site in large cells commencing division, freely diffusive FtsY can easily reach this place within few seconds. For *mreB-minD* and for *spoIIIE-ymfC,* we observed polar enrichment (**Fig. 5K,L**), as judged from the *x*-axis distribution.

Mixed behavior between mobile and confined localization, indicated by green tracks in **Fig. 5E-H**, is much more rarely observed than either confined or free mobility. This indicates than molecules only rarely switch between free diffusion and confinement, but rather stay in either state of mobility for an extended time.

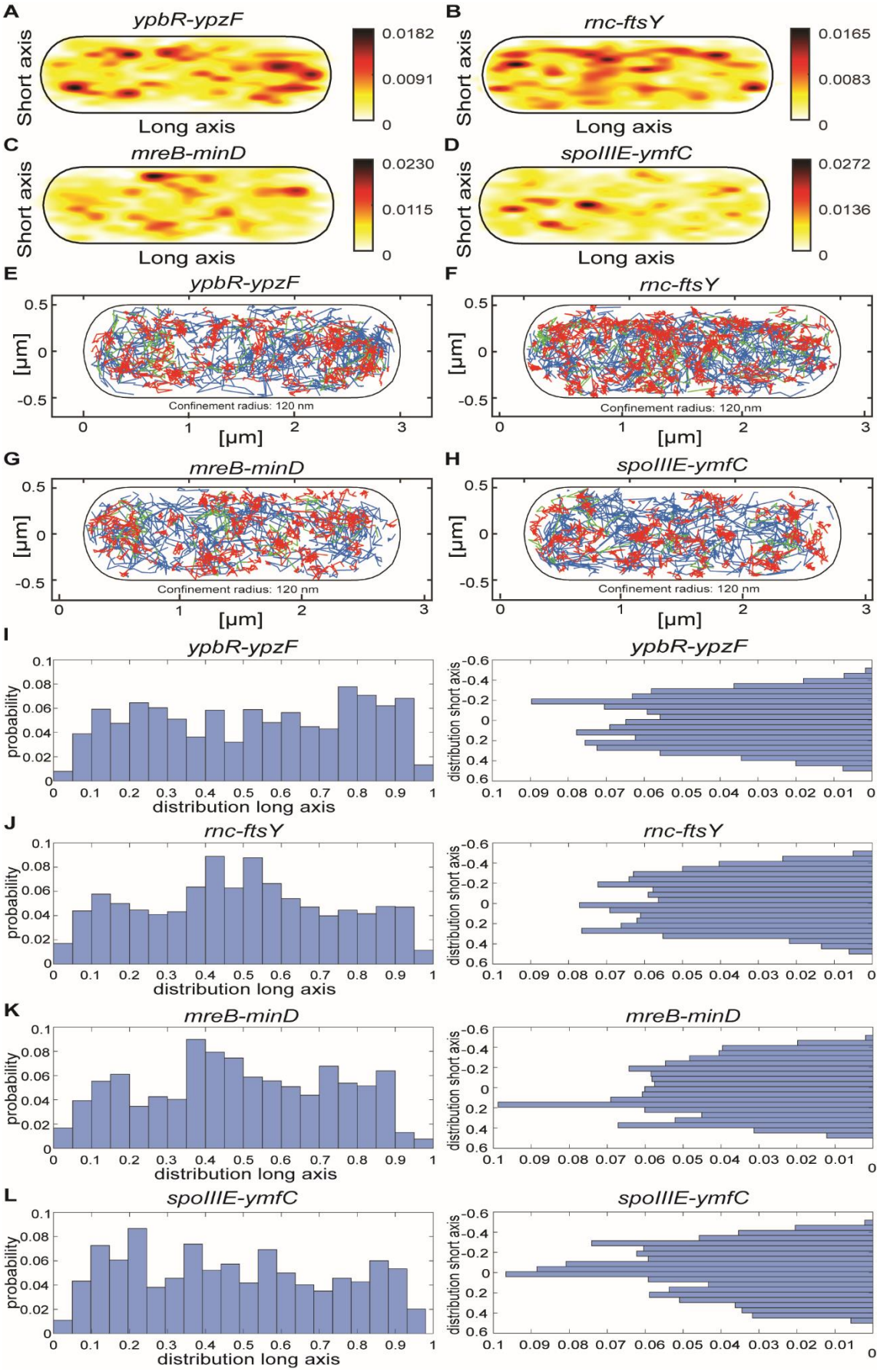

Fig. 5 Localization patterns of different mRNAs tagged with two MS2-binding sites.

All tracks of MS2-mVenus bound to 2x MS2-binding site tagged mRNAs are projected into a standardized cell of 1 x 3 µm. For heat maps, white to red represent low to high probability of localization of molecules. (**A**) MS2-mVenus + *ypbR-ypzF*_MS2-binding site 2x, (**B**) MS2-mVenus + *rnc-ftsY*_MS2-binding site 2x, (**C**) MS2-mVenus + *mreB-minD*_MS2-binding site 2x, (**D**) MS2-mVenus + *spoIIIE-ymfC*_MS2-binding site 2x. For confinement maps, blue represents freely diffusive tracks, red tracks restricted to a confined motion within a 120 nm circle for a minimum of 8 steps and green tracks with mixed behavior between mobile and confined motion. (**E**) MS2-mVenus + *ypbR-ypzF*_MS2-binding site 2x, (**F**) MS2-mVenus + *rnc-ftsY*_MS2-binding site 2x, (**G**) MS2-mVenus + *mreB-minD*_MS2-binding site 2x and (**H**) MS2-mVenus + *spoIIIE-ymfC*_MS2-binding site 2x. (**I-L**) Histograms showing probability of molecule localization along long (*x*) – or short (*y*) axis of cells. Histograms correspond to panel (**E-H**).

2.1.3.5 Rifampicin Stress Affects the Localization of *spoIIIE-ymfC* mRNA

As further test for the idea that the MS2 tag with two repeats of the MS2-binding site is useful for SMT, we tracked molecule fluorescence under Rifampicin stress. We used concentrations of Rifampicin where not all RNAP molecules might be inhibited, so some transcription should remain active. **Fig. 6** and **Fig. S4** show a similar change in the localization pattern of MS2-mVenus expressed without any binding site, and L1-mVenus, which showed exclusive accumulations at the cell poles (**Fig. 6A**,**B,E,F**). mRNA *spoIIIE-ymfC* showed the strongest effect. Under normal conditions, *spoIIIE-ymfC* had a higher density near the poles and the cell middle (future division sites) (**Fig. 6C**), whereas following Rifampicin treatment, membrane-proximal accumulation was lost; only some increased signal at the poles and the cell center remained (**Fig. 6D**). With regard to the confinement maps, MS2-mVenus only and L1-mVenus changed their pattern by stronger polar accumulation, which further suggests that MS2 might non-specifically bind to ribosomal RNA, whereas *spoIIIE-ymfC* mRNAs visually lost peripheral localization in favor or more central positioning (**Fig. 6G-L**). Interestingly, histograms of confined tracks revealed stronger polar accumulation of MS2-mVenus only, L1-mVenus and *spoIIIE-ymfC* following RNA depletion, as judged from the *x*-axis scans (**Fig. 6M-R**), whereas *y*-axis histograms reveal a shift of tracks away from the periphery of the cell toward the cell center, most pronounced for specifically labeled mRNA (**Fig. 6O,P**). Strongest changes seen for *spoIIIE-ymfC* mRNA in response to mRNA depletion support the idea of significant specificity in mRNA labeling versus non-specific MS2-mVenus binding.

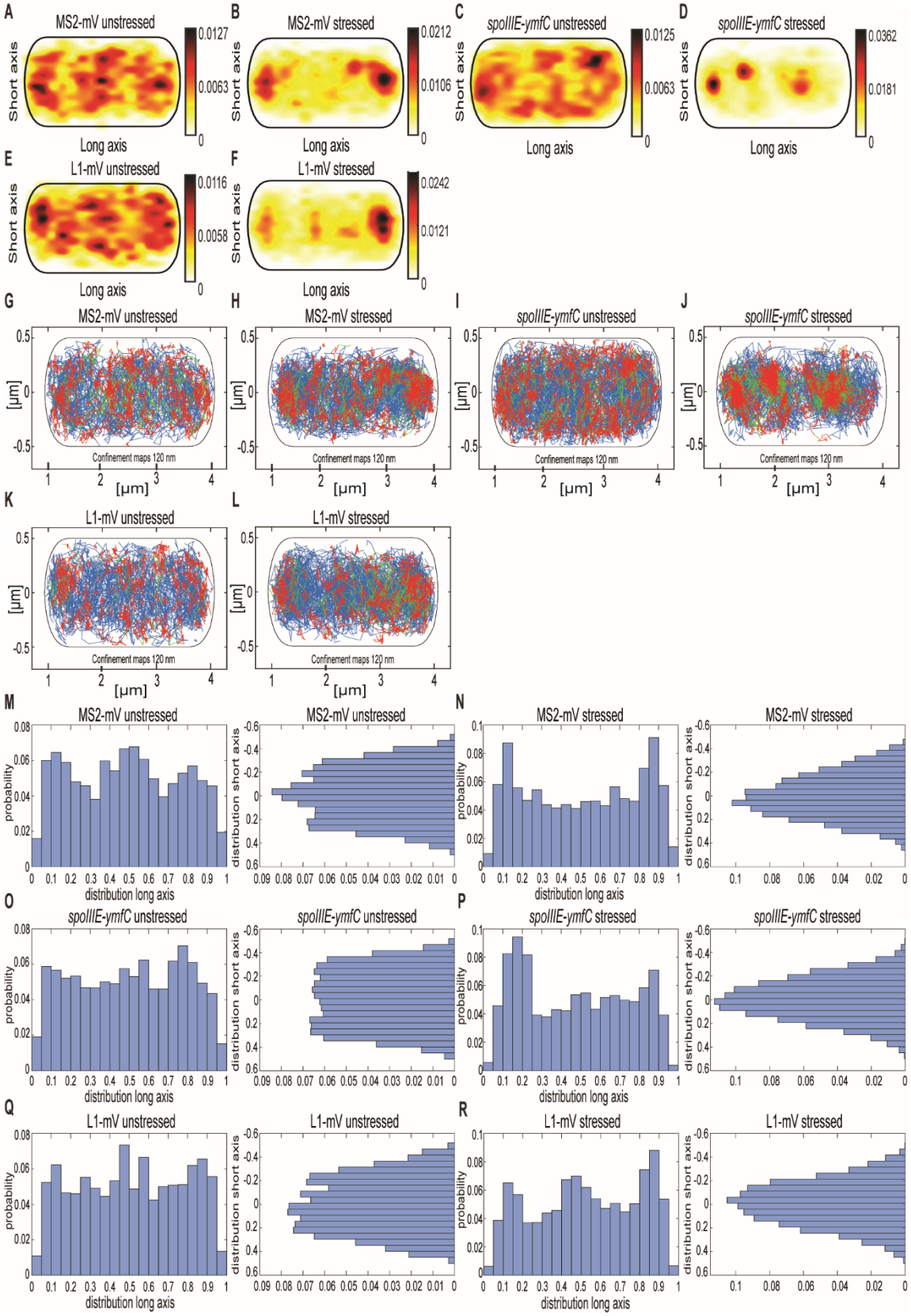

Fig. 6 Localization of MS2-mVenus, *spoIIIE-ymfC* and L1-mVenus with and without 50 µg Rifampicin.

All tracks of MS2-mVenus alone (**A,G**), or bound to 2x MS2-binding site tagged mRNA *spoIIIE-ymfC* (**C,I**), or the ribosomal protein L1-mVenus (**E,K**) are projected into a standardized cell of

1 x 3 µm. (**B,H**) *B. subtilis* cells expressing MS2-mVenus alone stressed for 40 minutes with 50 µg/ml Rifampicin (**D,J**) or bound to 2x MS2-binding site tagged mRNA *spoIIIE-ymfC,* or (**F,L**) ribosomal protein L1-mVenus. (**A-F**) Heat maps, from white to red, low to the probability of localization of molecules. (**G-L**) Confinement maps, blue represents freely diffusive tracks, red tracks restricted to confined motion within a circle of 120 nm for a minimum of 8 steps, green tracks having mixed behavior. (**M-R**) Histograms showing the probability of molecule localization occurring along long (*x*) – or short (*y*) axis of cells. Histograms correspond to panels (**G-L**).

Not only the localization pattern changed following downshift of RNAP activity, but also the single-molecule dynamics (**Fig. 7**). Here the effect was even more pronounced for *spoIIIE-ymfC* and L1 than for MS2 tag-only. DCs for the three populations remained similar for all three constructs (**Fig. 7B**). Population size of the static fraction decreased for MS2-mVenus only; the intermediate mobile fraction also decreased under mRNA depletion, whereas the high-mobile population increased (**Fig. 7A**). Thus, mRNA depletion led to higher mobility of MS2-mVenus. L1-mVenus showed a similar but stronger trend of increased mobility; the static fraction was less than halved, whereas the fastest ("free 50S subunits") fraction almost doubled (**Fig. 7A**). Interestingly, *spoIIIE-ymfC* dynamics changed differently from those of L1. The static mRNA population halved under Rifampicin treatment, and the high-mobile population increased from 48.9 to 63.6%, whereas the intermediate mobile population changed only little. This would fit to our idea that the static and intermediate mobile populations of L1 and the tested mRNAs are different stages of assembled ribosome, in which the static population could be the translating ribosome, which are similarly affected by a reduction in transcription activity.

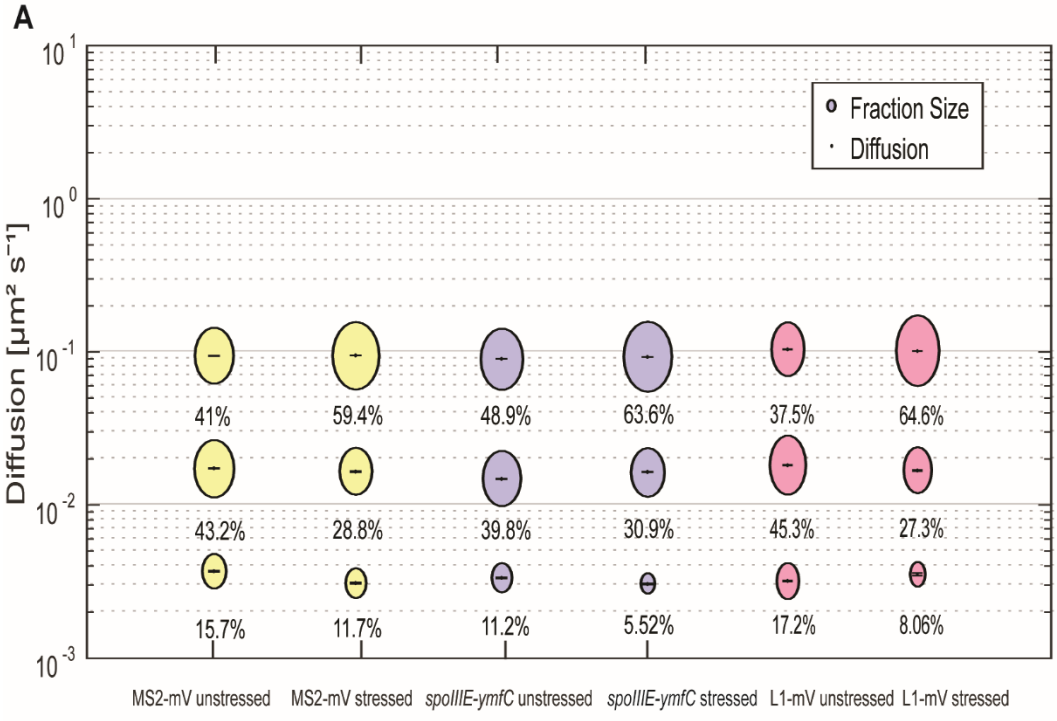

B

	MS2-mV unstressed	MS2-mV stressed	*spoIIIE-ymfC* unstressed	*spoIIIE-ymfC* stressed	L1-mV unstressed	L1-mV stressed
pop. 1 [%]	15.7% ± 0.002	11.7% ± 0.002	11.2% ± 0.001	5.52% ± 0.001	17.2% ± 0.002	8.06% ± 0.002
D1 [µm² s⁻¹]	0.004 ± 0	0.003 ± 0	0.003 ± 0	0.003 ± 0	0.003 ± 0	0.004 ± 0
pop. 2 [%]	43.2% ± 0.001	28.8% ± 0.001	39.8% ± 0.001	30.9% ± 0	45.3% ± 0.001	27.3% ± 0.001
D2 [µm² s⁻¹]	0.02 ± 0	0.02 ± 0	0.02 ± 0	0.02 ± 0	0.02 ± 0	0.02 ± 0
pop. 3 [%]	41% ± 0.001	59.4% ± 0.001	48.9% ± 0.001	63.6% ± 0	37.5% ± 0.001	64.6% ± 0.001
D3 [µm² s⁻¹]	0.1 ± 0	0.1 ± 0.001	0.1 ± 0.00	0.1± 0	0.1 ± 0.00	0.1± 0

Fig. 7 Rifampicin stress affects population sizes of mRNA and of ribosomal protein L1.

For the determination of the diffusive coefficient and the fraction size, square displacement analysis (SQD) was used. (**A**) The bubble plot shows the size of the fraction where each bubble is proportional to the area of its corresponding diffusion coefficients. MS2-mVenus is shown in yellow whereas the mRNA operon *spoIIIE-ymfC* is shown in purple. L1-mVenus is colored in pink. In table (**B**) – another way to display the SQD results - the data shown are the population sizes in % at a fixed DC that fits best to all three conditions, for better comparison if changes. For the stressed conditions, 50 µg/ml Rifampicin were added to the cells for 40 minutes.

2.1.3.6 Artificial mRNAs Behave Similar to Native mRNAs

As shown, the MS2 tag apparently binds to an unspecific target in *B. subtilis.* Due to a fortuitous mistake in our initial design, plasmids containing mRNA and (initially a single) MS2 site did not contain a terminator sequence shortly after the MS2-binding site, like for the shown samples previously. A downstream terminator sequence in the plasmid, approximately 1,700 bp after the MS2-binding site, terminated the artificial mRNA constructs. We took advantage of this collection of artificial mRNAs (original mRNA at 5' end, MS2 sequence in the middle, plasmid-derived 1,700 bp including terminator at the 3' end) and observed the behavior of mRNAs having different 5' portions. All constructs grew similarly as MS2-mVenus only-expressing cells (**Fig. S2**), suggesting that the extended mRNAs did not lead to any major problems for the cells. Even with one MS2 dimer bound to the MS2-binding site, we were able to track mRNA constructs (for JD analyses, see **Fig. S5**), whose static fractions were all considerably larger than for the cells expressing MS2-mVenus only (**Fig. 8Q**), again suggesting that we receive enough specific labeling of tagged mRNAs. Regarding the mRNAs encoding for mostly soluble proteins, (**Fig. 8A-D** and **Table 1**) we see the highest density in the heat map near the membrane and also a small amount at the pole, whereas confined localization of the mRNAs of ribosomal proteins *rplJ-rplL* and *rplK-rplA* can be detected in the cytoplasm, probably around the nucleoid [53]. The mRNA *hag*, which is monocistronic and encodes for flagellin, the largest extracellular part of the flagellum, is an exception [54]. Its mRNA is most evenly distributed and shows a strong midcell accumulation (**Fig. 8A** and **Fig. S6A**), whereas the other mRNAs showed different variations of the peripherally and polarly accumulation theme (**Fig. 8B-K** and **Fig. S6**). Interestingly, the heat maps for the two *ypbR-ypzF* constructs with two MS2 sites (**Fig. 5A,E**) and one site and artificial 3' end (**Fig. 8D,L**) are visually similar to each other, and likewise for mRNAs *rnc-ftsY* and *mreB-minD* (**Fig. 5**, **8**). This finding suggests that our observations made with the artificial mRNAs bear close resemblance to the ones made with the native constructs including just the two MS2-binding sites.

ComN is a transcription factor localized at the cell poles, whose transcript has also been shown to localize to the poles using FISH [15], and SecDF are integral membrane proteins involved in protein membrane insertion [55, 56]. *ylxM-rplS* encodes for SRP and ribosomal proteins, but also a 16S rRNA processing RNase and tRNA methyltransferase [53, 57, 58]. Thus, upper panels of the confinement maps from **Fig. 8** show mRNAs for operons containing open reading frames for soluble proteins (or membrane-associated DynA for the *ypbR* operon), and

lower panels represent mRNAs encoding membrane proteins (or membrane associated FtsY, **Table 1**). For all mRNAs, freely diffusive tracks are found through the nucleoid-containing cellular spaces. Although histograms of confined tracks show visual differences in membrane enrichment (depletion from the cell center), as judged from the *y*-axis scans, overall, there is no convincing general trend for mRNAs containing ORFs for membrane proteins towards the cell membrane (**Fig. S6E-H**), compared to those encoding soluble proteins (**Fig. S6A-D**); a majority of mRNAs tend to be depleted from the central cellular area (**Fig. S6**).

Concerning diffusion constants, for both *rnc-ftsY* constructs, these are comparable among all three populations, but the population size of the mobile population for two binding sites with 42.6% is approximately 50% larger than of *rnc-ftsY* with one binding site (27.8%), and the static population shrinks by 50% from 30.2% to 15%. This change in dynamics could reflect lowered translation efficiency of the artificially enlarged mRNA. For *mreB-minD,* no significant changes in the population sizes were observed, but DCs differ. Interestingly, with one binding site, D_1 (static) and D_2 (slow mobile) are less mobile than with two repeats. Despite of several other differences between the constructs, the general concept of three diffusive states for mRNAs holds true.

The largest difference between DCs were found for the slow mobile populations, the lowest being 0.0126 $\mu m^2 s^{-1}$ for *mreB-minD* and the highest of 0.0226 $\mu m^2 s^{-1}$ for *ypbR-ypzF.* The monocistronic mRNA *hag*, possibly containing the lowest number of translating ribosomes (we assume), appears to diffuse faster than most polycistronic mRNAs, with a DC of 0.0191 $\mu m^2 s^{-1}$, except of the operon mRNA of *ypbR-ypzF* (**Fig. 8Q,R**). D_3 of the different mRNAs varied between 0.081 $\mu m^2 s^{-1}$ and 0.104 $\mu m^2 s^{-1}$ (*hag* with the lowest and *rplJ-rplL* with the highest DC). Thus, assuming that the fast-mobile fraction corresponds to freely moving mRNA, size variations cause minor changes in mobility.

It could be argued that the MS2-system with two binding sites might be a better option to collect data for mRNA dynamics, looking at the number of tracks (**Table S1**), but the dynamics and localization patterns are quite similar between the one – and two MS2-binding sites constructs. Thus, motion of artificial mRNAs does not appear to differ much between native and synthetic mRNAs.

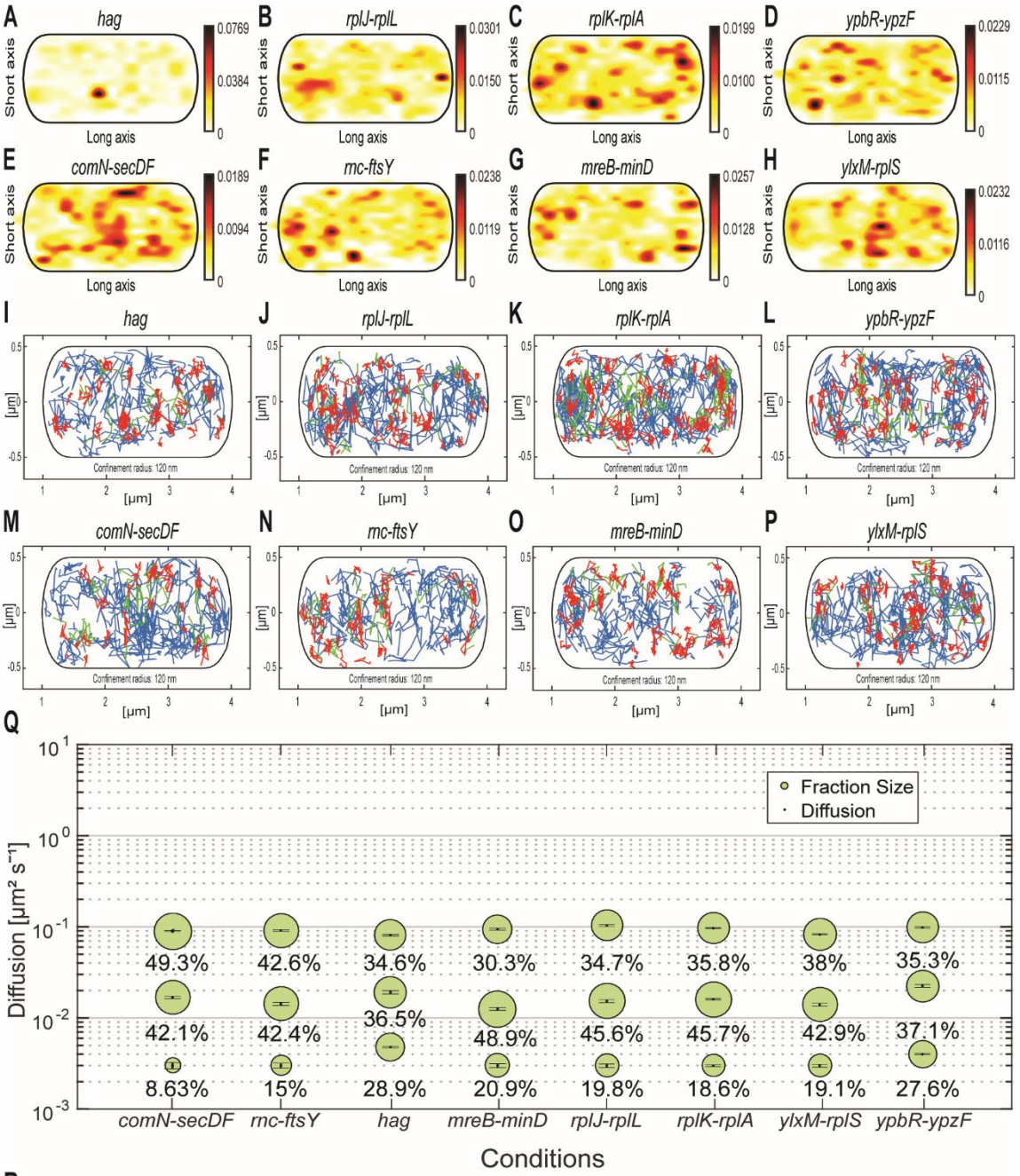

R

	comN-secDF	rnc-ftsY	hag	mreB-minD	rplJ-rplL	rplK-rplA	ylxM-rplS	ypbR-ypzF
pop. 1 [%]	8.63% ± 0.007	15% ± 0.012	28.9% ± 0.009	20.9% ± 0.014	19.8% ± 0.01	18.6% ± 0.005	19.1% ± 0.009	27.6% ± 0.006
D1 [μm² s⁻¹]	0.003 ± 0	0.003 ± 0	0.00479 ± 0	0.003 ± 0	0.003 ± 0	0.003 ± 0	0.003 ± 0	0.00401 ± 0
pop. 2 [%]	42.1% ± 0.006	42.4% ± 0.008	36.5% ± 0.006	48.9% ± 0.011	45.6% ± 0.007	45.7% ± 0.004	42.9% ± 0.006	37.1% ± 0.01
D2 [μm² s⁻¹]	0.0168 ± 0.001	0.0143 ± 0.001	0.0191 ± 0.001	0.0126 ± 0	0.0153 ± 0.001	0.0161 ± 0	0.014 ± 0	0.0226 ± 0.001
pop. 2 [%]	49.3% ± 0.006	42.6% ± 0.008	34.6% ± 0.006	30.3% ± 0.011	34.7% ± 0.007	35.8% ± 0.004	38% ± 0.006	35.3% ± 0.01
D3 [μm² s⁻¹]	0.0898 ± 0.001	0.0913 ± 0.002	0.081± 0.002	0.0941 ± 0.002	0.104 ± 0.002	0.0969 ± 0.001	0.0825 ± 0.001	0.0987 ± 0.002

Fig. 8 Artificially extended mRNAs approximately 1700 bp longer than native mRNAs, with one MS2-binding site, behave similar to native mRNAs with two MS2-binding sites.

(**A-H**) heat maps. (**A-D**) are mRNAs for soluble proteins, (**E-H**) for membrane associated or membrane proteins. From white to red is the low to high probability of localization. (**A**) MS2-

mVenus + *hag*_MS2-binding site 1x, (**B**) MS2-mVenus + *rplJ-rplL*_MS2-binding site 1x, (**C**) MS2-mVenus + *rplK-rplA*_MS2-binding site 1x, (**D**) MS2-mVenus + *ypbR-ypzF*_MS2-binding site 1x, (**E**) MS2-mVenus + *comN-secDF*_MS2-binding site 1x, (**F**) MS2-mVenus + *rnc-ftsY*_MS2-binding site 1x, (**G**) MS2-mVenus + *mreB-minD*_MS2-binding site 1x and (**H**) MS2-mVenus + *ylxM-rplS*_MS2-binding site 1x. (**I-P**) Confinement maps. Blue freely diffusive tracks, red confined tracks (120 nm circle, minimum of 8 steps), and green tracks with mixed behavior. (**I-L**) mRNAs for soluble proteins, (**M-P**) for membrane-associated or membrane proteins. (**I**) MS2-mVenus + *hag*_MS2-binding site 1x, (**J**) MS2-mVenus + *rplJ-rplL*_MS2-binding site 1x, (**K**) MS2-mVenus + *rplK-rplA*_MS2-binding site 1x, (**L**) MS2-mVenus + *ypbR-ypzF*_MS2-binding site 1x, (**M**) MS2-mVenus + *comN-secDF*_MS2-binding site 1x, (**N**) MS2-mVenus + *rnc-ftsY*_MS2-binding site 1x, (**O**) MS2-mVenus + *mreB-minD*_MS2-binding site 1x and (**P**) MS2-mVenus + *ylxM-rplS*_MS2-binding site 1x.

2.1.4 Discussion

Until recent developments of high and super resolution imaging methods, it was thought that transcription and translation in bacteria happen in a temporally and spatially coupled manner [1]. However, it has been shown that in *B. subtilis* and in *E. coli*, ribosomes are largely excluded from the central nucleoids, and approximately only 4% overlap with RNAP [12], which are found at the nucleoid [10]. This leads to the assumption that transcription and translation are spatial and temporarily separated. This does not account for all bacterial species, because in *C. crescentus,* chromosome loci, corresponding mRNA and ribosomes were found in close proximity, such that mRNAs stay near their transcript site [13].

In this study, we set out to study mRNA dynamics and localization at the highest possible resolution. We chose *B. subtilis,* an established model organism for Gram-positive bacteria, where it is known that transcription and translation occur in a spatially separated manner [8].

Using the MS2-system of the bacteriophage MS2 [19] and SMT, we used only two MS2-binding sites integrated into the 3’ end of four mRNAs, in order to cause as little deviation from native mRNAs as possible. With the caveat that MS2 appears to bind to some (likely ribosomal) RNA species in *B. subtilis* cells in a non-specific manner, we show that it is in principle possible to follow the movement of tagged sites on mRNA in a milliseconds time scale, assuming that individually tagged sites move similar to the entire mRNA molecule. Even given the noise generated by non-specifically binding MS2-mVenus protein, we found

evidence for mRNA movement through the entire cell, and for confined motion, indicative of mRNA being within a larger structure such as bound by translating ribosomes. In agreement with the finding that free ribosomal subunits can move throughout the cells, while translating 70S ribosomes and polysomes are present at polar regions and at peripheral site surrounding the nucleoid [37, 52], we found confined motion predominantly at sites excluded from the nucleoids, that is, the cell periphery and the cell poles. Although single-molecule data could be best explained by assuming three distinct populations of molecules with different average diffusion constants, we cannot exclude that only statically positioned mRNAs (engaged in translation) and freely mobile molecule exist. Whether there are two or three populations does not change the major finding of considerably fast diffusion for mRNA molecules, be it in complex with ribosomes or as free mRNA molecules. Experiments using inhibition of transcription supported this view. Thus, we conclude that mRNA molecules are not generally excluded from the nucleoids, but can diffuse through this subcellular space, allowing freedom for reaching different subcellular sites. Although we cannot prove that the fast-mobile fraction observed consists of MS2-mVenus specifically bound to the investigated mRNAs or to the non-specific RNA species, clearly the slow-mobile/static and medium-mobile fractions contain a large degree of specifically labeled mRNA molecules. Assuming a D of 0.02 $\mu m^2/s$ for medium-mobile diffusing mRNA molecules, and taking this constant as an estimate for 3D diffusion, on average, such a molecule would need less than 20 s to diffuse through a 3 µm large (spherical) cell, using $\tau = r^2/6D$. Assuming D of 0.01 for freely diffusing mRNAs, this number would drop to less than 4 s. Thus, mRNA molecules appear to have the possibility to reach different regions in a bacterial cell in a time frame of few seconds. Interestingly, diffusion of mRNA in eukaryotic cells has been determined to occur in a similar range [48, 49], although proteins generally show higher diffusion constants in eukaryotic than in bacterial cells.

We found little evidence for the assumption that mRNAs encoding for membrane proteins are localized and translated at the cell membrane [59]. In general, all tested mRNAs, which consisted of operons or of monocistronic mRNAs, showed confined motion at sites surrounding the nucleoids, that is, close to the cell membrane. mRNA operons encoding for membrane and cytosolic proteins – like *spoIIIE-ymfC* and *ylxM-rplS* – showed different degrees of membrane proximity for confined tracks but did not show clearly distinguishable patterns than mRNAs encoding solely soluble proteins, such as operons for ribosomal proteins. For mRNA encoding for flagellin that is secreted through the flagellar machinery to form the

filament outside of cells, we found a marked localization to the cell middle. As a caveat to these experiments, confined tracks for MS2-mVenus only also showed a preference for polar localization. However, given that half or more confined tracks for specifically labeled mRNAs can be accounted for by specific binding of MS2-mVenus, a generally higher degree of membrane proximity for mRNAs encoding membrane proteins, and thus for translation of membrane proteins at the membrane, should have been visible, but histograms of confined tracks did not show such a clear trend, although different patterns between mRNAs were apparent.

Our data are not in conflict of studies reporting stronger association of mRNAs encoding for membrane proteins with membranes than for mRNAs containing ORFs for soluble proteins observed in *E. coli* [16, 17]. It is also possible that although most mRNAs appear to be translated close to the cell membrane and at the cell poles, as seen in our study, mRNAs encoding membrane proteins are directly associated with the membrane, which is clearly the case of SRP-mediated membrane association of ribosomes translating nascent chains for membrane proteins.

Interestingly, observed diffusion constants for different mRNAs were rather similar. The populations with the highest DC, which we interpret to represent freely mobile molecules, showed a mobility much lower than that of even large proteins [31, 37] in agreement with the large size of mRNAs. Interestingly, these molecules diffused even through the nucleoids that have been discussed to present diffusion barriers within bacterial cells. Based on an optimal fitting of data, we found two additional populations, one with an extremely low DC of essentially static motion, between 0.003 – 0.005 $\mu m^2 s^{-1}$, likely composed of mRNA covered with many ribosomes (polysomes). Inhibition of RNA polymerase strongly decreased this population, supporting the idea of this population being involved in the translation process. An intermediate mobility fraction might be composed of mRNAs bound to 30S initiation complexes, that is, transition complexes; this population also decreased in size upon inhibition of translation.

To our knowledge, our study is the first report for CDs of ribosomal proteins in a Gram-positive bacterium. The observation of three diffusive populations agrees with findings made in *S. putrefaciens* [37]. A single DC was determined for freely diffusive ribosomal subunits or for translating ribosomes in *E. coli* [52]. Although our data can also be explained assuming two populations, we suggest that transition states between free subunits and translating 70S

ribosomes/polysomes are reflected by out-tracking analyses, because we implemented criteria to avoid overfitting of data (Bayesian information criterion) and implemented several statistical tests to find the optimal fits for observed data. Dynamics determined for mRNAs were similar to intermediate-mobile and static ribosome populations, supporting the idea of mRNAs diffusing freely, or more slowly as initiation complexes, and basically arresting at peripheral sites in the cell as translation complexes.

It has been argued that mRNAs can have specific sites of location within the non-compartmentalized bacterial cell [14, 60]. Our data are in no way contradictory, as we did observe differences in the pattern of localization of confined molecules for different mRNAs. In addition, polar localization described for mRNAs [15] is in agreement with our observation that confined motion of mRNAs (i.e., translation complexes) is prevalent at the polar areas of the cell. Thus, although out study failed to generate a system that is entirely specific for the labeled mRNAs to be studied, but is heavily blurred by non-specific binding of MS2 to unknown targets in *B. subtilis* (likely ribosomal RNA), our study provides fundamental data on single-molecule dynamics of mRNA molecules, and is thus an important step toward understanding molecule dynamics in bacteria in real time, and in understanding the intriguing asymmetric distribution of RNA molecules [17, 61] in a non-compartmentalized cell.

2.1.5 Acknowledgments

DATA AVAILABILITY STATEMENT

The original contributions presented in the study are included in the article/Supplementary Material, further inquiries can be directed to the corresponding author/s.

FUNDING

This work was supported by the DFG-funded research consortium TRR174.

2.1.6 Materials and Methods

Bacterial strains and growth conditions

Each *Bacillus subtilis* construct is in the wild type NCIB 3610, which possesses a plasmid for increased transformation efficiency with a *comI* mutation [62]. For cloning, the *Escherichia coli* strain DH5α was used. Both strains were cultivated in Luria-Bertani (LB) medium, for *B. subtilis* only for overnight cultures. *E. coli* was grown at 200 rpm and 37°C, while *B. subtilis* was cultivated at 250 rpm and 30°C. For single-molecule tracking *B. subtilis* was grown in $S7_{50}$ minimal medium(1% [wt/vol] fructose, 0.1% [wt/vol] glutamate, 0.004% [wt/vol] Casamino Acids [63] with the same temperature and speed. For the determination of the growth rate, it was measured with an optical density at 600 nm (OD_{600}). An OD of 0.7 was used for microscopy. Selection of the strains was accomplished by using the antibiotics ampicillin (100 µg/ml) for *E. coli* and chloramphenicol (5 µg/ml) and spectinomycin (100 µg/ml) for *B. subtilis*. For mRNA depletion, commonly 200 µg/ml is used, which also rapidly induces cell death in the culture. We used a lower concentration of 50 µg/ml, where dead cells were rarely seen during the first 40 min after drug addiction. An even lower concentration of 25 µg/ml was also used (**Supplementary Fig. 4**).

Strain construction

First the fusion protein MS2-mVenus was constructed in *E. coli* DH5α with the plasmid pSG1193 (ECE153). With this plasmid, the coat protein is set between the flanks of the alpha amylase *amyE*. After transformation in *B. subtilis*, a double crossover occurs with the *amyE* gene section between plasmid and bacterial chromosome and therefore this gene is

interrupted and no longer functional in *B. subtilis.* With this plasmid, a xylose promotor is set before the MS2-mVenus and therefore can be induced with xylose. Something, that was not done here. The strain MS2-mVenus in *B. subtilis* NCIB 3610 was then later on used to get the different mRNA constructs transformed into it.

For the mRNA constructs, the plasmid pHJDS [64] with a C-terminal fusion of one or two MS2-binding sites was used. After having the monocistronic and polycistronic mRNA constructs cloned with the MS2-binding site in *E. coli,* the constructs were cloned via a single-crossover event into *B. subtilis* MS2-mVenus at the original locus. Selection for the correct constructs was done by antibiotic resistance selection and test-PCR. L1-mVenus was made by using the plasmid pSG1164 with a C-terminal mVenus. With this plasmid also a single-crossover event occurs at the original locus in *B. subtilis.*

Preparation of NCIB 3610 constructs for microscopy

B. subtilis NCIB 3610 cells with only MS2-mVenus, MS2-mVenus + mRNA constructs, and L1-mVenus constructs were grown in $S7_{50}$ minimal medium at 30°C under shaking conditions to an OD of 0.7. For the cells, stressed with 25 and 50 µg/ml Rifampicin, it was added to the constructs and incubated for 40 minutes. Cells were spotted on coverslips (25 mm, Marienfeld) and covered with an agarose pad (1% (w/v)), made of $S7_{50}$ Medium and a smaller coverslip (12 mm, Marienfeld).

Single-molecule tracking, data acquisition- and analysis

Imaging was performed with a Nikon Eclipse Ti microscope equipped with a high numerical aperture objective (CFI Apochromat TIRF 100XC Oil, NA 1.49), an EM-CCD camera (ImagEM X2, Hamamatsu), and a YFP filter set (BrightLine 500/24, Beamsplitter 520 and BrightLine 542/27). mVenus fluorophores were excited by the central part of a laser beam (TOPTICA Beam Smart, 515 nm, max. power 100 mW) with a laser intensity of 20 mW. Each movie consists of 3000 frames and was recorded with an exposure time of 8, 20 and 75 ms, using Nikon NIS-Elements BR.

First, the videos were cut with Fiji (ImageJ) [65] and the first 500 to 1000 frames were cut off, to a point where only one or two signals were present in cells. Afterwards, the cell meshes were set with oufti [66]. For particle detection, U-track [67], a MATLAB software, was used. Here, the minimal length of tracks was set to 8, to avoid analyzing freely diffusive

molecules that diffuse slowly for a short time, and to link to points, no gaps for the particle detection was allowed. The Brownian search radius was set with the lower bound of 0 and the upper bound of 3. Data were analysed using SMTracker [32]. Here the Stationary Localization Analysis (SLA) panel for the confinement maps and dwell time analysis, Spatial distribution (SDA) panel for the heat maps and the Square Displacement Analysis (SQD) panel were used. R^2 was as a measure for goodness, a statistical tests such as Kolmogorov-Smirnov goodness of fit and null hypothesis significance were used to find the best fit to Rayleigh distributions. Bayesian information criterion was used to avoid overfitting of data. Although, at present, SMTracker allows only to differentiate up to 3 populations, assuming more than 3 populations presented overfitting of data from this study, based on a R value of "1" for using three populations.

With regard to the number of tracks (**Supplementary Table 1**), the MS2-system with two binding sites might be a better option to collect data for mRNA dynamics; however, the dynamics and localization patterns were quite similar between the one and two MS2-binding sites constructs. Thus, motion of artificial mRNAs does not appear to differ much between native and synthetic mRNAs.

2.1.7 References

1. Miller, O.L., Jr., B.A. Hamkalo, and C.A. Thomas, Jr., *Visualization of bacterial genes in action.* Science, 1970. **169**(3943): p. 392-5.
2. Fisher, J.K., et al., *Four-dimensional imaging of E. coli nucleoid organization and dynamics in living cells.* Cell, 2013. **153**(4): p. 882-95.
3. Cayley, S., et al., *Characterization of the cytoplasm of Escherichia coli K-12 as a function of external osmolarity. Implications for protein-DNA interactions in vivo.* J Mol Biol, 1991. **222**(2): p. 281-300.
4. Miczak, A., R.A. Srivastava, and D. Apirion, *Location of the RNA-processing enzymes RNase III, RNase E and RNase P in the Escherichia coli cell.* Mol Microbiol, 1991. **5**(7): p. 1801-10.
5. Khemici, V., et al., *The RNase E of Escherichia coli is a membrane-binding protein.* Mol Microbiol, 2008. **70**(4): p. 799-813.
6. Hamouche, L., et al., *Dynamic Membrane Localization of RNase Y in Bacillus subtilis.* mBio, 2020. **11**(1).
7. Campos, M. and C. Jacobs-Wagner, *Cellular organization of the transfer of genetic information.* Curr Opin Microbiol, 2013. **16**(2): p. 171-6.

8. Lewis, P.J., S.D. Thaker, and J. Errington, *Compartmentalization of transcription and translation in Bacillus subtilis.* EMBO J, 2000. **19**(4): p. 710-8.

9. Stracy, M., et al., *Live-cell superresolution microscopy reveals the organization of RNA polymerase in the bacterial nucleoid.* Proc Natl Acad Sci U S A, 2015. **112**(32): p. E4390-9.

10. Chai, Q., et al., *Organization of ribosomes and nucleoids in Escherichia coli cells during growth and in quiescence.* J Biol Chem, 2014. **289**(16): p. 11342-52.

11. Mascarenhas, J., M.H. Weber, and P.L. Graumann, *Specific polar localization of ribosomes in Bacillus subtilis depends on active transcription.* EMBO Rep, 2001. **2**(8): p. 685-9.

12. Bakshi, S., et al., *Superresolution imaging of ribosomes and RNA polymerase in live Escherichia coli cells.* Mol Microbiol, 2012. **85**(1): p. 21-38.

13. Montero Llopis, P., et al., *Spatial organization of the flow of genetic information in bacteria.* Nature, 2010. **466**(7302): p. 77-81.

14. Keren Nevo-Dinur, A.N.-S., Sigal Ben-Yehuda, Orna Amster-Choder, *Translation-Independent Localization of mRNA in E. coli.* Science, 25 FEBRUARY 2011. **VOL 331**.

15. dos Santos, V.T., A.W. Bisson-Filho, and F.J. Gueiros-Filho, *DivIVA-mediated polar localization of ComN, a posttranscriptional regulator of Bacillus subtilis.* J Bacteriol, 2012. **194**(14): p. 3661-9.

16. Benhalevy, D., et al., *Model Uracil-Rich RNAs and Membrane Protein mRNAs Interact Specifically with Cold Shock Proteins in Escherichia coli.* PLoS One, 2015. **10**(7): p. e0134413.

17. Moffitt, J.R., et al., *Spatial organization shapes the turnover of a bacterial transcriptome.* Elife, 2016. **5**.

18. Peabody, D.S., *The RNA binding site of bacteriophage MS2 coat protein.* EMBO J, 1993. **12**(2): p. 595-600.

19. Stockley, P.G., et al., *Probing sequence-specific RNA recognition by the bacteriophage MS2 coat protein.* Nucleic Acids Res, 1995. **23**(13): p. 2512-8.

20. Schonberger, J., U.Z. Hammes, and T. Dresselhaus, *In vivo visualization of RNA in plants cells using the lambdaN(2)(2) system and a GATEWAY-compatible vector series for candidate RNAs.* Plant J, 2012. **71**(1): p. 173-81.

21. Kannaiah, S. and O. Amster-Choder, *Methods for studying RNA localization in bacteria.* Methods, 2016. **98**: p. 99-103.

22. Garcia, J.F. and R. Parker, *MS2 coat proteins bound to yeast mRNAs block 5' to 3' degradation and trap mRNA decay products: implications for the localization of mRNAs by MS2-MCP system.* RNA, 2015. **21**(8): p. 1393-5.

23. Tutucci, E., et al., *An improved MS2 system for accurate reporting of the mRNA life cycle.* Nat Methods, 2018. **15**(1): p. 81-89.

24. van Gijtenbeek, L.A., et al., *On the Spatial Organization of mRNA, Plasmids, and Ribosomes in a Bacterial Host Overexpressing Membrane Proteins.* PLoS Genet, 2016. **12**(12): p. e1006523.

25. Kremers, G.-J., et al., *Cyan and Yellow Super Fluorescent Proteins with Improved Brightness, Protein Folding, and FRET Förster Radius.* Biochemistry, 2006. **45**(21): p. 6570-6580.

26. Femino, A.M., et al., *Visualization of single RNA transcripts in situ.* Science, 1998. **280**(5363): p. 585-90.

27. Golding, I. and E.C. Cox, *RNA dynamics in live Escherichia coli cells.* Proc Natl Acad Sci U S A, 2004. **101**(31): p. 11310-5.

28. Hernandez-Tamayo, R., et al., *Symmetric activity of DNA polymerases at and recruitment of exonuclease ExoR and of PolA to the Bacillus subtilis replication forks.* Nucleic Acids Res., 2019. **47**(16): p. 8521-8536.

29. Rosch, T.C., et al., *Single molecule tracking reveals spatio-temporal dynamics of bacterial DNA repair centres.* Sci Rep, 2018. **8**(1): p. 16450.

30. Burghard-Schrod, M., S. Altenburger, and P.L. Graumann, *The Bacillus subtilis dCMP deaminase ComEB acts as a dynamic polar localization factor for ComGA within the competence machinery.* Mol. Microbiol., 2020. **113**(5): p. 906-922.

31. Schibany, S., et al., *Single molecule tracking reveals that the bacterial SMC complex moves slowly relative to the diffusion of the chromosome.* Nucleic Acids Res, 2018. **46**(15): p. 7805-7819.

32. Rösch, T.C., et al., *SMTracker: a tool for quantitative analysis, exploration and visualization of single-molecule tracking data reveals highly dynamic binding of B. subtilis global repressor AbrB throughout the genome.* Sci Rep, 2018. **8**(1): p. 15747.

33. Weimann, L., et al., *A quantitative comparison of single-dye tracking analysis tools using Monte Carlo simulations.* PLoS One, 2013. **8**(5): p. e64287.

34. Sawant, P., et al., *A dynamin-like protein involved in bacterial cell membrane surveillance under environmental stress.* Environ Microbiol, 2016. **18**(8): p. 2705-20.

35. Dempwolff, F., et al., *The deletion of bacterial dynamin and flotillin genes results in pleiotrophic effects on cell division, cell growth and in cell shape maintenance.* BMC Microbiol, 2012. **12**: p. 298.

36. Braig, D., et al., *Two cooperating helices constitute the lipid-binding domain of the bacterial SRP receptor.* J Mol Biol, 2009. **390**(3): p. 401-13.

37. Mayer, B., et al., *Dynamics of Bacterial Signal Recognition Particle at a Single Molecule Level.* Front Microbiol, 2021. **12**: p. 663747.

38. Dersch, S., et al., *Super-Resolution Microscopy and Single-Molecule Tracking Reveal Distinct Adaptive Dynamics of MreB and of Cell Wall-Synthesis Enzymes.* Front Microbiol, 2020. **11**: p. 1946.

39. Dominguez-Escobar, J., et al., *Processive movement of MreB-associated cell wall biosynthetic complexes in bacteria.* Science, 2011. **333**(6039): p. 225-8.

40. Reimold, C., et al., *Motion of variable-length MreB filaments at the bacterial cell membrane influences cell morphology.* Mol Biol Cell, 2013. **24**(15): p. 2340-9.

41. Yu, Y., et al., *The Min System Disassembles FtsZ Foci and Inhibits Polar Peptidoglycan Remodeling in Bacillus subtilis.* mBio, 2020. **11**(2).

42. Strahl, H. and L.W. Hamoen, *Membrane potential is important for bacterial cell division.* Proc Natl Acad Sci U S A, 2010. **107**(27): p. 12281-6.

43. Resch, M., et al., *Insight into the induction mechanism of the GntR/HutC bacterial transcription regulator YvoA.* Nucleic Acids Res, 2010. **38**(7): p. 2485-97.

44. Fleming, T.C., et al., *Dynamic SpoIIIE assembly mediates septal membrane fission during Bacillus subtilis sporulation.* Genes Dev, 2010. **24**(11): p. 1160-72.

45. El Najjar, N., et al., *Single-Molecule Tracking of DNA Translocases in Bacillus subtilis Reveals Strikingly Different Dynamics of SftA, SpoIIIE, and FtsA.* Appl Environ Microbiol, 2018. **84**(8).

46. Castellana, M., S. Hsin-Jung Li, and N.S. Wingreen, *Spatial organization of bacterial transcription and translation.* Proc Natl Acad Sci U S A, 2016. **113**(33): p. 9286-91.

47. Gualerzi, C.O. and C.L. Pon, *Initiation of mRNA translation in bacteria: structural and dynamic aspects.* Cell Mol Life Sci, 2015. **72**(22): p. 4341-67.

48. Katz, Z.B., et al., *Mapping translation 'hot-spots' in live cells by tracking single molecules of mRNA and ribosomes.* Elife, 2016. **5**.

49. Yan, X., et al., *Dynamics of Translation of Single mRNA Molecules In Vivo.* Cell, 2016. **165**(4): p. 976-89.

50. Akanuma, G., et al., *Inactivation of ribosomal protein genes in Bacillus subtilis reveals importance of each ribosomal protein for cell proliferation and cell differentiation.* J Bacteriol, 2012. **194**(22): p. 6282-91.

51. Rosenberg, A., et al., *Dynamic expression of the translational machinery during Bacillus subtilis life cycle at a single cell level.* PLoS One, 2012. **7**(7): p. e41921.

52. Sanamrad, A., et al., *Single-particle tracking reveals that free ribosomal subunits are not excluded from the Escherichia coli nucleoid.* Proc Natl Acad Sci U S A, 2014. **111**(31): p. 11413-8.

53. Sohmen, D., et al., *Structure of the Bacillus subtilis 70S ribosome reveals the basis for species-specific stalling.* Nat Commun, 2015. **6**: p. 6941.

54. Holscher, T., et al., *Impaired competence in flagellar mutants of Bacillus subtilis is connected to the regulatory network governed by DegU.* Environ Microbiol Rep, 2018. **10**(1): p. 23-32.

55. Furukawa, A., et al., *Tunnel Formation Inferred from the I-Form Structures of the Proton-Driven Protein Secretion Motor SecDF.* Cell Rep, 2017. **19**(5): p. 895-901.

56. Neef, J., et al., *Relative contributions of non-essential Sec pathway components and cell envelope-associated proteases to high-level enzyme secretion by Bacillus subtilis.* Microb Cell Fact, 2020. **19**(1): p. 52.

57. Lovgren, J.M., et al., *The PRC-barrel domain of the ribosome maturation protein RimM mediates binding to ribosomal protein S19 in the 30S ribosomal subunits.* RNA, 2004. **10**(11): p. 1798-812.

58. Bystrom, A.S. and G.R. Bjork, *Chromosomal location and cloning of the gene (trmD) responsible for the synthesis of tRNA (m1G) methyltransferase in Escherichia coli K-12.* Mol Gen Genet, 1982. **188**(3): p. 440-6.

59. Buxbaum, A.R., G. Haimovich, and R.H. Singer, *In the right place at the right time: visualizing and understanding mRNA localization.* Nat Rev Mol Cell Biol, 2015. **16**(2): p. 95-109.

60. Fei, J. and C.M. Sharma, *RNA Localization in Bacteria.* Microbiol. Spectr., 2018. **6**(5).

61. Kannaiah, S., J. Livny, and O. Amster-Choder, *Spatiotemporal Organization of the E. coli Transcriptome: Translation Independence and Engagement in Regulation.* Mol Cell, 2019. **76**(4): p. 574-589 e7.

62. Konkol, M.A., K.M. Blair, and D.B. Kearns, *Plasmid-encoded ComI inhibits competence in the ancestral 3610 strain of Bacillus subtilis.* J Bacteriol, 2013. **195**(18): p. 4085-93.

63. Jaacks, K.J., et al., *Identification and characterization of genes controlled by the sporulation-regulatory gene spo0H in Bacillus subtilis.* J Bacteriol, 1989. **171**(8): p. 4121-9.

64. Defeu Soufo, H.J. and P.L. Graumann, *Dynamic movement of actin-like proteins within bacterial cells.* EMBO Rep., 2004. **5**(8): p. 789-794.

65. Schindelin, J., et al., *Fiji: an open-source platform for biological-image analysis.* Nature Methods, 2012. **9**(7): p. 676-682.

66. Paintdakhi, A., et al., *Oufti: an integrated software package for high-accuracy, high-throughput quantitative microscopy analysis.* Mol Microbiol, 2016. **99**(4): p. 767-77.

67. Jaqaman, K., et al., *Robust single-particle tracking in live-cell time-lapse sequences.* Nat Methods, 2008. **5**(8): p. 695-702.

2.1.8 Supplementary material

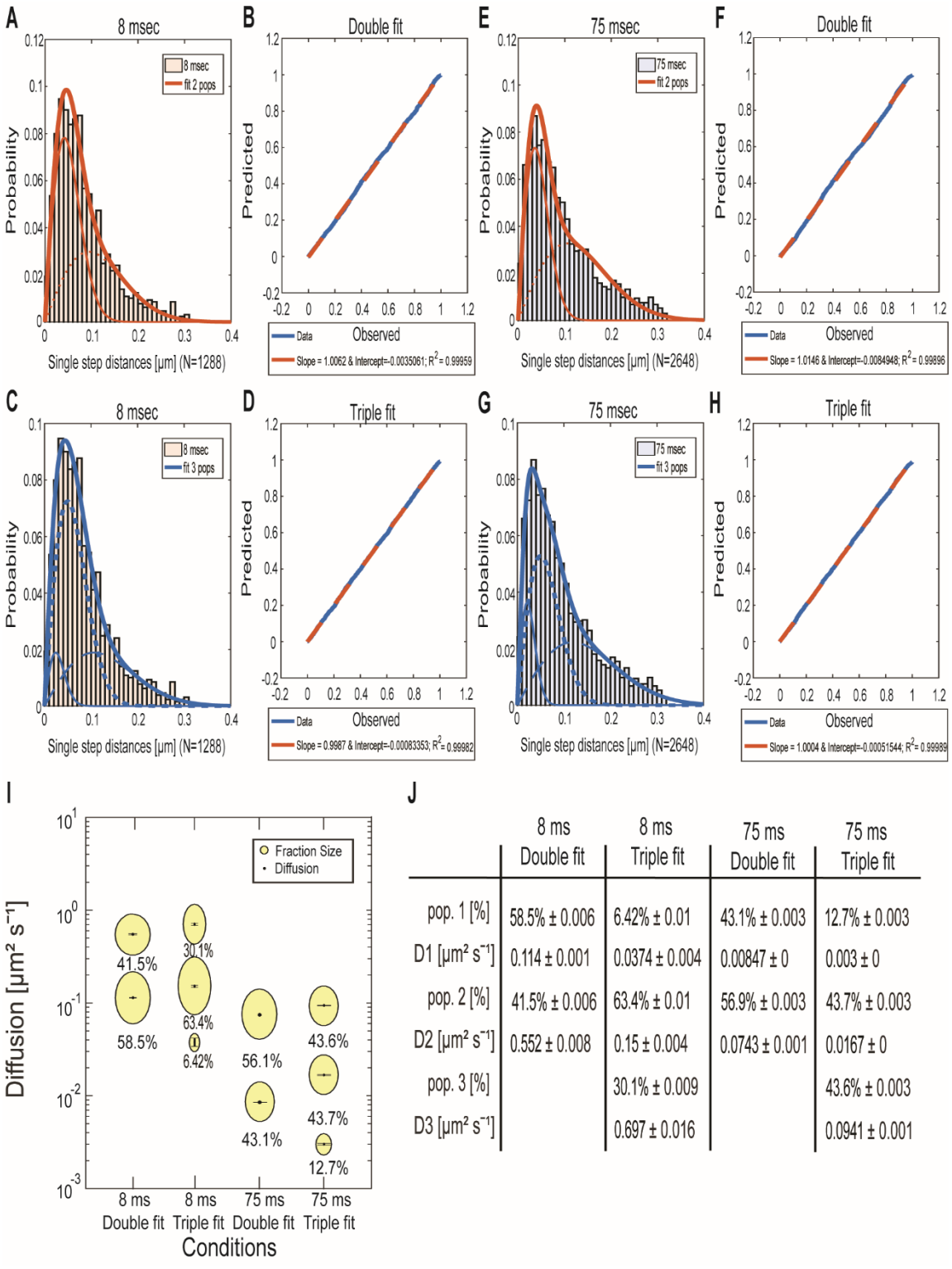

J

	8 ms Double fit	8 ms Triple fit	75 ms Double fit	75 ms Triple fit
pop. 1 [%]	58.5% ± 0.006	6.42% ± 0.01	43.1% ± 0.003	12.7% ± 0.003
D1 [µm² s⁻¹]	0.114 ± 0.001	0.0374 ± 0.004	0.00847 ± 0	0.003 ± 0
pop. 2 [%]	41.5% ± 0.006	63.4% ± 0.01	56.9% ± 0.003	43.7% ± 0.003
D2 [µm² s⁻¹]	0.552 ± 0.008	0.15 ± 0.004	0.0743 ± 0.001	0.0167 ± 0
pop. 3 [%]		30.1% ± 0.009		43.6% ± 0.003
D3 [µm² s⁻¹]		0.697 ± 0.016		0.0941 ± 0.001

Fig. S1 A minimum of two populations for MS2 protein are shown by the jump distance analysis.

JD analysis shows the distribution of the particles' displacements in a fixed time interval, plotted in a histogram (**A,C,E,G**). The probability-probability plots display the goodness of the

fit of predicted (red dotted lines) and measured data, shown with the blue solid lines (**B,D,F,H**). All triple fit models are shown in blue (**C,G**), double fits are depicted in red (**A,E**). Different dotted lines represent the subpopulations for a double or triple fit, while the solid lines represent the totality of the subpopulations. Double and triple fit, as well as the quantile-quantile plot in comparison to each other for the two different exposure times of the tracked MS2-mVenus fusion. (**A**) shows the double fit for the MS2 tag tracked with 8 ms exposure time and its belonging quantile-quantile plot (**B**). 75 ms is the other tested exposure time, with the double fit (**E**) and quantile-quantile plot (**F**). The triple fit for MS2-mVenus tracked with an exposure time of 8 ms (**C**), its quantile-quantile plot (**D**) and tracked with 75 ms exposure time (**G**) and its belonging quantile-quantile plot (**H**) are shown. For the determination of the diffusive coefficient and the fraction size, square displacement analysis (SQD) was used (**I**). The bubble plot shows the size of the fraction where each bubble is proportional to the area of its corresponding diffusion coefficients. Table (**J**) –displays SQD results - the shown data are the population sizes in % at its fixed, corresponding diffusion coefficient [$\mu m^2 s^{-1}$] for each condition.

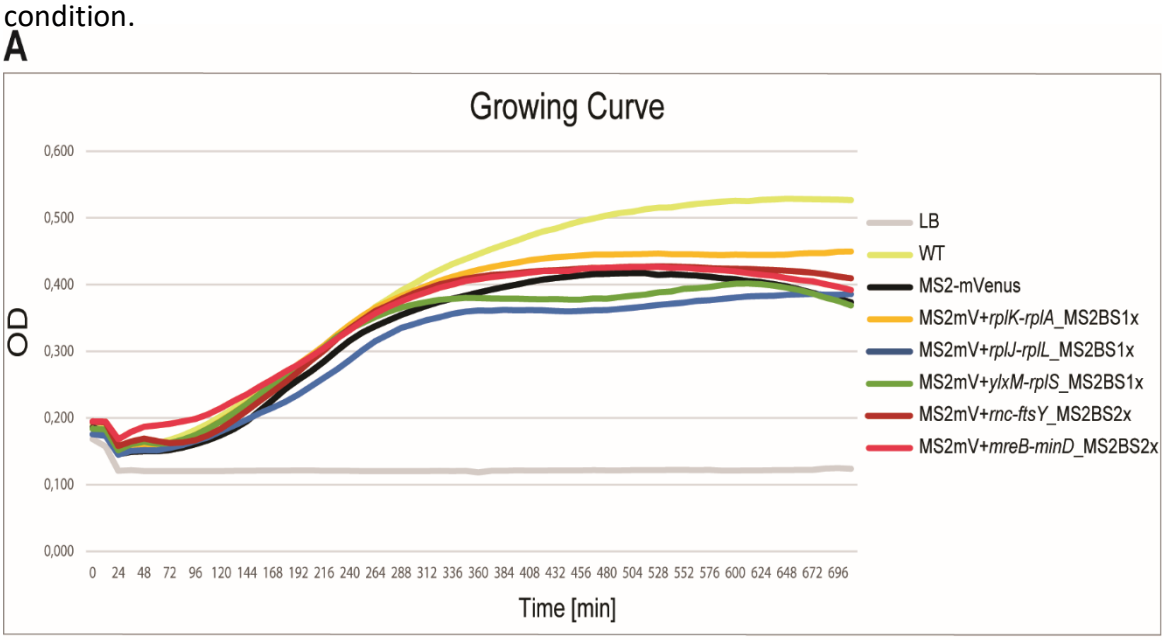

Fig. S2 Growth curves of constructs with the MS2-mVenus fusions.

Every 12 minutes, measurement of the optical density (OD) was done. For each condition, cells were grown in a 96 well plate with the rich media Luria-Bertani (LB). Each condition consists of a biological triplicate, done on three different days. Each replicate consists of eight technical replicates. The LB condition is growth media without cells, that acts as a control for the OD (in grey). WT is the other control for the growing behavior of *B. subtilis*, which consists of the *B. subtilis* wild type 3610 without any fusion, shown in yellow. MS2-mVenus is the MS2 coat

protein with a mVenus fusion, shown in black. Every mRNA construct consists also of the MS2-mVenus fusion. With one MS2-binding sites are the mRNAs MS2-mVenus +*rplK-rplA*_MS2BS1x (orange), MS2-mVenus + *rplJ-rplL*_MS2BS1x (blue) and MS2-mVenus + *ylxM-rplS*_MS2BS1x (green). With two MS2-binding sites are the mRNA constructs MS2-mVenus + *rnc-ftsY*_MS2BS2x (dark red) and MS2-mVenus + *mreB-minD*_MS2BS2x (red).

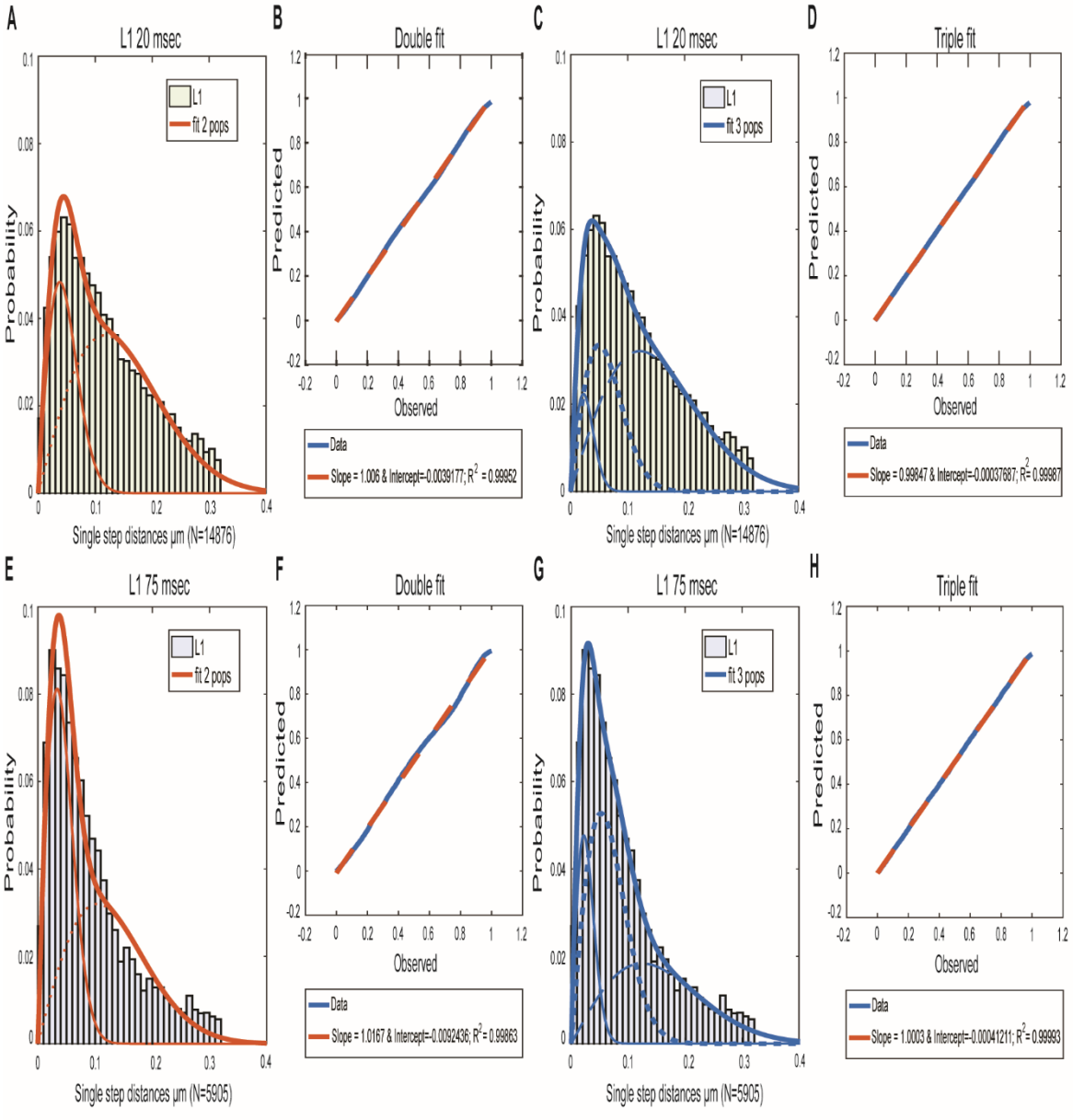

Fig. S3 Jump distance analysis of the tracked ribosomal protein L1 with two different exposure times.

Jump distance analysis shows the distribution of the particles' displacements in a fixed time interval, plotted in a histogram (**A,C,E,G**). The probability-probability plot displays the goodness of the fit of what is predicted (red dotted lines) and how the data actually behaves,

shown with the blue solid lines (**B,D,F,H**). All triple fit models are shown in blue (**C,G**), double fits are depicted in red (**A,E**). Different dotted lines represent the subpopulations for a double or triple fit, while the solid lines represent the totality of the subpopulations. Double and triple fit, as well as the quantile-quantile plot in comparison to each other for the three different exposure times of the tracked L1. (**A**) shows L1 tracked with 20 ms exposure time and its belonging quantile-quantile plot (**B**). For the tracking condition with 75 ms, the double fit (**E**) and the quantile-quantile plot (**F**) are shown. The triple fit for L1 tracked with an exposure time of 20 ms (**C**), its quantile-quantile plot (**D**), and tracked with 75 ms exposure time (**G**) and its quantile-quantile plot (**H**) are shown.

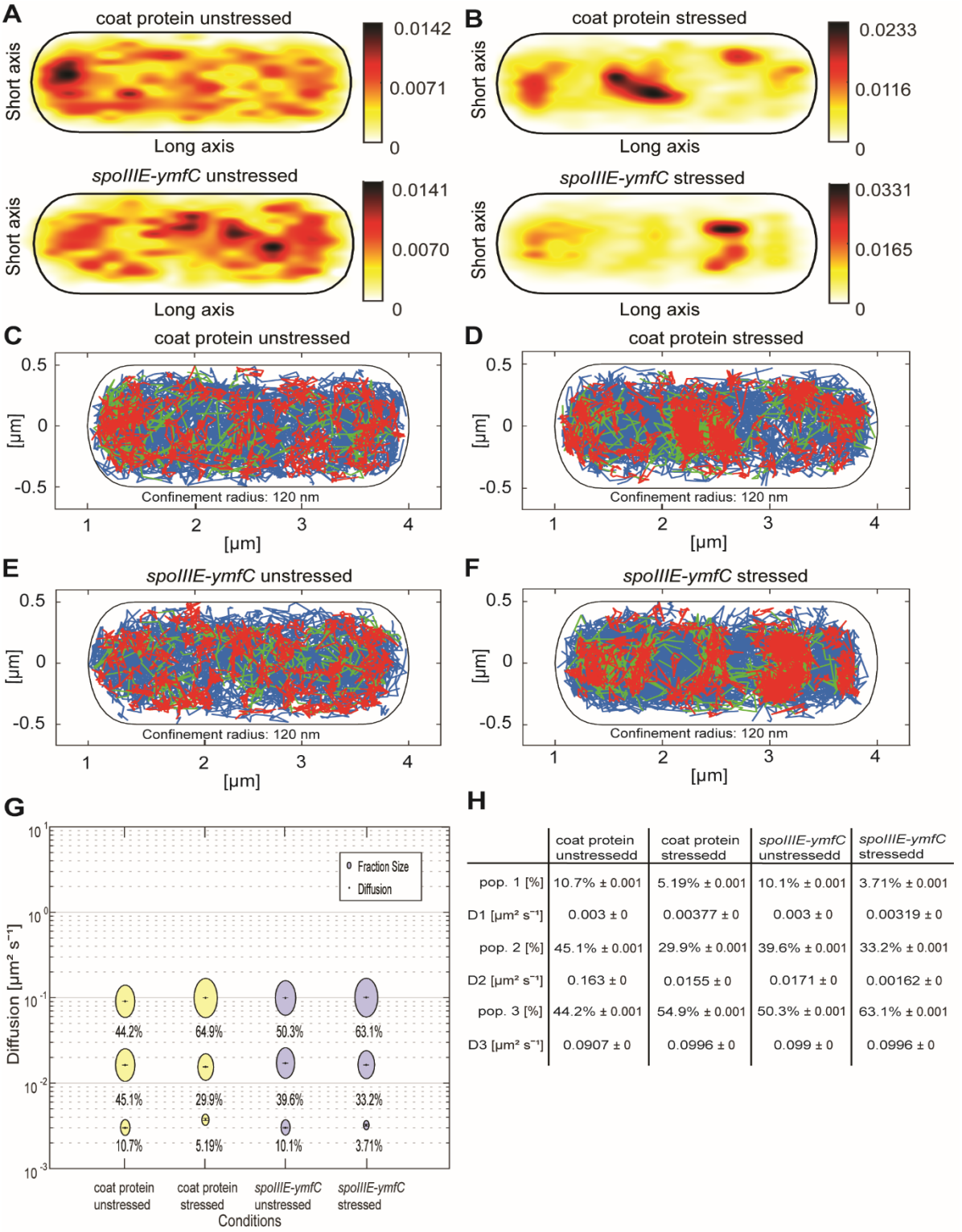

	coat protein unstressedd	coat protein stressedd	*spoIIIE-ymfC* unstressedd	*spoIIIE-ymfC* stressedd
pop. 1 [%]	10.7% ± 0.001	5.19% ± 0.001	10.1% ± 0.001	3.71% ± 0.001
D1 [µm² s⁻¹]	0.003 ± 0	0.00377 ± 0	0.003 ± 0	0.00319 ± 0
pop. 2 [%]	45.1% ± 0.001	29.9% ± 0.001	39.6% ± 0.001	33.2% ± 0.001
D2 [µm² s⁻¹]	0.163 ± 0	0.0155 ± 0	0.0171 ± 0	0.00162 ± 0
pop. 3 [%]	44.2% ± 0.001	54.9% ± 0.001	50.3% ± 0.001	63.1% ± 0.001
D3 [µm² s⁻¹]	0.0907 ± 0	0.0996 ± 0	0.099 ± 0	0.0996 ± 0

Fig. S4 Analysis of the coat protein and the mRNA *spoIIIE-ymfC* under Rifampicin stress.

For the stressed conditions, 25 µg/ml Rifampicin were added to the cells for 40 minutes. (**A-D**) In standardized cells of 1 x 3 µm, all tracks of the different fusions are projected. From white to red is the low to the high probability of distribution and spatial localization of the tracks represented for tracking with an exposure time of 75 ms for the (**A**) unstressed and (**B**)

stressed MS2-mVenus. (**C**) is the unstressed and (**D**) stressed mRNA MS2-mVenus + *spoIIIE-ymfC*_MS2-binding site 2x. (**E-H**) Also in standardized cells of 1 x 3 µm, all tracks of the two constructs are depicted. Blue represents free diffusive tracks, red are tracks that are restricted to a confined movement in a 120 nm circle with a minimum of 8 steps. In green are shown tracks with a mixed behavior between mobile and confined movement and vice versa. (**E**) is the MS2 tag MS2-mVenus without stress and in (**F**) under Rifampicin stress. (**G**) is the unstressed MS2-mVenus + *spoIIIE-ymfC*_MS2-binding site 2x and (**H**) the condition of the mRNA under Rifampicin stress. For the determination of the diffusive coefficient and the fraction size, square displacement analysis (SQD) was used (**I**). The bubble plot shows the size of the fraction where each bubble is proportional to the area of its corresponding diffusion coefficients. It can be distinguished between 3 populations, a static (lower bubbles), a slow mobile (middle bubbles) and a mobile (upper bubbles) fraction. In table (**J**) – another way to display the SQD results - the shown data are the population sizes in % at its fixed, corresponding diffusion coefficient [$\mu m^2 s^{-1}$] for each condition.

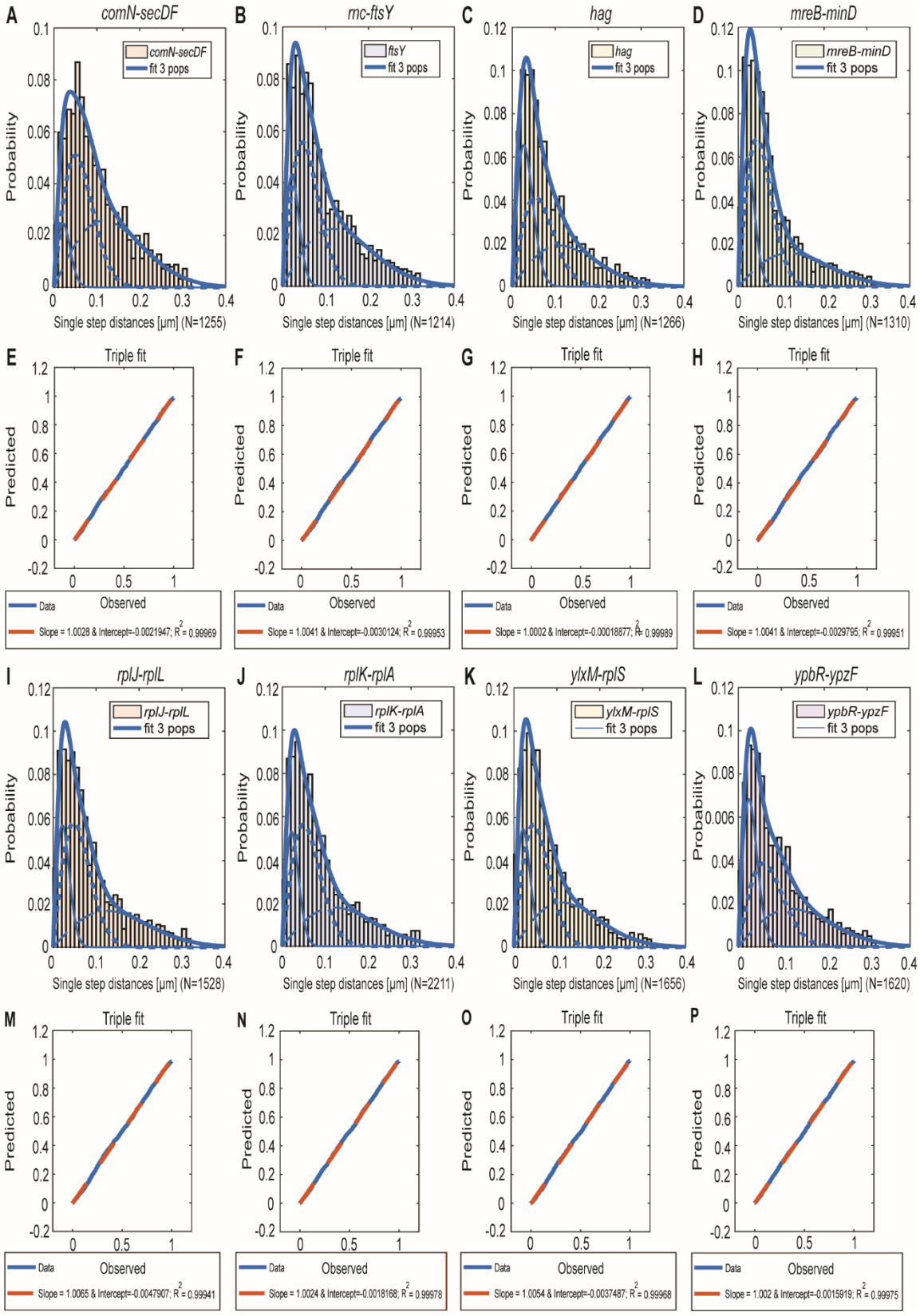

Fig. S5 Triple fit of eight different artificial mRNAs with one MS2-binding sites analysed with the jump distance analysis.

JD analysis shows the distribution of the particles' displacements in a fixed time interval, plotted in a histogram (**A-D,I-L**). The probability-probability plot displays the goodness of the

fit of what is predicted (red dotted lines) and how the data actually behaves, shown with the blue solid lines (**E-H,M-P**). All triple fit models are shown in blue. Different dotted lines represent the subpopulations for a triple fit, while the solid lines represent the totality of the subpopulations. The triple fit model of the jump distance analysis was chosen for all mRNAs: (**A**) MS2-mVenus + *comN-secDF*_MS2-binding site 1x and the belonging quantile-quantile plot (**E**), (**B**) MS2-mVenus + *rnc-ftsY*_MS2-binding site 1x and the belonging quantile-quantile plot (**F**), (**C**) MS2-mVenus + *hag*_MS2-binding site 1x and the belonging quantile-quantile plot (**G**), (**D**) MS2-mVenus + *mreB-minD*_MS2-binding site 1x and the belonging quantile-quantile plot (**H**), (**I**) MS2-mVenus + *rplJ-rplL*_MS2-binding site 1x and the belonging quantile-quantile plot (**M**), (**J**) MS2-mVenus + *rplK-rplA*_MS2-binding site 1x and the belonging quantile-quantile plot (**N**), (**K**) MS2-mVenus + *ylxM-rplS*_MS2-binding site 1x and the belonging quantile-quantile plot (**O**) and (**L**) MS2-mVenus + *ypbR-ypzF*_MS2-binding site 1x with its belonging quantile-quantile plot (**P**).

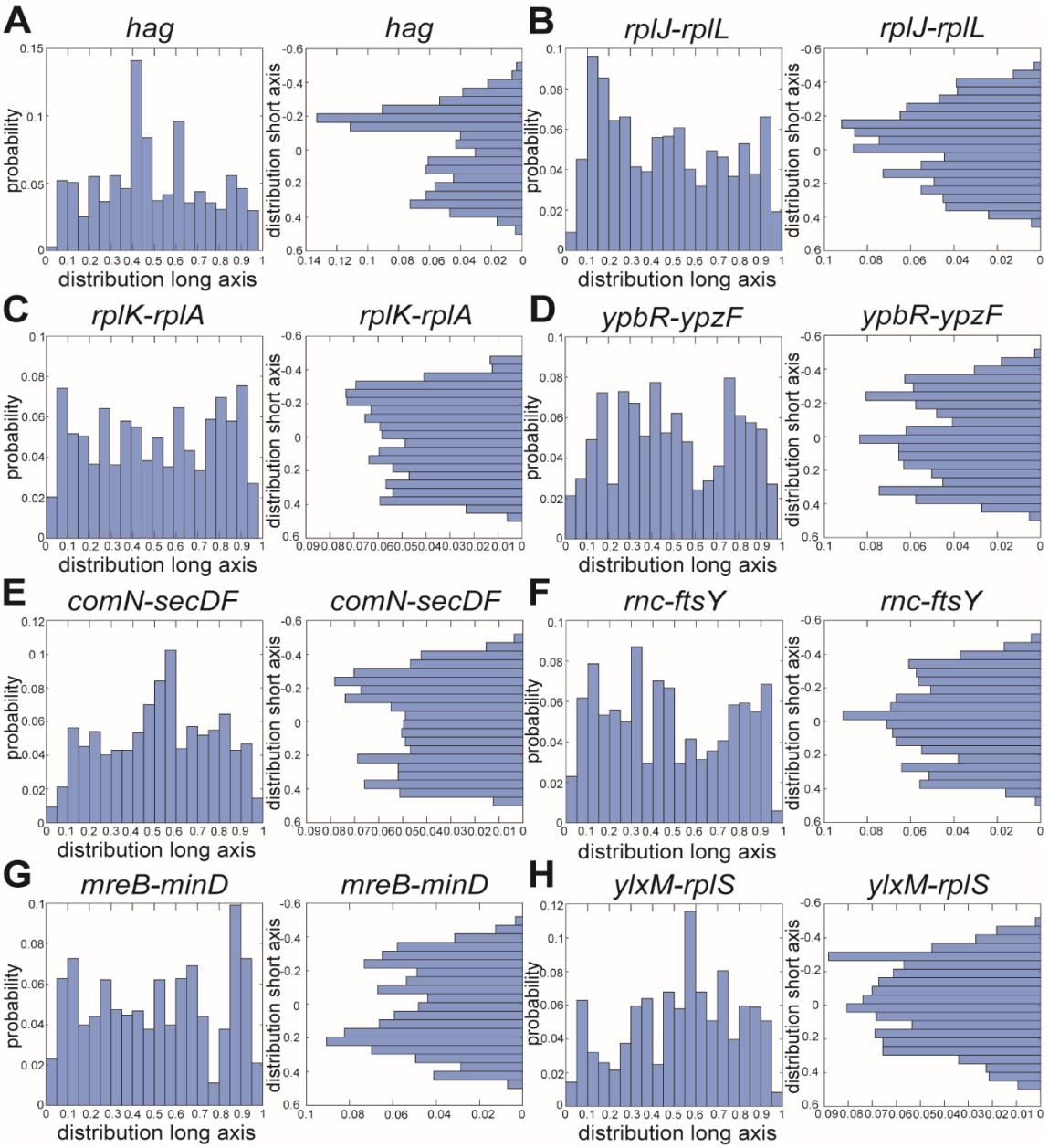

Fig. S6 Histogram of artificially extended mRNAs approximately 1700 bp longer than native mRNAs, with one MS2-binding site, show similar behavior to native mRNAs with two MS2-binding sites.

(**A-H**) Histograms showing the probability of molecule localization occurring along long (*x*) – or short (*y*) axis of cells. Histograms correspond to **Fig. 8I-P**.

(**A-D**) are mRNAs for soluble proteins, and (**E-H**) for membrane-associated or membrane proteins. (**A**) MS2-mVenus + *hag*_MS2-binding site 1x, (**B**) MS2-mVenus + *rplJ-rplL*_MS2-binding site 1x, (**C**) MS2-mVenus + *rplK-rplA*_MS2-binding site 1x, (**D**) MS2-mVenus + *ypbR-ypzF*_MS2-binding site 1x, (**E**) MS2-mVenus + *comN-secDF*_MS2-binding site 1x, (**F**) MS2-mVenus + *rnc-ftsY*_MS2-binding site 1x, (**G**) MS2-mVenus + *mreB-minD*_MS2-binding site 1x and (**H**) MS2-mVenus + *ylxM-rplS*_MS2-binding site 1x.

Table S1 Statistic of *B. subtilis* cells expressing MS2-system labelled mRNAs

A

	ypbR-ypzF	*rnc-ftsY*	*mreB-minD*	*spoIIIE-ymfC*
Cells	87	123	85	93
Cells with tracks	79	109	77	78
Tracks	297	651	245	263
Tracks per cell	4.08	5.41	3.28	3.59

B

	hag	*rplJ-rplL*	*rplK-rplA*	*ypbR-ypzF*	*comN-secDF*	*rnc-ftsY*	*mreB-minD*	*ylxM-rplS*
Cells	71	56	94	80	90	62	62	118
Cells with tracks	52	44	64	63	55	42	52	74
Tracks	110	136	190	150	133	113	123	158
Tracks per cell	2.12	3.06	2.50	2.62	1.94	2.63	2.38	2.00

(**A**) shows the statistics for the mRNAs with two MS2-binding sites, (**B**) are the artificial mRNAs with one MS2-binding site.

2.2 Article II

Assembly of *Bacillus subtilis* dynamin into membrane-protective structures in response to environmental stress is mediated by moderate changes in dynamics at a single molecule level

2.2.1 Abstract

Dynamin-like proteins are membrane-associated GTPases, conserved in bacteria and in eukaryotes, that can mediate nucleotide-driven membrane deformation or membrane fusion reactions. *Bacillus subtilis* DynA has been shown to play an important role in protecting cells against chemicals that induce membrane leakage, and to form an increased number of membrane-associated structures after induction of membrane stress. We have studied the dynamics of DynA at a single molecule level in real time, to investigate how assembly of stress-induced structures is accompanied by changes in molecule dynamics. We show that DynA molecule displacements are best described by the existence of three distinct populations, a static mode, a low-mobility and a fast-mobile state. Thus, DynA is most likely freely diffusive within the cytosol, moves along the cell membrane with a low mobility, and arrests at division sites or at stress-induced lesions at the membrane. In response to stress inducing membrane leakage, but not to general stress, DynA molecules become slightly more static, but largely retain their mobility, suggesting that only few molecules are involved in the repair of membrane lesions, while most molecules remain in a dynamic mode scanning for lesions. Our data suggest that even moderate changes in single molecule dynamics can lead to visible changes in protein localization patterns.

2.2.2. Introduction

Dynamins are a class of GTPases whose major function lies in the remodeling of biological membranes, most prominently in the mechanical, GTP-driven pinching off of membrane

vesicles. Other functions include organelle division and fusion of mitochondrial membranes [1]. Bacteria also contain dynamin-like proteins (DLP), whose functions lie in the involvement in bacterial cell division [2, 3] and response to membrane stress [4], likely in the resealing of holes in the membrane induced by chemical agents or phage evasion. Thus, the overarching scheme of dynamins are membrane fusion and fission [5].

Mechanochemical membrane remodeling involves different domains of dynamins, mediating membrane -binding and oligomerization, and GTP hydrolysis-driven conformational changes that can generate large membrane rearrangements [6]. In general, DLPs consist of a GTPase domain and a stalk domain, and often additional functional domains. The structure of a bacterial DLP has revealed a so-called paddle domain mediating binding to the lipid bilayer, and a conformational change upon GTP binding, resulting in bending and tabulation of membranes [7, 8]. Dimerization has also been shown to be important for membrane-binding.

DynA of *Bacillus subtilis* is one of the best studied members of the family of bacterial DLPs. Most bacteria contain two genes encoding for DLPs in an operon, whose products act as a heterotetramer [9]. In *B. subtilis*, there is only one gene, *ypbR,* but its corresponding DLP consist of two GTPase domains, with a low affinity to GTP, followed by a stalk and loop region [10]. Most likely, this gene has arisen through a gene duplication and fusion event.

Even though *B. subtilis* DynA binds to the membrane, it does not contain a transmembrane domain, like other heterotetrameric DLPs. Binding to and fusion of the membrane is accomplished by the two subunits, D1 and D2, which form intrinsic dimers and include the GTPase domain, stalk and loop. D1 might mediate the binding to the membrane, which is independent of nucleotide-binding, and also seems to be responsible for tethering together membranes. For this activity, DynA of *B. subtilis* needs Mg^{2+} to hydrolyse GTP [11]. D2 on the other hand seems to be more of a supporter for fusion and plays only a minor role for binding to the membrane. At the same time, it seems to be necessary for the stability of the binding and cluster formation at the membrane [12]. DynA might also interact with other proteins via its subdomains D1 and D2, and together with them may lead to membrane fusion [12, 13].

B. subtilis DynA has been shown to be present at the division septum, but also at sites along the lateral cell membrane [3]. After induction of membrane leakage, DynA foci increase in number at the cell membrane [4]. Importantly, a *dynA* deletion leads to sensitivity of cells towards membrane stress, most pronounced against agents that induce membrane leakage,

suggesting that dynamin mediates resealing of holes in the cell membrane [4]. A *dynA* deletion strain also acerbates the cell division phenotype of a *divIB* deletion [3], indicating that dynamin may also aid in membrane fusion of the invaginating division septum.

In this work, we wished to further characterize *B. subtilis* dynamin by studying its motion at a single molecule level and to analyze how the assembly of membrane-associated fluorescent foci of a functional DynA-fluorescent protein fusion is brought about by changes of molecule motion. We show that the dynamics of DynA can be best explained by assuming three populations of molecules with distinct diffusion coefficients. Induction of membrane stress and accompanying increase in membrane-associated assemblies are accompanied by only small changes in the size of DynA molecule populations, showing that visible rearrangements of proteins in a bacterial cell can be achieved by only small changes at a single molecule level.

2.2.3 Results

2.2.3.1 A DynA-mVenus fusion forms an increased number of foci in response to chemical inducing membrane leakage

We have previously shown that DynA-GFP accumulates at sites of cell division, but can also form visible foci at the cell membrane away from the division site [3]. The Bramkamp group has found that addition of Nisin, which induces membrane leakage for ions, induces the formation of fluorescent foci at the cell membrane [4]. Because DynA plays a protective role during membrane stress [4], we wished to investigate if other environmental stresses might lead to an accumulation of DynA at the membrane, and treated cells with different chemical and physical stresses. **Fig. 1A** shows that only a minority of exponentially growing cells (26%, Fig. 1B) showed fluorescent foci, predominantly close to mid cell (septal area) and at the cell poles and that the number of cells with foci was similar during heat and ethanol stress. However, as quantified in **Fig. 1B**, osmotic stress (sorbitol), osmotic and ionic stress (NaCl) and membrane stress (Nisin) lead to a large increase in the number of cells with foci, especially under Nisin and NaCl conditions. Compared with exponentially growing cells, where 25% contained a single focus and 1% several foci, 63% of Nisin-treated cells contained a single focus and 26% several foci; a total of 50% of cells treated with Sorbitol contained DynA-mV signals, and 86% of salt-treated cells (**Fig. 1B**). Following Nisin treatment, the ratio of signals at the

septum, the cell poles or the lateral membrane changed considerably, from roughly one third for each position (many places at the lateral cell membrane defining a "position") to 70% lateral membrane at the expense of septal and polar localization (**Fig. 1B**). These findings are in agreement with data from the Bramkamp laboratory showing a strong increase in membrane-associated foci after treatment with Nisin [4], and might imply that DynA assembles into visible structures after many kinds of stresses.

A

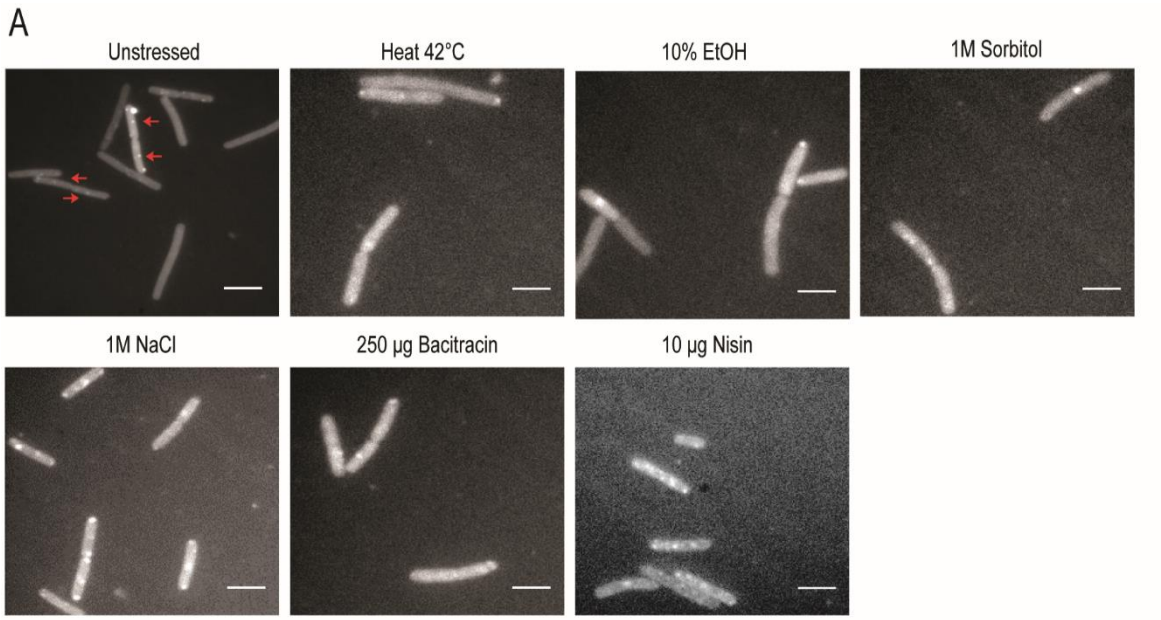

B

	unstressed	%	Heat 42°C	%	10% EtOH	%	1M Sorbitol	%	1M NaCl	%	250 µg Bacitracin	%	10 µg Nisin	%
cells total	302		123		132		54		155		351		391	
cells without *focus*	222	73.51	72	58.54	99	75.00	27	50.00	22	14.19	206	58.69	46	11.76
cells with one *focus*	76	25.17	45	36.59	27	20.45	24	44.44	104	67.10	138	39.32	245	62.66
cells with more than one *focus*	4	1.32	6	4.88	6	4.55	3	5.56	29	18.71	7	1.99	100	25.58
total number of *foci*	84		57		39		30		166		153		433	
pole	28	33.33	18	31.58	12	30.77	12	40.00	74	44.58	67	43.79	75	17.32
septum	26	30.95	24	42.11	16	41.03	12	40.00	43	25.90	26	16.99	56	12.93
membrane	30	35.71	15	26.32	11	28.21	6	20.00	49	29.52	60	39.22	302	69.75

Fig. 1 Epifluorescence analysis of DynA-mVenus foci arising in response to different stress conditions.

(**A**) YFP channels showing unstressed with foci mostly found at the septum, heat stressed cells (42°C), or cells after addition of 10% ethanol (EtOH), 1 M Sorbitol, 1 M NaCl, 250 µg Bacitracin,

or 10 µg Nisin. Cells were incubated for 30 minutes for each stress condition. Scale bar 2 µm. (**B**) shows the total number of counted cells for each condition, numbers of cells with or without *foci*, which can be also more than one *focus* per cell, and where they were localized. "membrane" refers to *foci* found at the cell membrane except for mid-cell ("septum") or at the cell poles ("pole").

2.2.3.2 DynA moves as three distinct fractions of mobility within cells

Because epifluorescence microscopy can only detect larger, static assemblies of molecules, but not diffusive molecules, we employed single molecule tracking to obtain more quantitative information on changes of DynA mobility. We investigated the dynamics of single DynA-mVenus molecules using "slim-field" illumination and bleaching of most fluorescent proteins until single molecules remain visible that can be efficiently tracked in real time [14-16]. We have previously shown that this approach leaves cells physiologically largely intact and harms them only to a small degree [17, 18]. We obtained an average track length of about 8 steps, and used tracks of 5 steps and longer for the analyses of diffusion constants and possible existence of several distinct populations of molecules using squared displacement analysis (SQD). **Fig. 2** shows jump distance (JD) evaluation of SQD data, indicating that the observed step size distributions can be best explained assuming 3 distinct populations (**Fig. 2A**), leaving almost no residuals when comparing observed data and modeled data (**Fig. 2B**). When only 2 populations are used (**Fig. 2C**), observed jump distances cannot be fully covered, and residuals remain in panel **D**, where the blue line deviates visibly from the dotted red line representing the modelled data. Although we do not want to overinterpret our data, we will continue assuming three diffusive populations, and will return to the idea of the existence of only two populations in the discussion section. For three population fits, we obtained the following diffusion constants (DC) and population sizes for DynA molecules in unstressed cells, using SMTracker 2.0: 15% of the molecules had a DC of 0.015 $\mu m^2 s^{-1}$, about 50% showed a DC of 0.122 $\mu m^2 s^{-1}$, and the fastest population of about 35% showed a DC of about 0.9 $\mu m^2 s^{-1}$ (**Fig**. **3A,B**). The later DC is characteristic of large cytosolic proteins [19, 20], while that of 0.15 $\mu m^2 s^{-1}$ reflects a rather static molecule, bound to a much larger structure, such as a ribosome [21]. Thus, 15% of DynA molecules appear to be statically positioned within a larger subcellular structure, while 35% are freely diffusive. We will come back to this point later, when we consider the spatial distribution of static and diffusive molecules. Taking into account the

findings that DynA is involved in the cell division process and is frequently observed at the septal area (see also **Fig. 2A**), a fraction of the static DynA molecules is likely bound to the Z-ring containing a variety of cell division proteins. If DynA indeed diffuses as three distinct fractions, the medium-mobile fraction might be molecules attached to the membrane, which would be expected to diffuse somewhat slower than cytosolic proteins, or molecules in a (pre) complex of an intermediate size. With the setup used, we cannot determine if molecules move along the membrane or within the cytosol, so the idea of an intermediate, membrane-associated DynA fractions remains a hypothesis.

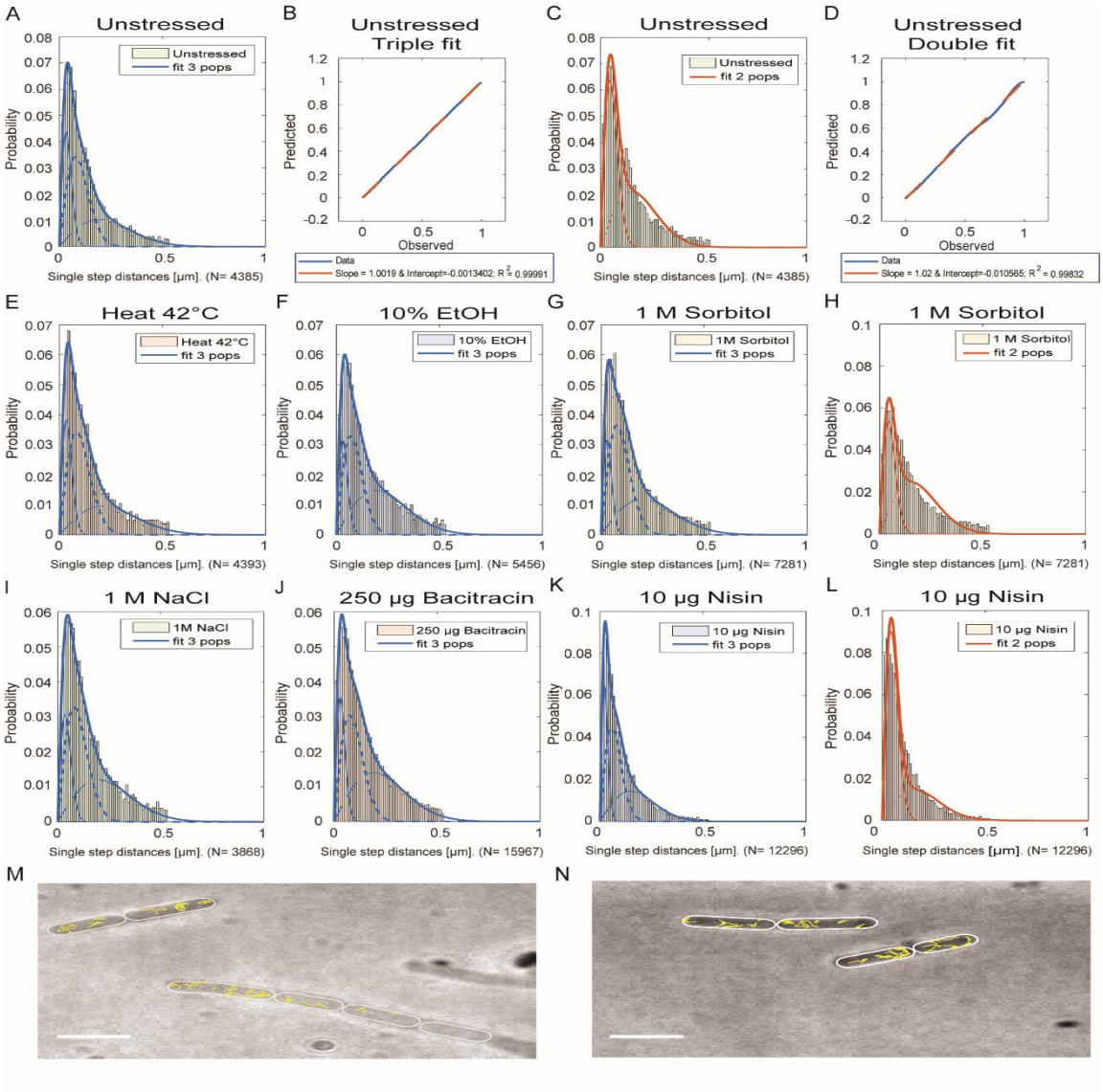

Fig. 2 Jump distance analysis (JD) of DynA-mVenus, showing the distribution of particle displacements in a fixed time interval, plotted in a histogram (A+C+E-L).

The quantile-quantile plots visualize the goodness of the fits, by comparing differences (blue line) between modelled (dashed line) and observed data (**B+D**). (**A**) Unstressed triple fit, (**B**)

quantile-quantile plot of the unstressed triple fit, (**C**) unstressed double fit, (**D**) quantile-quantile plot of the unstressed double fit. Because the data implicates a triple fit is the better option, the following conditions were analysed with a triple fit: (**E**) 42°C, (**F**) 10% EtOH, (**G**) 1M sorbitol, (**I**) 1M NaCl, (**J**) 250 µg Bacitracin, (**K**) 10 µg Nisin. In addition, double plots for the conditions 1M sorbitol (**H**) and 10 µg Nisin (**L**) are shown, to proof the usage of the better suited triple fit. Tracks of DynA under no stress are shown in yellow (**M, N**). Scale bar 2 µm.

To a first approximation, the JD distribution did not change markedly between exponentially growing cells and stressed cells (compare **Fig. 2A** with **2E** to **I**), except for Nisin-treated cells, in which JD visibly shifted left, towards slowed distances (**Fig. 2J**, compare with **2A**). This implies that DynA molecules have lower diffusion constants after treatment with Nisin. We quantified the percentage of molecules from the different diffusive populations and found slightly different values for DC for each condition, as well as different population sizes (data not shown). In order to better compare changes, we kept DC values constant (in fact, DCs were determined to best fit for all conditions), such that changes in molecule dynamics were only reflected in changes on population size. The bubble plot in **Fig. 3A** shows that heat stress led only to a marginal increase of the fast-mobility fraction, while ethanol treatment led to a roughly 30% increase in this fraction, at the expense of the medium-mobile fraction. Sorbitol treatment reduced the static fraction from 15 to 11.3% (i.e. relatively by about 25%), and enlarged the fast-mobility fraction by 24%. The strongest decrease in static molecules was observed after addition of sodium chloride, accompanied by an increase in the fast-mobile fraction. Also following Bacitracin treatment, DynA molecules became somewhat more mobile, however, as for the other stress conditions, this effect was not dramatic. Conversely, after the addition of Nisin, the size of the static fraction, assumed to be DynA molecules engaged in cell division or in repair of membrane damage, almost doubled, while the number of highly mobile molecules strongly decreased (**Fig. 3A**). These data support the idea of a specific Nisin-induced effect on DynA dynamics, and suggest that changes observed by the other stress conditions are likely more unspecific. However, although DynA provides protection for the cell against Nisin treatment, overall changes in the whole DynA molecule population are not profound, at least not as large as we would have expected. Only about 13% of all molecules move from a more mobile into a static mode, which we assume is the active form of DynA.

A

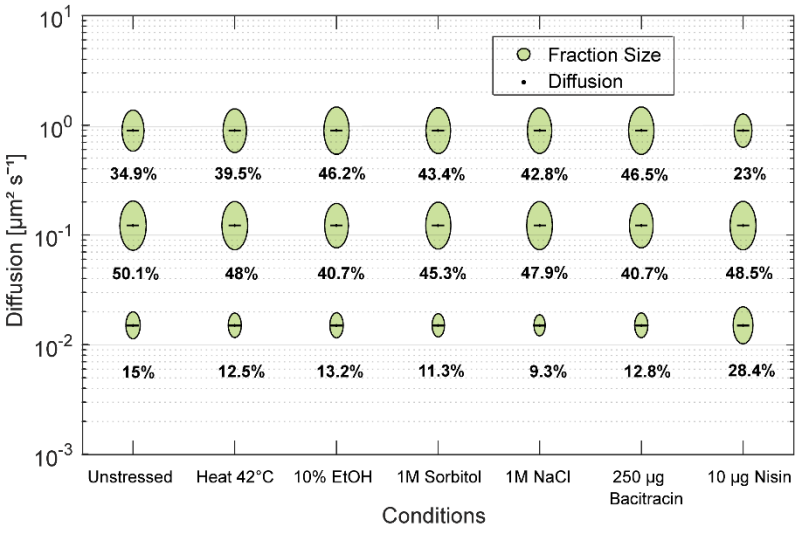

B

	Unstressed	Heat 42°C	10% EtOH	1M Sorbitol	1M NaCl	250 µg Bacitracin	10 µg Nisin
pop. 1 [%]	15 ± 0.002	12.5 ± 0.002	13.2 ± 0.002	11.3 ± 0.002	9.3 ± 0.002	12.8 ± 0.002	28.4 ± 0.002
D1 [µm² s⁻¹]	0.015 ± 0	0.015 ± 0	0.015 ± 0	0.015 ± 0	0.015 ± 0	0.015 ± 0	0.015 ± 0
pop. 2 [%]	50.1± 0.002	48 ± 0.002	40.7 ± 0.002	45.3 ± 0.002	47.9 ± 0.002	40.7 ± 0.002	48.5 ± 0.002
D2 [µm² s⁻¹]	0.122 ± 0.001	0.122 ± 0.001	0.122 ± 0.001	0.122 ± 0.001	0.122 ± 0.001	0.122 ± 0.001	0.122 ± 0.001
pop. 3 [%]	34.9 ± 0.002	39.5 ± 0.002	46.2 ± 0.002	43.4 ± 0.002	42.8 ± 0.002	46.5± 0.002	23 ± 0.002
D3 [µm² s⁻¹]	0.898 ± 0.008	0.898 ± 0.008	0.898 ± 0.008	0.898 ± 0.008	0.898 ± 0.008	0.898 ± 0.008	0.898 ± 0.008

Fig. 3 Analysis of the dynamics of DynA-mVenus under different stress conditions.

For the determination of the diffusion coefficients (DC) and the fraction sizes, SQD analyses with simultaneous fits for all conditions was used. This leads to the determination of a single value for D that fits best to all conditions, in order to allow for a better comparison of changes in population sizes. (**A**) The bubble plot shows the size of the fraction where each bubble is proportional to the area of its corresponding diffusion coefficients. In table (**B**) population 1 ("pop 1") refers to D1, and other sizes accordingly. Note that standard errors refer to fitting errors, not to differences between the biological triplicates, whose data were pooled for the analyses.

2.2.3.3 Stress conditions lead to visible changes in DynA localization and mobility

In order to further investigate changes in the localization and mobility of DynA, we generated heat maps, in which tracks from all cells are projected into a medium-sized cell and are displayed for frequent or infrequent presence. **Fig. 4A** shows a slight tendency for DynA to be present close to the cell membrane (**Fig. 4B** is a two-fold mirrored heat map), but even the frequent foci observed at the division site (**Fig. 1A**) do not shift this preference to the cell center. These data suggest that DynA molecules are distributed throughout the cell, i.e. within

the cytosol and at the membrane. Heat and Sorbitol stress induced an accumulation of DynA at the subpolar regions (**Fig. 4C/D**, and **G/H**), which might be due to some molecule aggregation due to un - or misfolding during heat or osmotic shock. Please note that heat maps were not normalized to each other because of the strong subpolar signals observed after heat and osmotic stress induction. Heat maps of ethanol, sodium chloride, and bacitracin stress did not induce any clear changes (**Fig. 4E/F, I/J** and **K/L**). Conversely, DynA molecules showed a higher preference towards membrane-proximal accumulation following Nisin treatment (**Fig. 4M,N**).

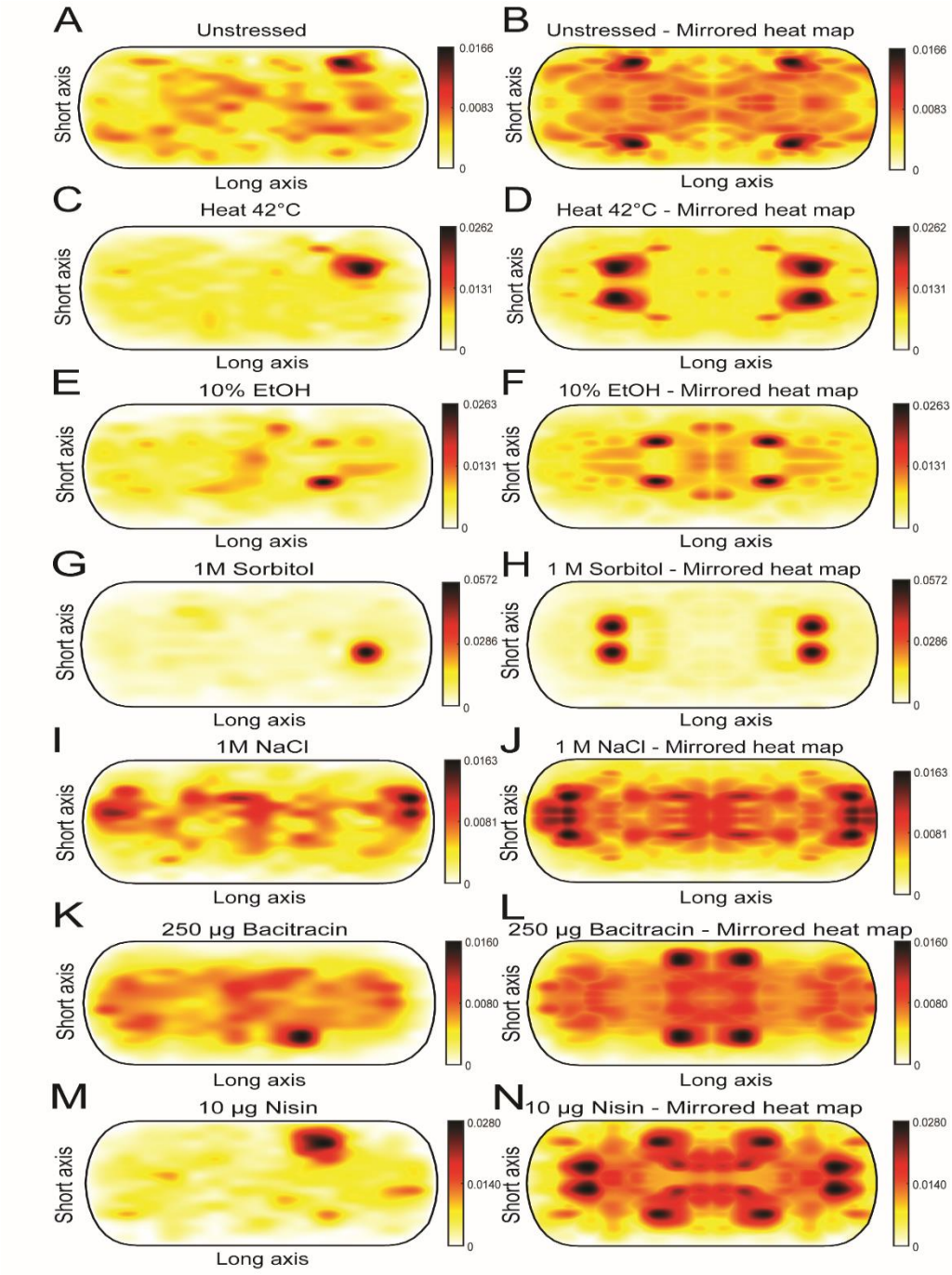

Fig. 4 Localization of Dyna-mVenus tracks under different stress conditions.

All tracks of one condition were projected into a standardized/medium size cell of 1 x 3 µm (**A,C,E,G,I,K,M**). In addition, mirrored heat maps, where the axes are mirrored, are shown, displaying symmetric localization of the diffusion molecules of DynA-mVenus (**B,D,F,H,J,L,N**). From white, via yellow to red is the low to high probability of distribution of the tracks. (**A**) Unstressed, (**B**) unstressed mirrored, (**C**) 42°C, (**D**) 42°C mirrored, (**E**) 10% EtOH, (**F**) 10% EtOH mirrored, (**G**) 1 M Sorbitol, (**H**) 1 M Sorbitol mirrored, (**I**) 1 M NaCl, (**J**) 1 M NaCl mirrored, (**K**) 250 µg Bacitracin, (**L**) 250 µg Bacitracin, (**M**) 10 µg Nisin, and (**N**) 10µg Nisin.

We also generated “confinement maps”, in which molecules showing little displacement for an extended time (confined motion) and freely diffusing molecules are displayed in a standardized cell. This analysis must not be confused with SQD analyses, because molecules with a low diffusion constant do not necessarily represent those showing confined motion for some time, although these two parameters will strongly overlap, and the analysis does not distinguish between e.g. populations of medium- or of high-mobility. For confinement maps, we used a radius of 120 nm (about three times the localization error in the setup) and defined confinement as molecules remaining within this radius for at least 8 time intervals. **Fig. 5** shows that during exponential growth (**Fig. 5A**), confined motion (red tracks) occurred throughout the cell, and frequently close to the cell membrane. The distribution of tracks along the length of cells (long-axis, or x-axis) is shown in **Fig. 5H**, left panel, distribution along the width (short/y axis) in **Fig. 5H**, right panel. Sorbitol and heat stress induced subpolar areas of increased confined motion (best seen in **Fig. 5I** and **K**, long axis), possibly reflecting places of enhanced protein aggregation. For ethanol sodium chloride and Bacitracin treatment, no clear changes were observed. Nisin treatment induced the strongest change in spatial dynamics, in that confined motion was observed in larger areas at the lateral cell membrane (**Fig. 5G**) including stronger signals at the cell poles (**Fig. 5N**, long axis), compared with unstressed cells (**Fig. 5A,H**). Accumulation of confined tracks at the poles changes the localization along the short cell axis seemingly away from the membrane (**Fig. 5N**, right panel, compare with **5H**). Additionally, transitions between confined motion and free diffusion, indicated by green tracks, was visibly increased following Nisin induced stress. The appearance of larger areas of confined motion after treatment with Nisin likely reflects the increased induction of foci seen in **Fig. 1**.

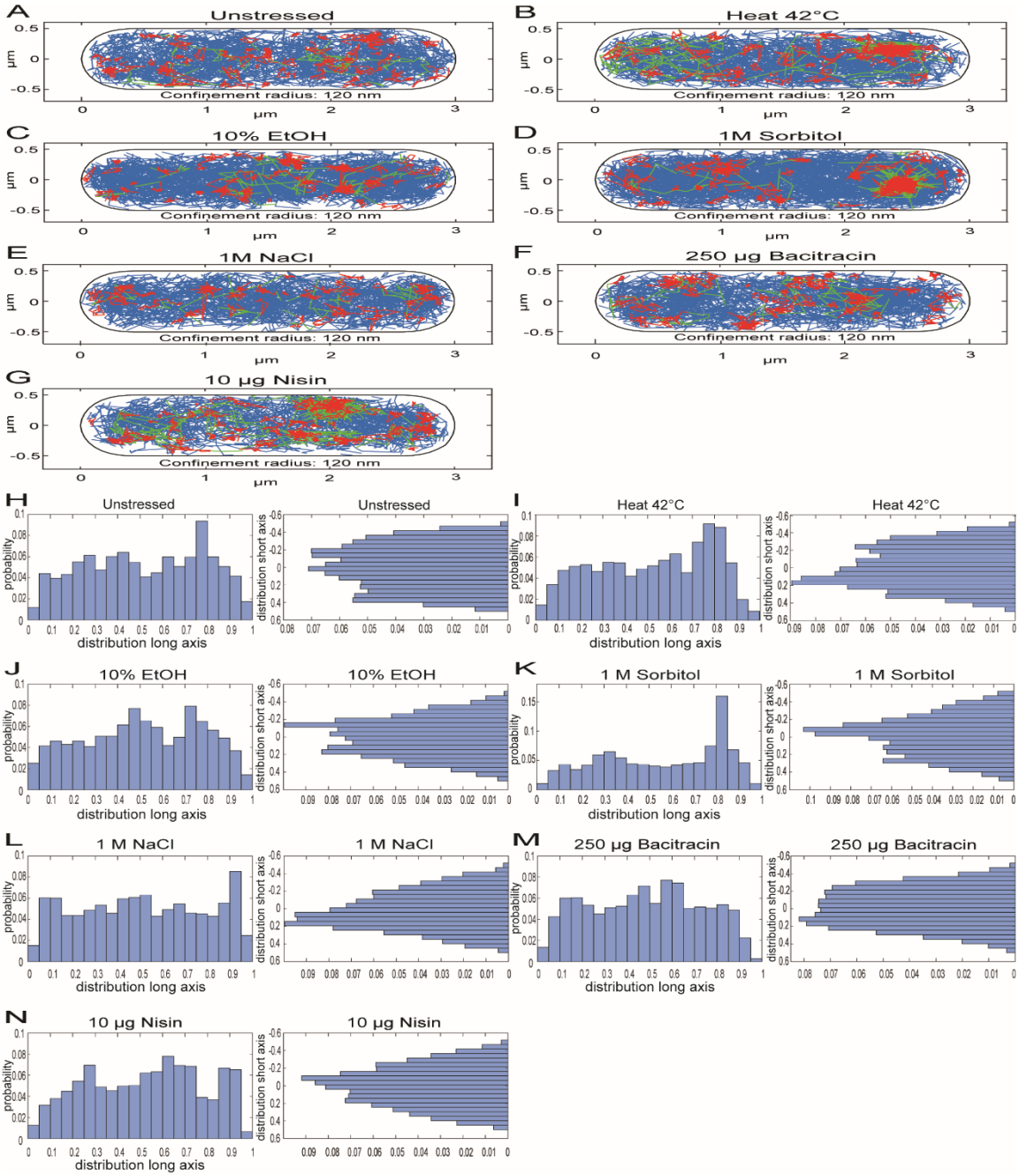

Fig. 5 Confined movement maps of DynA-mVenus under different stress conditions.

To visualize confined movement of DynA molecules, a radius of 120 nm was set in a standardized cell of 1 x 3 µm (**A-G**). A minimum of 8 steps was taken to indicate confined motion, shown in red. Freely diffusive tracks are shown in blue, mixed behavior between mobile and confined motion in green. (**A**) Unstressed, (**B**) 42°C, (**C**) 10% EtOH, (**D**) 1M sorbitol, (**E**) 1M NaCl, (**F**) 250 µg Bacitracin, (**G**) 10 µg Nisin. Histograms showing probability of molecule localization along long (*x*) – or short (*y*) axis of cells (**H-N**). Histograms correspond to panel (**A-G**).

2.2.3.4 Nisin-induced membrane stress leads only to a mild increase in dwell times of DynA

SQD analyzes for the dynamics, as well as heat and confinement maps for the localization, have shown that nisin addition leads to the clearest change in the behavior of DynA. The same is true when having a look at the residue time of DynA molecules. **Fig. 6** shows two possible fits for the molecules, which stay for a period of at least 8 time points within a radius of 120 nm. One-component fit with τ of 0.22 seconds fits well for DynA from non-stressed cells (**Fig. 6A**). The single decay curve already includes most of the data. Even if we assume two populations, the dwell times of τ_1 with 0.17 seconds and τ_2 with 0.23 seconds are close to each other. Note that due to molecule bleaching during acquisition, actual dwell times will be higher in cells, but for comparing dwell times between different conditions, estimates are sufficiently accurate. Around 88 ± 20% are included in τ_2, while the other 12 ± 20% belong to τ_1. This suggests that there is only one population of DynA molecules that arrests in motion for a considerable time. In comparison, the addition of nisin leads to two distinguish populations (**Fig. 6B**). The one-component fit does not include the whole data, while the two-component fit does. While τ_1 is with 0.18 seconds similar to the unstressed one, τ_2 increased strongly, to 0.35 seconds. This longer dwelling event occurred for roughly half of the molecules (48 ± 3.7%). Thus, we can assume that under nisin stress, there is a population which has a shorter average dwelling time (τ_1) similar to unstressed cells, while the long dwelling events (τ_2) refer to DynA molecules in the membrane that repair nisin-induced damage. Of note, the static population of molecules seen with SQD analyses of DynA, which almost doubled under nisin stress, will largely overlap with the population of molecules showing long dwelling events, but is not necessarily identical. Likewise, the population showing shorter dwell events likely conforms with the intermediate and fast populations in the SQD analysis, although even freely diffusive molecules can arrest for a short period of time. A single decay curve and thus a single average dwell time was also found for the other stress conditions, with no significant difference to the dwell time of exponentially growing cells (data not shown) compared to unstressed cells, except for bacitracin treatment (**Fig. 6C**), where two decay curves were determined, as well as a slightly higher dwell time for τ_2 of 0.28 seconds for half of the molecules (50 ± 9.1%). τ_1 on the other hand was similar to the Nisin-stressed condition with 0.22 seconds.

Thus, although a direct comparison of the SQD data with the dwell times cannot be made, it can be said that with both tools we are able to detect static DynA molecules. In both

models, under Nisin stress, DynA becomes more static and a clear difference in its single molecule dynamics can be seen. While with SQD analysis, a transition to a more static behavior under bacitracin stress was not apparent, the change in the dwelling events suggests that also under this condition DynA is recruited to the membrane, and induces membrane repair assemblies.

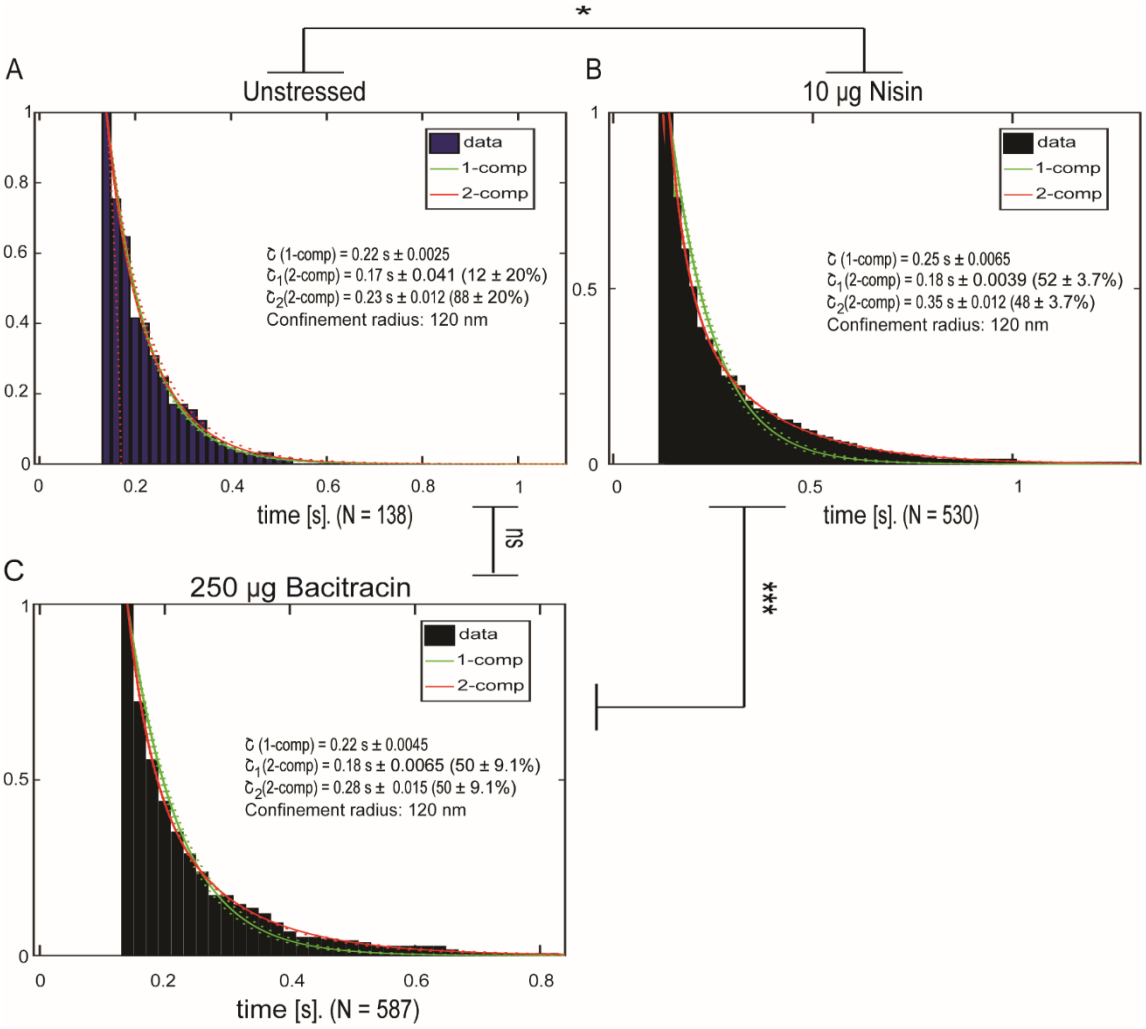

Fig. 6 Nisin stress leads to longer dwelling events.

The length of time of DynA molecules residue in a 120 nm circle for a minimum of 8 time points is shown for the unstressed condition (**A**), under 10 µg/ml Nisin stress for 30 minutes (**B**) and under 250 µg/ml Bacitracin stress for 30 minutes (**C**). τ describes the dwelling event for a one-component fit in green and τ_1 and τ_2 for a two-component fit in red. The average duration for the dwelling event is shown in seconds, while the amount of how many molecules residue in the defined circle of 120 nm with a minimum of 8 steps is depicted in percentage. Significant differences between the conditions are shown by * (α = 0,1),*** (α = 0,01) and ns (not significant).

2.2.4 Discussion

Bacterial cells have traditionally been regarded as organisms whose protein dynamics are largely governed by free Brownian diffusion of enzymes. While this may be true for a majority of cellular proteins, many proteins show assembly at distinct subcellular sites at all times, or even at specific times during the cell cycle [22]. It has also been found that diffusion can be anomalous within the bacterial cytoplasm, and its magnitude is affected by metabolic activity of the cell [23]. Thus, mobility in non-compartmentalized bacterial cells is non-trivial, and it is still unclear for most proteins complexes in which fashion they are assembled. Diffusion capture has been described for some processes, but other modes appear to be possible.

In our work, we wished to address the question of how molecule dynamics change for a protein known to form assemblies, based on fluorescence microscopy, at a given subcellular site, at a single molecule level, in order to monitor and describe changes between diffusive and bound molecules. We chose DynA from *B. subtilis*, a soluble protein that can associate with the cell membrane via a transmembrane-like dimeric subunit, D1. DynA was shown to assemble at the septum in a subset of cells within a growing population, colocalizing with FtsZ [3]. Based on genetic interactions, it was suggested that DynA plays a role in cell division, possible at the last step of fusion of the invaginating cell membrane. Increased membrane binding of DynA was inferred from wide field microscopy using a fluorescent protein fusion of DynA, when cells were treated with an agent inducing membrane leakage, lantibiotic Nisin, a compound produced by lactic acid bacteria, with a broad antibacterial spectrum amongst Gram positive bacteria. In order to obtain more insight into the dynamics of DynA assembly at the cell membrane, we used single molecule tracking, which not only localizes statically bound molecules, but also freely diffusing, mobile molecules. We found that DynA diffusion can be explained by assuming two distinct populations, and to an even better degree by assuming three populations. For a two population model, one would assume a freely diffusing part and a statically, membrane engaged part of molecules. We found minor changes in single molecule dynamics using two or three population models for general stress conditions, but considerable changes following Nisin treatment. For the purpose of this study, we chose a model with three population, which might be a better reflection of molecule dynamics within cells, keeping in mind that qualitatively, changes were similar no matter if two or three populations were assumed.

Nisin treatment induces or enhances the recruitment of DynA molecules to the cell

membrane, and the formation of fluorescent foci as seen by observing a functional fluorescent protein fusion to DynA [4] (**Fig. 1**). Rather than about 25% of cells showing a single DynA-mVenus focus at the cell membrane during exponential growth, about 80% of cells contain mostly several foci following Nisin treatment. We show that this observation made by wide field fluorescence microscopy involves only about 13% of the molecules, which change from being mobile (no matter if one or two mobile populations are assumed) to being static, using single molecule tracking. Accumulation of molecules moving in a confined manner occurred close to the cell membrane, as shown by confinement maps. Considerably longer dwell times that were observed between exponentially growing cells and Nisin-treated cells also underline that DynA becomes more static, by assembling in membrane repair complexes.

Using general stress factors such as heat, ethanol, osmotic and salt stress, we found a visual redistribution of molecules, in that especially after heat and osmotic stress, more molecule of DynA were found to cluster close to the cell poles. We interpret these findings to indicate that some molecules would denature and thus aggregate at the cell poles, possibly soon after translation, which occurs predominantly at the poles [24, 25]. However, we did not find any notable changes at a single molecule level after general and membrane stress, different from treatment with Nisin. An argument can be made that also Bacitracin treatment leads to significant changes of molecule dynamics, which can be seen for the confined motion, and increased average dwell times that were observed. Both Nisin and Bacitracin are antibiotics that bind to and affect the cycle of lipid II during cell wall synthesis, and Nisin induces membrane leakage [26]. These findings suggest that DynA is recruited to membrane damage if there is a specific leakage, e.g. through interference with lipid II components.

The data suggest that for repair of membrane leakage or generally membrane fusion, a minority of DynA molecules becomes statically involved/assemble at the membrane. The remaining molecules continue to be mobile, likely scanning the cell membrane for lesions. Our work shows that assembly of a protein at the cell membrane (in order to mediate membrane integrity) involves a small exchange in molecule dynamics and thus an induced diffusion/capture mechanism. We speculate that a large majority of protein assembly mechanisms involve diffusion/capture rather than specific membrane integration or proteolysis or other targeted mechanisms.

2.2.5 Acknowledgments

The work has funded by the research consortium TRR174, funded by the Deutsche Forschungsgemeinschaft (DFG).

2.2.6 Materials and Methods

Bacterial strains and growth conditions

Bacillus subtilis strain BG214 (also termed YB886) is a derivate of the strain 168. It is auxotrophic for tryptophan (*trp*C2) and methionine (*met*B5), therefore minimal media were supplemented with 50 mg/ml tryptophan and methionine, respectively [27]. For cloning, the *Escherichia coli* strain DH5α was used. Both strains were cultivated in Luria-Bertani (LB) medium, whereat it was used for *B. subtilis* only for overnight cultures. *E. coli* was grown at 200 rpm and 37°C, while *B. subtilis* was cultivated at 250 rpm and 30°C. For Epi-fluorescence and single-molecule tracking *B. subtilis* was grown in $S7_{50}$ minimal medium (1% [w/v] fructose, 0.1% [w/v] glutamate, 0.004% [w/v] Casamino Acids) [28] with the same temperature and speed. For the determination of the growth rate, it was measured with an optical density at 600 nm (OD_{600}). An OD_{600} of 0.8 was used for microscopy. Selection of the strains was accomplished by using the antibiotics ampicillin (100 µg/ml) for *E. coli* and chloramphenicol (5 µg/ml) for *B. subtilis*. In BG214 cells the xylose promotor was induced by adding 0.1% (w/v) xylose to the cells.

Strain construction

BG214 DynA_mVenus at the original locus was constructed by firstly creating the plasmid in *E. coli* DH5α. For this, the plasmid pSG1164 (ECE155) with a mVenus fluorophore was used. The last 500 bp of the 3'-end of DynA were cloned in front of the fluorophore. The cutting enzymes *Eco*RI and *Apa*I were used with the forward primer GCTAGAATTCGACAACAGCCTTA and the reverse primer GCATGGGCCCCATTTTTATTGTATTGTCTG, where the stop codon was removed. After transformation of this plasmid in *E. coli*, the plasmid was checked via sequencing and then used for transformation in *B. subtilis* BG 214. To get *B. subtilis* BG214 competent for DNA

uptake, an overnight culture of this strain was grown at 30°C and 200 rpm and inoculated in 10 ml of modified competence media to an OD_{600} of 0.08. Incubation at 37°C and 200 rpm for around 3 hours to an OD_{600} of 1.3-1.5. When this OD was reached, 2-3000 ng of plasmid DNA was added to 1 ml of the competent *B. subtilis* 168 cells and incubated at 37°C with 200 rpm for 2 hours. Last, the cells were streaked on a LB agar plates with the needed antibiotics (chloramphenicol) for selection and incubated overnight at 30°C. Colonies were screened for a positive clone via PCR (forward primer CATCCATGGATGACAGATCAAAACAGAAAA, reverse primer CCTTACTCGAGTTTGGATCCTTACTTGTACAGCTCGTCCATGCCG) and by antibiotic selection.

Preparation of BG214 DynA-mVenus for microscopy

B. subtilis BG214 DynA-mV cells were grown in $S7_{50}$ minimal medium at 30°C under shaking conditions to an OD_{600} of 0.8. Afterwards, the cells were stressed with 1M Sorbitol, 1M NaCl, 10% EtOH, 250 µg Bacitracin or 10 µg Nisin for 30 minutes and 42°C in a shaking bath for 30 minutes. Cells were spotted on coverslips (25 mm, Marienfeld) and covered with a 1% agarose pad (w/v), made of $S7_{50}$ Medium and a smaller coverslip (12 mm, Marienfeld).

Epifluorescence microscopy

A Zeiss Axio observer Z1 microscope with a Cascade II:512 Photometrics camera was used for imaging. The magnification of the objective was 100x, while the magnification of the optivar was 1.6x. The total magnification was 160x. The camera chip was 512 x 512 with a pixel size of 16 µm x 16 µm. Images were acquired using Metamorph, acquisition was done with an exposure time of 3000 ms using a YFP filter.

Single-molecule tracking, data acquisition- and analysis

Imaging was performed with a Nikon Eclipse Ti microscope equipped with a high numerical aperture objective (CFI Apochromat TIRF 100XC Oil, NA 1.49), an EM-CCD camera (ImagEM X2, Hamamatsu) and a YFP filter set (BrightLine 500/24, Beamsplitter 520 and BrightLine 542/27). mVenus fluorophores were excited by the central part of a laser beam (TOPTICA Beam Smart,

515 nm, max. power 100 mW) with a laser intensity of 150 W cm^{-1}. Each movie consists of 3000 frames and was recorded with an exposure time of 20 ms, using Nikon NIS-Elements BR.

First, the videos were cut with Fiji (ImageJ) [29] and the last 2000 frames were used. Afterwards, the cell meshes were set with oufti [30]. For particle detection, U-track [31], a MATLAB software, was used. Here, the minimal length of tracks was set to 5 and to link to points, no gaps for the particle detection was allowed. Data were analyzed using software SMTracker 2.0 [32]. In this program, the Stationary Localization Analysis (SLA) panel was used for dwell time analysis and heat maps, and the Square Displacement Analysis (SQD) panel for calculation of diffusion constants are population sizes and confinement maps. SQD uses the squared, 2-dimensional radial displacement of molecules, generating a cumulative distribution function (CDF) of squared. For a given number of diffusive states, the algorithm implemented in SQD performs a simultaneous nonlinear least square fit to the experimental CDFs. SMTracker estimates the most approximate number of diffusive groups found in the experimental data using the Bayesian information criterion (BIC), which also help to avoid overfitting of data. To obtain the uncertainty on the estimation of the fitting parameters the main dataset is split into two subsets, train and test. Fitting estimation is run using only the training subset, and evaluating on set of the test data. The training subset is methodologically split into 10 independent folds without any common data point, and the fitting is performed in each of these. Final estimation of the parameters is obtained after determining the mean, and the error is the sum of the standard error for the mean and the 95% confidence intervals obtained from the fitting procedure. Normalization is done according to standard procedures, sizes of bins in histograms was adjusted to yield the visually best representation of data.

2.2.7 References

1. Ramachandran, R. and S.L. Schmid, *The dynamin superfamily.* Curr. Biol., 2018. **28**(8): p. R411-R416.
2. Schlimpert, S., et al., *Two dynamin-like proteins stabilize FtsZ rings during Streptomyces sporulation.* Proc. Natl. Acad. Sci. U S A, 2017. **114**(30): p. E6176-E6183.
3. Dempwolff, F., et al., *The deletion of bacterial dynamin and flotillin genes results in pleiotrophic effects on cell division, cell growth and in cell shape maintenance.* BMC Microbiol., 2012. **12**: p. 298.
4. Sawant, P., et al., *A dynamin-like protein involved in bacterial cell membrane surveillance under environmental stress.* Environ. Microbiol., 2016. **18**(8): p. 2705-2720.
5. Antonny, B., et al., *Membrane fission by dynamin: what we know and what we need to know.* EMBO J., 2016. **35**(21): p. 2270-2284.

6. Jimah, J.R. and J.E. Hinshaw, *Structural Insights into the Mechanism of Dynamin Superfamily Proteins.* Trends Cell Biol., 2019. **29**(3): p. 257-273.
7. Low, H.H. and J. Lowe, *A bacterial dynamin-like protein.* Nature, 2006. **444**(7120): p. 766-769.
8. Low, H.H., et al., *Structure of a bacterial dynamin-like protein lipid tube provides a mechanism for assembly and membrane curving.* Cell, 2009. **139**(7): p. 1342-1352.
9. Liu, J., J.K. Noel, and H.H. Low, *Structural basis for membrane tethering by a bacterial dynamin-like pair.* Nat. Commun., 2018. **9**(1): p. 3345.
10. Praefcke, G.J. and H.T. McMahon, *The dynamin superfamily: universal membrane tubulation and fission molecules?* Nat Rev Mol Cell Biol, 2004. **5**(2): p. 133-47.
11. Burmann, F., et al., *A bacterial dynamin-like protein mediating nucleotide-independent membrane fusion.* Mol Microbiol, 2011. **79**(5): p. 1294-304.
12. Guo, L. and M. Bramkamp, *Bacterial dynamin-like protein DynA mediates lipid and content mixing.* FASEB J, 2019. **33**(11): p. 11746-11757.
13. Burmann, F., P. Sawant, and M. Bramkamp, *Identification of interaction partners of the dynamin-like protein DynA from Bacillus subtilis.* Commun Integr Biol, 2012. **5**(4): p. 362-9.
14. Reyes-Lamothe, R., D.J. Sherratt, and M.C. Leake, *Stoichiometry and architecture of active DNA replication machinery in Escherichia coli.* Science, 2010. **328**(5977): p. 498-501.
15. Kleine Borgmann, L.A., et al., *The bacterial SMC complex displays two distinct modes of interaction with the chromosome.* Cell Rep., 2013. **3**(5): p. 1483-1492.
16. Schibany, S., et al., *Single molecule tracking reveals that the bacterial SMC complex moves slowly relative to the diffusion of the chromosome.* Nucleic Acids Res., 2018. **46**(15): p. 7805-7819.
17. El Najjar, N., et al., *Bacterial cell growth is arrested by violet and blue, but not yellow light excitation during fluorescence microscopy.* BMC Mol. Cell. Biol., 2020. **21**(1): p. 35.
18. Dersch, S., et al., *Super-Resolution Microscopy and Single-Molecule Tracking Reveal Distinct Adaptive Dynamics of MreB and of Cell Wall-Synthesis Enzymes.* Front. Microbiol., 2020. **11**: p. 1946.
19. Schenk, K., et al., *Rapid turnover of DnaA at replication origin regions contributes to initiation control of DNA replication.* PLoS Genet., 2017. **13**(2): p. e1006561.
20. Rosch, T.C., et al., *Single molecule tracking reveals spatio-temporal dynamics of bacterial DNA repair centres.* Sci. Rep., 2018. **8**(1): p. 16450.
21. Sanamrad, A., et al., *Single-particle tracking reveals that free ribosomal subunits are not excluded from the Escherichia coli nucleoid.* Proc. Natl. Acad. Sci. U S A, 2014. **111**(31): p. 11413-11418.
22. Shapiro, L. and R. Losick, *Dynamic spatial regulation in the bacterial cell.* Cell, 2000. **100**(1): p. 89-98.
23. Parry, B.R., et al., *The bacterial cytoplasm has glass-like properties and is fluidized by metabolic activity.* Cell, 2014. **156**(1-2): p. 183-194.
24. Lewis, P.J., S.D. Thaker, and J. Errington, *Compartmentalization of transcription and translation in Bacillus subtilis.* EMBO J., 2000. **19**(4): p. 710-718.
25. Mascarenhas, J., M.H. Weber, and P.L. Graumann, *Specific polar localization of ribosomes in Bacillus subtilis depends on active transcription.* EMBO Rep., 2001. **2**(8): p. 685-689.
26. El Jastimi, R., K. Edwards, and M. Lafleur, *Characterization of permeability and morphological perturbations induced by nisin on phosphatidylcholine membranes.* Biophys. J., 1999. **77**(2): p. 842-852.
27. Yasbin, R.E., P.I. Fields, and B.J. Andersen, *Properties of Bacillus subtilis 168 derivatives freed of their natural prophages.* Gene, 1980. **12**(1-2): p. 155-9.
28. Jaacks, K.J., et al., *Identification and characterization of genes controlled by the sporulation-regulatory gene spo0H in Bacillus subtilis.* J Bacteriol, 1989. **171**(8): p. 4121-9.
29. Schindelin, J., et al., *Fiji: an open-source platform for biological-image analysis.* Nature Methods, 2012. **9**(7): p. 676-682.

30. Paintdakhi, A., et al., *Oufti: an integrated software package for high-accuracy, high-throughput quantitative microscopy analysis.* Mol Microbiol, 2016. **99**(4): p. 767-77.
31. Jaqaman, K., et al., *Robust single-particle tracking in live-cell time-lapse sequences.* Nat Methods, 2008. **5**(8): p. 695-702.
32. Oviedo-Bocanegra, L.M., et al., *Single molecule/particle tracking analysis program SMTracker 2.0 reveals different dynamics of proteins within the RNA degradosome complex in Bacillus subtilis.* Nucleic Acids Res., 2021.

3 UNPUBLISHED RESULTS

3.1 Functionality of MS2-mVenus in cells with and without mRNAs with a MS2-binding site

3.1.1 Growth behavior of cells expressing the MS2-system

The coat protein of the RNA bacteriophage MS2 has a specific binding site, a RNA loop, which to it binds. This binding site is also part of the MS2 bacteriophage. The MS2-binding site has been found to be an advantageous technique for RNA labeling in living cells [154, 155]. As described earlier, in most studies, different numbers of repeats of the 19 nt short MS2-binding site were fused on the 3'-end of mRNAs, in the beginning 96 repeats, nowadays six and twelve repeats are more common [107, 207]. This means that six or twelve coat proteins, fused together with a fluorophore, can also bind to it. The dimeric coat protein is only 13.7 kDa small, GFP or its derivates, which are mostly used, have a size of around 27 kDa. Even though this might not sound big, six MS2 tags, each with at least one fluorophore on it, become pretty huge. This could possibly have an influence on the behavior of the smaller, target mRNA. This is one reason why only one binding site or a second repeat was used in my work.

A known influence of the MS2 tag on the target mRNAs is that it delays the degradation of it. In yeast, binding of the MS2 tag to the MS2-binding site at the 5' or 3'-end of the mRNA, an accumulation of short mRNAs bound to the coat protein was observed [208]. This could potentially also lead to wrong localization patterns. Nevertheless, this has only been observed in yeast, where it also leads to other problems of mRNA processing in the nucleoid. It seems that starving conditions increase this effect further [209].

To investigate, if the use of the MS2-system can be justified for this work, the correct expression of the fusion of the MS2 tag with the monomeric fluorophore mVenus was tested first. Therefore, a western blot was performed with a specific first antibody against GFP and its derivates and a second one against the first antibody. The fusion protein should have a size of around 41 kDa. Even though the blotting to the membrane leads to a slight uneven transfer of the protein and ladder, as **Fig. 3.1** shows, a well visible lane can be detected at this size, while no signal can be detected in the negative control. One coat protein is fused to one mVenus and this fusion is fully expressed.

Although already included in the Supplement of Manuscript 1, the growth curve is again discussed in more detail here to verify a possible influence of the MS2-system on the

cells. Looking at the cells containing the MS2-mVenus fusion, an effect on the growth behavior can be observed (**Fig. 3.2**). In the *B. subtilis* wild type strain 3610, an optical density up to 0.53 is reached, while the strain MS2-mV + *rplK-rplA*_MS2BS1x is the one that reaches the highest optical density for strains containing the MS2-mVenus fusion. It reaches an optical density of 0.45. The least growing *B. subtilis* strain containing the MS2-mVenus fusion is MS2-mV + *rplJ-rplL*_MS2BS1x. It reaches an optical density of around 0.39. Independent of one or two MS2-binding sites, all the other constructs optical density lay in between those two strains. Even for the strain MS2-mVenus, which does not co-express any MS2-binding site, the optical density achieved is more or less in the middle of the optical densities reached, at about 0.42. When having a look at the growth behavior over time, it seems that the MS2 tag might have an influence here as well. Both the lag phase and the range of the exponential growth phase are quite similar to the wild type. After almost 5 hours (between 288-312 minutes), where the wild type is still growing continuously, the growing curves start to flatten for all constructs containing the MS2 tag. One hour later, after 6 hours, the stationary growth phase is reached for those strains. After a total growing time of 10 hours, the first strains - MS2-mVenus, MS2-mV + *ylxM-rplS*_MS2BS1x and MS-mV + *mreB-minD*_MS2BS2x -, start to die off. The other strains are still in the stationary growth phase. Meanwhile, the cells of the wild type strain have also reached the stationary growth phase.

Thus, we can assume that the MS2 tag seems to have an effect on the cells. At the same time, it appears that the existence of the MS2-binding site has nothing to do with it. Therefore, the cautious assumption can be made that the MS2-binding site and the binding of the MS2 tag to the mRNA via its binding site do not really influence the target mRNAs. Even though the MS2 tag appears to affect the growing behavior, the optical density reached is still in a satisfactory range. Reaching the stationary growth phase at an earlier time – where now the possible decay of mRNA degradation could play a more crucial role – does not lead to a fast dying of the cells. It should be mentioned that in daily working situations, the overnight cultures showed a similar optical density as strains without the MS2 tag. Nevertheless, the exponential growth phase was important for this work. Because this is identical to the *B. subtilis* wild type strain 3610, it can therefore be assumed that doing the experiments with the different mRNA strains containing the MS2 tag is not a problem in the exponential growth phase.

To proof this further, a motility assay was performed to demonstrate that the binding

of the MS2 tag does not influence the mRNA and its associated protein (**Fig. 3.3**). For this, the mRNA *hag* was chosen. This mRNA encodes for the flagellin protein, whose subunits form one flagellum [210]. If this mRNA or the protein is impaired by the MS2-binding site or by the binding of the MS2 tag to it, the *B. subtilis* strain containing the MS2-mV + *hag*_MS2BS1x construct should show this in its motility behavior. We would then expect the cells to swarm less or not at all on the 0.3% soft agar plate. This could be because there are fewer or impaired flagella, or because there are none due to problems with the translation of the mRNA *hag*. However, already at the timepoint 2 (**Fig. 3.2B,F**), so two hours after adding *B. subtilis* cells on the soft agar plate, both, the wild type and the strain MS2-mV + *hag*_MS2BS1x show similar behavior. The starting point at which the cells were added is well to see, as early as at timepoint 0 (**Fig. 3.1A,E**). A halo is visible around it, showing how far the cells are integrated into the soft agar. Also, small branches are visible, especially in the MS2-mV + *hag*_MS2BS1x cells, showing how much the cells integrate into the soft agar. At timepoint t5 (**Fig. 3.1C,G**) the swarming of the cells continued and is still similar between those two strains. Small branches are still there, but are not visible well any longer. After a total of 24 hours (**Fig. 3.3D,H**), the entire soft agar plates is fully covered by the cells. Biofilm formation, beginning at the starting point, is also well to see in both the wild type and cells expressing the MS2-mV + *hag*_MS2BS1x construct. A stronger halo around the biofilm is seen too, better for the wild type, but also present in the MS2-mV + *hag*_MS2BS1x strain. Therefore, functional flagella can be assumed. To verify this further, staining of the flagella would be necessary.

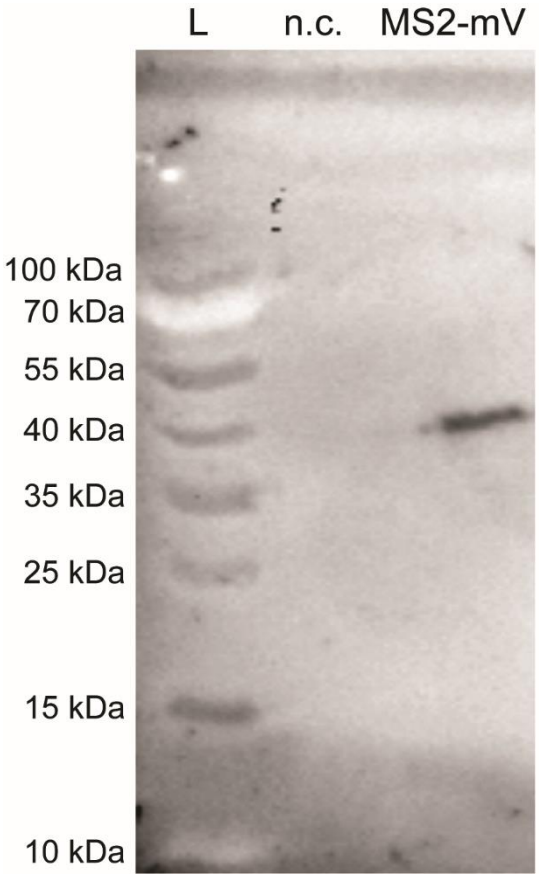

Fig. 3.1 Western blot of the NCIB 3610 *Bacillus subtilis* cells transformed with the MS2 tag, shows an expression of the MS2-mVenus fusion.

For the gel electrophoresis, a 12% SDS-PAGE gel was used. The sample was concentrated to an OD of 1. After the transfer of the fusion protein from the SDS-PAGE to the membrane, an antibody against GFP, that works for mVenus too, was used. mVenus is 26.9 kDa small and the MS2 tag is 13.7 kDa small. Together it has a size of 40.6 kDa. The negative control (n.c.) are *B. subtilis* 3610 wild type cells without any fluorophore in them. L is a prestained protein ladder by ThermoFischer, which displays the protein size from 10-180 kDa.

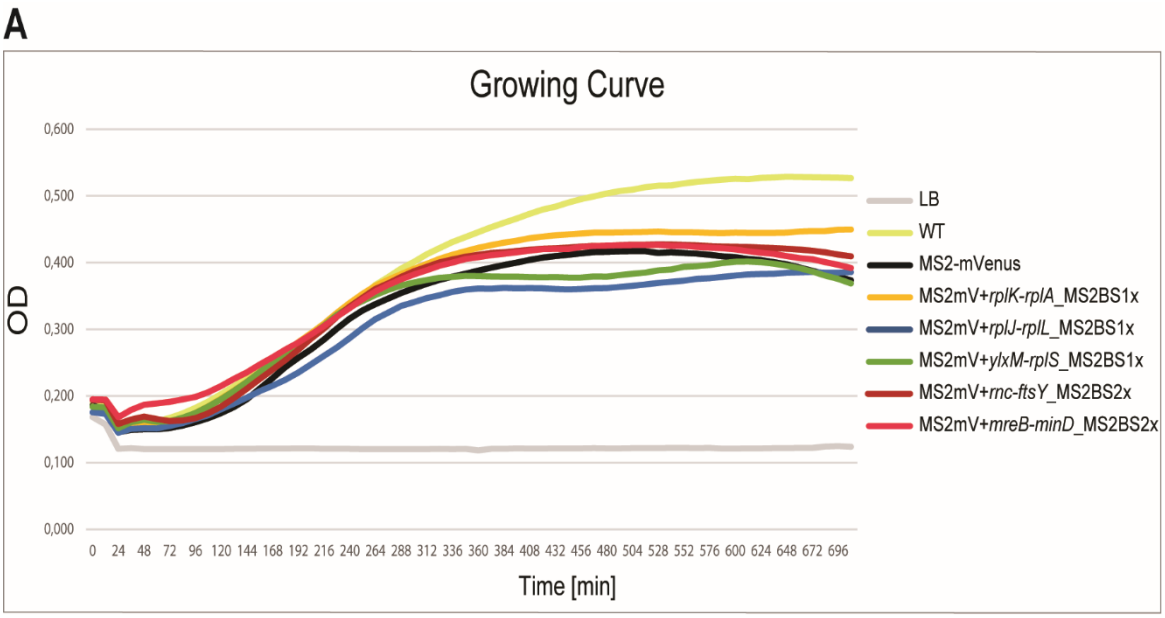

Fig. 3.2 Cells expressing constructs with the coat protein_mVenus grow to a lower density.

Every 12 minutes, measurement of the optical density (OD) was done. For each condition, cells were grown in a 96 well plate with the rich media Luria-Bertani (LB). Each condition consists of a biological triplicate, done on three different days. Each replicate consists of eight technical replicates. The LB condition is growth media without cells, that acts as a control for the OD (in grey). WT is the other control for the growing behavior of *B. subtilis*, which consists of the *B. subtilis* wild type 3610 without any fusion, shown in yellow. MS2-mVenus is the MS2 coat protein with a mVenus fusion, shown in black. Every mRNA construct consists also of the MS2-mVenus fusion. With one MS2-binding sites are the mRNAs MS2-mVenus +*rplK-rplA*_MS2BS1x (orange), MS2-mVenus + *rplJ-rplL*_MS2BS1x (blue) and MS2-mVenus + *ylxM-rplS*_MS2BS1x (green). With two MS2-binding sites are the mRNA constructs MS2-mVenus + *rnc-ftsY*_MS2BS2x (dark red) and MS2-mVenus + *mreB-minD*_MS2BS2x (red).

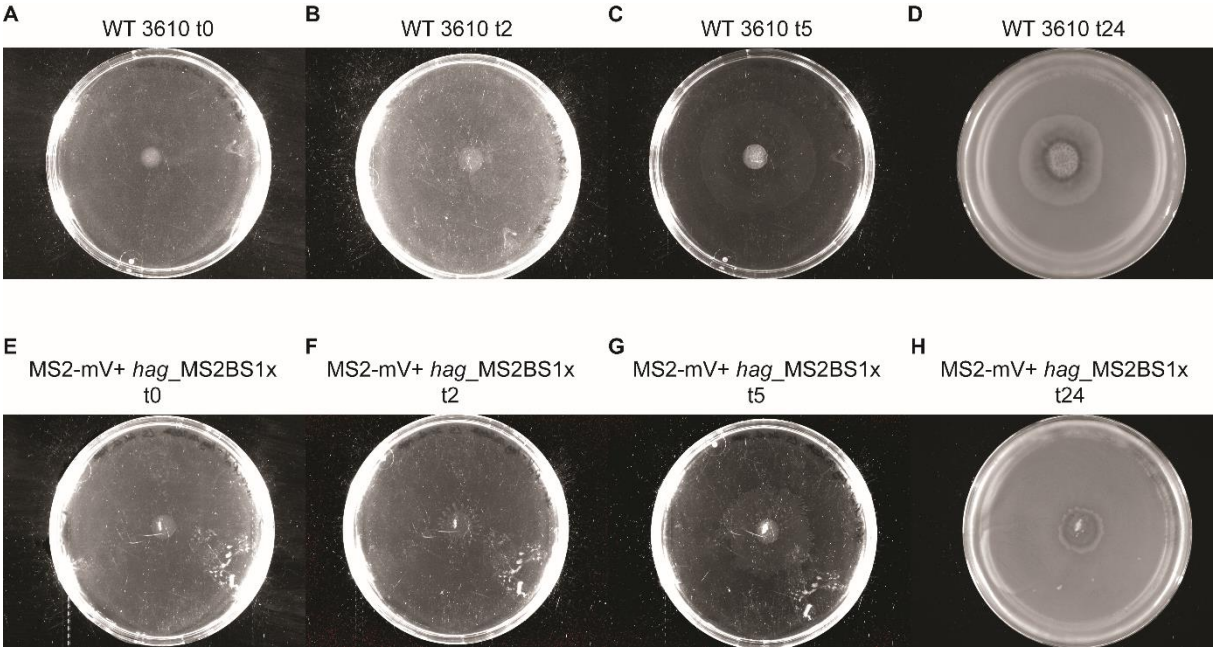

Fig. 3.3 Motility assay reveals no reduction in functionality on protein level with mRNA, bound to the MS2 tag.

5µl cell suspension of the *B. subtilis* wild type 3610 and the mRNA construct MS2-mV + *hag*_MS2BS1x were dropped in the middle of a 0.3% soft agar plate. Directly after this, at timepoint 0, the first picture of the wild type (**A**) and MS2-mV + *hag*_MS2BS1x (**E**) was taken. After two hours, t2, a second picture for the wild type (**B**) and MS2-mV + *hag*_MS2BS1x (**F**) was taken. 5 hours later, for the wild type (**C**) and MS2-mV + *hag*_MS2BS1x (**G**) the next picture was taken. The last time point is after 24 hours, (**D**) the wild type, (**H**) MS2-mV + *hag*_MS2BS1x.

3.1.2 Localization behavior of unbound MS2-tag and its dynamics in comparison to tagged mRNAs

Although already included in Manuscript 1 and its supplement, the dynamics and localization behavior of the MS2-tag is again discussed in more detail here to verify the use of the MS2-system. In a further step, a comparison between the MS2 tag alone and co-expression with an MS2BS-tagged mRNA is conducted. For this purpose, single-molecule tracking was performed with two different exposure times (8 and 75 ms). A third one, 20 ms, was discarded, as it did not add any real value. The same is true for the test tracking of mRNAs with 20 and 100 ms exposure time, as the best results were achieved with an exposure time of 75 ms. Only this data set was used.

First, the dynamics of MS2-mVenus will be explained and compared with the example mRNA *ypbR*-ypzF, used for this purpose. By using the jump distance analysis (JD) with the jump

square displacement parameters, as well as the probability-probability plot for the MS2-mVenus tag tracked with 8 ms, two populations can be assumed (**Manuscript 1**, **Fig. 1A,B,G,H** + **S1A-D, I,J**). This is surprising, as I expected only one freely diffusing population. To ensure the correctness of the fits and models, several tests were used. JD analysis is based on squared displacement analysis (SQD) [159, 160, 211]. It shows the probability of particles during a given time interval by assuming two-dimensional Brownian motion. To find out how many populations can be detected, depending on an average diffusion constant, the Rayleigh distribution was used. The use of the Bayesian Information Criterion also ensures an overfitting of the data [212]. Further tests were used to assure the correctness of the used models. For the JD analysis a R^2 test was done to measure the goodness of the fit, e.g., for one or two populations. The Kolmogorov-Smirnov-Goodness-of-Fit and null hypothesis significance test are statistical tests used. The used probability-probability plot shows, whether or not the modeled data and the observed data differ. A high deviation indicates a low quality for the goodness of the fit, while a low deviation shows a high quality for the goodness of the fit [159, 160]. By taking this all into consideration and selecting the best model of two populations, as suggested by the SMTracker, there is no mistake that two populations exist for the MS2-tag when tracked with a fast exposure time of 8 ms. It can be assumed that no free mVenus is visible here, since an exposure time of 5 ms is needed for its detection [213]. The mobile population seems to be freely diffusive, while the more static population does not look like a real static population. It can already be said that the diffusion coefficient (DC) of 0.114 $\mu m^2 s^{-1}$ corresponds to a slower but not static population. For example, the DC of the slow mobile population of DynA-mVenus is 0.122 $\mu m^2 s^{-1}$, which was tracked with an exposure time of 20 ms.

The data of the fast tracked MS2-mVenus construct were a surprise that an unspecific binding event might occur. However, this population could also be explained by assuming that the MS2-tag might bump against the cell wall or the poles or larger proteins, causing it to slow down. When tracking this now with a longer exposure time of 75 ms, the data of the MS2-mVenus tag tracked show not only two populations, but also a possible third one (**Manuscript 1**, **Fig. 1 C,D,G,H** + **S1E-J**). Assuming two populations, which is already a good fit, the DC becomes slower, which can be explained throw the use of a higher exposure time and is 0.0743 $\mu m^2 s^{-}1$ for the mobile population and 0.00847 $\mu m^2 s^{-}1$ for the static population. When assuming a third population, it could be possible that the previously observed slower

population has now been split into the slow mobile of 0.0167 $\mu m^2 s^{-1}$ and static populations of 0.003 $\mu m^2 s^{-1}$. This static population is now truly static, where more or less no movement can be assumed at all.

Due to a possible third population, when tracked with 75 ms exposure time, a possible binding event in an unspecific manner for MS2-mVenus seems possible. At first glance, this are no good news, but compared to the tested mRNA, the population sizes change, even though the DC's are similar (**Manuscript 1**, **Fig. 3**). Only around 13% of MS2-mVenus shows the static population, while around 87% are more mobile. On the other hand, the static population increases to around 25%, when looking at the MS2-mVenus + *ypbR-ypzF*_MS2BS2x construct, while the mobile population decreases, but not the slow mobile one. This leads to the hypothesis that the static population represents mRNA to be translated (this will be further addressed under **4.1**), while the slow mobile and mobile population could be MS2-mVenus that bind something unspecific in the cells, or some another event, like more or less free diffusive MS2-mVenus for the mobile population, which bumps into the cell wall, etc., also further discussed under section **4.1**. Regardless, as I will explain in more detail later in section **4.1**, the static population is the one of interest that is most likely to displace mRNAs in a fully assembled ribosome where translation occurs.

Furthermore, if we consider the localization behavior of the MS2-tag with 8 and 75 ms, an obvious free diffusive behavior is observable (**Manuscript 1**, **Fig. 1I,J**). No specific localization is visible, which is also underlined by the low probability of distribution and spatial localization, which is projected by color. Only twice a higher probability of distribution is given. It can be argued, this could be a specific binding or the result of bumping into the membrane, since it occurs near it. Even if a specific binding would take place, a clear difference can be seen when looking at the localization behavior of the tested mRNA (**Manuscript 1**, **Fig. 5A,E**). Here, the *ypbR-ypzF* mRNA shows a higher probability of distribution and a distinct spatial localization. There is an inherent difference between the MS2-mVenus alone and bound to a mRNA. This clearly indicates that the use of this tag is more in its favor than against.

To ensure that the static population observed in cells expressing only MS2-mVenus is not MS2-mVenus bound to other mRNAs without any tag, cells were stressed with the RNA-polymerase inhibitor Rifampicin (**Manuscript 1**, **Fig. 6,7+S4**). Because of the concentration used, 50 and 25 µg/ml, a total inhibition of transcription does not occur (note: for total inhibition, a concentration of 200 µg/ml is needed). No cells are dying here. However, this is

enough, since a clear difference is already noticeable with a low concentration of 25 µg/ml (**Manuscript 1**, **Fig. S4**). Therefore, mRNAs are still available in the stressed cells, but to a decreased number. This data also underlines that the MS2-system can be used to analyse mRNAs. Although the DC did not change much, the important observation is that both the tested mRNA construct, MS2-mVenus + *spoIIIE-ymfC*_MS2BS2x, and ribosomal protein L1 [67] show a drastic decrease for the static population of around 50-55% (with the addition of 50 µg/ml Rifampicin), whereas cells expressing only MS2-mVenus show a decrease in the static population of 25% (**Manuscript 1**, **Fig. 7**). There are also obvious changes in the slow mobile population for MS2-mVenus and L1, with a decrease of roughly 34% for MS2-mVenus cells and about 40% for L1, whereas there is not much change here for MS2-mVenus + *ypbR-ypzF*_MS2BS2x. Although mRNA depletion lead to a more mobile MS2-mVenus, it is possible that based on these findings, MS2-mVenus in cells lacking a MS2-binding site, binds nonspecifically to something else. This will be further addressed under **4.1**. Because of the strong affinity for the MS2BS, which was also reported by other groups [154, 208, 214], this unspecific binding behavior does not seem to play a crucial role when the binding site is co-expressed during mRNA-observation.

It should be said that the MS2-tag might not be a tool with no downsides and the data must be interpreted carefully, but at least one-third to one-half of the data should be MS2-mVenus bound to the MS2-binding site of a labelled mRNA and therefore can be used.

3.2 Two residence times for MS2BS labelled native mRNA constructs

In addition to the localization of the mRNAs as well as their dynamics (see **Manuscript 1**), I would like to briefly discuss the dwell times of the tested mRNAs. Here, the dwell time relates to the tracks moving within a 120 nm radius with a minimum of 8 steps, the same conditions as for the confined localization. The dwell time is described by τ and can be divided into one or two populations. The average dwell time refers to two populations.

For the four native mRNA constructs with two MS2BS, two residence times can be assumed (**Fig. 3.4**). This can be seen not only in the differences in population sizes for one- and two-component fits, but also in the amount of data used for this purpose. If one population is assumed (in green), part of the data is not covered. If, on the other hand, the two-component fit (in red) is used, most of the data set is covered, which can be seen well in **Fig. 3.4B**.

For *ypbR-ypzF* (**Fig. 3.4A**), we see a shorter dwell event of 0.73 ± 0.015 seconds, which

affects 86 ± 5.2% of the 229 tracks used for it. The remaining 14% ± 5.2% have a dwell time of 1.5 ± 0.28 seconds, which is more than twice as long. The average dwell time here is 0.882 ± 0.037 seconds. The other three mRNA constructs display similar behavior. As such, the first population of the two-component fit for *rnc-ftsY* (**Fig. 3.4B**) is 0.77 ± 0.011 seconds long and affects 75 ± 2.8% of the 507 tracks used for it. The second residence time is slightly longer than that of *ypbR-ypzF* at 1.7 ± 0.088 seconds, with a size of 25 ± 2.8%. The average dwell time is 1.034 ± 0.045 seconds. For *mreB-minD* (**Fig. 3.4C**), the first dwell event is 0.78 ± 0.033 seconds long. The population size for this is 78 ± 13%. The second dwell event, which is just over twice as long, lasts 1.3 ± 0.25 seconds and covers the remaining 22 ± 13% of the 192 tracks used for this purpose. The average dwell time is 0.971 ± 0.051 seconds. It is almost identical to *spoIIIE-ymfC* with 0.973 ± 0.056 seconds (**Fig. 3.4D**). For the first residence time we obtain a value of 0.79 ± 0.023 seconds and affects 84 ± 6.6% of the 205 tracks used for this purpose. The second residence time is as long as for *rnc-ftsY* with 1.7 ± 0.31 seconds and affects the remaining 16 ± 6.6% of the tracks. In general, the two dwell times for the two-component fit between the four mRNAs tested are similar. This is also true when considering only the one-component fit, where the residence times range from 0.8-0.91 seconds.

As has already become clear in Manuscript 1 and will be discussed further in Section **4.1.1**, the static population (**Manuscript 1**, **Fig. 3**), which is recognizable in the localization as a confined localization (**Manuscript 1**, **Fig. 5**), appears to represent a translation event. Since the same conditions apply for the dwell times as for the confined localization, it can be assumed that the dwell times refer to mRNAs that are being translated. In this context, the longer residence time could represent the actual translation of the mRNAs, while the approximately half-long residence time relates to mRNAs that are about to be translated, where the 70S ribosome assembly has not yet been fully accomplished. However, it could also be that the first, larger population of the two-component fit refers to mRNAs that are translated by polysomes, i.e., by many ribosomes at the same time, so that the actual dwell time can be shortened. If, on the other hand, an mRNA is translated by only one ribosome, the dwell time will be longer, since an mRNA is usually translated more than once. At the same time, it could also be the other way around, since the presence of polyribosomes increases the frequency of translation and the mRNA is also more accessible to additional ribosomes, which increases the residence time. Regardless of what is the case, one would have to assume in this context that the mRNAs under investigation are translated by both single ribosomes

and polyribosomes, but this cannot be verified further here.

Looking now at the artificial mRNAs with one MS2BS (**Fig. 3.5C**), a difference to the above four described native mRNAs becomes obvious. A two-component fit no longer seems to be present. The mean deviations in the population sizes are too severe for this, as shown by the examples of *rplK-rplA* and *rnc-ftsY*. Here, *rplK-rplA* has a size of 83.4% for the first population of the two-component fit and the second population is only 16.6% large, but the mean deviation is 30.1%. *rnc-ftsY*, on the other hand, has an even larger first fraction of 92.2% and a smaller, second fraction of 7.83% with a mean deviation of 3.4%. Therefore, a two-component fit cannot be safely assumed. Although the residence times for the first population are similar to those of native mRNAs (**Fig. 3.4**) with 0.77-0.85 seconds, the dwell times for the second fraction are sometimes significantly longer, such as the 3.3 seconds for *hag* and 3.6 seconds for *rplJ-rplL*, with a mean deviation of 13 seconds for the latter.

For the artificial mRNA constructs *ypbR-ypzF*, *mreB-minD* and *ylxM-rplS*, on the other hand, it is obvious that only one fraction is present, since a population size of 0% is present for the two-component fit for the second, longer residence time. Since *ypbR-ypzF* and *mreB-minD* in particular, which were also tested with two MS2BS and have a two-component fit, have only one population here, it is reasonable to assume that incorrect cloning and the presence of the translation terminator too late lead to this significant difference. The residence time for translation of these mRNAs is shortened to 0.79-0.85 seconds. Translation no longer appears to function as efficiently as with the native mRNAs with two MS2BS. Reasons for this could be that translation is terminated earlier, due to misfolding at the 3' end, or the artificial mRNAs are only translated by single ribosomes. An effect on the lifespan of mRNAs is also possible, although a possible delay in degradation by the MS2-system is only known in yeast whereas the mRNAs are shortened [208]. This cannot be further verified here. Regardless of the number of MS2BS and regardless of the correct placement of the translation terminator, on average 78% of the tracks of native mRNAs and on average 72% of the tracks of artificial mRNAs exhibit confined localization and thus have the appropriate residence times.

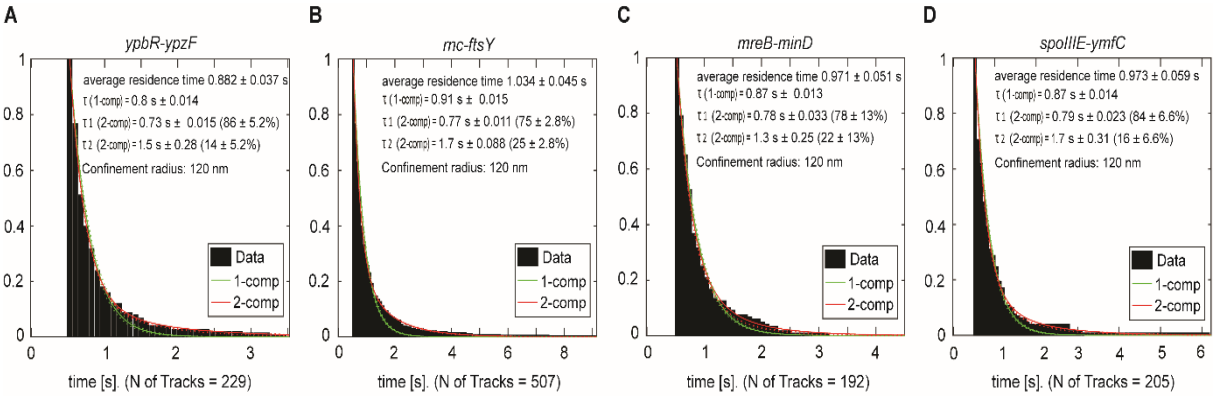

Fig. 3.4 Two different dwell events for mRNAs with two MS2-binding sites can be found.

The length of time of mRNA molecules residue in a 120 nm circle for a minimum of 8 time points is shown for the mRNAs (**A**), MS2-mVenus + *ypbR-ypzF*_MS2-binding sites 2x, (**B**) MS2-mVenus + rnc-ftsY_MS2-binding sites 2x, (**C**) MS2-mVenus + *mreB_minD*_MS2-binding sites 2x and (**D**) MS2-mVenus + *spoIIIE-ymfC*_MS2-binding sites 2x. The average residence time is shown first. τ describes the dwelling event for a one-component fit in green and τ_1 and τ_2 for a two-component fit in red. The duration for the dwelling event is shown in seconds, while the amount of how many molecules residue in the defined circle of 120 nm with a minimum of 8 steps is depicted in percentage. The number of tracks, that were used for this analysis are shown under the graphs.

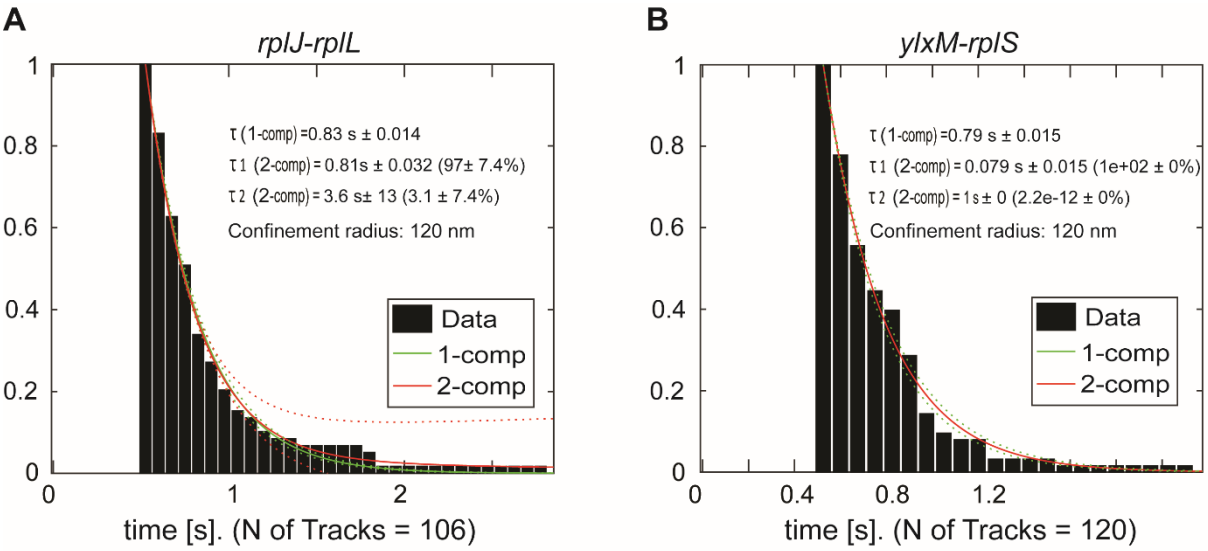

C

	hag	*rplJ-rplL*	*rplK-rplA*	*ypbR-ypzF*	*comN-secDF*	*rnc-ftsY*	*mreB-minD*	*ylxM-rplS*
average residence time [s]	0.95 ± 0.087	0.899± 0.052	0.896 ± 0.052	0.895 ± 0.045	0.859 ± 0.058	0.927 ± 0.083	0.878 ± 0.04	0.836 ± 0.035
τ [s]	0.84 ± 0.018	0.83 ± 0.014	0.84 ± 0.017	0.85 ± 0.018	0.81 ± 0.014	0.83 ± 0.024	0.84 ± 0.096	0.79 ± 0.015
τ1 [s]	0.81 ± 0.014	81 ± 0.032	0.77 ± 0.066	0.85 ± 0.018	0.8 ± 0.015	0.77 ± 0.031	0.84 ± 0.099	0.79 ± 0.015
Fraction τ 1 [%]	96.8 ± 1.75	96.9 ± 7.41	83.4 ± 30.1	100 ± 0	99.7 ± 0.3	92.2 ± 6.87	100 ± 0	100 ± 0
τ2 [s]	3.3 ±. 2.7e+06	3.6 ± 13	1.4 ± 0.93	0.93 ± 0	2.2e-14 ± 0	3.1 ± 3.4	0.92 ± 0	1 ± 0
Fraction τ 2 [%]	3.18 ± 1.75	3.14 ± 7.41	16.6 ± 30.1	0 ± 0	0.311 ± 0.3	7.83 ± 6.87	0 ± 0	0 ± 0
Number of Tracks	84	106	130	107	73	76	89	120

Fig. 3.5 One dwell event for artificial mRNAs with one MS2-binding sites can be found.

The length of time of mRNA molecules residue in a 120 nm circle for a minimum of 8 time points is shown. An example for a mRNA with a one- and two-component fit for the dwell events is (**A**), MS2-mVenus + *rplJ-rplL*_MS2-binding sites 1x. A one-component fit is suggested. An example for a mRNA with a one-component fit of 100% is MS2-mVenus + *ylxM-rplS*_MS2-binding sites 1x (**B**). τ describes the dwelling event for a one-component fit in green and τ_1 and τ_2 for a two-component fit in red. All artificial mRNAs with one MS2-binding site are shown in table (**C**). Even though a one-component fit is suitable with 100%, a two-component fit is also always shown. The duration for the dwelling event is shown in seconds, while the amount of how many molecules residue in the defined circle of 120 nm with a minimum of 8 steps is depicted in percentage. The number of tracks, that were used for this analysis are shown in the table and under the graphs. An average residence time is also shown.

3.3 Possible co-localization of the polycistronic mRNA *ypbR-ypzF* and its encoded protein DynA

To find out more about the localization behavior of mRNAs, I decided to co-express a tagged mRNA and its corresponding protein - as a fusion protein with a fluorophore - parallel to the

mRNA experiments (see **Manuscript 1).** In this way, I hoped to gain more information about whether or not mRNAs are translated near the site where their corresponding proteins are later required, as suggested by the Amster-Choder group. To accomplish this, I decided to use the dynamin-like protein DynA and the polycistronic mRNA *ypbR-ypzF*. This operon contains two genes, *ypbS* and *ypzF*, whose protein functions are unknown, whereas *ypbR* encodes DynA. DynA is also known by the less common name YpbR. This protein is a GTPase and belongs to the bacterial dynamin-like protein family [215, 216]. Unlike other members of this family, DynA does not possess a transmembrane domain and binds only loosely to the membrane, mainly through the D1 subunit and partially through the D2 subunit [204]. With these two subunits, DynA forms an intrinsic dimer that includes the GTPase domain, a stalk region, and a loop. In particular, D1 is important for mediating membrane binding [199]. It appears that DynA also acts as a scaffold for other proteins that may be involved in membrane fusion and is necessary for stability [204, 206]. Together, membrane fusion can be accomplished. DynA is found mainly near the lateral membrane site and also at the division septum [125], as well as free diffusive in the cytoplasm (see **Manuscript 2**).

ypbR-ypzF is a polycistronic mRNA that was studied in Manuscript 1. There, this mRNA can be found in a confined localization pattern mainly in the cytoplasm - probably around the nucleoid -, near the membrane and at the poles. With this localization, it is not yet shown whether there is a possible co-localization between protein and its transcript or not. DynA can at least be found in the same areas. To investigate this further, we used the native mRNA of *ypbR-ypzF* tagged with the binding site for the MS2 tag of the MS2-system. The monomeric mVenus fluorophore, a derivative of GFP [217], was fused to the MS2 tag. Simultaneously, DynA fused to the blue fluorescent protein CFP was expressed at the native locus. DynA-CFP and MS2-mVenus + *ypbR-ypzF*_MS2BS2x were therefore expressed together in the cells. First, a wide-field fluorescence image of DynA-CFP was acquired. Then, the MS2-mVenus + *ypbR-ypzF*_MS2BS2x construct was tracked with an exposure time of 75 ms. Later, an overlay of the projections of the MS2-mVenus + *ypbR-ypzF*_MS2BS2x tracks was done in ImageJ [218]. An overlay was again generated using this and the fluorescence image from DynA-CFP. These results can be seen in **Fig. 3.6.**

Three different examples were used to illustrate the results. First, the wide-field fluorescent image of DynA-CFP is shown (**Fig. 3.6A,D,E**). Not in each cell foci for DynA can be seen. In **Fig**. **3.6**, closer inspection of the selected cells reveals foci at the poles and in the

middle of the cells, probably in the septum, which is consistent the findings from Manuscript 2. Tracks of the *ypbR-ypzF* mRNA in yellow can be observed mainly near the membrane, cytosol, and poles, which fits our findings in Manuscript 1 (**Fig. 3.6B**). An overlap with the DynA-CFP foci can be assumed here. In this case, the cells are quite full of the mRNA track projections. A better example is **Fig**. **3.6D,E**, where one foci for DynA-CFP is visible near the membrane and at the pole. In the overlay in **Fig. 3.6E** a clear overlap between the mRNA and the protein is observable. This time, fewer mRNA tracks can be seen, which are also located in the cytosol and near the membrane, but are further away from the foci. Only one mRNA projection is directly above the DynA-CFP foci and one is very close to it. Of course, these settings cannot define more precisely whether the observed DynA foci were freshly translated by the overlapping *ypbR-ypzF* mRNA or by a spatially separated mRNA at an earlier time point. At least this shows a potential co-localization of a mRNA with its corresponding protein. Something similar is also seen in the next example. This time, the DynA foci are located in two different cells at the septum – or at least in the middle of the cell in the cytoplasm - and once in the cytosol (**Fig. 3.6E**). Not many tracks are visible in the overlapping image with the *ypbR-ypzF* mRNA track projections (**Fig. 3.6F**). Those tracks that are visible are localized at the poles and co-localize with the foci at the septal site and the cytosol. It can be assumed that the mRNA localization in the middle of the cell might be in a nucleoid-free region, which is enabled by an upcoming cell division.

In this work, I also tried to do the same experiment with the mRNA *hag,* which encodes for the flotillin protein [219], and the protein FliM, which is part of the flagellar motor [220]. Because the flotillin protein is transported out of the cell, this protein has not been suitable. In contrast, a protein that is part of the flagellar motor should work as well. However, due to cloning issues, this was not possible. In retrospect, based on the localization behavior of *hag,* a co-localization of the mRNA with FliM should not be very likely. *hag,* as a mRNA encoding for an extracellular protein, could co-localize with the flagellar motor or not following the theory that a mRNA is translated near the site where its corresponding protein is required. Our findings in Manuscript 1 underline the suggestion that mRNAs for extracellular proteins are most likely to be translated in the cytoplasm, as suggested by a study in *E. coli* [105].

Since the *ypbR-ypzF* mRNA from the SMT experiments (see **Manuscript 1**) has a similar localization pattern to the arrangement used with ImageJ, it can be assumed that what we see is a true mRNA signal and not background noise. However, cells with too much signal,

like in **Fig. 3.6B**, do not really seem to be suitable. Nevertheless, this shows that this method of using an overlap of mRNA track projections with wide-field fluorescent images of the corresponding protein works. Of course, these results are not enough to say that a mRNA and its corresponding protein co-localize, but it at least gives an indication that this is a possible theory. More of those co-localization experiments need to be done. For example, with other mRNAs and/or the system can be improved, including by switching to a different setup. Systems in which fixed cells are used are not recommended.

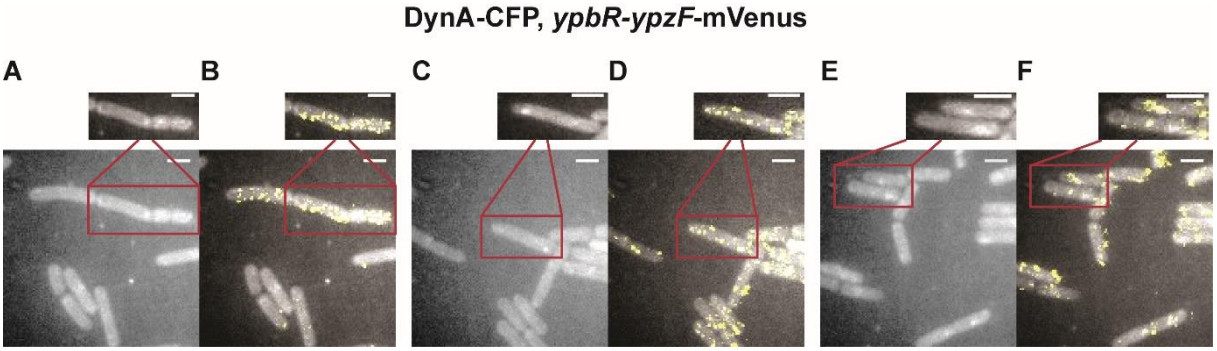

Fig. 3.6 Overlay of the tracked MS2-mVenus + *ypbR-ypzF*_MS2BS2x with DynA-CFP wide-field fluorescent pictures.

All cells express DynA-CFP and MS2-mVenus + *ypbR-ypzF*_MS2BS2x. DynA-CFP Epifluorescence pictures, taken with are depicted in (**A**), (**C**) and (**E**). An enlarged view on the selected cells is shown above the whole picture. (**B**), (**D**) and (**F**) show the overlay of MS2-mVenus + *ypbR-ypzF*_MS2BS2x tracks in yellow with DynA-CFP. Also here, selected cells are shown above the whole picture. The selected cells are marked in a red box. Red arrows indicate DynA-CFP foci. The scale bar on the upper right side is 1 µm. For DynA-CFP fluorescence imaging, an exposure time of 3000 ms was used, while for single-molecule tracking, the exposure time was set to 75 ms.

3.4 L1-mVenus is fully functional

L1 is one of the ribosomal proteins of the large subunit 50S of the ribosome [67, 221]. In this work, not only was the polycistronic mRNA *rplK-rplA* used, which translates into different ribosomal proteins like L1, but L1 also served as a comparison for the behavior of mRNAs and their dynamics. While comparing the localization and dynamics, it was possible to underline the findings that mRNAs with the MS2-system tagged were tracked and that it can be assumed that the mRNAs behave more or less naturally. An overlap in the dynamics and the localization was observed. To proof that the L1-mVenus construct was fully expressed and functional, a

western blot was performed (**Fig. 3.7**).

L1 itself is only 24.77 kDa small. Fused together with the 26.9 kDa small mVenus, this fusion protein is 51.67 kDa big. Because up to one-third of the total proteins in *Escherichia coli* is made up of ribosomal proteins, depending on the growth conditions [222, 223], different amounts of a concentration with an optical density of 5 were tested to avoid overloading of the sample. In each case, a lane with the correct size of around 52 kDa is visible. Independent of the used amount, unknown lanes are visible at around 17 and 27 kDa. The 17 kDa signal could be a lysosome that is about 15 kDa small [224]. This is an often-reported lane and was analysed once by our lab by sending this sample for testing. The other lane could be free mVenus. Not as good to see are other lanes are between L1-mVenus and the possible free mVenus lane. This could be due to the degradation of the fusion protein. The L1-mVenus sample was gathered and then frozen overnight. This step could lead to a possible degradation of the protein. Nevertheless, the majority of the L1-mVenus is fully expressed by the cells and if any free mVenus was tracked during single-molecule tracking, it was not much.

The single-molecule tracking results underline this (see **Manuscript 1**), but also the localization pattern (**Fig. 3.8**) fits the findings of our labs a few years ago [127]. There we see mainly strong signals at the poles, but also at the membrane (**Fig. 3.8A-C**). No signal is seen in special areas in the cell center, probably where the nucleoid might be. Clear and strong signal around this area, is especial good visible in **Fig. 3.8C**. Diffusive signal is rare. With this, it can be assumed that the L1-mVenus fusion is functional. The degradation observed in the western blot may possibly be caused by the overnight freezing.

All in all, it is believable that the L1-mVenus fusion is functional and therefore a good tool to compare its localization with the mRNA localization. Also, a comparison of the dynamics is possible and therefore highly recommended for this work.

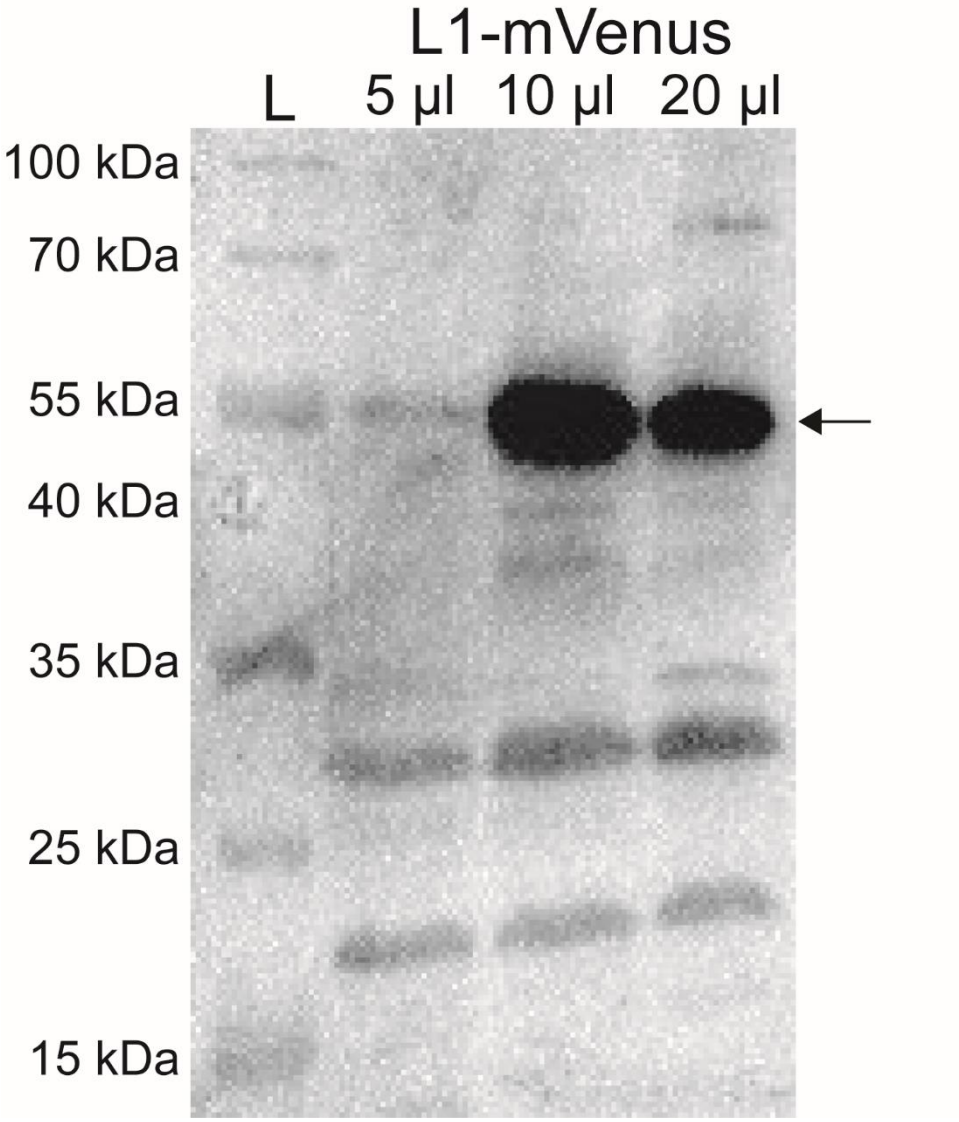

Fig. 3.7 Western blot of NCIB 3610 *Bacillus subtilis* cells, show an expression of the ribosomal protein L1-mVenus fusion.

For the gel electrophoresis, a 12% SDS-PAGE gel was used. For the SDS-PAGE, the L1-mVenus sample was concentrated to an OD of 5. After the transfer of the fusion protein from the SDS-PAGE to the membrane, an antibody against GFP, that works for mVenus too, was used. mVenus is 26.9 kDa small and L1 is 24.77 kDa small. Together it has a size of 51.67 kDa. Three different volumes were used for the SDS-PAGE, 5, 10 and 20 µl. L is a prestained protein ladder by ThermoFischer, which displays the protein size from 10-180 kDa.

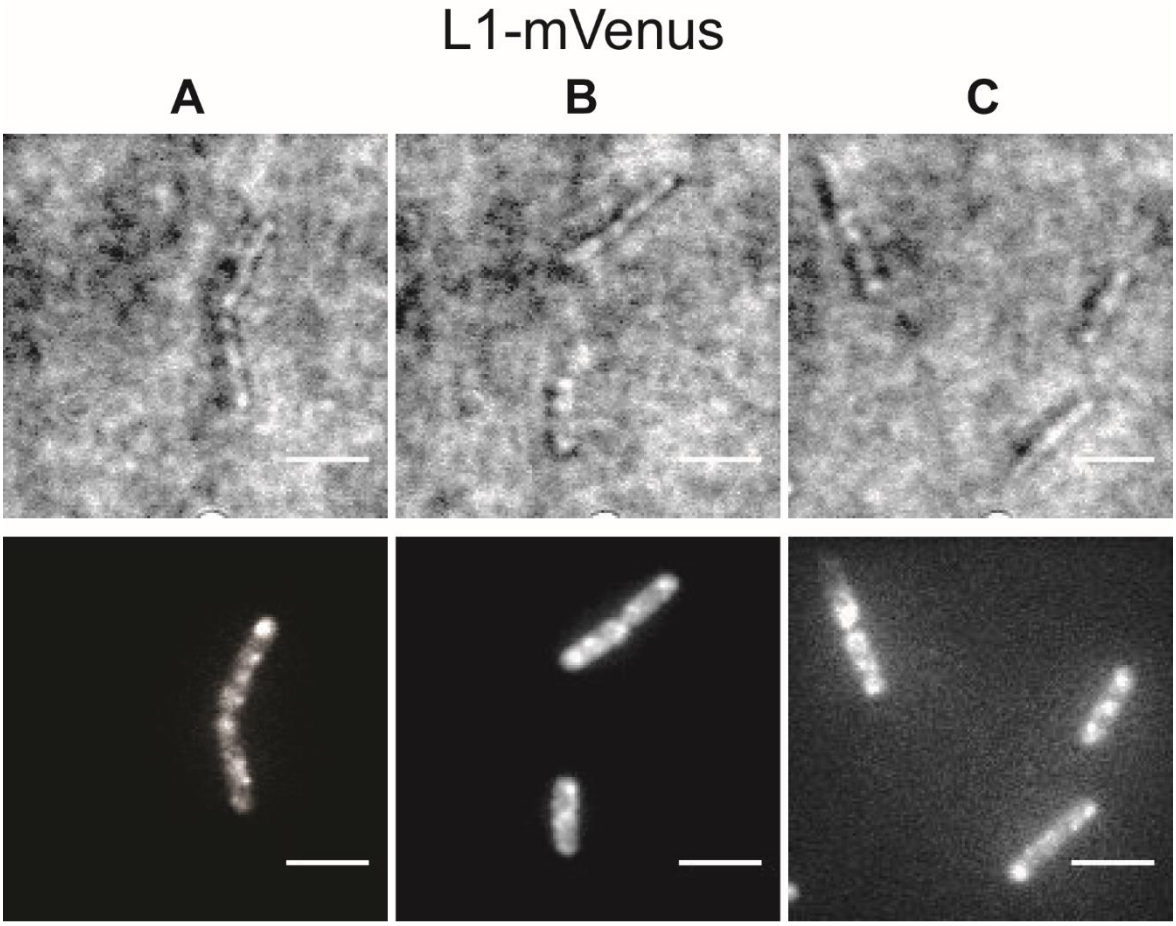

Fig. 3.8 Wide-field fluorescent pictures shows a known localization pattern in *B. subtilis*.

The same Nikon Eclipse Ti microscope, that was used for single-molecule tracking of L1-mVenus, was also used to do the wide-field fluorescent microscopy of L1-mVenus. An exposure time of 500 ms was used. (**A**) to (**C**) show *B. subtilis* cells, expressing the L1-mVenus fusion protein with different localizations. In the upper lanes, bright field pictures are depicted, in the lower lanes the fluorescent pictures. Scale bar 2 µm.

3.5 Further characterization of DynA-mVenus under different stress conditions

3.5.1 Western Blot of DynA

As already described, DynA is a dynamin-like protein of *B. subtilis* and is involved in the final membrane fusion during cell division [125, 199]. This membrane-associated GTPase binds to the membrane via its subunit D1 and partially via the D2 subunit. It is an intrinsic dimer that also functions as a scaffold for other protein that may be involved in membrane fusion [199, 206]. In this study, DynA fused to two different fluorophores were used. For the co-localization of the mRNA with its corresponding protein, under point **3.2**, it is fused together with a CFP.

For the molecule counting (**Fig. 3.10**+**3.11**) and Manuscript 2, it is fused with the GFP derivate mVenus, a monomeric fluorophore. A western blot was performed to proof the functionality of both DynA fusion proteins and that they are expressed in full length (**Fig. 3.9**). DynA itself is quite large with 137.16 kDa. Both fluorophores are 26.9 kDa small. Fused to DynA, the fusion proteins are 164.06 kDa big. To mention is that the same antibody can be used against both fluorophores, as it is an antibody against GFP and its derivates. A strong lane below 30 kDa is visible for the positive control, p.c., where purified GFP was used to test if the antibody works fine, because of the nature of mVenus and CFP as GFP derivates.

When looking at the western blot, only weak lanes are visible for DynA-mVenus and DynA-CFP depicted by the numbers 2) and 3) in **Fig. 3.9**. Although these lanes are weak, they are still of the correct size. It seems that DynA is expressed at a low level in *B. subtilis* cells, which we have already realized from single-molecule tracking (**Fig. 3.11**) and Epifluorescence microscope, where not each cell expresses the protein (**Fig. 3.6**+**3.11**). To control the procedure of extracting the DynA-mVenus fusion protein from the whole cell lysate, the membrane protein SpoIIIE, which was also fused with a mVenus fluorophore, was extracted from the whole cell lysate in parallel, in exactly the same way. The construct is 113.89 kDa in total and a stronger, but still weak, lane for SpoIIIE-mVenus is visible. In this control, as well as in the two samples of the DynA fusion proteins, an additional lane can be seen at around 70 kDa. It may not be degradation of the proteins, but rather an unspecific lane in *B. subtilis.* Because of the same unspecific lane seen for each construct, we assume that even though the lanes around 165 kDa are weak, those are indeed the DynA-mVenus and DynA-CFP constructs.

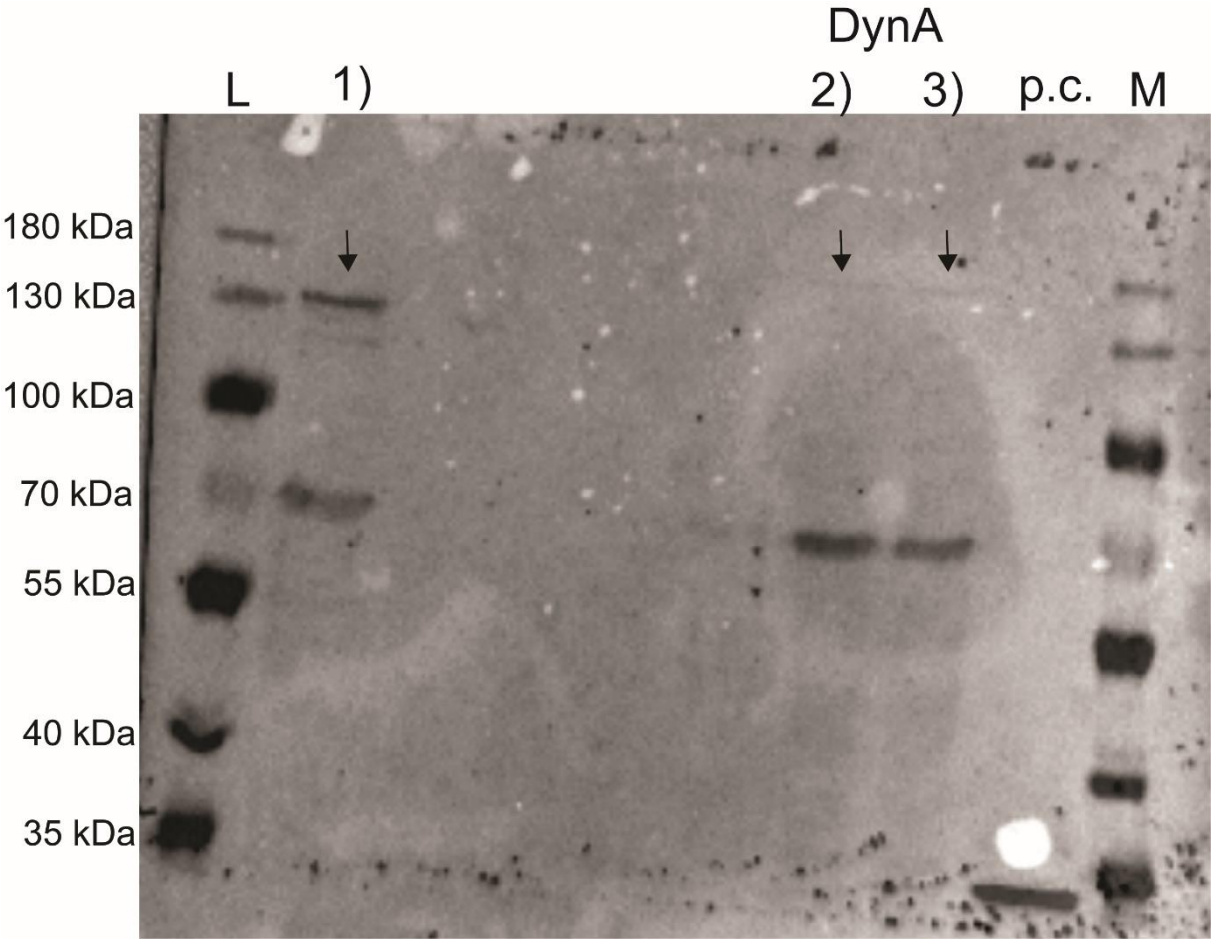

Fig. 3.9 Western blot of NCIB 3610 *Bacillus subtilis* cells, show an expression of the protein DynA-mVenus and DynA-CFP fusion.

For the gel electrophoresis, an 8% SDS-PAGE gel was used. For the SDS-PAGE, the DynA samples were concentrated to an OD of 5. After the transfer of the fusion protein from the SDS-PAGE to the membrane, an antibody against GFP, that works for mVenus and CFP too, was used. mVenus and CFP are 26.9 kDa small, and DynA is 137.16 kDa big. (**1**) is a control for preparation of the samples. For this, SpoIIIE-mVenus was used, which is 113.89 kDa big in total. (**2**) DynA-mVenus is 164.06 kDa and (**3**) DynA-CFP has the same kDa size. p.c is the positive control, which is purified GFP. L is a prestained protein ladder by ThermoFischer, which displays the protein size from 10-180 kDa.

3.5.2 Counting of the number of DynA-mVenus molecules under different stress conditions shows monomeric and dimeric fractions.

Single-molecule tracking already revealed, small changes on the molecule level are enough, to have an influence on the dynamics of DynA and therefore on the protection of the cells through membrane leakage. We also assume this is enough for an induced diffusion/capture mechanism to obtain membrane integrity surveillance (see **Manuscript 2**). We were also able

to show that most of the membrane stressors tested did not affect the dynamics of DynA at the single molecule level, with the exception of the antibiotics Nisin and slightly Bacitracin. Something similar was observed for the localization at the single-molecule level. Also, when considering the number of foci and their localization, the clearest change was observed under Nisin stress, even though sodium chloride (NaCl) leads to an increased number of foci, too (**Manuscript 2**, **Fig.1B**). To gather more information on the behavior of DynA, the number of molecules of DynA was counted and evaluated (**Fig. 3.10**). For this purpose, the "molecule quantification" tool of the SMTracker was used [159, 160]. Here, the molecules of each cell are counted indirectly if they are fused to a fluorophore, whose signal can in turn be detected by this tool. Wild type cells of NCIB 3610 *B. subtilis* cells, expressing no fluorophore at all, were also treated the same way as cells containing the DynA-mVenus fusion. This was done to subtract any background noise such as autofluorescence of *B. subtilis* cells. This also counts for cells expressing DynA-mVenus under several stress conditions. For this setup, every condition had its own wild type cells stressed and the experiment was done on the same day to minimize any external influences. Also, for the slide preparation, the agarose pads used were made with the same agar for each condition to minimize any influence here as well. An image of the pad with no cell is also necessary for the counting of molecules to subtract any background noise of the pad.

Another reason to perform the molecule counting was that we observed a relatively low number of tracks per cell of 3.7 for DynA-mVenus with no stress (**Fig. 3.11H**) via single-molecule tracking. This barely changes under heat stress and doubles under 250 µg Bacitracin and 10% ethanol (EtOH) stress. An increase of up to 11.54 tracks per cell can be observed under 1M sorbitol stress. The biggest effect is visible after adding 1M NaCl (20.18 tracks per cell) and stressing the cells for 30 minutes with 10 µg Nisin, resulting in a tenfold increase in the number of tracks per cell, with 29.64. This fits with our findings that Nisin and NaCl stress leads to an increase in foci per cell (**Manuscript 2, Fig. 1**). Surprisingly, this is not observed for the number of fluorophores in the molecular counting data (**Fig. 3.10A-D, M-O**). Here we can count the number of DynA-molecules by counting the fluorophores fused to them. The highest number of molecules of DynA-mVenus is seen under osmotic stress (**Fig. 3.10D**), with 140.55 ± 16.64. This is followed by DynA-mVenus under 1M NaCl stress (**Fig. 3.10M**), with a number of 120.68 ± 12.04 fluorophores, followed by DynA-mVenus under 250 µg Bacitracin stress (**Fig. 3.10N**), with 106.55 ± 9.53 fluorophores. **Fig. 3.10E** shows the 10% EtOH condition, where

94.86 ± 7.99 fluorophores can be counted. The next conditions show a drastic decrease in the fluorophore number of DynA-mVenus, with 47.42 ± 3.35 fluorophores counted under heat stress (**Fig. 3.10B**), and 10 µg Nisin stress leading to only 30.9 ± 5.77 fluorophores counted (**Fig. 3.10O**). In the unstressed condition, 18.77 ± 2.43 fluorophores are counted (**Fig. 3.10A**).

A drastic increase in the number of fluorophores was expected for NaCl and Nisin stress, which we observe only for the NaCl condition. After addition of Bacitracin and sorbitol to the cells, we also see an increased number of fluorophores, but not for DynA-mVenus expressing cells in EtOH and heat conditions. As we can see for DynA-mVenus with and without Nisin stress, both conditions show that many cells do not have many fluorophores in them, which we expected for DynA-mVenus unstressed (**Fig. 3.10A,O**). Mainly, the data show a number of fluorophores below 20. The same can be seen for DynA-mVenus under heat stress (**Fig. 3.10C**). The distribution of fluorophores in the cells is not even. This is obvious in **Fig. 3.10A,B,G**, where we see no or barely any tracks (depicted in blue) in some cells, where other cells have more. The number of tracks shown here is counted in a different way than the number of fluorophores (**Fig. 3.11G**). Here, a track was detected only if it appeared at least for 5 frames in a Brownian search radius of 0 to 5. On the other hand, looking at the conditions with the highest number of fluorophores, we see up to 450 fluorophores under sodium chloride stress, whereas the addition of sorbitol, Bacitracin and ethanol results in more than 200 fluorophores. Looking at the tracks displayed in different cells, here we see more often an even distribution of tracks throughout the cells, like in the sorbitol (**Fig. 3.11D**) and more or less in the ethanol (**Fig. 3.11C**) conditions. Here, more or less each cell has a signal in it, as shown also by the distribution of the number of fluorophores, with fluorophores rarely seen below a number of 50. A wider range, but still an even distribution of the fluorophores is seen for DynA-mVenus under Bacitracin stress (**Fig. 3.10N**), whereas the distribution in the cells seems to be more or less even (**Fig. 3.11F**). At the same time, DynA-mVenus not only exhibits one of the highest numbers of fluorophores after addition of 1M NaCl, but also ranks second in the number of tracks per cell. When looking at the tracks depicted in the cells (**Fig. 3.11E**), they seem to be crowded. Tracks can be seen more or less everywhere. It is important to mention again that the number of tracks is counted differently than the number of fluorophores. This is not equitable. It is a help to understand why the cells show more or fewer tracks under certain conditions. It is also important if the cells show an even expression of tracked DynA-mVenus. In untreated cells it would be possible that DynA is expressed only at

a low level because it is mainly required during cell division or membrane leakage, especially Nisin-induced ones. Why after the addition of Nisin, DynA-mVenus is not highly expressed in each cell, is not clear. We cannot say why the number of fluorophores counted here does not meet our expectations, except for a few conditions, for example, osmotic and ionic stress caused by NaCl and the unstressed one. Still then, the average number of fluorophores is much higher than the tracks per cell. Even though a direct comparison between those two methods is not possibly, it should give a hint of what we can expect. For another protein, Dgck, where the tracks per cell were also very low, the number of fluorophores was also still low with around 5 [225]. The 18.77 fluorophores counted for DynA-mVenus are still much more, while the number of tracks was similar for both proteins. The differences in the definition of a track versus molecular quantification could be an explanation, as well as the lesser-known regulatory mechanism of DynA by the housekeeping sigma factor SigA [226, 227], which will be discussed further under **4.2.1**.

It has been previously reported that DynA functions as an intrinsic dimer, but it could potentially also interact with another DynA to form a homodimer. It is possible that it only forms dimers when membrane fusion must occur [178]. We have also shown that DynA movements are best explained by assuming three different populations, with the static population likely being the one in which membrane fusion occurs. Therefore, one possibility could be that the other two populations are DynA molecules moving in the cell in a monomeric state. To address this, molecule quantification was also used. **Fig. 3.10I-L** and **S-U** show the bleaching steps of the DynA-mVenus fusion protein. By looking at the bleaching of the fluorophore, it is possible to determine different fractions. If a second bleaching step occurs and therefore is double the first fraction, it may be a dimer if the first fraction is assumed to be a monomer. However, it is also possible that the first fraction is a dimer and the second fraction would be then a tetramer. Hence, the biological context should not be disregarded, because it plays a crucial role.

For DynA-mVenus, two fractions can be observed (**Fig. 3.10I**). The first bleaching step includes 64% of the molecules with an average of 5.443 photons. A second bleaching step is seen with 12.369 photons for 36% of the molecules, which is about twice the photons of the first bleaching step. In the biological context, it makes sense that around two-thirds of the DynA molecules are monomers, which are moving around in the cells, probably scanning the cell for membrane leakage. Only DynA molecules that fuse together membranes, due to

membrane leakage or during cell division, would be found as dimers. The doubling of photons can be explained by the assumption that one dimer bleaches out over the same time as two monomers.

Something similar can be observed for DynA molecules under 250 µg Bacitracin stress (**Fig. 3.10T**) and the mechanic membrane stress of 42°C (**Fig. 3.10J**). In both conditions, we have two bleaching steps. Under heat and Bacitracin stress, the assumed monomeric fraction is 69% and the average bleaching steps under heat are 6.289 photons and 4.969 photons for Bacitracin. For the other 31%, the average bleaching step is again about twice as large of the first one, with 12.613 photons under heat stress and 9.995 photons under Bacitracin stress. Cells treated with 1M sorbitol and 1M NaCl show an increase in the assumed monomeric fraction compared to the unstressed condition. With 1M sorbitol, 78% of the observed bleaching molecules have an average bleaching step of 5.785 photons (**Fig. 3.10L**). For the supposed dimeric fraction, which is 21% small, an average bleaching step of 14.836 photons was observed. Under 1M NaCl stress, DynA molecules are found with 73% in the assumed monomeric state, where the average bleaching step is 5.780 photons, whereas the assumed dimer fraction of 27% has an average bleaching step of 10.602 photons (**Fig. 3.10S**). Under ethanol and Nisin stress, an increase of the supposed monomeric fraction is again observed (**Fig. 3.11K,U**). This time, under 10% ethanol stress, 7.008 photons were observed for the assumed monomers, which make up of 85% of the molecules. For the other 15% molecules of the supposed dimeric fraction, 17.272 photons were observed. Under Nisin stress, something similar happens. The first fraction is 82% big, with 10.743 photons for an average bleaching step. The observed average bleaching step for the supposed dimeric fraction is around the double, with 20.998 photons. This fraction is 18% big.

The unstressed condition displays DynA in a normal state in *B. subtilis*. The assumption of two-third of the molecules being monomers and the other third being dimers makes sense in the biological context, as the single-molecule data of Manuscript 2 already showed a mainly diffusive population for DynA molecules. That DynA does not really change below 42°C also fits with the other microscopy data of Manuscript 2, where no real changes to the normal condition were observed. That Bacitracin stress also leads to no real change on the molecule level also fits to the other microscopy data. Only slight changes in the residence time and possibly in localization are shown, but those changes are not prominent. A possible reason for the detected changes in the monomeric and dimeric states of DynA under the other stress

conditions, will be further explained in section **4.2.1**, as well as a possible tetrameric oligomerization event of DynA under Nisin treatment.

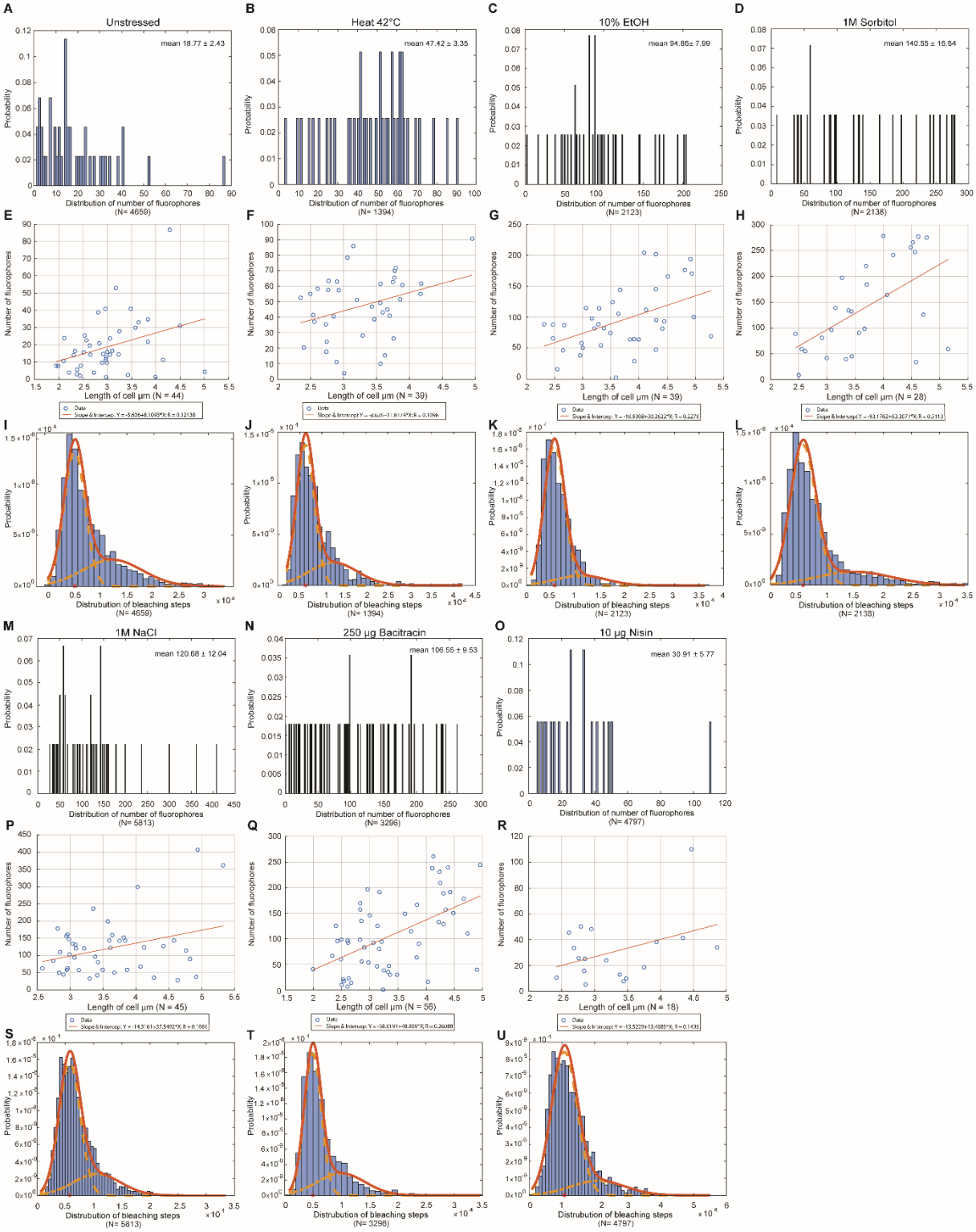

Fig. 3.10 Molecule counting of DynA-mVenus under different stress conditions.

Distribution of the number of fluorophores per cell containing DynA-mVenus in exponential growth phase under (**A**) unstressed condition with an average of 18.77 ± 2.43 fluorophores,

(**B**) 42°C heat stress with an average of 47.42 ± 3.35 fluorophores, (**C**) 10% EtOH stress with an average of 94.86 ± 7.99 fluorophores, (**D**) 1M Sorbitol stress with an average of 140.55 ± 16.64 fluorophores, (**M**) 1M NaCl stress with an average of 120.68 ± 12.04 fluorophores, (**N**) 250 µg Bacitracin stress with an average of 106.55 ± 9.53 fluorophores and (**O**) 10 µg Nisin stress with an average of 30.91 ± 5.77 fluorophores. A correlation between number of fluorophores and size is not to see for (**E**) the unstressed condition, (**F**) under heat stress, (**G**) 10% EtOH stress, (**H**) 1M Sorbitol stress, (**P**) 1M NaCl stress, (**Q**) 250 µg Bacitracin stress and (**R**) 10 µg Nisin stress. The distribution of bleaching steps shows monomeric and potential dimeric DynA-mVenus molecules for (**I**) the unstressed condition, (**J**) under heat stress, a smaller dimeric population for (**K**) 10% EtOH stress, (**L**) 1M Sorbitol stress, (**S**) 1M NaCl stress, (**T**) 250 µg Bacitracin stress and again a smaller dimeric fraction for (**U**) 10 µg Nisin stress. For each stress condition, cells were stressed for 30 minutes. N is the total number of fluorophores for the distribution of fluorophores and the distribution of bleaching steps and also the number of cells for the linear regression relation between cell length and the number of fluorophores.

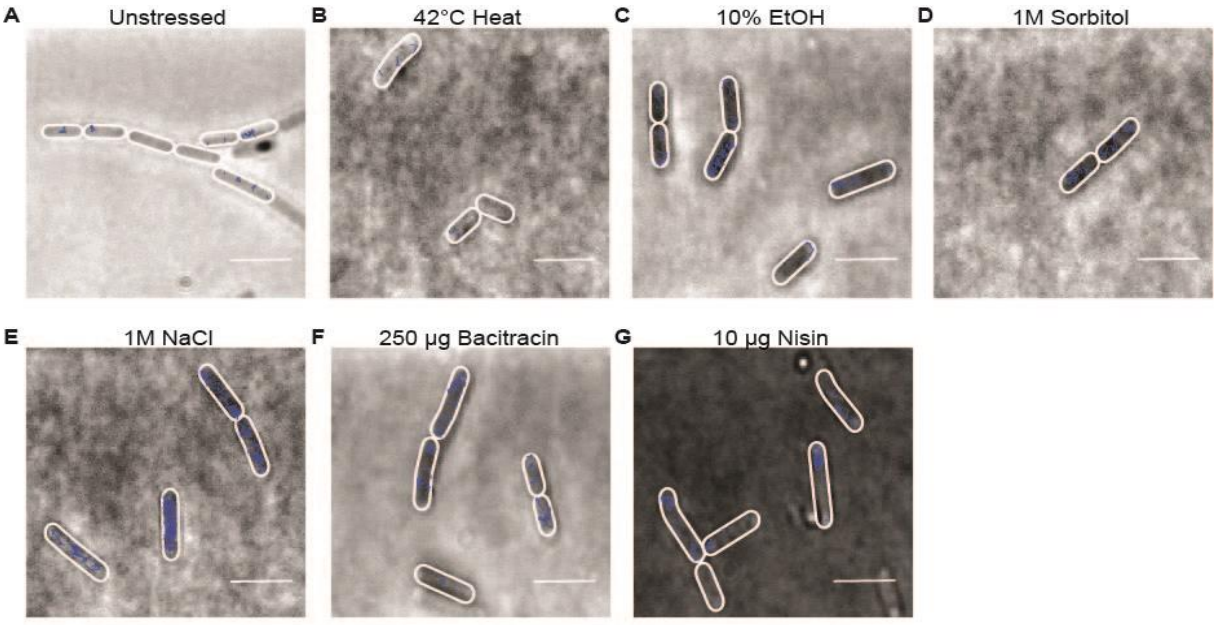

H

	Unstressed	42°C Heat	10% EtOH	1M Sorbitol	1M NaCl	250 µg Bacitracin	10 µg Nisin
Cells	24	41	39	29	45	65	25
Cells with tracks	21	38	37	29	45	62	25
Tracks	89	183	261	284	880	463	643
Tracks/cell	3.7	5.4	7.1	11.5	20.2	7.5	29.7

Fig. 3.11 Overview of tracks in *B. subtilis* cells, expressing DynA-mVenus, under different stress conditions used for molecule counting.

From **A-G** are *B. subtilis* 3610 cells shown, that express the DynA-mVenus fusion. In blue, tracks of the movement of DynA-mVenus are depicted. To count as a track, it needs to exist

for at least 5 frames with no gap and in a Brownian search radius of 0-5 pixel. Different conditions were used, (**A**) is DynA-mVenus under normal circumstances, (**B**) under 42°C heat stress, (**C**) under 10% ethanol stress, (**D**) under 1M Sorbitol stress, (**E**) under 1M sodium chloride stress, (**F**) under 205 µg Bacitracin stress and (**G**) under 10 µg Nisin stress. The table (**H**) depicts the total number of cells for each condition, how many of them can be found with tracks, how many tracks are detected and how many tracks per cell are there. Cells were incubated for 30 minutes for each stress condition. Scale bar 2 µm.

3.5.3 DynA dwell times change under Nisin treatment

In addition to the SDQ simultaneous analysis and confined localization used (see **Manuscript 2**), the behavior of DynA was further characterized by looking at its dwell time. For this, the same data set was used as for the dynamics and localization data. The dwell time here applies to the tracks moving within a 120 nm radius with a minimum of 8 steps, the same conditions as for the confined localization. DynA alone probably has more likely one dwell event of 0.22 ± 0.0025 seconds (**Fig. 3.12A,D**). Two different dwell events can also be assumed. However, it must be taken into account that the mean deviation is 20%, where the first population with a residence time of 0.17 ± 0.041 seconds is only 11.8% and the second population is 88.2% and has a residence time of 0.23 ± 0.013 seconds. Therefore, it is reasonable to assume only one dwell event. Of the 667 DynA tracks, only 21% met the condition for dwell times and were used for this purpose. This is also true for the observation of the confined localization.

Looking at the different stress factors, there is no particular variation in the residence time under heat (0.26 ± 0.0048 sec.) and ethanol stress (0.25 ± 0.0051 sec.) or osmotic (0.24 ± 0.0043 sec.) and osmotic ionic stress (0.2 ± 0.0051 sec.) for the one-component fit (**Fig. 3.12D**). However, there is a difference if we assume that there are two different dwell events. Here, the shorter residence time resembles DynA without stress (0.18-0.24 sec.), but the population size turns out to be much larger, with 74-90%. The mean deviation here is partly so big that the second, clearly smaller fraction can be attributed to the deviation, as it is the case for DynA in untreated cells. This can be seen very clearly under heat and sodium chloride stress. But also under ethanol and sorbitol stress this population becomes very small (maximum up to 9% considering the mean deviation). At the same time, a significant prolongation of the residence time can be observed in some cases for these stress factors (0.28-065 sec.). These very long dwell times for DynA do not fit in any way with the observed dynamics of DynA, where a larger population would then be expected in the static population.

Furthermore, if we compare what percentage of the total DynA tracks experience a dwell event under the different stressors, these values again closely resemble the DynA molecules expressed by untreated cells. Under heat stress 20% are in a dwell event and thus also a confined localization, while under ethanol and sorbitol stress it is 19% and under sodium chloride stress only 17% DynA molecules. Moreover, the average lifetime of the tracks, given in frames/sec, are similar with 7.2-7.9, whereas an average lifetime of 7.6 frames/sec was found for DynA. Therefore, I assume that the stress factors listed above do not lead to any real change in the residence times.

This is different in cells treated with Bacitracin and Nisin (**Fig. 3.12B,C**). A first indication is the average lifetime of the tracks. Although under Bacitracin stress this does not really change (7.7 frames/sec), it increases significantly under Nisin stress to 9.7 frames/sec (**Fig. 3.12D**). Using these two antibiotics, the ratio of DynA molecules changes in a dwell event. Here, there are clearly two different dwell times, with almost identical, equal ratios between the different populations. Thus, τ1 under Bacitracin stress is 0.18 ± 0.0065 seconds long and the associated fraction is 49.7 ± 9.11% in size. The second residence time is 0.28 ± 0.015 seconds long and 50.3 ± 9.11% large. Under Nisin treatment, the second dwell time is even prolonged to 0.35 ± 0.012 seconds. This fraction is 47.5 ± 3.69% in size. The remaining 52.5 ± 3.69% have a residence time of 0.18 ± 0.0039 seconds. It is obvious that there are two different dwell times among these two antibiotics. In addition, the percentage of tracks involved in the dwell event also increases and thus also have the confined localization. Under Bacitracin stress it increases to 25% of all tracks and under Nisin stress even to 38%. Especially the influence of Nisin on DynA molecules is also reflected in the SQD simultaneous analysis, where the static population increases. This is not visible for DynA molecules under Bacitracin treatment. However, since almost 600 tracks of the nearly 2400 tracks show this change in the residence times, there seems to be no error due to a small amount of data. A slight change in the localization (**Manuscript 2**, **Fig. 4+5**) is also recognizable. Given is the fact of the distinct change in behavior of the DynA molecules under Nisin stress, which could be observed throughout this work.

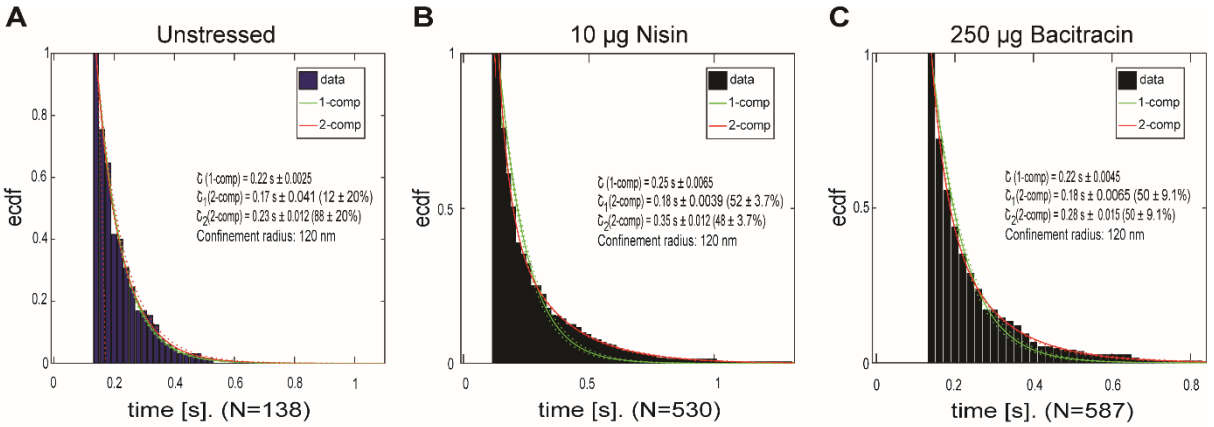

D

	Unstressed	42°C Heat	10% EtOH	1M Sorbitol	1M NaCl	250 µg Bacitracin	10 µg Nisin
Cells	194	149	81	96	55	142	20
Cells with tracks	166	116	72	96	54	142	20
Tracks	667	642	861	1059	624	2385	1412
average lifetime [frames/s]	7.6/0.15	7.8/0.16	7.3/0.15	7.9/0.15	7.2/0.14	7.7/0.15	9.7/0.19
av. residence time [s]	0.249 ± 0.017	0.281 ± 0.021	0.282 ± 0.026	0.275 ± 0.019	0.222 ± 0.014	0.241 ± 0.008	0.275 ± 0.011
τ [s]	0.22 ± 0.0025	0.26 ± 0.0048	0.25 ± 0.0051	0.24 ± 0.0043	0.2 ± 0.0051	0.22 ± 0.0045	0.25 ± 0.0065
τ1 [s]	0.17 ± 0.041	0.24 ± 0.014	0.22 ± 0.0056	0.23 ± 0.0045	0.18 ± 0.012	0.18 ± 0.0065	0.18 ± 0.0039
Fraction τ1 [%]	11.8 ± 20.3	84.4 ± 15.1	86.8 ± 4.25	90.3 ± 3.25	73.6 ± 22.4	49.7 ± 9.11	52.5 ± 3.69
τ2 [s]	0.23 ± 0.012	0.47 ± 0.02	0.6 ± 0.12	0.65 ± 0.14	0.3 ± 0.084	0.28 ± 0.015	0.35 ± 0.012
Fraction τ2 [%]	88.2 ± 20.3	15.6 ± 15.1	13.2 ± 4.25	9.75 ± 3.25	26.4 ± 22.4	50.3 ± 9.11	47.5 ± 3.69
Number of Tracks	138	128	167	198	109	587	530

Fig. 3.12 Overview of tracks and dwell events in *B. subtilis* cells, expressing DynA-mVenus, under different stress conditions used for localization and dynamics analyses.

One dwell event can be found for DynA-mVenus (**A,D**), also under 42°C heat stress (**D**), under 10% ethanol stress (**D**), under 1M Sorbitol stress (**D**), under 1M sodium chloride stress (**D**), and two dwell events for DynA-mVenus under 250 µg Bacitracin stress and (**B,D**), and under 10 µg Nisin stress (**C,D**). The table (**D**) depicts the total number of cells for each condition, how many of them can be found with tracks, how many tracks are detected and the average life time for them in frames per seconds. Furthermore, the duration for one and two dwelling events is shown in seconds, while the amount of how many molecules residue in the defined circle of 120 nm with a minimum of 8 steps is depicted in percentage. The number of tracks, that were used for this analysis are shown in the table and under the graphs. An average residence time is also shown. Cells were incubated for 30 minutes for each stress condition.

4. General Discussion

4.1. Analysis of the localization behavior and the dynamics of several mRNAs and L1 in *B. subtilis* via single-molecule tracking

Transcription and translation are basic, and necessary processes for life, which can be found in each organism. The assumption that these processes are coupled in prokaryotes has an advantage. This would mean that by binding to the nascent mRNA, too early transcription termination in a Rho-dependent manner could not occur, and it could protect against early degradation [73]. This could be the case in bacteria such as *Caulobacter crescentus*, where the chromosome fills the entire cell [80], where the Jacobs-Wagner group observed co-localization of ribosomes with the nucleoid as well as mRNAs remaining near their transcription site [228]. Therefore, they propose that the chromosome serves as a template for the mRNA to be translated, although it does not have to explicitly lead to the coupling of transcription and translation, but at least this occurs in close spatial proximity to each other [228].

In contrast, other model bacteria such as *Escherichia coli* and *Bacillus subtilis* have a nucleoid that contains the chromosome and occupies the central area of the cell, but leaves out the poles as well as the center in large cells that are about to divide [98]. In *E. coli*, one study found that approximately 80% of all 70S ribosomes were found outside the nucleoid [101]. Further studies even found the majority of all 70S ribosomes outside the nucleoid, while the two ribosomal subunits could be found unbound in the nucleoid [78, 102], possibly leading to nucleoid expansion in rapidly growing *E. coli* [78] In addition, only 4% of RNA polymerases and ribosomes colocalize in the nucleoid [79]. This indicates a separation of transcription and translation. The Amster-Choder group therefore proposes the model that mRNAs localize where their subsequent protein product localizes [81]. Thus, mRNAs for soluble proteins are thought to be translated in the cytoplasm, whereas the mRNA of membrane proteins are translated near or at the membrane, which has been observed to be the case by several groups [81, 103-105]. Operons encoding both cytosolic and membrane proteins are thought to have a priority for membrane proteins that are dependent on the SRP [81, 107].

However, the Amster-Choder group already observed that 10-15% of mRNAs might show coupling of transcription and translation in fast growing cells, whereas the other mRNAs localize with their corresponding protein [79, 229]. In contrast, another group has speculated

that the majority of mRNAs in *E. coli* show coupled transcription and translation, but some mRNAs are probably translated outside the nucleoid in ribosome-rich regions [230]. In general, there are conflicting reports where mRNAs could be found in the nucleoid or surrounding it [99], while other groups found the exact opposite [106]. In addition, there are few reports on the dynamics of mRNAs in *E. coli*, which was either determined indirectly [231] or where the diffusion coefficient of 70S ribosomes was described [102].

In this work, by using the MS2-system, I was able to determine the DC of mRNAs that are just about to be translated in *B. subtilis*, with almost no movement and slower DC than that described in *E. coli*. At least one other population can be assumed where the assembly of the ribosome takes place, to which the mRNA is bound. I found the same for the ribosomal protein L1, which has yet other populations of ribosome assembly, and probably a free population where L1 is maximally bound to the free 50S subunit, described for the first time in a Gram-positive bacterium. The mRNA localization I observed is consistent with both presented models to some extent. Thus, mRNAs encoding soluble proteins are found at the poles and in the cytoplasm, whereas mRNAs can also be found surrounding the nucleoid, where possible coupling of transcription and translation is possible. At the same time, mRNA encoding membrane proteins, among others, have, in my opinion, a tendency towards the cell membrane. In the following, the obtained findings of this study will be discussed in detail.

4.1.1 Localization pattern of several mRNAs in *B. subtilis*

With single-molecule tracking and by using the SMTracker tool, data were obtained of the localization and the dynamics of the tested mRNAs. First, I will discuss the localization behavior of the mRNAs, starting with the mRNAs tagged with two MS2-binding sites.

Three observations apply to all mRNA constructs tested in *B. subtilis*. 1.) Mobile signal is present in the confined maps mainly in the cell center, as well as in the cytoplasm (**Fig. 4.1E**). The poles and cell periphery show little signal there. 2.) In the confinement maps, signals for mixed behavior is rarely visible. There are not many transient events leading from more diffusive to confined localization and vice versa. 3.) Regardless of which proteins a mRNA encodes, defined localization is found in the cytoplasm, including surrounding the nucleoid, and at the poles (**Fig. 4.1B,C**). In large cells about to divide, where the nucleoid is no longer present at the cell poles and in the middle of the cell, but makes room for the invaginating septum [98], mRNAs can be found in the nucleotide-free region in the septal region (**Fig. 4.1D**).

I hypothesized that where mRNAs localize longer, their translation occurs. This is

supported by finding a static localization of ribosomal protein L1, an observation made not only in this work but also previously by our group [127]. More on this in a moment.

Of interest is that, in my opinion, mRNAs encoding solely soluble proteins (*rplJ-rplL, rplK-rplA*) localize in a confined manner only at the sites described above. Here, I cannot observe a helical distribution in the cytoplasm as described by the Amster-Choder group [81]. Among other reasons, I think that some mRNAs show a somewhat specified localization, depending on where the subsequent protein product localizes. For example, co-expression of *ypbR-ypzF* with the protein Dyna shows a partial localization match. No clear statement can be made as to whether the observed co-localization means that the protein originated from the co-localizing mRNA or arose independently elsewhere within the cell and diffused there, and the observed co-localization is a coincident event. At least for mRNAs encoding membrane proteins only (*comN-secDF*) an altered localization is observable. Here, a tendency toward the cell periphery and signal directly at the membrane is detectable (**Fig. 4.1A**). This also applies to operons encoding both cytosolic and membrane proteins (*mreB-minD*, *rnc-ftsY*, *spoIIIE-ymfC*, among others), where a certain proportion of mRNAs are translated near or at the cell periphery. This makes sense since these membrane proteins rely on the SRP for proper integration into the membrane [107]. At the same time, the heat maps do not show this tendency so clearly. Since the probability of distribution of all tracks is considered here and not only that of the confined localization, these deviations might occur. Whether or not there is a preference of mRNAs for membrane proteins to be translated cannot be further verified here, since all mRNAs localize in the cytoplasm and poles, as mentioned above. Even if this is not the case, the example of FtsY in *Shewanella putrefaciens* shows that proteins can move rapidly through the cell to get to where they are needed [232]. Some alignment with the Amster-Choder group model is therefore provided. Other groups have also found specific mRNAs in various organisms at the sites where the associated protein later localizes [103-105].

The mRNA *hag* is an exception. Its corresponding flagellin protein is localized in the extracellular. Even though this protein is transported out of the cell at some point, no export signal at the moment is known, according to SubtiWiki. My findings show a clear cytosolic localization pattern for *hag.* This phenome has also been observed in *E. coli* [101, 105]. It is known that a lot of proteins of the extracellular depend on the Sec-pathway and partially also of the SRP [233], but this is not true for all. The same paper also discussed that proteins independent of the Sec-pathway can be found in the cytoplasm before being transported out

of the cell. Therefore, it is plausible to assume that those proteins are also translated in the cytoplasm, and *hag* might be one of them, as my findings suggest.

Thus, my assumption that some mRNAs might have a specific localization, depending on the localization of their corresponding protein, is not unfounded. Nevertheless, my results do not contradict the model of the Jacobs-Wagner group, in which the transcript remains in proximity to the transcription site [80]. Plenty of signal could be detected in the cytoplasm and around the presumed nucleoid. Although there appears to be no coupling between transcription and translation in *B. subtilis*, in part because of the barely existing overlap of 70S ribosomes with RNAP in *E. coli* [101], mRNAs do not necessarily appear to diffuse far from their transcription site, on condition that the gene to be transcribed is transcribed at the nucleoid periphery by the RNAP. In other organisms and also for other genes in *B. subtilis*, coupling of transcription and translation has not been ruled out [73, 100, 230] but has not been clearly observed in this work.

As mentioned earlier, the ribosomal protein L1 of the large subunit shows similar localization behavior as the tested mRNAs, which speaks for the functionality of the MS2-system, but also supports my assumption that translation events are observed. Interestingly, a confined localization in the cell center with the presumed nucleoid can be seen very well when looking at the data with 20 ms exposure time. However, this confined signal in the nucleoid decreases greatly when microscopy was performed with a higher exposure time. This suggests that the individual ribosomal proteins diffuse freely in the cells and appear to be most mobile in the nucleoid. It seems that the more mobile it is, the more it is found in the cell center, while significantly more static populations can be observed primarily at the poles, in the cytoplasm, and at the membrane, which is also the case in epifluorescence images [127] (**Fig. 3.8**). For the more mobile populations, it can be assumed that L1 is part of the free 50S subunit, whereas the more static signals, among others at the poles, represent a fully or almost fully assembled ribosome, with the 30S and 50S subunits bound in the 70S ribosome (**Fig. 4.2C**). The observed confined signal for the mRNAs then means that there the mRNA is bound to the ribosome and possibly already being translated, while more mobile mRNAs form possibly the translation-initiation complex with the 30S subunit and probably diffuse out of the nucleoid into the cytoplasm. The finding of the two unbound subunits of the ribosome mainly in the nucleoid in *E. coli* supports this assumption [102]. At the same time, outside the nucleoid should be the majority of the complete 70S ribosome, indicating more static

populations, which was also observed in this study. Moreover, *E. coli* and *B. subtilis* are similar in many aspects [23], which is why I think it is plausible that my results from L1 correspond to those in *E. coli*, which in turn confirms my assumption of translation of mRNAs.

To ensure that the specific localization observed was indeed the mRNA constructs labeled with the MS2-system, SMT was performed with the addition of Rifampicin. Before the addition of the transcriptional inhibitor Rifampicin, confined localization of *spoIIIE-ymfC* is visible at the membrane, poles, cell periphery and cytoplasm, leaving the cell center free. Free diffuse signal is seen throughout the cell. After the addition of 25 or 50 µg/ml Rifampicin, a clear discrepancy is observed as the signal at the membrane and poles is completely lost. The detected signal is now located throughout the inner part of the cell, including the cell center. Something that is not observed in cells expressing only the MS2-mVenus tag. There it tends to accumulate near the poles and in the cell center after the adding of Rifampicin. The same can be observed for L1. This indicates that the MS2-system appears to bind nonspecifically to ribosomal RNA, which makes up the majority of RNAs in bacteria [234]. Therefore, a truly specific localization pattern for certain mRNAs may be missed. In addition, it appears that the MS2-tag may diffuse into the compact nucleoid, possibly by binding to rRNA, leading to a blurred result. Thus, the different localization patterns may only apply to a portion of the mRNAs. However, the reduced rate of transcription makes it clear that the specific localization of the mRNA disappears, which is in favor of the assumption that translation taking place. The accumulation in the nucleoid after the inhibition of RNAP suggests that the low level of transcribed mRNA remains there. On the other hand, the small amount of mRNA that is still transcribed continues to be translated at the poles by the ribosomes, which accumulate there in greater numbers. The fact that barely any confined localized mRNA is found in the nucleoid in untreated cells suggests that no translation takes place there, especially since the DNA cluster is usually very compact [98, 113] and, therefore, offers little space for the translation apparatus, which leads me to the assumption that there is a separation of translation and transcription in *B. subtilis*.

It is known that during translation a mRNA copy is translated more than once, depending on the cells' need and, among other things, the lifetime of a mRNA to save resources [79]. There is no reason for big movement of mRNA during translation. The observed residence time, which confirms my assumption of translating mRNA, refers only to tracks found in confined localization. The residence times of the four mRNAs with two MS2BS show

that 14-25% of the static molecules have a long dwell time of 1.3-1.7 seconds, while the other percentage still has a long dwell time of 0.73-0.79 seconds. This applies to an average of 78% of all tracks, so a high percentage of mRNAs exhibit the confined localization. One explanation for the two different residence times could be that the shorter dwell time refers to mRNAs that are not yet translated but are about to be, and the longer residence time represents the actual translation. However, it could also be that the presence of polyribosomes or single ribosomes on mRNAs play a role here, leading to either a longer or shorter residence time of the mRNA, but one should keep in mind the incorporation rate of amino acids [98, 101]. It cannot be clearly stated which dwell time corresponds to the presence of polyribosomes or not. The cloning error of the artificial mRNAs leads to an interesting behavior, highlighting that the more static populations are involved in translation. Artificial mRNAs have a residence time of only 0.84 seconds on average, which is slightly longer than the shorter residence time for mRNAs with two MS2BS. This applies to an average of 72% of all tracks. Although the majority of the tracks have confined localization, the incorrect cloning may lead to early terminated translation, which we see in the shortened residence time. However, the influence of the MS2-system causes an altered lifetime of mRNAs in yeast, as the MS2-system can lead to delayed degradation, but of shortened mRNAs [208]. This could also be the case here, whereby protein production does not appear to be greatly affected. Whether this is actually the case cannot be verified here. Fact is, the MS2-system has an influence on growth, but this is independent of the MS2BS (**Fig. 3.2**). In the end, however, protein production seems to be fine, as the mRNAs also encode essential proteins, among others, and the cells show no impairment in morphology and growth [235] and the growth assay with MS2-mVenus + *hag*_MS2BS1x shows no differences compared to the WT. Experiments with other components of the translational machinery underline my assumption that translation of mRNA can be observed here. It is known that in *E. coli* translation of proteins occurs at a rate of 8-20 aa/sec [98, 236]. By tRNA tracking, it was also found that translation initiation and elongation have residence times of 50 and 100 ms for certain tRNAs [101]. In eukaryotes, a translation time of about one second was found for β-actin mRNA [75]. All in all, it can therefore be assumed that a dwell time of maximum 1.7 seconds is not too long for the observation of a translation event and could even be longer, considering that the bleaching of the molecules could lead to a shorter dwell event than would be the case in reality.

The last thing to discuss is the mobile population, which can be found primarily in the

center of the cell (**Fig. 4.1E**). This is likely to be freely diffusing mRNA, possibly forming the translation-initiation complex with the 30S subunit in the nucleoid after transcription and leaving the nucleoid. The presence of the unbound 30S subunit supports that the translation-initiation complex is formed in the nucleoid [102]. Outside the nucleoid, possibly already on the way out due to the localization of L1, the assembly of the ribosome takes place. Translation of the mRNA occurs at the above-listed sites outside the nucleoid, consistent with the results for the 70S ribosome in *E. coli* [101, 102].

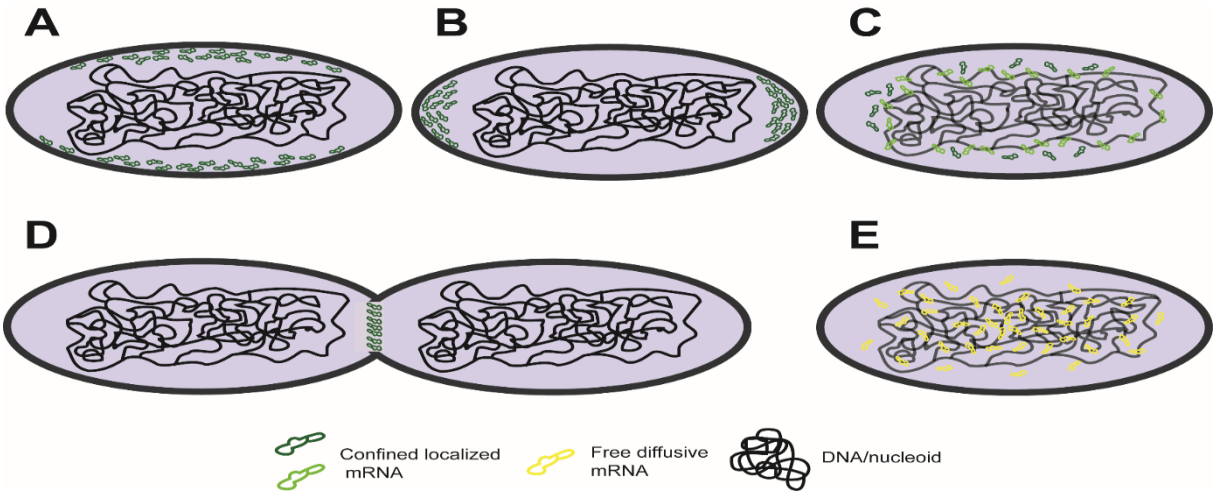

Fig. 4.1 Model of the localization of mRNA in *B. subtilis*. Based on the findings of the localization data of mRNAs in *B. subtilis* gained by single-molecule tracking.

Confined localization of mRNA at the membrane and cell periphery/near the membrane **(A)**, at the poles **(B)**, in the cytoplasm around the nucleoid as well as at the periphery of the nucleoid **(C)** and in the septal area of large dividing cells **(D)**. Diffusive signal is found throughout the cell, and accumulating in the cell center **(E)**. mRNA in yellow represent free diffusing mRNA, and in green represents mRNA with confined localization. Confined localization data was defined as signal found within a radius of 120 nm for a minimum of 8 steps. mRNA shown in lighter green is located within the nucleoid, while dark green mRNAs are outside of the nucleoid.

4.1.2 mRNA and L1 dynamics in *B. subtilis*

In this work, SMT was used to investigate not only the localization of the various mRNAs and L1, but also, for the first time, their dynamics in a Gram-positive bacterium. Here, the dynamics of the mRNAs can be divided into at least two different populations, while for L1 possibly more than three populations exist. To avoid overfitting, the Bayesian Information Criterion was used [212], among others, as well as several statistic tests to ensure the accuracy of the data [159,

160]. Looking at the three different populations proposed by the SMTracker, the diffusion constants (DC) between the individual mRNAs and also L1 are in general similar. Yet, this is also true for the MS2-tag alone, again suggesting nonspecific binding to rRNA. Nevertheless, a major difference can be seen in the population sizes. Here, a clear discrepancy between the static (D_1) and the mobile population (D_3) of mRNAs can be seen in comparison with the MS2-tag. The generated data under Rifampicin stress further illustrates this, as the slow mobile (D_2) and mobile populations increase for the MS2-tag and more closely resembles the behavior of L1. However, D_1 remains almost unchanged, unlike for the tested mRNAs. Their static population decreases by half, as it does for L1, and the mobile population increases in size for it. These results allow several conclusions. 1.) The suspicion strengthens that the MS2-tag interacts with the ribosome or its components, which leads to the fact that 2.) no reliable statement can be made regarding the mobile population for the mRNA constructs, since the background noise due to the MS2-tag overshadows this to a certain extent. 3.) The other two populations can be investigated further, with the static population likely being the translation of the mRNAs.

Looking now at the individual populations, one can see that the mobile population with 0.08-0.1 $\mu m^2 s^{-1}$ for the mRNAs and 0.1 $\mu m^2 s^{-1}$ for L1 do not show a particularly fast DC. However, looking at L1 with a faster exposure time, we get a tripling of the DC to 0.337 $\mu m^2 s^{-1}$ for D_3 and an approximate halving to 0.0594 $\mu m^2 s^{-1}$, for D_2, while D_1 with 0.0163$\mu m^2 s^{-1}$ D_2 corresponds to D2 at an exposure time of 75 ms (0.0181 $\mu m^2 s^{-1}$), which fits as far as the DC of unbound 30S subunits with 0.12 $\mu m^2 s^{-1}$ is similar [79]. Thus, many different intermediate steps can be assumed for L1, which can be explained by the complex assembly of the ribosome, with the mobile population with the faster exposure time more representative of L1 bound in the large subunit, as it corresponds to the DC of free 30S and 50S subunits with 0.4 $\mu m^2 s^{-1}$ in *E. coli* [102, 231]. The various intermediate steps represent a movement towards the poles, the cytoplasm and the cell periphery where translation later occurs [127] (**Fig. 4.2C**). This can also explain the slow mobile population of mRNAs (0.0126-0.0226 $\mu m^2 s^{-1}$), where this represents at least the translation-initiation-complex with the 30S subunit, although other transition complexes may be included, possibly also the intermediate step where the 70S ribosome interacts with the Shine-Dalgarno sequence of the mRNA at the 5' end, but translation does not yet occur. The same applies to the mobile population, where the formation of the translation-initiation-complex can be assumed and the slow mobile population then

represents further intermediates, although no reliable statement can be made for the mobile population because of the background noise of the MS2-tag. Assuming a DC of 0.02 $\mu m^2 s^{-1}$, these slow mobile mRNA molecules would take less than 20 seconds to diffuse through a spherical cell of 3 µm, assuming 3D diffusion where $\tau = r^2/6D$. Even if a lower DC is assumed, mRNA molecules should have enough time to reach anywhere in the cell.

70S ribosomes, where translation process was assumed, were observed to have a DC of 0.055 $\mu m^2 s^{-1}$ in *E. coli* [102] and a theoretical DC for mRNAs during translation, in which the average DC of polyribosomes was used, is similar to this [231], while another work estimated a DC of 0.02 $\mu m^2 s^{-1}$ [237] for it. In eukaryotes, a similar DC of 0.047-0.4 $\mu m^2 s^{-1}$ was found for mRNA diffusion [75, 77], while the 60S ribosomal subunit has a much higher DC of 0.31 $\mu m^2 s^{-1}$ [238] with proteins generally having higher DC in eukaryotes than in prokaryotes. My data suggest that even slower DCs for mRNAs exist at least in *B. subtilis*. Not only did the used statistical tests, such as the R^2 test, Kolmogorov-Smirnov-Goodness-of-Fit and null hypothesis significance test [159, 160], ensure that a correct number of populations was used, these tests also show that using two populations excludes some of the data set. The DC of the slow mobile and static populations are below the DC observed in *E. coli*. Only one group found a DC for mRNAs during translation in a range of 0.001-0.03 $\mu m^2 s^{-1}$ using 96 repeats of MS2BS, where the 96 fluorophore-MS2 dimers can be expected to influence the mRNA [153]. But only a small number of cells were used in the study. My downsized MS2-System shows that D_1 represents more or less standstill with 0.003 $\mu m^2 s^{-1}$. The same DC can be observed for L1 and is evidence for the translation of mRNA by the 70S ribosome. It can be assumed that translation is done by single ribosomes as well as polyribosomes. As was noted in the 70's, the ratio of free subunits to actively translating ribosomes in *E. coli* is about 15-85% [239]. It can be speculated that not only polyribosomes and 70S ribosomes are represented in the 85%, but also the intermediate states, since only free, unbound subunits are represented in the remaining 15%. A ratio I could observe similarly for L1 – and was observed in *S. putrefacient* [232] - and the mRNAs, assuming the slow mobile population for the ribosomal intermediates and the static population representing the 70S ribosomes and polyribosomes involved in translation. Furthermore, in this work, no dependency of translation time on mRNA size was observed (native mRNAs of 3200-5500 bp, artificial mRNAs of about 2500-7200 bp).

If one considers now where the mRNAs show a confined localization and connects this with the dynamics data, a translation of the mRNAs at the poles, in the cytoplasm and around

the nucleoid can be assumed, as for some mRNAs also in the cell periphery and directly at the membrane (**Fig. 4.2A,D**). More mobile mRNA, on the other hand, will be primarily present around nucleoid (**Fig. 4.2B,D**), where the mRNA here already forms the translation-initiation-complex with the 30S subunit. During diffusion out of the nucleoid, the ribosome continues to assemble by binding the 50S subunit, forming various intermediates until the complete 70S ribosome is formed and translation occurs (**Fig. 4.2**).

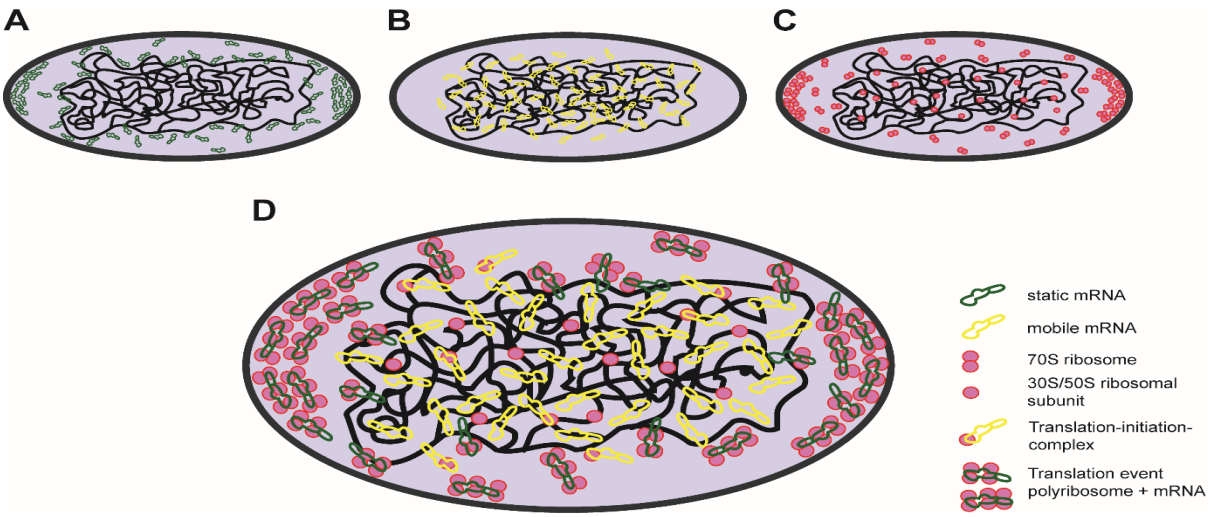

Fig. 4.2 Model of mRNAs dynamics and where it is translated in *B. subtilis*.

Based on the findings of the localization and dynamic data of mRNAs and L1 in *B. subtilis* gained by single-molecule tracking. Static mRNA (in green) is localized at the membrane and cell periphery/near the membrane, at the poles, in the cytoplasm around the nucleoid as well as at the periphery of the nucleoid **(A)**. Diffusive signal (in yellow) of mRNA is found throughout the cell, and accumulating in the cell center **(B)**. 70S ribosomes (two red circles) are found at the poles, the membrane, cell periphery/near the membrane, in the cytoplasm and around the nucleoid, while the ribosomal subunits (on red circle) are found in the nucleoid **(C)**. **(D)** is the final model where translation of mRNAs by suspected polyribosomes occurs at the poles, the membrane, in the cell periphery/near the membrane, in the cytoplasm, and in the nucleoid periphery. Mobile mRNAs, including the translation-initiation-complex, depicted in yellow and/or with the ribosomal subunit bound to it, are found throughout the cell, and accumulating in the cell center. For a better understanding, mRNAs of the slow mobile population were not shown bound in an assembling ribosome but may be found throughout the cell. Septal localization of mRNAs in large dividing cell are not shown for the purpose of a better understandable illustration.

4.2 Analysis of the behavior of DynA under different stress conditions

The combination of single-molecule tracking with the SMTracker software offers a variety of advantages. In this work, I already mentioned the use of the DynA protein for co-localization experiments with its mRNA, *ypbR-ypzF*, and the behavior of this mRNA has been thoroughly investigated. Therefore, it is not farfetched to gain more information about the protein as well. To do this for each protein would be too much. Much research is also being done by other groups on some of the proteins translated by the mRNAs tested [108, 117, 125, 129, 232]. Although DynA is a well-studied bacterial dynamin-like protein, question about its function, especially under membrane stress, have not been fully answered yet and thus the potential is there to figure out more. Hence, I wanted to characterize this protein in more detail. Not many interaction partners of DynA are known [206] and how membrane fusion is accomplished is also not fully understood, only possible mechanisms [204]. How important is its role in cell division and membrane integrity? Our group already started to find out more about this [125], while the Bramkamp group tried to find out more about DynA and its interaction with the membrane [199, 204], while also testing it under environmental stress [124]. They did this by using different antibiotics and phages, but no other stress factors were used for the membrane. Therefore, I wanted to answer the question of what specific membrane stressors DynA responds to and, more importantly, also look for the dynamic behavior of DynA in general, but also under stress. The Bramkamp group reported an effect after adding the antibiotics Bacitracin and Nisin and under phage invasion. For this reason, I decided to use those two antibiotics, as well as several membrane stresses. In a collaboration with the Bramkamp group, the behavior of DynA under phage infection has already been investigated (unpublished data). With this approach, I was able to characterize DynA more and I was able to find out that DynA only reacts to specific membrane stresses and moves around the cell with at least two, possibly three distinct populations of mobility.

4.2.1 Molecule counting of DynA under different stress conditions is not explicit

Already by doing the Epifluorescence microscopy experiments with DynA-mVenus, I realized that signal is not detectable in each cell. Single-molecule tracking revealed that the majority of cells expressing this protein only at low concentration. At least, the low number of tracks per cell of 3.7 lead to this assumption. At the same time, different stress factors lead to a higher number of tracks per cell. Especially under sodium chloride and Nisin stress it increased about 5-8 times. The other conditions also lead to an increase of around 2-3 times. To

investigate this further, I used the “molecule quantification” tool of the SMTracker. By counting the mVenus fluorophore via its fluorescence, the number of DynA molecules can be counted, as well as if it can be found in a monomeric, dimeric, tetrameric, etc. state.

The findings of the number of molecules of DynA under different stress conditions do not show an explicit behavior. In some instances, the results fit the expectation. For example, DynA-mVenus has the lowest molecule number of an average of around 19 molecules per cell, while this increases to 121 molecules under sodium chloride stress. At the same time, the number of molecules under Nisin stress only increases to 31. There is a clear discrepancy to spot. Also in most other conditions, where there was only a 3-5-fold increase in the number of tracks per cell, the number of molecules counted increased much more, in a range from 95 to 141. It is quite difficult to explain those strong differences. The number of tracks per cell originates from the same data set as for molecule quantification. Therefore, the data should fit together in a much better way. An explanation could be that for the analyses of the molecule number, much more data is taken into consideration, which is sorted out by the requirement to detect a track for the analyses of the tracks per cell but also for the localization and dynamics of DynA. At least the “molecule quantification” tool is working fine for comparison of different proteins with each other [225]. In theory, it should also work for comparing a protein under different conditions, regardless of the biological fluctuations in a cell.

Also of interest is the distribution of the bleaching steps, which provides information on how many molecules are found in a monomeric, dimeric, etc. state. The distribution of bleach steps indicates a two-thirds monomeric state for DynA under most conditions and the other state might be a dimeric state. This fits with previous findings that DynA not only function as an intrinsic dimer but also oligomerizes with itself to form a dimer, whereas only the dimeric state is required for membrane fusion [178, 199]. If the percentage for the monomeric state increases, like under sorbitol, sodium chloride and ethanol stress, this would also explain why the number of fluorophores increases. More DynA molecules do not mean that they are needed for membrane fusion and therefore are found in a mainly monomeric state, which is further underlined by the dynamic data in **4.4.2**. Interestingly, a distinct difference is observed under Nisin treatment, where a mainly dimeric state of 82% is present and the remaining 18% DynA molecules could be in a tetrameric state. The average number of photons counted leads to this assumption. For the monomers (data of Nisin stress is not

taken into consideration), the average bleaching step is around 5.879 photons, while the average bleaching step for the dimers is 12.948 photons. Only DynA under Nisin stress has an average bleaching step of 12.948 photons and of 20.998 photons, which are about the double of the bleaching steps for the assumed monomers and dimers. Formation of a tetramer has not previously been reported for DynA, only dimerization. However, a kinetic experiment of the subunits of D1 and D2 *in vitro* demonstrated possible formation of a tetramer by the D1 subunit [199]. Furthermore, there are other dynamin proteins in eukaryotes that can form tetramers. [180, 181]. Another explanation could also be that the pore formation through Nisin treatment could lead to more than one pore in close proximity. Two dimers of DynA would then be counted as a tetramer, even though the molecules are recruited to different pores in the membrane. Therefore, the molecule counting depicts a high number of monomers for DynA under Nisin stress and the smaller fraction of 18% are dimers. This might be the case if only a small number of DynA molecules are recruited to the membrane to repair it, which is somehow visible in the dynamic data (see **4.4.2**).

All in all, the molecule quantification does not offer a clear answer as to why the number of fluorophores increases so drastically, but this is not represented in the tracks or tracks per cell. Also, the question of what happens to DynA under Nisin stress cannot be answered in a satisfying way by just looking at the molecule quantification. A repeat of the molecule qualification with several biological replicates therefore might be reasonable. Despite all this, a possible oligomerization of DynA towards a tetramer should not be disregarded.

4.2.2 Distinct changes in localization and dynamics of DynA under Nisin stress

In this section, I will provide an insight into the localization behavior and dynamics of DynA under different stress factors. For this purpose, both epifluorescence microscopy and SMT were used.

Epifluorescence microscopy shows the expected localization for DynA at the septum, the membrane, and the poles, where roughly one-third of the protein localizes at each of those sites, respectively [124, 125]. This does not change much under heat, ethanol, and sorbitol stress. Mainly, the foci number increases at the septum and poles, which might be due to the exponential growth state. For no stress, cells of an OD_{600} of 0.8 were used, while for all stress conditions, cells with an OD_{600} of 0.8 were stressed with the appropriate stress factors for 30 min. This can explain the increase in foci at the septum and poles. A slight

increase in foci at the membrane and pole and a decrease at the septum are observed under Bacitracin treatment. Under osmotic stress, introduced by the adding of sorbitol, the number of foci in general increases. This effect is stronger under sodium chloride and Nisin stress. The number of cells with more than one focus also increases, which has been reported previously for Nisin treatment [124], while no change in the distribution of foci is observed under sodium chloride stress. Under Nisin treatment, a two- to threefold increase of foci at the membrane is observed. This fits with the results of the Bramkamp group who reported a clear effect of DynA under Nisin stress [124].

SMT reveals a similar localization behavior. Especially when looking for confined localization under Nisin stress, a preferential localization at the membrane can be observed. This is also observed to some extent for DynA molecules under Bacitracin stress, while this cannot be said for all other conditions. The reason for the increase of DynA molecules with a mixed behavior (from mobile to confined localization and vice versa) at the membrane under both antibiotic treatments might be that more DynA molecules transition from a diffusive state to a static, confined localized state for membrane fusion. After membrane fusion, they detach from the membrane and scan the cell for further pores in the membrane. Interestingly, the localization data also reveals that, independent of any stress factors, a lot of DynA signal can be found in the cytoplasm, where it seems to diffuse freely, which has not been shown before. The Bramkamp group stated this once, but did not present any data [178]. This can also be observed very well in the heat maps. Especially under sodium chloride and Bacitracin stress, a higher probability of distribution in the cytoplasm can be seen. The reason for this may be that no SMT but other microscopy were performed for dynamic imaging of DynA - accept the given statement of Marc Bramkamp with no data presenting -, and therefore only more static signal was detected by doing for example epifluorescence microscopy, FRAP and similar procedures. The dynamic data of DynA further underlines this. This would also make sense in a biological context. DynA does not consist of several transmembrane domains, just a small anchor at the D1 subunit that allows it to bind to the membrane [204], which may lead to its agile behavior. This will be discussed more thoroughly in the following.

At this time, no dynamic studies about DynA are reported. It makes sense to assume at least two different populations for it. A mobile one, where DynA is not involved in any membrane fusion, and a static one, where membrane fusion mediated by DynA occurs (**Fig.4.3**). With single-molecule tracking, I was even able to detect a third population that fits

to the localization data. JD analyses with only two populations clearly do not include the whole data. Furthermore, SQD simultaneous analysis was used. This means that the DC's for each population are fixed between the different conditions, based on the average DC of each condition. With this, changes in the population sizes can be detected more easily.

In a normal state of the cell, DynA already shows three different populations for its mobility. This also applies to DynA under any tested stresses. For the mobile population, a freely diffusive state can be assumed. Its DC (0.898 ± 0.008 $\mu m^2 s^{-1}$) is in the range of freely diffusing cytosolic proteins [240], but faster than proteins of similar composition, which include a membrane anchor but no transmembrane domain [117]. With its also large population size of around one-third – already once indicated by the Bramkamp group [178] -, DynA can be assumed to move in the cell in a freely diffusive state. The static population (0.015 ± 0 $\mu m^2 s^{-1}$) also fits other cytosolic proteins with its DC [240], while the slow mobile population (0.122 ± 0.001 $\mu m^2 s^{-1}$) lays in a good range between the other two. When taking this into the biological context, the three populations can be best explained by the following assumption: One-third of DynA molecules move freely in the cell, while half of it is in an intermediate state. Here, DynA molecules could be moving near the membrane or in the membrane, searching for a possible leakage of the membrane. It cannot be said weather the protein moves in the membrane and is therefore slower or weather the protein is only temporarily attached to the membrane and leaves it when no membrane leakage can be found before scanning the next area for any membrane damage. Meanwhile, the static population is attached to the Z-ring during cell division, as it is known that DynA localizes at the septal area and plays a role in cell division [125], but also is attached to the membrane and mediates membrane fusion, if necessary. When taking the findings of the molecule counting with the bleaching steps into consideration (see **4.2.1**) , it is highly possible that in the mobile and intermediate populations (which are more than two-thirds), Dyna molecules are monomeric, while it dimerizes during membrane fusion, as previously suggested [204].

If DynA reacts to membrane stress, an increase of the static population would be expected. This is definitely the case when Nisin was added. Here, the static population roughly doubles, while for each other condition this population did not change or mainly decreases by 3% compared to the unstressed condition. Also, under Nisin stress only, the mobile population meanwhile decreases by 12%, while the slow mobile population did not change. This can be explained by assuming that more of the free diffusing DynA molecules

are scanning for a possible membrane leakage, while at the same time more DynA molecules become static when they encounter membrane damage. Therefore, an increase in the slow mobile population is not observed. Whether oligorimerization to a dimer or tetramer occurs cannot be verified here.

Nevertheless, an increase from 15% to 28% of the static population is not much when looking also at the increase of foci. The findings of the dwell times may provide an explanation for this, which are used to further characterize the static population, where confined localization can be assumed.

First of all, I have to mention that only under Nisin stress and slightly under Bacitracin stress any changes were detectable. Therefore, the other stresses are not discussed (**Fig. 3.12**). In a normal cell state, DynA probably shows one dwell event, perhaps two (21% of the tracks showing confined localization). With two residence times, the mean deviation is 20%. Since one population covers only 12% and the other 88%, this high mean could also imply that there is only one population with a dwelling event of 0.22 sec. Even assuming two populations, the residence times do not differ much, with 0.17 sec and 0.23 sec. Under Nisin but also Bacitracin stress, this changes clearly (38% and 25% of the tracks showing confined localization), which fits the dynamic data. Two distinct dwell events are observed here. Both residence times occur for around 50% of the static molecules, respectively, where only the second fraction shows an increase of the residence time to 0.28 sec. under Bacitracin stress. Under Nisin treatment, the second population shows a strong increase in the residence time, doubling to 0.35 sec, further proving the effect of Nisin on the behavior of static DynA molecules. It also indicates an influence of Bacitracin on DynA, although this was not observed in the SDQ simultaneous analysis. Still, the prolonged residence time does not seem really long in comparison to the mRNAs. However, if we compare it with the membrane protein DgcK and the soluble protein DgcP [225], their residence times are one power smaller and the residence time of DynA is not as short-lived, but still not time-consuming. As mentioned in **4.1**, one should keep in mind that here an influence by bleaching of the molecules can lead to shorter dwell times. When taken into consideration that not so many more DynA molecules seem to be involved in membrane fusion, it can be assumed that the mediation for membrane fusion and the fusion itself does not need much time. Therefore, the searching, finding and repair of membrane lesions is a highly dynamic and not time-intensive process.

For the purpose of this work, I was able to characterize DynA more and have been able to give an idea about the reaction of DynA to various membrane stresses and its dynamics. DynA molecules can be divided into three populations, with each population performing a different task. One new, freely diffusing fraction mainly in the cytoplasm, an intermediate one that scans the membrane for any damage, and a static population in which DynA is involved in membrane fusion at the membrane or also during cell division at the septal area (**Fig.4.3**). Moreover, localization and dynamic data emphasizes that DynA seems to react to special kind of membrane damage. Both Bacitracin and Nisin are antibiotics that lead to membrane damage by taking advantage of lipid II components [241-243]. The fact that DynA is also recruited to the membrane after phage infection [124] and behaves similarly in localization, dynamic and dwell event analysis (unshown data), further underlines that specific pores in the membrane lead to a reaction by DynA, as previously suggested by the Bramkamp group [124]. Even though some membrane stresses, like ionic and osmotic membrane stress, lead to an increase of DynA molecules in the cell, they are not recruited to the membrane for any membrane fusion. More research is also needed on the regulation of DynA on a translational level, probably mainly about the housekeeping σ-factor SigA, which plays an important role in the major vegetative growth phase and under stress conditions, and also controls the expression of DynA [226, 227]. In general, it seems that small changes at the molecular level are enough for an obvious rearrangement of DynA molecules and also to some degree for the surveillance and mediation of membrane integrity.

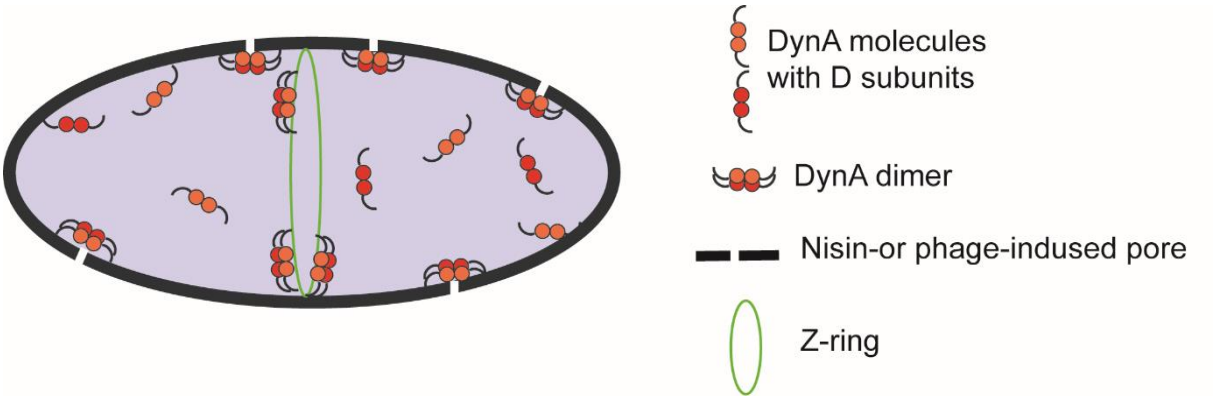

Fig. 4.3 Populations of DynA in *B. subtilis* and its localization behavior.

DynA molecules move freely diffusely in the cytoplasm or are bound as a dimer to the Z-ring during cell division or to nisin/phage-induced pores in the membrane to enable membrane fusion. A third population scans the membrane for possible damage.

5 GENERAL MATERIAL & METHODS

5.1 Material

5.1.1 Reagents and kits

All chemicals used in this work were standard chemicals, purchased by different companies. Those were Carl Roth (Karlsruhe, Germany), Sigma Aldrich (Steinheim, Germany).

Enzymes, used for DNA modification, reagents used for molecular and cloning and genetic manipulations, as well as DNA polymerases and for PCR, needed further reagents like dNTPs and reaction buffers, were used by New England Biolabs (Frankfurt a. M., Germany). Kits for Gel extraction and PCR purification by Qiagen (Hilden, Germany) were used. For plasmid extraction, the kit GenElute^{TM} Plasmid miniprep by Sigma-Aldrich (Steinheim, Germany) were purchased. Chromosomal isolation was performed by using the innuPREP Bacteria DNA kit of Analytik Jena GmbH (Jena, Germany). For DNA staining, Midori Green Advance was supplied by Nippon Genetics Japan (Düren, Germany). Size standards for DNA by New England Biolabs (Frankfurt a. M., Germany) were used, size standards for proteins were obtained from Thermo Fischer Scientific (Schwerte, Germany).

5.1.2 Oligonucleotides

For this work, all oligonucleotides were ordered from Sigma Aldrich (Steinheim, Germany) and adjusted to 100 pmol μl^{-1} with ddH_2O. They were stored at -20°C. All used oligonucleotides are listed in the appendix (A8.2).

5.1.3 Vectors

Different vectors were used for this work. A list of all of them can be found in the appendix (A8.3). To get more insight into the behavior, dynamics and localization of mRNAs (see also **2.1)**, as well as to find out more about DynA and its behavior under different stress conditions (see also **2.2)**, vectors of the pSG series were used [244], as well as an own vector, fusing parts of vectors of the pSG series together. With the used vectors, C-terminal fusions of the own target gene with different fluorescent proteins are possible. The chosen target gene- or gene fragments were integrated into the chromosome by homologous recombination via a double crossover event at the ectopic *amyE* site, which codes for α-amylase or via a single crossover event, which is a Campbell-type integration at the original locus. When using a vector, targeting the *amyE* site, the gene of interest is flanked by gene parts of *amyE*. After a successful integration at the *amyE* site in *B. subtilis*, those cells can no longer degrade starch.

By screening for these cells, a successful integration was confirmed. Gene expression, as well as a correct expression of genes in an operon, was controlled by an artificial xylose-inducible Pxyl promoter, which is part of all used vectors.

The *amyE* site vector pSG1193 was used to bring a gene of the MS2 bacteriophage, fused with the fluorescent protein mVenus, into *B. subtilis* cells. Besides the lack of starch degradation, cells containing this vector also had a spectinomycin (spec) resistance. A vector, pHJDS MS2BS, was constructed by taking the multiple cloning site of pSG1193 (ECE153) and the vector backbone of pSG1164(ECE155). The fluorescent protein was replaced by the MS2-binding site. This vector was used for the monocistronic and polycistronic mRNA constructs with one and two MS2-binding sites. Screening for successfully transformed vectors into the cells was confirmed by an amphenicol (amp) resistance in *E. coli* cells or a chloramphenicol (cm) resistance in *B. subtilis* cells. pSG1164 was used for the construction of DynA-mVenus and DynA-CFP. Also here, screening for successfully transformed vectors were confirmed by an amp resistance in *E. coli* cells or a cm resistance in *B. subtilis* cells. For the DynA-CFP strain, an exchange of chloramphenicol to tetracycline (tet) resistance was done by the resistance change vector pCM::Tet via a double-crossover recombination event *in vivo* [245]. Screening for successfully transformed cells was gained by selection for cells, containing the Tet resistance while a simultaneous loss of the Cm resistance.

5.1.4 Bacterial strains

The *E. coli* strain DH5α was used for the propagation of the constructs [246, 247]. One of the used *B. subtilis* strains, BG214, is a derivate of the laboratory domesticated strain 168 [248]. This strain was used for the work with the DynA-mVenus construct. For all the other constructs, the undomesticated strain NCIB3610 with a *comI* mutation for a better plasmid-transformable was used [249]. The constructed strains, used in this work, are listed in the appendix (A8.4).

5.2 Microbiological and cell biological methods

5.2.1 Bacterial growth and supplements

For cloning and propagation of vectors and plasmids, *E. coli* DH5α cells were cultivated overnight under aerobic conditions at 37°C in Luria-Bertani (LB) (see **Table 5.1**) medium with constant shaking of 200 rpm or on LB 1.5% (w/v) agar plates, purchased by Carl Roth (Karlsruhe, Germany). Liquid and solid media were prepared according to the manufacturer's instructions and were sterilized by autoclaving for 30 minutes at 121°C and 2 bar.

Overnight cultures of *B. subtilis* strains were cultivated under aerobic conditions at 30°C in LB media with constant shaking of 200 rpm. Cultivation on LB 1.5% (w/v) agar plates also happened at 30°C for strains of the frozen stock, prior to inoculation in liquid media. For transformation use, *B. subtilis* strains were cultivated under aerobic conditions in Modified Competence media (MC media, see **Table 5.1**) at 37°C. Strains, used for microscopy, were cultivated in the minimal media $S7_{50}$ (see **Table 5.1**). To sterilize the MC media and $S7_{50}$ media, a sterile filtration (pore size 0.2 µm) was performed. For constructs in the strain BG214, minimal media were supplemented with 50 µg/ml tryptophan and methionine, respectively. For overnight growing, media were supplemented with antibiotics. The final concentrations used, can be found in **Table 5.2**. For the motility assay, cells were growing on LB 0.3% (w/v) soft agar plates at 30°C.

Table 5.1 Bacterial growth media

Medium	Composition	Final concentration
LB medium	Trypton	10 g/l
	Yeast extract	5 g/l
	NaCl	10 g/l
	Agar-Agar	15 g/l
	pH 7.0 ± 0.2	
$S7_{50}$ medium	10 x $S7_{50}$ salts	1 x
	100 x $S7_{50}$ metals	1 x
	D-fructose	1% (w/v)
	Glutamic acid	0.5 mM
	Casamiino acids	0.004% (w/v)
	H_2O	
	50% Xylose	0.5% (w/v)
	H_2O (Xylose)	
10 x $S7_{50}$ salts	MOPS	500 mM
	$(NH_4)_2SO_4$	100 mM
	KH_2PO_4	50 mM
	adjusted pH to 7.0 (KOH)	
100 x $S7_{50}$ metals	$MgCl_2$	0.2 M
	$CaCl_2$	70 mM
	$MnCl_2$	5 mM
	ZnCl	0.1 mM
	Thiamine-HCL	0.01 mg/ml
	HCL	2 mM
	$FeCl_3$	0.5 mM

10 x MC medium (20 ml, pH 7.0)	K_2HPO_4 x 3 H_2O	2.81 g
	K_2HPO_4	1.05 g
	D-Glucose	4 g
	$KC_5H_8NO_4$	0.4 g
	Casein hydrolysate	0.2 g
	300 mM Sodium citrate	2 ml
	22 mg/ml ferric ammonium citrate	0.2 ml
1x MC medium (10 ml)	10 x MC medium	1ml
	1M $MgSO_4$	0.333 ml
	H_2O	8.7 ml

5.2.1.1 Stress conditions while bacterial growth

Cells, expressing the DynA-mVenus construct, were stressed with different substances (see also **2.2** and **Table 5.2**). A final concentration of 1M sorbitol, 1M NaCl, 10% (w/v) ethanol, 250 µg/ml Bacitracin and 10 µg/ml Nisin were used. This was added to cells, already growing in $S7_{50}$ minimal media at 30°C with constant shaking of 200 rpm. Those cells were in the exponential growth phase. Incubation with the different stress factors was done for 30 minutes. Heat stress at 42°C was accomplished by shifting the cells into a shaking bath with 42°C and 200 rpm.

Stress experiments with Rifampicin, purchased by Sigma Aldrich (Steinheim, Germany), were done by adding 25 or 50 µg/ml to cells in the exponential growth phase. Incubation of 40 minutes followed.

5.2.1.2 Preparation of *B. subtilis* cells for microscopy

All *B. subtilis* strains used for microscopy were grown in $S7_{50}$ minimal medium at 30°C under shaking conditions to an OD of 0.7-0.9. If necessary, cells were stressed (see **5.2.1.1**). Cells were spotted on coverslips (25mm, Marienfeld) and covered with an agarose pad (1% (w/v), made of $S7_{50}$ Medium and a smaller coverslip (12mm, Marienfeld). All coverslips were cleaned before use by sonication in Hellmanex II solution (1% v/v) for 45-60 min, followed by sonification in ddH_2O for 30 min.

Table 5.2 Media supplements and antibiotics

Antibiotics/supplement	Final concentration
Ampicilin (Amp)	100 µg/ml
Chloramphenicol (Cm)	5 µg/ml
Tetracyclin (Tet)	20 µg/ml
Spectinomycin (Spec)	100 µg/ml
D-Xylose (Xyl)	0.5% (w/v)
Rifampicin (Rif)	25/50 µg/ml
Bacitracin	250 µg/ml
Ethanol (EtOH)	10% (w/v)
Nisin	10 µg/ml
Sodiumchloride (NaCl)	1M
Sorbitol	1M

5.2.2 Storage of bacteria

All bacterial strains were stored at -80°C for long-time storage. For this, cells were harvest in the exponential growth phase and subsequently supplemented with a final concentration of 20% (w/v) of glycerol.

5.2.3 Determination of cell density

The optical density (OD) of cells was measured in cuvettes of Sarstedt (Nümbrecht, Germany). Cuvettes have a thickness of 1 cm. With the Ultrospec™ 10 cell density meter (Amersham Pharmacia Biotech) at a wavelength of 600 nm (OD_{600}) measurements were performed. First, a cuvette with sterile media was measured to subtract the background of the media. After this, measurement of the actual sample could happen. A volume of 1 ml was used. A value of 0.1 corresponds to a cell density of approximately $1x10^8$ cells ml^{-1}.

5.2.4 Motility assay

To test the swarming behavior of the *B. subtilis* wild type NCIB 3610 and cells expressing MS2-mV + *hag*_MS2BS1x, fresh LB 0.3% (w/v) soft agar plates were prepared one day before. 5 µl per cell suspension were spotted in the middle of the soft agar plates. Cells in the exponential growth phase, with an OD_{600} of 0.6-0.8 were used for this. Plates were incubated at 30°C for 24 hours. At different time points, directly after adding the bacterial cells to the plate, after two, five, eight and 24 hours, pictures were taken with ChemiDoc™ MP Imaging System by BIO-RAD (Feldkirchen, Germany).

5.3 Molecular biological methods

5.3.1 Isolation of chromosomal DNA

To isolate chromosomal DNA of *B. subtilis,* the innuPREP Bacteria DNA kit by Jena Analytik (Jena, Germany) was used. Cells were grown in test tubes overnight in LB at 30°C. 1,5-2 ml of the overnight cultures were then used for centrifugation, to gain the bacterial cell pellet. All centrifugation steps to gain the chromosomal DNA occurred for 2 minutes at 13000 rpm with the Eppendorf 5424R centrifuge. The supernatant was discarded and 200 µl TE buffer was added. The pellet was re-suspended in the buffer. After this, 1,5 µl lysozyme (stock solution 100 mg/ml) was added and carefully mixed by vortexing to isolate the chromosomal DNA. For a complete lysis of the sample, it was incubated at 37°C for several minutes. After full lysis, 200 µl of Lysis Solution TLS and 25 µl of Proteinase K were added and mixed by vortexing. Incubation at 50°C for 15 minutes followed. Next, 400 µl of the Binding Solution TBS was added and thoroughly mixed by vortexing and pipetting the solution several times. The whole solution was then transferred into a spin filter, which was in a 2 ml receiver tube. One centrifugation step was performed and the spin filter was placed into a new receiver tube. Now the chromosomal DNA should be bound to the filter. A wash step with 500 µl of the Washing Solution HS was next, followed by vortexing. The spin filter was placed into a new receiver tube. A second wash step happened with the next Washing Solution MS, by adding 750 µl of it, followed again by a centrifugation step. Again, into a new receiver tube, the spin filter was placed. To remove any remains of alcohol from the wash buffers, a centrifugation step was performed. Into a 1.5 ml tube, the spin filter was placed. To gain the chromosomal DNA out of the filter, 50 µl ddH_2O was added and a final step of centrifugation was performed. To measure the concentration of the extracted DNA, a NanoDrop Lite ND-100 (Thermo Fischer Scientific) was used. Storage at 4°C in the fridge.

5.3.2 Plasmid isolation

For the plasmid isolation of *E. coli* DH5α, the GenElute^{TM} Plasmid miniprep kit of Sigma-Aldrich (Steinheim, Germany) was used. Cells were grown overnight in LB media at 37°C. 1,5-2 ml of the overnight cultures were then used for centrifugation, to gain the bacterial cell pellet. Most centrifugation steps to gain the plasmid DNA occurred for 2 minutes at 13000 rpm with the Eppendorf 5424R centrifuge. The pellet was resuspended in 200 µl Resuspension Solution by pipetting. After this, 200 µl of Lysis Solution was added and carefully mixed. The next step was

incubation for 5 minutes. Next, 350 µl Neutralization Solution was added and mixed by 6 times inverted. 10 minutes centrifugation was performed. Before transferring the supernatant into the spin filter, 500 µl of the Column Preparation Solution was added to the spin filter, centrifuged and the flow-through discarded. The supernatant than was added to the spin filter and centrifuged. The flow-through was discarded. 500 µl of the Wash Solution 1 was added and centrifuged. After discarding the flow-through, 750 µl of the Wash Solution 2 was added and centrifuged. The empty spin filter was centrifuged again, to get rid of any residues of the wash solutions. After relocating the spin filter into a clean 1.5 ml tube, 50 µl ddH_2O was added and to gain the plasmid DNA, the last step of centrifugation was performed. A NanoDrop Lite ND-100 (Thermo Fischer Scientific) was used to measure the concentration of the extracted plasmid DNA. Storage at 4°C in the fridge.

5.3.3 Polymerase chain reaction – PCR

For analytical and preparative purposes, specific DNA fragments were amplified via polymerase change reaction (PCR) [250]. For a standard PCR reaction, 1x reaction (5x Phusion® High-Fidelity reaction buffer, NEB) was used, as well as 200 µM dNTPs and 0.5 µM of each oligonucleotide (primer), 3 % (v/v) DMSO (dimethyl sulfoxide) and 0.02 U/µl polymerase (Phusion® HighFidelity DNA Polymerase, NEB). Chromosomal DNA (50-100 ng) or plasmid DNA (10-30 ng) was used. For each PCR reaction, the thermocycler by Biometra was used. The protocol for PCRs is shown below (**Table 5.3**). The annealing temperature depended on the used primers. To calculate the correct temperature, the online tool of NEB was used (https://tmcalculator.neb.com/#!/main). The used Phusion polymerase can do 1000 bps in one minute. The duration for the elongation step was chosen depending on the length of the target DNA fragment. By agarose gel electrophoresis (see **5.3.4**), the PCR fragments were analysed and purified out of the gel with the QIAquick Gel Extraction kit or were purified of salt, enzymes and nucleotides by the QIAquick® PCR Purification Kit, both kits of Qiagen.

Table 5.3 PCR program-and thermocycling conditions

Step	Temperature	Time	
Initial denaturation	95°C	2 min	
Denaturation	95°C	30 sec	
Annealing	53-69°C	30 sec	30 cycles
Extension	72°C	60 sec/kb	

Final extension	72°C	5 min
Hold	4°C	∞

5.3.4 Agarose gel electrophoresis

To analyse the size and quality of DNA fragments after PCR, after modification of plasmids or to check DNA after plasmid isolation and PCR purifications, a horizontal agarose gel electrophoresis was performed. Due to the agarose, DNA molecules are separated by size. As a standard, a 1% (w/v) gel was used. For bigger DNA fragments, a 0.8% (w/v) and for smaller DNA fragments a 1.5% (w/v) agarose gel was used. The agarose was dissolved in 1x TAE-buffer and heated up in a microwave. The liquid gel was then poured into the horizontal gel casts. To stain the DNA, 0.01% (w/v) MidoriGreen (Nippon Genetics Europe GmbH) was added, which can be visualized by UV-light. To load the DNA, it was diluted with 6x loading dye of NEB first. For the electrophoresis, 100-140 V (Electrophoresis power supply, Consort EV243) was used. To visualize the DNA, a UV-transilluminator was used.

50 x TAE-Buffer	Tris-Acetate pH8.2-8.4	2 M
	EDTA	0.05 M

5.3.5 Molecular cloning

For molecular cloning and therefore to construct new plasmids to bring them into *B. subtilis*, and everything, that belonged to this, like isolation of plasmid and chromosomal DNA, PCR reactions, specific digestions and ligation were performed according to the standard protocol [251]. Besides classic cloning, also some constructs were made according to the so-called Gibson Assembly protocol [252]. Here, specific digestion and ligation of plasmid with one or more DNA fragments are done more or less simultaneously.

5.3.6 DNA sequencing

To verify, if the construct after molecular cloning were correct, purified plasmid DNA (see **5.3.2**) was send for sequencing. The offer of two different companies was used, whereas a concentration of purified plasmids of 50-100 ng/µl was used. The companies chosen for DNA sequencing were GATC Biotech (Konstanz, Germany) and Eurofins Genomics (Ebersberg, Germany), which are now fused together to Eurofins Genomics Germany GmbH (Ebersberg, Germany).

5.3.7 Preparation of chemical- and electrocompetent *E. coli* cells and transformation

To get the target constructs into *B. subtilis* cells, first, the constructs need to get transformed into *E. coli* cells. For this DH5α cells were made competent by a chemical or an electro procedure. A standard protocol for chemical competent *E. coli* cells was used. For this purpose, fresh DH5α cells were inoculated for an overnight culture in LB and were grown at 37°C. On the next day, in a 1 L flask, 125 ml SOB media was inoculated with the *E. coli* overnight culture to an OD_{600} of 0.005. At room temperature and 200 rpm, the culture was cultivated up to an OD_{600} of 0.6, which took around 30 hours. The culture in the flask was then incubated for 10 min on ice. All the following steps occurred on ice or at 4°C. Centrifugation of the culture at 2500 rpm for 10 min (rotor: SX4750, centrifuge AllegraR X-15R, Beckman Coulter). The supernatant was discarded and the pellet was resuspended with cold 50 ml TB-buffer. Next, an incubation step for 15 min on ice followed. Again, centrifugation at 2500 rpm for 10 min. The supernatant was discarded and the pellet resuspended with 12 ml cold TB-buffer. Adding of 900 µl DMSO to the suspension and thoroughly mixing it. Aliquotation of 200 µl of the now chemical competent DH5α cells, respectively and freezing first in liquid nitrogen and storage at -80°C.

For transformation, the chemical competent DH5α cells were unfrozen on ice. If a ligated reaction was transformed, 10 µl of it was used or in the case of the transformation of a closed plasmid, 100 ng DNA was used. After adding the DNA, incubation of the cells on ice for 20-30 minutes. A heat shock for 90 sec at 42°C followed. 600 µl of prewarmed LB media was added to the cells. After this, the cells were incubated for 5 minutes on ice. Next, incubation of the DH5α cells for one hour at 37°C and 200 rpm. Last, the cells were streaked on a LB agar plates with the needed antibiotics for selection (for all *E. coli* strains, final concentration of 100µg/ml ampicillin was used) and incubated overnight at 37°C.

In case to gain electrocompetent DH5α cells, an overnight culture of fresh DH5α cells in 10 ml LB media at 37°C was incubated. On the next day, 3 ml of the overnight culture were used to inoculate 300 ml of prewarmed LB media. Incubation at 37°C and 200 rpm to an OD_{600} of 0.6 µl. After this, incubation on ice for 15-30 minutes. 50 ml of the DH5α culture was filled into 6 sterile falcons, respectively. Centrifugation for 15 min at 4°C with 4500 rpm (centrifuge AllegraR X-15R, Beckman Coulter). The supernatant was discarded and the pellets were resuspended with 50 ml cold ddH_2O, respectively. Repeat of the centrifugation step. The supernatant was discarded and the pellets resuspended in 25 ml ddH_2O. Out of the 6 falcons,

always two were merged to 3 falcons, with a total amount of 25 ml ddH_2O. Repeat of centrifugation. The supernatant was discarded. Now the three falcons are merged into one, while the pellets were resuspended with 2 ml cold ddH_2O. Repeat of the centrifugation step and the supernatant was discarded. Resuspending of the pellet with 600 µl cold ddH_2O. Repeat of the centrifugation step. The supernatant was discarded. The pellet was resuspended in 600 µl cold 10% glycerin (w/v). Aliquots of 40 µl of the now electrocompetent DH5α cells, respectively, were done and then the aliquots were frozen first in liquid nitrogen and stored at -80°C.

Transformation of 10 µl of a ligate reaction or 100 ng DNA of a closed plasmid was used with electrocompetent DH5α cells. First, dialysis of the DNA for one hour on a special membrane in a water bath. After this, the DH5α cells, mixed with the DNA, were filled into a cold cuvette. A current pulse of 25 kV was given to the cells. 900 µl prewarmed LB media was added and the cells were incubated at 37°C with 200 rpm for 90 minutes. Last, the cells were streaked on a LB agar plates with the needed antibiotics for selection (for all *E. coli* strains, final concentration of 100µg/ml ampicillin was used) and incubated overnight at 37°C.

TB-Buffer	HEPES pH 6.7	10 mM
	$CaCl_2$	15 mM
	KCl	250 mM
	$MnCl_2$	55 mM

5.3.8 Preparation and transformation of competent *B. subtilis* cells

Different subpopulations of *B. subtilis* can take up exogenous DNA, because of their natural competence, which occurs during the transition of the exponential growth phase to the stationary growth phase. Normally, the NCIB3610 strain is under laboratory conditions not able to take up DNA, because of the plasmid-encoded competence inhibitor ComI. The strain NCIB3610, which was used in this study besides BG214, has a *comI* mutation, *comI*^{Q12L}, which leads to a low competent *B. subtilis* strain [249]. An overnight culture of this strain or BG214, grown at 30°C and 200 rpm, was used to inoculate 10 ml of 1x MC media (**Table 5.1**) to an OD_{600} of 0.08. Incubation at 37°C and 200 rpm for around 3 hours to an OD_{600} of 1.3-1.5. When this OD was reached, 1000 ng of chromosomal DNA or 2-3000 ng of plasmid DNA was added to 1 ml of the competent *B. subtilis* cells and incubated at 37°C with 200 rpm for 2 hours. Last, the cells were streaked on a LB agar plates with the needed antibiotics for selection (**Table 5.2**) and incubated overnight at 30°C.

5.4 Biochemical methods

5.4.1 Sodium-dodecyl sulfate polyacrylamide gel electrophoresis (SDS-PAGE)

Performance of a SDS-PAGE is a common way to distinguish proteins under denaturation conditions according to their mass. Self-made polyacrylamide gels were prepared with 12% (w/v) or 8% (w/v). Composition of the gels, according to Laemmli [253] is shown in **Table. 5.4**. The mini-PROTEAN® system by BIO-RAD was used. The protein samples were mixed with a 5x SDS loading buffer, then boiled at 95°C for 7 minutes or incubated for one hour at room temperature and then loaded to the gel. As a size control, the pre-stained protein ladder by ThermoFischer, which displays the protein size from 10-180 kDa, was used. Electrophoresis with 100-120 V was performed with MiniPROTEAN® Tetra Cell by BioRad and Electrophoresis power supply, Consort EV243.

Table 5.4 Compositions of the gel for SDS-PAGE

SDS-gel	Composition	Volume for two gels
Stacking gel	Acrylamide	4 ml
	Tris pH 8.8	3.75 ml
	H_2O	7 ml
	10% SDS	150 µl
	TEMED	7.5 µl
	10% APS	76 µl
8% Running gel	Acrylamide	990 µl
	Tris pH 6.8	1.875 ml
	H_2O	4.5 ml
	10% SDS	75 µl
	TEMED	5 µl
	10% APS	50 µl
12% Running gel	Acrylamide	6 ml
	Tris pH 6.8	3.75 ml
	H_2O	5 ml
	10% SDS	150 µl
	TEMED	7.5 µl
	10% APS	75 µl

5.4.2 Western blotting and immunodetection of fusion proteins

After the SDS-Page (see **5.4.1**), the protein gets transferred onto a nitrocellulose membrane (pore size 2 µm; 82 mm thick; Protran BA83, Whatman™, GE Healthcare) via the standard

protocol for semi-dry Western blots [254]. For this, the PerfectBlue™ Semi-Dry-Blotter Sedec™ (VWR Peqlab) cast was used. The nitrocellulose membrane laid between six wet layers of Rotilabo® blotting paper (Roth, 0.35 mm thick), which means three under and three above the nitrocellulose membrane. The blotting paper and the nitrocellulose membrane were soaked with the transfer buffer. On top of the nitrocellulose membrane, and therefore under three blotting papers, the SDS-PAGE gel was laid on it. The electrotransfer was performed for 70 min (12% SDS-PAGE) or 120 min (8% SDS-PAGE) at 0.8 mA per cm2 of gel area.

After the transfer of the protein bound to a fluorescent protein to the nitrocellulose membrane, the membrane was blotted overnight in the blocking solution of 5% (w/v) milk at 4°C (see **Table 5.5**). On the next day, the membrane was washed three times for 10 minutes with PBS-T. After this, a first antibody for detection - by using a specific antibody against GFP (dilution 1:500) – was used overnight at 4°C. The antibody was added in 5% (w/v) milk. A secondary antibody against the first antibody (mouse-α-rabbit-HRP), which also contains a conjugated horseradish peroxidase (dilution 1:10.000, Sigma), was used. Before applying the second antibody, three wash steps with PBS-T for 10 min were performed. The second antibody was also added into 5% (w/v) milk and the membrane was incubated with it for one hour at RT. After this, the three wash steps were repeated. For visualization of the fusion proteins by chemiluminescence, an enzymatic reaction of luminol via oxidation of the IgG coupled horseradish peroxidase was utilized. For this, solution 1 and 2 were mixed prior to the signal detection and the membrane was incubated for 1-3 minutes with it (see **Table 5.5**). For detection, the ChemiDoc™ MP Imaging System (BIO-RAD) was used.

Table 5.5 Compositions of media for immunodetection of fusion proteins

Medium	Composition	Final concentration
PBS-T	Na_2HPO_4	0.8 mM
	NaH_2PO_4	2 mM
	NaCl	10 mM
	Tween 20	0.1% (v/v)
Blocking solution	PBS-T with 5% skim milk powder	
Solution 1	Luminol	2.5 mM
	Coumaric acid	0.4 mM
	Tris-HCL pH 8.5	100 mM

Solution 2	H_2O_2	0.018% (v/v)
	Tris-HCL pH 8.5	100 mM

5.5 Microscopy

5.5.1 Fluorescence microscopy

Fluorescent microscopy is a procedure of microscopy, which can be tracked down to its beginning of the 20th century, where August Köhler was one of the first to describe this special method of microscopy [255]. Fluorescence microscopy takes advantage of the autofluorescence of different structures of plants and animals for example plant components like the chlorophyll [256]. Besides this, not each structure in cells are auto-fluorescent. To visualize those, fluorescent dyes and fluorescent proteins are used. Fluorescent dyes are most commonly used in cell biology, microbiology, medicine and more, to stain different structures of all kinds of cells. Fluorescent proteins are also used widely used to image a target molecule in a cell [257]. To visualize the fluorescent protein via fluorescence microscopy, the fluorescent protein needs to get excited. For this, light with a certain wavelength is used. There, electrons take up photons, which leads to a higher energy state. This process is also called absorption. After the electron falls back to its ground state of energy, the uptaken photon is released. Here, energy is released as light. This emission of light is what then can be seen as a fluorescent signal. This occurs normally from the lowest energy level, which follows the Kasha-rule [258]. The emitting photon then shows a displacement to the long-wavelength, less energized spectrum of light. The remaining energy is given off as heat to the sample, also known as Stokes-shift [259]. In most cases of fluorescent molecules, the wavelength for excitation and emission can be found in a spectrum of similar wavelengths. Therefore, if more than one fluorophore is used for one sample, it should be taken care, that the excitation and emission wavelength for the different fluorophores are not too similar to each other. Because short-wavelength is energy-rich, while long-wavelength are energy-low, it adds up to start with the fluorescent protein of the long-wavelength spectrum. This is not always possible. Exceptions will be explained in **5.5.2.1**.

Besides the already explained requirements of a specific and short spectrum of wavelength for excitation and emission, it is important, that the probability of the photon uptake is high and also the emission of the photon to have a good intensity and brightness of the signal. Otherwise, it is difficult to visualize this event. Another important requirement for

a good fluorophore is a long lifetime, as well as low bleaching [260]. Under normal conditions, it is desirable to have fluorophores that can be excited more than once. Worth mentioning is, that with the common fluorescence microscopy, structures smaller than the microscopic resolution limit cannot be distinguished well. It cannot be said if the observable signal is produced by one molecule or more molecules in close proximity. Therefore, different methods and advanced microscopes like STED [261]-and-SIM microscopy [262] - also belonging to the fluorescence microscopy field - show better results in high-resolution.

In this work, different fluorescent proteins were used, to visualize proteins and mRNAs. The used fluorescent proteins were all derivates of the green fluorescent protein (GFP) of the jellyfish *Aequorea victoria* [263]. As the name already suggests, GFP is fluorescent in the green wavelength. The range for excitation is 309-501 nm and for emission it is 448-624 nm but the peaks for excitation are at a wavelength of 395 nm and for emissions at 509 nm [264]. mVenus is a monomeric derivate of the dimeric GFP and its peak for excitation is at a wavelength of 515 nm and for emissions at 527 nm. The range for excitation is 351-578 nm and for emission it is 485-648 nm. Even though the range of usable wavelength of mVenus is in a similar range to GFP, the main excitation and emission range is more compact and therefore a better option for microscopy [217]. The halftime of the photostability is 24.1 sec in *Saccharomyces cerevisiae* and 50.4 sec in HEK239A cells and therefore this fluorophore seems good enough for the use of this work, even though no tests in bacteria were performed [265]. Only for mVenus this data is known at the moment. Besides this, mVenus is an established fluorophore, just like GFP. The other used fluorescent proteins used in this work, is the dimeric cyan fluorescent protein (CFP), which's peak for excitation is at a wavelength of 456 nm and for emissions at a wavelength of 480 nm. The range for excitation is 302-470 nm and for emission it is 455-597 nm [217, 266].

5.5.1.1 Epifluorescence microscopy

Epifluorescence microscopy is an established procedure of microscopy and belongs to the wide-field microscopy, because a widespread area of the sample gets illuminated. The general setup resembles the one of bright-field microscopy. Besides an ocular, arm, base, stage, objective lenses and objectives, coarse and fine focus and the illumination for the bright-field, an additional UV-light with belonging excitation filters – which only let pass light with specific wavelength – exists. The beam splitter is used to lead the excitation wavelength through the objective to the sample, where the fluorophore gets excited. At the same time, the now more

long-wave signal, which gets emitted by the fluorophores of the sample, can pass the beam splitter and is recorded by, for example, a camera, as a picture or movie. At least it goes in the direction of the ocular. Because the beam splitter is not 100% accurate, a small amount of excitation light can pass it and goes to the ocular. A blocking filter stops this and no excitation light gets through to the ocular.

In a "normal" fluorescence microscope, the different filters are located together in a block above the objective. Because the used microscope in this work has this block with the filters in it beneath the objective, it is called an inversive microscope. The used microscope is the Zeiss Axio observer Z1 microscope with the camera Cascade II:512 Photometrics. The magnifications of the objective were 100x, while the magnification of the ocular was 1.6x. The total magnification was 160x. The camera chip was 512x512 and 16 µm x 16 µm. With the program-Metamorph (Molecular Devices, Sunnyvale, CA, USA) the settings were done. The acquisition of DynA-mVenus was done with an exposure time of 3000 ms and a YFP filter was used.

5.5.1.2 Wide-field fluorescence microscopy

Wide-field fluorescence microscopy is part of the fluorescence microscopy and also epifluorescence microscopy belongs to it. Here, as the name already suggests, a wide-field of the sample is illuminated. Because for some experiments not the microscope under **5.5.1** was used but another one, and due to the use of a laser and not an UV-light, for distinguishing reason, this part here is just called wide-field fluorescence microscopy. Also, it is still slightly different then epifluorescence microscopy. Even though the sample is illuminated in a wide-field, the specific slim laser used here leads to a strong excitation of the fluorescent molecules to a specific spot of the sample by underfilling the back aperture of the objective lens, which leads to a concentrated, parallel illumination on this specific spot of the sample and therefore leads to a faster bleaching of the molecules. Due to this, a lower exposure time can be used.

Imaging was performed with a Nikon Eclipse Ti microscope equipped with a high numerical aperture objective (CFI Apochromat TIRF 100XC Oil, numerical aperture (NA) 1.49), an EM-CCD camera (ImagEM X2, Hamamatsu) and a YFP filter set (BrightLine 500/24, Beamsplitter 520 and BrightLine 542/27). mVenus fluorophores were excited by the central part of a laser beam (TOPTICA Beam Smart, 515 nm, max. power 100 mW) with a laser intensity of 20 mW. Each image was taken with an exposure time of 500 ms, using Nikon NIS-Elements BR.

5.5.2 Single-molecule tracking

Nowadays, microscopes and technologies get better and better to study processes in eukaryotes and prokaryotes. To give an example, fluorescence recovery after photobleaching (FRAP) is a common tool to study phosphor bi-and monolayers, dynamics and migration of molecules in cells [267, 268]. Another method to study the dynamics of molecules is single-molecule tracking (SMT), also known as single-particle tracking. With this method, individual behaviors of molecules and their diffusive behaviour can be analysed [269], as well as processes like transcription [270], translation [173], replication[240] and signal transduction [271], to name a few. As the name already suggests, for SMT, molecules on a single-molecule or particles on a single-particle level are needed. For this, a specific laser setup is crucial. For a better understanding, a repeat of the explanation of the laser, used for wide-field fluorescence microscopy (**5.5.1.2**) will be given. Even though it still belongs to wide-field microscopy, due to the specific slim laser used here, a strong excitation of the fluorescent molecules to a specific spot of the sample by underfilling the back aperture of the objective lens, is given. This leads to a concentrated, parallel illumination on this specific spot of the sample and therefore leads to a faster bleaching of the molecules. Due to this, not only a lower exposure time can be used, but also the fluorescent proteins are bleached to the minimum, where only single fluorescent proteins – or for example fluorophores of dimers in the case of single-particle tracking -, which already regenerated from the strong bleaching, can be detected. The intensity of the excitation is of a factor of around 100 higher than compared with epifluorescence [169]. **Fig. 5.1** shows the bleaching behavior of L1-mVenus over time. At the beginning of the strong excitation, a lot of signal arises (a), but soon, most of it bleaches out fast (b). The decay of the curve is rapid. A plateau is reached (c), which corresponds with single recovered fluorescent molecules, that can be tracked for a short time, before bleaching out again.

With SMT, the dynamic of single molecules within a medium can be observed in a two-or-three-dimensional way, which is referred to as trajectories. In this work, single molecules were observed in two dimensions [272] to analyse the protein DynA under different stress conditions, but mainly different mRNAs, to observe their localization patterns and dynamic behavior. To be sure, that no background noise shines through the cell and the chances to detect any background noise, the used coverslips are cleaned thoroughly with 1% Hellmanex and ddH_2O.

SMT can only reveal its information if a software is used to analyse the gained data. This is a crucial step. For this, our group developed a tool, called SMTracker [159, 160]. Before this tool is usable, the taken videos need to be prepared. To analyse only molecules on a single-molecule level, frames in a range of 1000-2500 frames or 1500-2500 frames were used (**Fig. 5.1**). For this, ImageJ was used [218]. Next step was to define what a cell is, so that the program later on cannot detect background noise as a false-positive signal. This was done with Oufti [273]. For particle detection, U-track [274], a MATLAB software, was used. Here, in the case of DynA-mVenus tracking, the minimal length of tracks was set to 5 and to link to points, no gaps for the particle detection were allowed. For the analysis of the different mRNAs, the MS2-tag and L1, a minimal length of tracks was set to 8. To link two points, no gaps for the particle detection was allowed. The Brownian search radius was set with the lower bound of 0 and the upper bound of 3. This was done to get rid of most of the possible unbound MS2-tags in the data set. Last, the SMTracker version 1.5 and 2.0 itself were used [159, 160]. This software gives information about the number of tracks detected, tracks per cell, length of the cell, lifetime of tracks and more in the "import" panel. Also there, the tool for the quantification of molecules (see **3.5.2**) can be found. The SMTracker also displaces the localization of molecules in so-called heat maps, where the probability of distribution is displaced by color in the "Spatial distribution" (SDA) panel. There the distribution of the tracks can also be found in the form of histograms along the x- and y-axes. Another way to represent localization, are the confinement maps, where a defined, confined movement in a 120 nm radius and with a tracking length of the molecules are shown (the settings are selected manually). There it is not only possible to see, which molecules move in a diffusive and which ones in a confined way in the cell, but also an intermediate state can be observed, where molecules with a mixed behavior between mobile and confined movement and vice versa are displayed. The described tool can be found in the "Stationary Localization Analysis" (SLA) panel. Besides the tools to gain more information about the localization of molecules, the dynamics can also be analysed. Three different models exist, but only was used. The "Gaussian Mixture Model" (GMM), the "Apparent Diffusion" (APPD) model and the model for the "Square displacement analysis" (SQD). The SQD was chosen to analyse all data. First of all, with the jump distance analysis (JD) - part of the SQD panel - we get the probability of particles how they might distribute in a fixed time interval via two-dimensional Brownian motion, with the use of square displacement analysis parameter [159, 160, 211], while the probability-

probability plot shows us how the actual data behave to its predictions for the goodness of the fit (see **Manuscript 1+2**). The SQD then gives the possibility to distinguish those populations via their different diffusive coefficients, which takes the cumulative distribution function of square displacements as its basis. With this, we get the probability of molecules remaining in a circle over time [159, 160]. This model was chosen to get the information of possible changes of the diffusive coefficients and the change in population size of DynA under different stress conditions. Also, I wanted to be able to see, if different mRNAs differ in their dynamic because of their size. To answer those questions, SQD was the best option to choose. Last, the SLA panel also gives some information on the dynamic of molecules, more precisely about the residence time of static molecules (see **Manuscript 1-2**). With this tool, it is possible to look for changes in the dwelling event τ, for example, DynA under different conditions, but also to compare two or more proteins. Only static molecules are taken into consideration and two possible models are displaced. The first model shows the behavior of the static molecules for one dwelling event, while the second model assumes two different dwelling events. It also displaces the population sizes for this and therefore the likelihood, that there occur two of those dwelling events or only one. A possible significant difference between two or more conditions is also provided.

Most of the single-molecule tracking done in this work was performed with the Nikon Eclipse Ti microscope. All information of the used microscope, laser and everything else that belongs to it, can be found under **5.5.1.** For the tracking of DynA-mVenus, an exposure time of 20 ms was used, L1-mVenus and the MS2-tag mVenus were tracked with 20 and 75 ms, and each mRNA construct with 75 ms exposure time. The laser intensity of 20 mW was used and 3000 frames for the movies were taken, respectively.

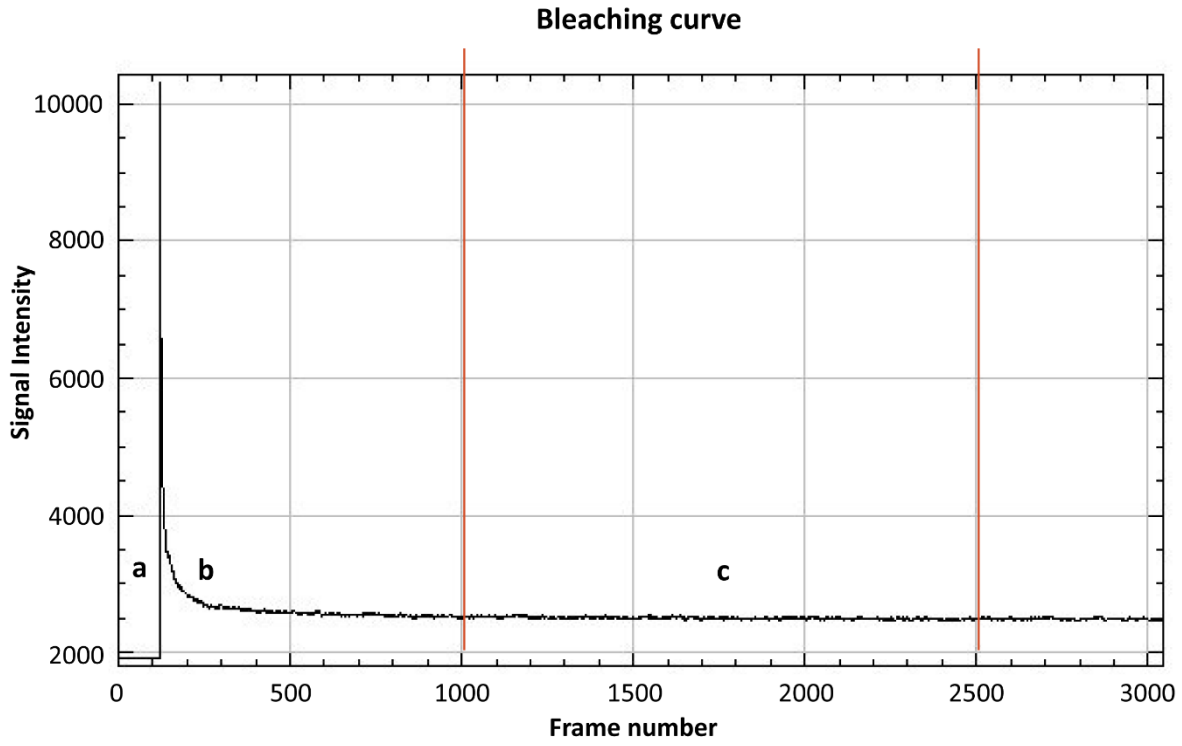

Fig. 5.1 An example of a bleaching curve by using a movie of L1-mVenus.

Number of frames is shown on the y-axis. The x-axis displays the signal intensity. The image was created through the software ImageJ-win64. a) displays the rise of the signal from zero, after turning on the laser. b) shows the decay of signal while the movie is filmed, also known as bleaching curve. c) displays the plateau of signal, where only single molecules are visible before they bleach out and new fluorophores replace them. Two red lines frame the area, which is mostly used, while the other frames are cut away.

5.5.2.1 Combination of single-molecule tracking and wide-field fluorescence microscopy

For the combination of single-molecule tracking and epifluorescence microscopy (see **3.3**) another microscope than before was used. This was an Olympus IX71, with a high numerical objective (x100 objective UAPON 100×OTIRF, NA 1.49) and an electron-multiplying CCD (EMCCD) camera iXon Ultra (Andor Technology, Belfast, UK), with a laser diode of 514 nm for mVenus excitation and a laser diode of around 405 nm for CFP excitation. Each movie was taken with an exposure time of 75 ms and 3000 frames, respectively. Pictures with wide-field fluorescent microscopy were performed with an exposure time of 3000 ms.

In this set-up, the mRNA operon *ypbR-ypfzF* and one of its belonging protein DynA were analysed. The constructs MS2-mVenus + *ypbR-ypfzF*_MS2BS2x and DynA-CFP were used. As explained under **5.5.1**, in general, the fluorophore with the most long-wavelength is used

first, because it is less energy-rich. Mostly, with this, the fluorophore which is on the short-wavelength spectrum does not get excited. But it could be the other way around, if the short-wavelength fluorophore is excited first. Therefore, MS2-mVenus + *ypbR-ypfzF*_MS2BS2x should be excited first. In this work, this was not done, for a good reason. One reason, but not the main one, was, that the recording of a SMT movie of MS2-mVenus + *ypbR-ypfzF*_MS2BS2x takes roughly around 4 minutes. So, we wanted to be sure, to exclude any influence of this long acquisition time on the DynA protein. Even though, a real influence might not occur at all. The main reason was, that DynA is a protein, that is not expressed in each cell constantly, as shown in **Manuscript 2** and discussed in **3.4.2**. To be sure, to use *B. subtilis* cells, that express the DynA-CFP fusion protein, first, the wide-field fluorescent pictures of cells were taken. If there was a DynA-CFP signal detectable, the single-molecule tracking was performed directly after this.

5.6 Software

To gain the DNA sequences of *B. subtilis* genes, the SubtiWiki server was used (http://subtiwiki.uni-goettingen.de/).

To align and compare DNA sequences the EMBOSS NEEDLE alignment tool (https://www.ebi.ac.uk/Tools/psa/emboss_needle/) was utilized.

Microscope images were analysed by making use of MetaMorph 6.3-Software (Meta Imaging Software), Fiji ImageJ, and the MATLAB independent version of Oufti (2021 Oufti, Jacobs-Wagner Lab), as well as MATLAB (© 1994-2021 The MathWorks, Inc.).

For statistical analysis, Excel 2016 (Microsoft) was used. To visualize and assemble data, Adobe Illustrator (version 16.0.3) was utilized.

6 BIBLIOGRAPHY

1. Kvenvolden, K., et al., *Evidence for extraterrestrial amino-acids and hydrocarbons in the Murchison meteorite.* Nature, 1970. **228**(5275): p. 923-6.
2. Miller, S.L., *A production of amino acids under possible primitive earth conditions.* Science, 1953. **117**(3046): p. 528-9.
3. Woese, C.R., *The Genetic Code, the Molecular Basis for Genetic Expression*. 1967, New York: Harper & Row.
4. Gilbert, W., *Origin of life - The RNA world.* NATURE, 1986. **319**: p. 618.
5. Crick, F.H., *The origin of the genetic code.* J Mol Biol, 1968. **38**(3): p. 367-79.
6. Powner, M.W., B. Gerland, and J.D. Sutherland, *Synthesis of activated pyrimidine ribonucleotides in prebiotically plausible conditions.* Nature, 2009. **459**(7244): p. 239-42.
7. Westheimer, F.H., *Polyribonucleic acids as enzymes.* Nature, 1986. **319**(6054): p. 534-5.
8. Schoning, K., et al., *Chemical etiology of nucleic acid structure: the alpha-threofuranosyl-(3'-->2') oligonucleotide system.* Science, 2000. **290**(5495): p. 1347-51.
9. Zhang, L., A. Peritz, and E. Meggers, *A simple glycol nucleic acid.* J Am Chem Soc, 2005. **127**(12): p. 4174-5.
10. Wachtershauser, G., *Evolution of the first metabolic cycles.* Proc Natl Acad Sci U S A, 1990. **87**(1): p. 200-4.
11. Wachtershauser, G., *Before enzymes and templates: theory of surface metabolism.* Microbiol Rev, 1988. **52**(4): p. 452-84.
12. Wickramasinghe, N.C., D.T. Wickramasinghe, and E.J. Steele, *Cometary panspermia and origin of life?* Adv Genet, 2020. **106**: p. 5-20.
13. Hoagland, M.B., et al., *A soluble ribonucleic acid intermediate in protein synthesis.* J Biol Chem, 1958. **231**(1): p. 241-57.
14. Simons, R.W. and N. Kleckner, *Biological regulation by antisense RNA in prokaryotes.* Annu Rev Genet, 1988. **22**: p. 567-600.
15. Caprara, M.G. and T.W. Nilsen, *RNA: versatility in form and function.* Nat Struct Biol, 2000. **7**(10): p. 831-3.
16. Avner, P. and E. Heard, *X-chromosome inactivation: counting, choice and initiation.* Nat Rev Genet, 2001. **2**(1): p. 59-67.
17. Barrick, J.E. and R.R. Breaker, *The distributions, mechanisms, and structures of metabolite-binding riboswitches.* Genome Biol, 2007. **8**(11): p. R239.
18. Wang, J., et al., *Non-coding RNAs and Their Roles in Stress Response in Plants.* Genomics Proteomics Bioinformatics, 2017. **15**(5): p. 301-312.
19. Yakovchuk, P., E. Protozanova, and M.D. Frank-Kamenetskii, *Base-stacking and base-pairing contributions into thermal stability of the DNA double helix.* Nucleic Acids Res, 2006. **34**(2): p. 564-74.
20. Alberts, B.e.a., *Molecular biology of the cell*. 2015, New York and Abingdon: Norton & Company.
21. Campbell, N.A., Reece, J.B. Campbell et al Biology. 2009: Pearson Education.
22. Gowrishankar, J. and R. Harinarayanan, *Why is transcription coupled to translation in bacteria?* Mol Microbiol, 2004. **54**(3): p. 598-603.
23. Lewis, P.J., S.D. Thaker, and J. Errington, *Compartmentalization of transcription and translation in Bacillus subtilis.* EMBO J, 2000. **19**(4): p. 710-8.
24. Watson, J., Backer TA., Bell, SP., Gann, A., Levine, M., Losik, R., Harrison, SC., *Molecular Biology of the Gene*. 2014: Benjamin-Cummings Publishing Company.
25. Butler, J.E. and J.T. Kadonaga, *The RNA polymerase II core promoter: a key component in the regulation of gene expression.* Genes Dev, 2002. **16**(20): p. 2583-92.
26. Dvir, A., *Promoter escape by RNA polymerase II.* Biochim Biophys Acta, 2002. **1577**(2): p. 208-223.

27. Orphanides, G., T. Lagrange, and D. Reinberg, *The general transcription factors of RNA polymerase II.* Genes Dev, 1996. **10**(21): p. 2657-83.
28. Wade, J.T. and K. Struhl, *The transition from transcriptional initiation to elongation.* Curr Opin Genet Dev, 2008. **18**(2): p. 130-6.
29. Hodges, C., et al., *Nucleosomal fluctuations govern the transcription dynamics of RNA polymerase II.* Science, 2009. **325**(5940): p. 626-8.
30. Arndt, K.M. and C.M. Kane, *Running with RNA polymerase: eukaryotic transcript elongation.* Trends Genet, 2003. **19**(10): p. 543-50.
31. Richardson, J.P., *Rho-dependent termination and ATPases in transcript termination.* Biochim Biophys Acta, 2002. **1577**(2): p. 251-260.
32. Farnham, P.J. and T. Platt, *Rho-independent termination: dyad symmetry in DNA causes RNA polymerase to pause during transcription in vitro.* Nucleic Acids Res, 1981. **9**(3): p. 563-77.
33. Prescott, E.M., et al., *Transcriptional termination by RNA polymerase I requires the small subunit Rpa12p.* Proc Natl Acad Sci U S A, 2004. **101**(16): p. 6068-73.
34. Richard, P. and J.L. Manley, *Transcription termination by nuclear RNA polymerases.* Genes Dev, 2009. **23**(11): p. 1247-69.
35. Boulikas, T., *Nuclear localization signals (NLS).* Crit Rev Eukaryot Gene Expr, 1993. **3**(3): p. 193-227.
36. Darnell, J.E., Jr., *Reflections on the history of pre-mRNA processing and highlights of current knowledge: a unified picture.* RNA, 2013. **19**(4): p. 443-60.
37. Gilbert, W., *Why genes in pieces?* Nature, 1978. **271**(5645): p. 501.
38. Lerner, M.R., et al., *Are snRNPs involved in splicing?* Nature, 1980. **283**(5743): p. 220-4.
39. Hedberg, A. and S.D. Johansen, *Nuclear group I introns in self-splicing and beyond.* Mob DNA, 2013. **4**(1): p. 17.
40. Marcotrigiano, J., et al., *Cocrystal structure of the messenger RNA 5' cap-binding protein (eIF4E) bound to 7-methyl-GDP.* Cell, 1997. **89**(6): p. 951-61.
41. Walczak, S., et al., *A novel route for preparing 5' cap mimics and capped RNAs: phosphate-modified cap analogues obtained via click chemistry.* Chem Sci, 2017. **8**(1): p. 260-267.
42. Visa, N., et al., *A nuclear cap-binding complex binds Balbiani ring pre-mRNA cotranscriptionally and accompanies the ribonucleoprotein particle during nuclear export.* J Cell Biol, 1996. **133**(1): p. 5-14.
43. Banerjee, A.K., *5'-terminal cap structure in eucaryotic messenger ribonucleic acids.* Microbiol Rev, 1980. **44**(2): p. 175-205.
44. Konarska, M.M., R.A. Padgett, and P.A. Sharp, *Recognition of cap structure in splicing in vitro of mRNA precursors.* Cell, 1984. **38**(3): p. 731-6.
45. Gao, M., et al., *Interaction between a poly(A)-specific ribonuclease and the 5' cap influences mRNA deadenylation rates in vitro.* Mol Cell, 2000. **5**(3): p. 479-88.
46. Ryan, K., O. Calvo, and J.L. Manley, *Evidence that polyadenylation factor CPSF-73 is the mRNA 3' processing endonuclease.* RNA, 2004. **10**(4): p. 565-73.
47. Logan, J., et al., *A poly(A) addition site and a downstream termination region are required for efficient cessation of transcription by RNA polymerase II in the mouse beta maj-globin gene.* Proc Natl Acad Sci U S A, 1987. **84**(23): p. 8306-10.
48. Zhuang, Y., H. Zhang, and S. Lin, *Polyadenylation of 18S rRNA in algae(1).* J Phycol, 2013. **49**(3): p. 570-9.
49. Hunt, A.G., et al., *Arabidopsis mRNA polyadenylation machinery: comprehensive analysis of protein-protein interactions and gene expression profiling.* BMC Genomics, 2008. **9**: p. 220.
50. Quaresma, A.J., R. Sievert, and J.A. Nickerson, *Regulation of mRNA export by the PI3 kinase/AKT signal transduction pathway.* Mol Biol Cell, 2013. **24**(8): p. 1208-21.
51. Tian, B., et al., *A large-scale analysis of mRNA polyadenylation of human and mouse genes.* Nucleic Acids Res, 2005. **33**(1): p. 201-12.
52. Tian, B. and J.L. Manley, *Alternative polyadenylation of mRNA precursors.* Nat Rev Mol Cell Biol, 2017. **18**(1): p. 18-30.

53. Shell, S.A., et al., *Elevated levels of the 64-kDa cleavage stimulatory factor (CstF-64) in lipopolysaccharide-stimulated macrophages influence gene expression and induce alternative poly(A) site selection.* J Biol Chem, 2005. **280**(48): p. 39950-61.
54. Voorma, H.O., et al., *Turnip Yellow Mosaic Virus Rna: A Polycistronic Messenger for Polypeptide Synthesis by Escherichia Coli Ribosomes.* Biochim Biophys Acta, 1964. **87**: p. 691-3.
55. Kaine, B.P., R. Gupta, and C.R. Woese, *Putative introns in tRNA genes of prokaryotes.* Proc Natl Acad Sci U S A, 1983. **80**(11): p. 3309-12.
56. LaRoche-Johnston, F., et al., *Bacterial group II introns generate genetic diversity by circularization and trans-splicing from a population of intron-invaded mRNAs.* PLoS Genet, 2018. **14**(11): p. e1007792.
57. Rauhut, R. and G. Klug, *mRNA degradation in bacteria.* FEMS Microbiol Rev, 1999. **23**(3): p. 353-70.
58. Arnold, T.E., J. Yu, and J.G. Belasco, *mRNA stabilization by the ompA 5' untranslated region: two protective elements hinder distinct pathways for mRNA degradation.* RNA, 1998. **4**(3): p. 319-30.
59. Hambraeus, G., K. Karhumaa, and B. Rutberg, *A 5' stem-loop and ribosome binding but not translation are important for the stability of Bacillus subtilis aprE leader mRNA.* Microbiology (Reading), 2002. **148**(Pt 6): p. 1795-1803.
60. Osada, Y., R. Saito, and M. Tomita, *Analysis of base-pairing potentials between 16S rRNA and 5' UTR for translation initiation in various prokaryotes.* Bioinformatics, 1999. **15**(7-8): p. 578-81.
61. August, J.T., P.J. Ortiz, and J. Hurwitz, *Ribonucleic acid-dependent ribonucleotide incorporation. I. Purification and properties of the enzyme.* J Biol Chem, 1962. **237**: p. 3786-93.
62. Anantharaman, V., E.V. Koonin, and L. Aravind, *Comparative genomics and evolution of proteins involved in RNA metabolism.* Nucleic Acids Res, 2002. **30**(7): p. 1427-64.
63. O'Hara, E.B., et al., *Polyadenylylation helps regulate mRNA decay in Escherichia coli.* Proc Natl Acad Sci U S A, 1995. **92**(6): p. 1807-11.
64. Chang, S.A., et al., *Kinetics of polynucleotide phosphorylase: comparison of enzymes from Streptomyces and Escherichia coli and effects of nucleoside diphosphates.* J Bacteriol, 2008. **190**(1): p. 98-106.
65. Nagaike, T., T. Suzuki, and T. Ueda, *Polyadenylation in mammalian mitochondria: insights from recent studies.* Biochim Biophys Acta, 2008. **1779**(4): p. 266-9.
66. Walter, M., J. Kilian, and J. Kudla, *PNPase activity determines the efficiency of mRNA 3'-end processing, the degradation of tRNA and the extent of polyadenylation in chloroplasts.* EMBO J, 2002. **21**(24): p. 6905-14.
67. Akanuma, G., et al., *Inactivation of ribosomal protein genes in Bacillus subtilis reveals importance of each ribosomal protein for cell proliferation and cell differentiation.* J Bacteriol, 2012. **194**(22): p. 6282-91.
68. Ben-Shem, A., et al., *The structure of the eukaryotic ribosome at 3.0 A resolution.* Science, 2011. **334**(6062): p. 1524-9.
69. Lopez-Lastra, M., A. Rivas, and M.I. Barria, *Protein synthesis in eukaryotes: the growing biological relevance of cap-independent translation initiation.* Biol Res, 2005. **38**(2-3): p. 121-46.
70. Munk, K., Dersch, P., Eikmanns, B., Eikmanns, M., Fischer, R., Jahn, D., Jahn, M., Nethe-Jaenchen, R., Requena, N., Schultze, B., *Mikrobiologie*. Taschenbuch Biologie, Mikrobiologie 2008, Stuttgart: Georg Thieme Verlag.
71. Ganoza, M.C., et al., *Mechanism of protein chain termination: further characterization of a mutant defective in a new protein synthesis factor.* Proc Natl Acad Sci U S A, 1973. **70**(1): p. 31-5.
72. Slayter, H.S., et al., *The Visualization of Polyribosomal Structure.* J Mol Biol, 1963. **7**: p. 652-7.

73. Miller, O.L., Jr., B.A. Hamkalo, and C.A. Thomas, Jr., *Visualization of bacterial genes in action.* Science, 1970. **169**(3943): p. 392-5.
74. Warner, J.R., P.M. Knopf, and A. Rich, *A multiple ribosomal structure in protein synthesis.* Proc Natl Acad Sci U S A, 1963. **49**: p. 122-9.
75. Katz, Z.B., et al., *Mapping translation 'hot-spots' in live cells by tracking single molecules of mRNA and ribosomes.* Elife, 2016. **5**.
76. Ostroff, L.E., et al., *Polyribosomes redistribute from dendritic shafts into spines with enlarged synapses during LTP in developing rat hippocampal slices.* Neuron, 2002. **35**(3): p. 535-45.
77. Yan, X., et al., *Dynamics of Translation of Single mRNA Molecules In Vivo.* Cell, 2016. **165**(4): p. 976-89.
78. Bakshi, S., et al., *Time-dependent effects of transcription- and translation-halting drugs on the spatial distributions of the Escherichia coli chromosome and ribosomes.* Mol Microbiol, 2014. **94**(4): p. 871-87.
79. Bakshi, S., et al., *Superresolution imaging of ribosomes and RNA polymerase in live Escherichia coli cells.* Mol Microbiol, 2012. **85**(1): p. 21-38.
80. Campos, M. and C. Jacobs-Wagner, *Cellular organization of the transfer of genetic information.* Curr Opin Microbiol, 2013. **16**(2): p. 171-6.
81. Keren Nevo-Dinur, A.N.-S., Sigal Ben-Yehuda, Orna Amster-Choder, *Translation-Independent Localization of mRNA in E. coli.* Science, 25 FEBRUARY 2011. **VOL 331**.
82. Rudner, D.Z. and R. Losick, *Protein subcellular localization in bacteria.* Cold Spring Harb Perspect Biol, 2010. **2**(4): p. a000307.
83. Defeu Soufo, H.J. and P.L. Graumann, *Bacillus subtilis actin-like protein MreB influences the positioning of the replication machinery and requires membrane proteins MreC/D and other actin-like proteins for proper localization.* BMC Cell Biol, 2005. **6**(1): p. 10.
84. Dempwolff, F., et al., *Bacillus subtilis MreB orthologs self-organize into filamentous structures underneath the cell membrane in a heterologous cell system.* PLoS One, 2011. **6**(11): p. e27035.
85. Cabeen, M.T. and C. Jacobs-Wagner, *The bacterial cytoskeleton.* Annu Rev Genet, 2010. **44**: p. 365-92.
86. Jones, L.J., R. Carballido-Lopez, and J. Errington, *Control of cell shape in bacteria: helical, actin-like filaments in Bacillus subtilis.* Cell, 2001. **104**(6): p. 913-22.
87. Yu, X.C. and W. Margolin, *FtsZ ring clusters in min and partition mutants: role of both the Min system and the nucleoid in regulating FtsZ ring localization.* Mol Microbiol, 1999. **32**(2): p. 315-26.
88. Fleming, T.C., et al., *Dynamic SpoIIIE assembly mediates septal membrane fission during Bacillus subtilis sporulation.* Genes Dev, 2010. **24**(11): p. 1160-72.
89. Levin, P.A. and R. Losick, *Transcription factor Spo0A switches the localization of the cell division protein FtsZ from a medial to a bipolar pattern in Bacillus subtilis.* Genes Dev, 1996. **10**(4): p. 478-88.
90. Govindarajan, S., et al., *The general phosphotransferase system proteins localize to sites of strong negative curvature in bacterial cells.* mBio, 2013. **4**(5): p. e00443-13.
91. Lenarcic, R., et al., *Localisation of DivIVA by targeting to negatively curved membranes.* EMBO J, 2009. **28**(15): p. 2272-82.
92. Maddock, J.R. and L. Shapiro, *Polar location of the chemoreceptor complex in the Escherichia coli cell.* Science, 1993. **259**(5102): p. 1717-23.
93. Miczak, A., R.A. Srivastava, and D. Apirion, *Location of the RNA-processing enzymes RNase III, RNase E and RNase P in the Escherichia coli cell.* Mol Microbiol, 1991. **5**(7): p. 1801-10.
94. Raskin, D.M. and P.A. de Boer, *Rapid pole-to-pole oscillation of a protein required for directing division to the middle of Escherichia coli.* Proc Natl Acad Sci U S A, 1999. **96**(9): p. 4971-6.
95. Webb, C.D., et al., *Bipolar localization of the replication origin regions of chromosomes in vegetative and sporulating cells of B. subtilis.* Cell, 1997. **88**(5): p. 667-74.

96. Ebersbach, G., et al., *A self-associating protein critical for chromosome attachment, division, and polar organization in caulobacter.* Cell, 2008. **134**(6): p. 956-68.
97. Umbarger, M.A., et al., *The three-dimensional architecture of a bacterial genome and its alteration by genetic perturbation.* Mol Cell, 2011. **44**(2): p. 252-64.
98. Fisher, J.K., et al., *Four-dimensional imaging of E. coli nucleoid organization and dynamics in living cells.* Cell, 2013. **153**(4): p. 882-95.
99. Kuhlman, T.E. and E.C. Cox, *Gene location and DNA density determine transcription factor distributions in Escherichia coli.* Mol Syst Biol, 2012. **8**: p. 610.
100. Fan, H., et al., *Transcription-translation coupling: direct interactions of RNA polymerase with ribosomes and ribosomal subunits.* Nucleic Acids Res, 2017. **45**(19): p. 11043-11055.
101. Chai, Q., et al., *Organization of ribosomes and nucleoids in Escherichia coli cells during growth and in quiescence.* J Biol Chem, 2014. **289**(16): p. 11342-52.
102. Sanamrad, A., et al., *Single-particle tracking reveals that free ribosomal subunits are not excluded from the Escherichia coli nucleoid.* Proc Natl Acad Sci U S A, 2014. **111**(31): p. 11413-8.
103. Dugar, G., et al., *The CsrA-FliW network controls polar localization of the dual-function flagellin mRNA in Campylobacter jejuni.* Nat Commun, 2016. **7**: p. 11667.
104. Pilhofer, M., et al., *Fluorescence in situ hybridization for intracellular localization of nifH mRNA.* Syst Appl Microbiol, 2009. **32**(3): p. 186-92.
105. Moffitt, J.R., et al., *Spatial organization shapes the turnover of a bacterial transcriptome.* Elife, 2016. **5**.
106. Valencia-Burton, M., et al., *RNA visualization in live bacterial cells using fluorescent protein complementation.* Nat Methods, 2007. **4**(5): p. 421-7.
107. van Gijtenbeek, L.A., et al., *On the Spatial Organization of mRNA, Plasmids, and Ribosomes in a Bacterial Host Overexpressing Membrane Proteins.* PLoS Genet, 2016. **12**(12): p. e1006523.
108. Angelini, S., S. Deitermann, and H.G. Koch, *FtsY, the bacterial signal-recognition particle receptor, interacts functionally and physically with the SecYEG translocon.* EMBO Rep, 2005. **6**(5): p. 476-81.
109. Braig, D., et al., *Two cooperating helices constitute the lipid-binding domain of the bacterial SRP receptor.* J Mol Biol, 2009. **390**(3): p. 401-13.
110. Herskovitz, M.A. and D.H. Bechhofer, *Endoribonuclease RNase III is essential in Bacillus subtilis.* Mol Microbiol, 2000. **38**(5): p. 1027-33.
111. Durand, S., L. Gilet, and C. Condon, *The essential function of B. subtilis RNase III is to silence foreign toxin genes.* PLoS Genet, 2012. **8**(12): p. e1003181.
112. Mitra, S. and D.H. Bechhofer, *Substrate specificity of an RNase III-like activity from Bacillus subtilis.* J Biol Chem, 1994. **269**(50): p. 31450-6.
113. Schibany, S., et al., *Single molecule tracking reveals that the bacterial SMC complex moves slowly relative to the diffusion of the chromosome.* Nucleic Acids Res, 2018. **46**(15): p. 7805-7819.
114. Kleine Borgmann, L.A., et al., *The bacterial SMC complex displays two distinct modes of interaction with the chromosome.* Cell Rep, 2013. **3**(5): p. 1483-92.
115. Graumann, P.L., R. Losick, and A.V. Strunnikov, *Subcellular localization of Bacillus subtilis SMC, a protein involved in chromosome condensation and segregation.* J Bacteriol, 1998. **180**(21): p. 5749-55.
116. Wang, X., et al., *The SMC condensin complex is required for origin segregation in Bacillus subtilis.* Curr Biol, 2014. **24**(3): p. 287-92.
117. Dersch, S., et al., *Super-Resolution Microscopy and Single-Molecule Tracking Reveal Distinct Adaptive Dynamics of MreB and of Cell Wall-Synthesis Enzymes.* Front Microbiol, 2020. **11**: p. 1946.
118. Dominguez-Escobar, J., et al., *Processive movement of MreB-associated cell wall biosynthetic complexes in bacteria.* Science, 2011. **333**(6039): p. 225-8.

119. Mirouze, N., et al., *MreB-Dependent Inhibition of Cell Elongation during the Escape from Competence in Bacillus subtilis.* PLoS Genet, 2015. **11**(6): p. e1005299.
120. Yu, Y., et al., *The Min System Disassembles FtsZ Foci and Inhibits Polar Peptidoglycan Remodeling in Bacillus subtilis.* mBio, 2020. **11**(2).
121. Strahl, H. and L.W. Hamoen, *Membrane potential is important for bacterial cell division.* Proc Natl Acad Sci U S A, 2010. **107**(27): p. 12281-6.
122. Resch, M., et al., *Insight into the induction mechanism of the GntR/HutC bacterial transcription regulator YvoA.* Nucleic Acids Res, 2010. **38**(7): p. 2485-97.
123. El Najjar, N., et al., *Single-Molecule Tracking of DNA Translocases in Bacillus subtilis Reveals Strikingly Different Dynamics of SftA, SpoIIIE, and FtsA.* Appl Environ Microbiol, 2018. **84**(8).
124. Sawant, P., et al., *A dynamin-like protein involved in bacterial cell membrane surveillance under environmental stress.* Environ Microbiol, 2016. **18**(8): p. 2705-20.
125. Dempwolff, F., et al., *The deletion of bacterial dynamin and flotillin genes results in pleiotrophic effects on cell division, cell growth and in cell shape maintenance.* BMC Microbiol, 2012. **12**: p. 298.
126. Sohmen, D., et al., *Structure of the Bacillus subtilis 70S ribosome reveals the basis for species-specific stalling.* Nat Commun, 2015. **6**: p. 6941.
127. Mascarenhas, J., M.H. Weber, and P.L. Graumann, *Specific polar localization of ribosomes in Bacillus subtilis depends on active transcription.* EMBO Rep, 2001. **2**(8): p. 685-9.
128. Ogura, M. and T. Tanaka, *The Bacillus subtilis late competence operon comE is transcriptionally regulated by yutB and under post-transcription initiation control by comN (yrzD).* J Bacteriol, 2009. **191**(3): p. 949-58.
129. dos Santos, V.T., A.W. Bisson-Filho, and F.J. Gueiros-Filho, *DivIVA-mediated polar localization of ComN, a posttranscriptional regulator of Bacillus subtilis.* J Bacteriol, 2012. **194**(14): p. 3661-9.
130. Furukawa, A., et al., *Tunnel Formation Inferred from the I-Form Structures of the Proton-Driven Protein Secretion Motor SecDF.* Cell Rep, 2017. **19**(5): p. 895-901.
131. Rubio, A., X. Jiang, and K. Pogliano, *Localization of translocation complex components in Bacillus subtilis: enrichment of the signal recognition particle receptor at early sporulation septa.* J Bacteriol, 2005. **187**(14): p. 5000-2.
132. von Loeffelholz, O., et al., *Structural basis of signal sequence surveillance and selection by the SRP-FtsY complex.* Nat Struct Mol Biol, 2013. **20**(5): p. 604-10.
133. Williams, M.L., et al., *YlxM is a newly identified accessory protein that influences the function of signal recognition particle pathway components in Streptococcus mutans.* J Bacteriol, 2014. **196**(11): p. 2043-52.
134. Honda, K., et al., *Cloning and characterization of a Bacillus subtilis gene encoding a homolog of the 54-kilodalton subunit of mammalian signal recognition particle and Escherichia coli Ffh.* J Bacteriol, 1993. **175**(15): p. 4885-94.
135. Lovgren, J.M., et al., *The PRC-barrel domain of the ribosome maturation protein RimM mediates binding to ribosomal protein S19 in the 30S ribosomal subunits.* RNA, 2004. **10**(11): p. 1798-812.
136. Bystrom, A.S. and G.R. Bjork, *Chromosomal location and cloning of the gene (trmD) responsible for the synthesis of tRNA (m1G) methyltransferase in Escherichia coli K-12.* Mol Gen Genet, 1982. **188**(3): p. 440-6.
137. Mirel, D.B. and M.J. Chamberlin, *The Bacillus subtilis flagellin gene (hag) is transcribed by the sigma 28 form of RNA polymerase.* J Bacteriol, 1989. **171**(6): p. 3095-101.
138. Hwang, W.Y., et al., *Efficient genome editing in zebrafish using a CRISPR-Cas system.* Nat Biotechnol, 2013. **31**(3): p. 227-9.
139. Wiedenheft, B., S.H. Sternberg, and J.A. Doudna, *RNA-guided genetic silencing systems in bacteria and archaea.* Nature, 2012. **482**(7385): p. 331-8.
140. O'Connell, M.R., et al., *Programmable RNA recognition and cleavage by CRISPR/Cas9.* Nature, 2014. **516**(7530): p. 263-6.

141. Moter, A. and U.B. Gobel, *Fluorescence in situ hybridization (FISH) for direct visualization of microorganisms.* J Microbiol Methods, 2000. **41**(2): p. 85-112.
142. Femino, A.M., et al., *Visualization of single RNA transcripts in situ.* Science, 1998. **280**(5363): p. 585-90.
143. Bratu, D.P., et al., *Visualizing the distribution and transport of mRNAs in living cells.* Proc Natl Acad Sci U S A, 2003. **100**(23): p. 13308-13.
144. Tyagi, S. and F.R. Kramer, *Molecular beacons: probes that fluoresce upon hybridization.* Nat Biotechnol, 1996. **14**(3): p. 303-8.
145. Ansorge, W.J., *Next-generation DNA sequencing techniques.* N Biotechnol, 2009. **25**(4): p. 195-203.
146. Lee, J.H., et al., *Fluorescent in situ sequencing (FISSEQ) of RNA for gene expression profiling in intact cells and tissues.* Nat Protoc, 2015. **10**(3): p. 442-58.
147. Ouellet, J., *RNA Fluorescence with Light-Up Aptamers.* Front Chem, 2016. **4**: p. 29.
148. Paige, J.S., K.Y. Wu, and S.R. Jaffrey, *RNA mimics of green fluorescent protein.* Science, 2011. **333**(6042): p. 642-6.
149. Dolgosheina, E.V., et al., *RNA mango aptamer-fluorophore: a bright, high-affinity complex for RNA labeling and tracking.* ACS Chem Biol, 2014. **9**(10): p. 2412-20.
150. Daigle, N. and J. Ellenberg, *LambdaN-GFP: an RNA reporter system for live-cell imaging.* Nat Methods, 2007. **4**(8): p. 633-6.
151. Schonberger, J., U.Z. Hammes, and T. Dresselhaus, *In vivo visualization of RNA in plants cells using the lambdaN(2)(2) system and a GATEWAY-compatible vector series for candidate RNAs.* Plant J, 2012. **71**(1): p. 173-81.
152. Tutucci, E., et al., *An improved MS2 system for accurate reporting of the mRNA life cycle.* Nat Methods, 2018. **15**(1): p. 81-89.
153. Golding, I. and E.C. Cox, *RNA dynamics in live Escherichia coli cells.* Proc Natl Acad Sci U S A, 2004. **101**(31): p. 11310-5.
154. Stockley, P.G., et al., *Probing sequence-specific RNA recognition by the bacteriophage MS2 coat protein.* Nucleic Acids Res, 1995. **23**(13): p. 2512-8.
155. Peabody, D.S., *The RNA binding site of bacteriophage MS2 coat protein.* EMBO J, 1993. **12**(2): p. 595-600.
156. Gustafsson, M.G., *Surpassing the lateral resolution limit by a factor of two using structured illumination microscopy.* J Microsc, 2000. **198**(Pt 2): p. 82-7.
157. Metzler, R., et al., *Anomalous diffusion models and their properties: non-stationarity, non-ergodicity, and ageing at the centenary of single particle tracking.* Phys Chem Chem Phys, 2014. **16**(44): p. 24128-64.
158. Manzo, C. and M.F. Garcia-Parajo, *A review of progress in single particle tracking: from methods to biophysical insights.* Rep Prog Phys, 2015. **78**(12): p. 124601.
159. Rösch, T.C., et al., *SMTracker: a tool for quantitative analysis, exploration and visualization of single-molecule tracking data reveals highly dynamic binding of B. subtilis global repressor AbrB throughout the genome.* Sci Rep, 2018. **8**(1): p. 15747.
160. Oviedo-Bocanegra, L.M., et al., *Single molecule/particle tracking analysis program SMTracker 2.0 reveals different dynamics of proteins within the RNA degradosome complex in Bacillus subtilis.* Nucleic Acids Res, 2021. **49**(19): p. e112.
161. Ober, R.J., et al., *Quantitative Aspects of Single Molecule Microscopy.* IEEE Signal Process Mag, 2015. **32**(1): p. 58-69.
162. Zander, C., Enderlein, J., Keller, R.A., *Single Molecule Detection in Solution: Methods and Applications*. 2002: Wiley-VCH Verlag GmbH & KGaA.
163. Berg, H.C., *How to track bacteria.* Rev Sci Instrum, 1971. **42**(6): p. 868-71.
164. Salthammer, T., *Numerical simulation of pile-up distorted time-correlated single photon counting (TCSPC) data.* J Fluoresc, 1992. **2**(1): p. 23-7.
165. Myong, S., et al., *Repetitive shuttling of a motor protein on DNA.* Nature, 2005. **437**(7063): p. 1321-5.

166. Betzig, E., et al., *Imaging intracellular fluorescent proteins at nanometer resolution.* Science, 2006. **313**(5793): p. 1642-5.
167. Manley, S., et al., *High-density mapping of single-molecule trajectories with photoactivated localization microscopy.* Nat Methods, 2008. **5**(2): p. 155-7.
168. El Najjar, N., et al., *Bacterial cell growth is arrested by violet and blue, but not yellow light excitation during fluorescence microscopy.* BMC Mol Cell Biol, 2020. **21**(1): p. 35.
169. Plank, M., G.H. Wadhams, and M.C. Leake, *Millisecond timescale slimfield imaging and automated quantification of single fluorescent protein molecules for use in probing complex biological processes.* Integr Biol (Camb), 2009. **1**(10): p. 602-12.
170. Chung, H.S., J.M. Louis, and W.A. Eaton, *Experimental determination of upper bound for transition path times in protein folding from single-molecule photon-by-photon trajectories.* Proc Natl Acad Sci U S A, 2009. **106**(29): p. 11837-44.
171. Liu, S.L., et al., *Effectively and efficiently dissecting the infection of influenza virus by quantum-dot-based single-particle tracking.* ACS Nano, 2012. **6**(1): p. 141-50.
172. Elf, J., G.W. Li, and X.S. Xie, *Probing transcription factor dynamics at the single-molecule level in a living cell.* Science, 2007. **316**(5828): p. 1191-4.
173. English, B.P., et al., *Single-molecule investigations of the stringent response machinery in living bacterial cells.* Proc Natl Acad Sci U S A, 2011. **108**(31): p. E365-73.
174. Suzuki, D.T., T. Grigliatti, and R. Williamson, *Temperature-sensitive mutations in Drosophila melanogaster. VII. A mutation (para-ts) causing reversible adult paralysis.* Proc Natl Acad Sci U S A, 1971. **68**(5): p. 890-3.
175. Kochs, G., et al., *Self-assembly of human MxA GTPase into highly ordered dynamin-like oligomers.* J Biol Chem, 2002. **277**(16): p. 14172-6.
176. Niemann, H.H., et al., *Crystal structure of a dynamin GTPase domain in both nucleotide-free and GDP-bound forms.* EMBO J, 2001. **20**(21): p. 5813-21.
177. Pai, E.F., et al., *Refined crystal structure of the triphosphate conformation of H-ras p21 at 1.35 A resolution: implications for the mechanism of GTP hydrolysis.* EMBO J, 1990. **9**(8): p. 2351-9.
178. Bramkamp, M., *Structure and function of bacterial dynamin-like proteins.* Biol Chem, 2012. **393**(11): p. 1203-14.
179. Oh, P., D.P. McIntosh, and J.E. Schnitzer, *Dynamin at the neck of caveolae mediates their budding to form transport vesicles by GTP-driven fission from the plasma membrane of endothelium.* J Cell Biol, 1998. **141**(1): p. 101-14.
180. Smirnova, E., et al., *A model for dynamin self-assembly based on binding between three different protein domains.* J Biol Chem, 1999. **274**(21): p. 14942-7.
181. Muhlberg, A.B., D.E. Warnock, and S.L. Schmid, *Domain structure and intramolecular regulation of dynamin GTPase.* EMBO J, 1997. **16**(22): p. 6676-83.
182. Ochoa, G.C., et al., *A functional link between dynamin and the actin cytoskeleton at podosomes.* J Cell Biol, 2000. **150**(2): p. 377-89.
183. Henley, J.R., et al., *Dynamin-mediated internalization of caveolae.* J Cell Biol, 1998. **141**(1): p. 85-99.
184. Lemmon, M.A. and K.M. Ferguson, *Signal-dependent membrane targeting by pleckstrin homology (PH) domains.* Biochem J, 2000. **350 Pt 1**: p. 1-18.
185. Gold, E.S., et al., *Dynamin 2 is required for phagocytosis in macrophages.* J Exp Med, 1999. **190**(12): p. 1849-56.
186. Thompson, H.M., et al., *The large GTPase dynamin associates with the spindle midzone and is required for cytokinesis.* Curr Biol, 2002. **12**(24): p. 2111-7.
187. Antonny, B., et al., *Membrane fission by dynamin: what we know and what we need to know.* EMBO J, 2016. **35**(21): p. 2270-2284.
188. Chernomordik, L.V. and M.M. Kozlov, *Protein-lipid interplay in fusion and fission of biological membranes.* Annu Rev Biochem, 2003. **72**: p. 175-207.

189. Kozlovsky, Y. and M.M. Kozlov, *Membrane fission: model for intermediate structures.* Biophys J, 2003. **85**(1): p. 85-96.
190. Smirnova, E., et al., *A human dynamin-related protein controls the distribution of mitochondria.* J Cell Biol, 1998. **143**(2): p. 351-8.
191. Janzen, C., G. Kochs, and O. Haller, *A monomeric GTPase-negative MxA mutant with antiviral activity.* J Virol, 2000. **74**(17): p. 8202-6.
192. Hermann, G.J., et al., *Mitochondrial fusion in yeast requires the transmembrane GTPase Fzo1p.* J Cell Biol, 1998. **143**(2): p. 359-73.
193. McQuibban, G.A., S. Saurya, and M. Freeman, *Mitochondrial membrane remodelling regulated by a conserved rhomboid protease.* Nature, 2003. **423**(6939): p. 537-41.
194. Yoon, Y., et al., *A novel dynamin-like protein associates with cytoplasmic vesicles and tubules of the endoplasmic reticulum in mammalian cells.* J Cell Biol, 1998. **140**(4): p. 779-93.
195. Gu, X. and D.P. Verma, *Phragmoplastin, a dynamin-like protein associated with cell plate formation in plants.* EMBO J, 1996. **15**(4): p. 695-704.
196. Uthaiah, R.C., et al., *IIGP1, an interferon-gamma-inducible 47-kDa GTPase of the mouse, showing cooperative enzymatic activity and GTP-dependent multimerization.* J Biol Chem, 2003. **278**(31): p. 29336-43.
197. Prakash, B., et al., *Structure of human guanylate-binding protein 1 representing a unique class of GTP-binding proteins.* Nature, 2000. **403**(6769): p. 567-71.
198. Low, H.H. and J. Lowe, *A bacterial dynamin-like protein.* Nature, 2006. **444**(7120): p. 766-9.
199. Burmann, F., et al., *A bacterial dynamin-like protein mediating nucleotide-independent membrane fusion.* Mol Microbiol, 2011. **79**(5): p. 1294-304.
200. Gao, S., et al., *Structure of myxovirus resistance protein a reveals intra- and intermolecular domain interactions required for the antiviral function.* Immunity, 2011. **35**(4): p. 514-25.
201. Ford, M.G., S. Jenni, and J. Nunnari, *The crystal structure of dynamin.* Nature, 2011. **477**(7366): p. 561-6.
202. Low, H.H., et al., *Structure of a bacterial dynamin-like protein lipid tube provides a mechanism for assembly and membrane curving.* Cell, 2009. **139**(7): p. 1342-52.
203. Gasper, R., et al., *It takes two to tango: regulation of G proteins by dimerization.* Nat Rev Mol Cell Biol, 2009. **10**(6): p. 423-9.
204. Guo, L. and M. Bramkamp, *Bacterial dynamin-like protein DynA mediates lipid and content mixing.* FASEB J, 2019. **33**(11): p. 11746-11757.
205. Dempwolff, F. and P.L. Graumann, *Genetic links between bacterial dynamin and flotillin proteins.* Commun Integr Biol, 2014. **7**(5).
206. Burmann, F., P. Sawant, and M. Bramkamp, *Identification of interaction partners of the dynamin-like protein DynA from Bacillus subtilis.* Commun Integr Biol, 2012. **5**(4): p. 362-9.
207. Kannaiah, S. and O. Amster-Choder, *Methods for studying RNA localization in bacteria.* Methods, 2016. **98**: p. 99-103.
208. Garcia, J.F. and R. Parker, *MS2 coat proteins bound to yeast mRNAs block 5' to 3' degradation and trap mRNA decay products: implications for the localization of mRNAs by MS2-MCP system.* RNA, 2015. **21**(8): p. 1393-5.
209. Heinrich, S., et al., *Stem-loop RNA labeling can affect nuclear and cytoplasmic mRNA processing.* RNA, 2017. **23**(2): p. 134-141.
210. Kodgire, P. and K.K. Rao, *hag expression in Bacillus subtilis is both negatively and positively regulated by ScoC.* Microbiology (Reading), 2009. **155**(Pt 1): p. 142-149.
211. Weimann, L., et al., *A quantitative comparison of single-dye tracking analysis tools using Monte Carlo simulations.* PLoS One, 2013. **8**(5): p. e64287.
212. Kass, R.E., Wassermann, L., *A Reference Bayesian Test for Nested Hypotheses and its Relationship to the Schwarz Criterion.* Journal of the American Statistical Association 1995. **90**(431).
213. Kubitscheck, U., et al., *Imaging and tracking of single GFP molecules in solution.* Biophys J, 2000. **78**(4): p. 2170-9.

214. Buxbaum, A.R., G. Haimovich, and R.H. Singer, *In the right place at the right time: visualizing and understanding mRNA localization.* Nat Rev Mol Cell Biol, 2015. **16**(2): p. 95-109.
215. Ramachandran, R. and S.L. Schmid, *The dynamin superfamily.* Curr Biol, 2018. **28**(8): p. R411-R416.
216. Schlimpert, S., et al., *Two dynamin-like proteins stabilize FtsZ rings during Streptomyces sporulation.* Proc Natl Acad Sci U S A, 2017. **114**(30): p. E6176-E6183.
217. Kremers, G.J., et al., *Cyan and yellow super fluorescent proteins with improved brightness, protein folding, and FRET Forster radius.* Biochemistry, 2006. **45**(21): p. 6570-80.
218. Schindelin, J., et al., *Fiji: an open-source platform for biological-image analysis.* Nature Methods, 2012. **9**(7): p. 676-682.
219. Holscher, T., et al., *Impaired competence in flagellar mutants of Bacillus subtilis is connected to the regulatory network governed by DegU.* Environ Microbiol Rep, 2018. **10**(1): p. 23-32.
220. Ward, E., et al., *Organization of the Flagellar Switch Complex of Bacillus subtilis.* J Bacteriol, 2019. **201**(8).
221. Rosenberg, A., et al., *Dynamic expression of the translational machinery during Bacillus subtilis life cycle at a single cell level.* PLoS One, 2012. **7**(7): p. e41921.
222. Bremer, H. and P.P. Dennis, *Modulation of Chemical Composition and Other Parameters of the Cell at Different Exponential Growth Rates.* EcoSal Plus, 2008. **3**(1).
223. Brunschede, H., T.L. Dove, and H. Bremer, *Establishment of exponential growth after a nutritional shift-up in Escherichia coli B/r: accumulation of deoxyribonucleic acid, ribonucleic acid, and protein.* J Bacteriol, 1977. **129**(2): p. 1020-33.
224. Proctor, V.A. and F.E. Cunningham, *The chemistry of lysozyme and its use as a food preservative and a pharmaceutical.* Crit Rev Food Sci Nutr, 1988. **26**(4): p. 359-95.
225. Kunz, S., et al., *Cyclic di-GMP Signaling in Bacillus subtilis Is Governed by Direct Interactions of Diguanylate Cyclases and Cognate Receptors.* mBio, 2020. **11**(2).
226. Delumeau, O., et al., *The dynamic protein partnership of RNA polymerase in Bacillus subtilis.* Proteomics, 2011. **11**(15): p. 2992-3001.
227. Irnov, I., et al., *Identification of regulatory RNAs in Bacillus subtilis.* Nucleic Acids Res, 2010. **38**(19): p. 6637-51.
228. Montero Llopis, P., et al., *Spatial organization of the flow of genetic information in bacteria.* Nature, 2010. **466**(7302): p. 77-81.
229. Buskila, A.A., S. Kannaiah, and O. Amster-Choder, *RNA localization in bacteria.* RNA Biol, 2014. **11**(8): p. 1051-60.
230. Bakshi, S., H. Choi, and J.C. Weisshaar, *The spatial biology of transcription and translation in rapidly growing Escherichia coli.* Front Microbiol, 2015. **6**: p. 636.
231. Castellana, M., S. Hsin-Jung Li, and N.S. Wingreen, *Spatial organization of bacterial transcription and translation.* Proc Natl Acad Sci U S A, 2016. **113**(33): p. 9286-91.
232. Mayer, B., et al., *Dynamics of Bacterial Signal Recognition Particle at a Single Molecule Level.* Front Microbiol, 2021. **12**: p. 663747.
233. Kostakioti, M., et al., *Mechanisms of protein export across the bacterial outer membrane.* J Bacteriol, 2005. **187**(13): p. 4306-14.
234. Scott, M., et al., *Interdependence of cell growth and gene expression: origins and consequences.* Science, 2010. **330**(6007): p. 1099-102.
235. Formstone, A. and J. Errington, *A magnesium-dependent mreB null mutant: implications for the role of mreB in Bacillus subtilis.* Mol Microbiol, 2005. **55**(6): p. 1646-57.
236. Guet, C.C., et al., *Minimally invasive determination of mRNA concentration in single living bacteria.* Nucleic Acids Res, 2008. **36**(12): p. e73.
237. Mika, J.T. and B. Poolman, *Macromolecule diffusion and confinement in prokaryotic cells.* Curr Opin Biotechnol, 2011. **22**(1): p. 117-26.
238. Politz, J.C., R.A. Tuft, and T. Pederson, *Diffusion-based transport of nascent ribosomes in the nucleus.* Mol Biol Cell, 2003. **14**(12): p. 4805-12.

239. Forchhammer, J. and L. Lindahl, *Growth rate of polypeptide chains as a function of the cell growth rate in a mutant of Escherichia coli 15.* J Mol Biol, 1971. **55**(3): p. 563-8.
240. Schenk, K., et al., *Rapid turnover of DnaA at replication origin regions contributes to initiation control of DNA replication.* PLoS Genet, 2017. **13**(2): p. e1006561.
241. Johnson, B.A., H. Anker, and F.L. Meleney, *Bacitracin: A New Antibiotic Produced by a Member of the B. Subtilis Group.* Science, 1945. **102**(2650): p. 376-7.
242. Hickey, R.J., *Bacitracin, its manufacture and uses.* Prog Ind Microbiol, 1964. **5**: p. 93-150.
243. Soomro, A.H., T. Masud and Kiran Anwaar*, *Role of Lactic Acid Bacteria (LAB) in Food Preservation*
and Human Health – A Review. Pakistan Journal of Nutrition, Asian Network for Scientific information, 2002. **1 (1)**.
244. Feucht, A. and P.J. Lewis, *Improved plasmid vectors for the production of multiple fluorescent protein fusions in Bacillus subtilis.* Gene, 2001. **264**(2): p. 289-97.
245. Steinmetz, M. and R. Richter, *Plasmids designed to alter the antibiotic resistance expressed by insertion mutations in Bacillus subtilis, through in vivo recombination.* Gene, 1994. **142**(1): p. 79-83.
246. Woodcock, D.M., et al., *Quantitative evaluation of Escherichia coli host strains for tolerance to cytosine methylation in plasmid and phage recombinants.* Nucleic Acids Res, 1989. **17**(9): p. 3469-78.
247. Taylor, R.G., D.C. Walker, and R.R. McInnes, *E. coli host strains significantly affect the quality of small scale plasmid DNA preparations used for sequencing.* Nucleic Acids Res, 1993. **21**(7): p. 1677-8.
248. Burkholder, P.R. and N.H. Giles, Jr., *Induced biochemical mutations in Bacillus subtilis.* Am J Bot, 1947. **34**(6): p. 345-8.
249. Konkol, M.A., K.M. Blair, and D.B. Kearns, *Plasmid-encoded ComI inhibits competence in the ancestral 3610 strain of Bacillus subtilis.* J Bacteriol, 2013. **195**(18): p. 4085-93.
250. Mullis, K., et al., *Specific enzymatic amplification of DNA in vitro: the polymerase chain reaction.* Cold Spring Harb Symp Quant Biol, 1986. **51 Pt 1**: p. 263-73.
251. Sambrook, J., E.F. Fritsch, and T. Maniatis, *Molecular cloning, A laboratory manual*. 1989, Cold Spring Harbor, NY: Cold Spring Harbor Laboratory Press. xxxviii + 1546 pp.
252. Gibson, D.G., et al., *Enzymatic assembly of DNA molecules up to several hundred kilobases.* Nat Methods, 2009. **6**(5): p. 343-5.
253. Laemmli, U.K., *Cleavage of structural proteins during the assembly of the head of bacteriophage T4.* Nature, 1970. **227**(5259): p. 680-5.
254. Harlow, E., Lane, D., *A laboratory manual*. Vol. 579. 1988, New York: New York: Cold Spring Harbor Laboratory.
255. Murphy, D.B., *Fundamentals of light microscopy and electronic imaging*. 2001, New York: Wiley-Liss, Inc.
256. Zhu, X.G., et al., *Chlorophyll a fluorescence induction kinetics in leaves predicted from a model describing each discrete step of excitation energy and electron transfer associated with Photosystem II.* Planta, 2005. **223**(1): p. 114-133.
257. Lichtman, J.W. and J.A. Conchello, *Fluorescence microscopy.* Nat Methods, 2005. **2**(12): p. 910-9.
258. Kasha, M., *Characterization of Electronic Transitions in Complex Molecules.* Discussions of the Faraday Society, 1950. **9**: p. 14-19.
259. Gispert, J.R., *Coordination Chemistry*. 2008, Weinhehim: Wiley-VCH.
260. Yikun, C., Yongxin, G., Yujun, H., Gang, Z., Hui, W., Yuchen, W., Qin-Pei, W., Huaqin, C., *Determining Essential Requirements for Fluorophore Selection in Various Fluorescence Applications Taking Advantage of Diverse Structure–Fluorescence Information of Chromone Derivatives.* Journal of Medicinal Chemistry, 2020: p. 1001-1017.
261. Westphal, V., et al., *Video-rate far-field optical nanoscopy dissects synaptic vesicle movement.* Science, 2008. **320**(5873): p. 246-9.

262. Gustafsson, M.G., et al., *Three-dimensional resolution doubling in wide-field fluorescence microscopy by structured illumination.* Biophys J, 2008. **94**(12): p. 4957-70.
263. Ormo, M., et al., *Crystal structure of the Aequorea victoria green fluorescent protein.* Science, 1996. **273**(5280): p. 1392-5.
264. Arosio, D., et al., *Spectroscopic and structural study of proton and halide ion cooperative binding to gfp.* Biophys J, 2007. **93**(1): p. 232-44.
265. Lee, J., et al., *Versatile phenotype-activated cell sorting.* Sci Adv, 2020. **6**(43).
266. Heim, R., D.C. Prasher, and R.Y. Tsien, *Wavelength mutations and posttranslational autoxidation of green fluorescent protein.* Proc Natl Acad Sci U S A, 1994. **91**(26): p. 12501-4.
267. Axelrod, D., et al., *Mobility measurement by analysis of fluorescence photobleaching recovery kinetics.* Biophys J, 1976. **16**(9): p. 1055-69.
268. Day, C.A., et al., *Analysis of protein and lipid dynamics using confocal fluorescence recovery after photobleaching (FRAP).* Curr Protoc Cytom, 2012. **Chapter 2**: p. Unit2 19.
269. Stracy, M., et al., *In vivo single-molecule imaging of bacterial DNA replication, transcription, and repair.* FEBS Lett, 2014. **588**(19): p. 3585-94.
270. Stracy, M., et al., *Live-cell superresolution microscopy reveals the organization of RNA polymerase in the bacterial nucleoid.* Proc Natl Acad Sci U S A, 2015. **112**(32): p. E4390-9.
271. Kusumi, A., et al., *Tracking single molecules at work in living cells.* Nat Chem Biol, 2014. **10**(7): p. 524-32.
272. Anthony, S., L. Zhang, and S. Granick, *Methods to track single-molecule trajectories.* Langmuir, 2006. **22**(12): p. 5266-72.
273. Paintdakhi, A., et al., *Oufti: an integrated software package for high-accuracy, high-throughput quantitative microscopy analysis.* Mol Microbiol, 2016. **99**(4): p. 767-77.
274. Jaqaman, K., et al., *Robust single-particle tracking in live-cell time-lapse sequences.* Nat Methods, 2008. **5**(8): p. 695-702.

7 ABBREVIATIONS

amp	amphenicol
ATP	adenosine triphosphate
A-site	aminoacyl-tRNA-binding site
(B)DLP	(bacterial) dynamin-like proteins
bp	base pair
cm	chloramphenicol
CFP	cyan fluorescent protein
D(C)	diffusion coefficient/constant
(ds)DNA	(double strand) deoxyribonucleotide acid
cDNA	circular deoxyribonucleotide acid
EM-CCD	electron multiplying charge-coupled device
ER	endoplasmic reticulum
E-site	exit site
FiSH	fluorescence *in situ* hybridization
GDP	guanosine diphosphate
GED	GTPase effector domain
GFP	green fluorescent protein
GMM	Gaussian mixture model
GTP	guanosine triphosphate
GTPase	guanosine triphosphatase
JD(A)	jump distance analysis
kan	kanamycin

kDa	kilo Dalton
LB	Luria-Bertani
min(s)	minute(s)
ms	millisecond(s)
MS2BP	MS2-binding protein
MS2BS	MS2-binding site
NA	numerical aperture
NLS	nuclear localization sequence
nt	nucleotide
OD	optical density
ORF	open reading frame
PA-FP	photoactivatable fluorescent proteins
PALM	photoactivated localization microscopy
PAM	protospacer adjacent motif
PCR	polymerase change reaction
PH	pleckstrin-homology
Pol I	DNA-polymerase I
Pol II	RNA-polymerase II
PRD	proline-rich domains
P-site	peptidyl-tRNA-binding site
PSF	point spread function
RBS	ribosome binding site
rif	rifampicin
RNA	ribonucleotide acids

mRNA	messenger RNA
pre-mRNA	precursor messenger RNA
ncRNA	non-coding RNA
rRNA	ribosomal RNA
tRNA	transfer RNA
RNAP	RNA-polymerase
rpm	revolution per minute
σ-factor	sigma factor
s/sec	second(s)
SDA	spatial distribution analysis
SDS-PAGE	Sodium-dodecyl sulfate polyacrylamide gel electrophoresis
SLA	stationary localization analysis
SMT	single-molecule tracking
snRNP	small nuclear ribonucleoproteins
spec	spectinomycin
SPT	single-particle tracking
SQD	square displacement analysis
SRP	signal-recognition particle
τ	tau
TCSPC	time-correlated single-photon counting
tet	tetracycline
TIRM	total-internal-reflection microscopy
UTR	untranslated regions
WT	wild type

xyl	xylose
YFP	yellow fluorescent protein

8 APPENDIX

8A.1 Movies

Movie S1: Single-molecule tracking of exponential *B. subtilis* NCIB3610 producing MS2-mVenus

Movie S2: Single-molecule tracking of exponential *B. subtilis* NCIB3610 producing MS2-mVenus

Movie S3: Single-molecule tracking of exponential *B. subtilis* NCIB3610 producing MS2-mVenus + *ypbR-ypzF*_MS2BS2x

Movie S4: Single-molecule tracking of exponential *B. subtilis* NCIB3610 producing MS2-mVenus + *rnc-ftsY*_MS2BS2x

Movie S5: Single-molecule tracking of exponential *B. subtilis* NCIB3610 producing MS2-mVenus + *mreB-minD*_MS2BS2x

Movie S6: Single-molecule tracking of exponential *B. subtilis* NCIB3610 producing MS2-mVenus + *spoIIIE-ymfC*_MS2BS2x

Movie S7: Single-molecule tracking of exponential *B. subtilis* NCIB3610 producing MS2-mVenus + *comN-secDF*_MS2BS1x

Movie S8: Single-molecule tracking of exponential *B. subtilis* NCIB3610 producing MS2-mVenus + *rnc-ftsY*_MS2BS1x

Movie S9: Single-molecule tracking of exponential *B. subtilis* NCIB3610 producing MS2-mVenus + *hag*_MS2BS1x

Movie S10: Single-molecule tracking of exponential *B. subtilis* NCIB3610 producing MS2-mVenus + *mreB-minD*_MS2BS1x

Movie S11: Single-molecule tracking of exponential *B. subtilis* NCIB3610 producing MS2-mVenus + *rplJ-rplL*_MS2BS1x

Movie S12: Single-molecule tracking of exponential *B. subtilis* NCIB3610 producing MS2-mVenus + *rplK-rplA*_MS2BS1x

Movie S13: Single-molecule tracking of exponential *B. subtilis* NCIB3610 producing MS2-mVenus + *ylxM-rplS*_MS2BS1x

Movie S14: Single-molecule tracking of exponential *B. subtilis* NCIB3610 producing MS2-mVenus + *ypbR-ypzF*_MS2BS1x

Movie S15: Single-molecule tracking of exponential *B. subtilis* NCIB3610 producing L1-mVenus

Movie S16: Single-molecule tracking of exponential *B. subtilis* NCIB3610 producing L1-mVenus

Movie S17: Single-molecule tracking of exponential *B. subtilis* NCIB3610 producing MS2-mVenus under 50 µg/ml Rifampicin stress

Movie S18: Single-molecule tracking of exponential *B. subtilis* NCIB3610 producing MS2-mVenus + *spoIIIE-ymfC*_MS2BS2x under 50 µg/ml Rifampicin stress

Movie S19: Single-molecule tracking of exponential *B. subtilis* NCIB3610 producing L1-mVenus under 50 µg/ml Rifampicin stress

Movie S20: Single-molecule tracking of exponential *B. subtilis* BG214 producing DynA-mVenus

Movie S21: Single-molecule tracking of exponential *B. subtilis* BG214 producing DynA-mVenus under 42°C heat stress

Movie S22: Single-molecule tracking of exponential *B. subtilis* BG214 producing DynA-mVenus under 10% ethanol stress

Movie S23: Single-molecule tracking of exponential *B. subtilis* BG214 producing DynA-mVenus under 1 M sorbitol stress

Movie S24: Single-molecule tracking of exponential *B. subtilis* BG214 producing DynA-mVenus under 1 M sodium chloride stress

Movie S25: Single-molecule tracking of exponential *B. subtilis* BG214 producing DynA-mVenus under 250 µg/ml Bacitracin stress

Movie S26: Single-molecule tracking of exponential *B. subtilis* BG214 producing DynA-mVenus under 10 µg/ml Nisin stress

For the movies 2-14, 16-19: Time intervals: 75 ms upon continuous illumination with 515 nm

For the movies 15, 20-26: Time intervals: 20 ms upon continuous illumination with 515 nm

For the movie 1: Time intervals: 8 ms upon continuous illumination with 515 nm

Scale bars: 2 µm

All movies are provided on the attached DVD.

8A.2 List of oligonucleotides

Lists are provided as MS word files on the attached DVD.

8A.3 List of plasmids

Lists are provided as MS word files on the attached DVD.

8A.4 List of strains

Lists are provided as MS word files on the attached DVD.

CURRICULUM VITAE

Page 120 (Curriculum vitae) contains personal data. It is therefore not part of the online publication.

ACKNOWLEDGMENTS

[redacted]

[redacted]